The Spectrum of Molecular Oxygen

Paul H. Krupenie

View Online

Export Citation

ARTICLES YOU MAY BE INTERESTED IN

The Spectrum of Molecular Oxygen

Paul H. Krupenie

Optical Physics Division, National Bureau of Standards, Washington, D.C. 20234

This is a critical review and compilation of the observed and predicted spectroscopic data on O_2 and its ions O_2^-, O_2^+, and O_2^{2+}. The ultraviolet, visible, infrared, Raman, microwave, and electron paramagnetic resonance spectra are included. Each electronic band system is discussed in detail, and tables of band origins and heads are given. The microwave and EPR data are also tabulated. Special subjects such as the dissociation energy of O_2, perturbations, and predissociations are discussed. Potential energy curves are given, as well as f-values, Franck-Condon integrals, and other intensity factors. A summary table lists the molecular constants for all known electronic states of O_2 and O_2^+. Electronic structure and theoretical calculations are also discussed.

Key words: Critical review; electronic spectrum; molecular oxygen; potential energy curves; rotational spectrum; spectroscopic constants.

Contents

423

J. Phys. Chem. Ref. Data, Vol. 1, No. 2, 1972

Figures

1. Introduction

This report, the second[1] in a series on the spectra of diatomic molecules, includes a review of the literature (through February 1971) on the spectra of O_2^-,[2] O_2, O_2^+, and O_2^{2+},[3] and a compilation of critically evaluated numerical data on band positions, molecular constants, energy levels, potential energy curves, transition probabilities, and other molecular properties derived from the spectrum. Though emphasis is on the gas phase, condensed oxygen is considered in discussions of Raman spectra, simultaneous transitions, e.g., $2(^1\Delta_g) \rightarrow 2(^3\Sigma_g^-)$, and the so called high pressure bands. The cited references are mainly those from which the tabulated numerical data are taken, but include also some which deal with interpretation and history.

O_2 is the dominant molecule in thermochemistry and is the second most abundant constituent in the earth's atmosphere. The dissociation, predissociation, and band systems of molecular oxygen play an important role in the aurora, airglow, and nightglow.[4] Molecular oxygen is an important constituent of stellar atmospheres (including that of the sun) and possibly of planetary atmospheres. Meeks and Lilley [269][5] have suggested that the microwave spectrum (60 GHz) can be used as a probe of the thermal structure of the earth's atmosphere and as a space probe of planetary atmospheres.

In laboratory studies below 2000 Å, spectrographs have to be evacuated because of the strong absorption of light by the O_2, $B\ ^3\Sigma_u^- - X\ ^3\Sigma_g^-$ Schumann-Runge transition; more than 99 percent of this absorption is due to the dissociation continuum (1750–1300 Å).

The ionization potentials of O_2 are known from conventional spectroscopy of O_2^+, from Rydberg series limits, photon impact (UV absorption), photoionization, electron impact, and photoelectron spectroscopy. An extremely useful review of electron spectroscopy, electron impact, photoelectron spectroscopy, and Penning ionization has been given by Berry [38].

Topics not considered in detail in this review include absorption coefficients, collision and photon cross sections, photoionization and absorption cross sections, collision detachment cross sections, dissociative recombination coefficients, ion-electron recombination, and charge transfer collision cross sections.

Photoionization cross section measurements have been recently reviewed by Schoen [350]. Autoionization of O_2 Rydberg states has been qualitatively discussed by Price [319]. Cook and Ching [93] have discussed in detail the divergence of measured absorption coefficients.

Two very useful reviews concerning spectra should

be mentioned: Wallace [396] has tabulated band heads for O_2 and O_2^+ transitions, as well as term values and rotational constants for the various states; Gilmore [161] has summarized a great deal of information about the potential energy curves of O_2 and its ions. In addition, a capsule summary of many O_2 transitions and the conditions under which they are observed is contained in a review by Herzberg [190] on forbidden transitions in diatomic molecules. Singlet molecular oxygen (principally $a\ ^1\Delta_g$ and $b\ ^1\Sigma_g^+$) has been reviewed by Wayne [404]. The possibly important role of reactivity of oxygen with pollutants is mentioned in a discussion of the relation of laboratory measurements to atmospheric chemistry.

Reproductions of spectra are not given here but can be found in references cited in table 1 as well as in "The Identification of Molecular Spectra" by Pearse and Gaydon [316].

2. Electronic Structure of O_2 and Its Ions

2.1. Electronic Structure of O_2 and O_2^+

The order of the molecular orbitals (MO's) for O_2 has been given by Mulliken[6] [284]:

$$1\sigma_g < 1\sigma_u < 2\sigma_g < 2\sigma_u < 3\sigma_g < 1\pi_u < 1\pi_g < 3\sigma_u.$$
$$K \quad\ K \quad\ b \quad\ a \quad\ b \quad\ b \quad\ a \quad\ a$$

The bonding character of each orbital is designated as K (inner), b (bonding), or a (anti-bonding). $1\sigma_g$ and $1\sigma_u$ are virtually atomic $1s$ orbitals; $2\sigma_g$ and $2\sigma_u$ are modified $2s$; all other orbitals no longer resemble their separated (atomic) form. The electron configuration which gives rise to the ground state, $X\ ^3\Sigma_g^-$, and also to the observed states $a\ ^1\Delta_g$ and $b\ ^1\Sigma_g^+$, is $KK(2\sigma_g)^2(2\sigma_u)^2(3\sigma_g)^2(1\pi_u)^4$ $(1\pi_g)^2$. The possible states originating from excited configurations are summarized in table 2.

O_2 is one of the few paramagnetic molecules with an even number of electrons; the ground state has a permanent magnetic moment due to unpaired spins. Prediction of the ground state as $^3\Sigma$ was an early success of the molecular orbital method and an early failure of the Heitler-London method. Only by "reexamination" was Heitler-London theory able to predict the correct gound state.

Seven known stable states of the neutral molecule arise from the two lowest electron configurations (table 1). A repulsive $^3\Pi_u$ state is inferred from ab initio calculations and from the predissociation of the $B\ ^3\Sigma_u^-$ state. All bound states which dissociate to ground state atoms have been observed. This inference is based on the semi-empirical potential curves for the unobserved states determined by Vanderslice et al. [387] and Gilmore [161], and from configuration interaction (CI) calculations by

---

[1] The first volume of this series is "The Band Spectrum of Carbon Monoxide," Nat. Bur. Stand. (U.S.), Nat. Stand. Ref. Data Ser., NSRDS–NBS 5 (1966).

[2] Data on O_2^- is mainly from study of the solid. Gas phase O_2^- has been observed as a product of various ion-molecule reactions (Fehsenfeld et al., J. Chem. Phys. 45, 1844–5 (1966)). See sec. 2.4.

[3] O_2^{2+} is known only from electron impact experiments and theoretical calculations.

[4] For details see, e.g., McCormac and Omholt [261] and Roach [332].

[5] Figures in brackets indicate the literature references in Section 15.

[6] Another commonly used notation designates the orbitals as
$$\sigma_g 1s < \sigma_u 1s < \sigma_g 2s < \sigma_u 2s < \sigma_g 2p < \pi_u 2p < \pi_g 2p < \sigma_u 2p.$$

Schaefer and Harris [344]. (See also [187].) Five other states, recently observed, arise from unknown or uncertain excited electron configurations. In addition there have been observed numerous states belonging to Rydberg series. Eight states of O_2^+ are known. Configurations for seven of them are established.

The electronic structure for a number of states of O_2 and O_2^+ has been given by Mulliken [284]. A weakly bound state at about 6.5–7 eV, dissociating to $^3P_g +$ ^1D_g, was hinted at, but such state has not been observed. Mulliken's summary of the lower ionizations of O_2 is given below.

Electron ionized	O_2^+ state
$1\pi_g$ (from $X\ ^3\Sigma_g^-$)	$X\ ^2\Pi_g$
$1\pi_u$ (from $X\ ^3\Sigma_g^-$)	$a\ ^4\Pi_u, A\ ^2\Pi_u$
$1\pi_u$ (from $^1\Delta_g$)	$^2\Pi_u\ (A = 195),\ ^2\Phi_u$
$1\pi_u$ (from $^1\Sigma_g^+$)	$^2\Pi_{ui}\ (A = -195)$
$3\sigma_g$ (from $X\ ^3\Sigma_g^-$)	$b\ ^4\Sigma_g^-, B\ ^2\Sigma_g^-$
$(2\sigma_u)$ (from $X\ ^3\Sigma_g^-$)	$c\ ^4\Sigma_u^-$

The configuration $(1\pi_u)^3(1\pi_g)^2$ includes three $^2\Pi_u$ states, only one of which is known (bound). All three should combine with the ground state of the ion. (See the recent discussion of these $^2\Pi_u$ states by Dixon and Hull [115]; this is mentioned in sec. 2.5.)

Nordheim-Pöschel [300], using a valence bond approach, has estimated the relative separation between a number of low-lying states of O_2, and has shown, qualitatively, that $^3\Pi$ states would not lie at low energies. Indeed, no stable $^3\Pi$ state of O_2 has been identified. It was further concluded that $^3\Sigma_u^-$ and $^3\Sigma_g^+$ states arising from $^3P + {}^1D$ are repulsive. One of the two possible $^3\Sigma_u^-$ states derivable from these atomic products, the B state, has been observed and is stable. No $^3\Sigma_g^+$ state is known.

Miller et al. [276] have shown from observed magnetic hyperfine structure of $^{16}O^{17}O$ that the unpaired electrons in the O_2 bond are primarily $p\pi$ rather than $p\sigma$ and have concluded that "electron configurations which put unpaired electrons in the $p\sigma$ orbit are unimportant in the O_2 molecule."

Lal [248] reported seeing new bands in the visible and UV regions which could not be fitted into other known systems (e.g., $B-X$, O_2 or $A-X$, O_2^+). He therefore inferred the existence of a new state of O_2^+, likely $^2\Pi$, which would perturb $A^2\Pi_u$ around $v=6$. No numerical data were published. Such a $^2\Pi$ state is unknown, and Lal's correlation of such state with $^4S_u + {}^1D_g$ is incorrect.

2.2. Numerical Calculations

a. Semiempirical

Moffitt [280] has shown the need to include configuration interaction to obtain reasonable excitation energies relative to the ground state and correct dissociation

products. By using an intuitive modification of the single configuration MO method he predicted the relative order of O_2 states derived from $\pi_u^4\pi_g^2$ and $\pi_u^3\pi_g^3$ configurations. Both $^1\Sigma_u^-$ and $^3\Delta_{ui}$ were predicted as bound ($^1\Sigma_u^-$ at higher energy), and both were predicted to lie below $A\ ^3\Sigma_u^+$. Experimentally the tentative order is $c\ ^1\Sigma_u^-$, $C\ ^3\Delta_{ui}$, both below the A state. Both c and C states dissociate to ground state atoms. Moffitt also showed that the ionic state $^3\Sigma_u^-$ dissociates to $^1D + {}^3P$ because of the non-crossing rule.

Watari [402], treating O_2 as a six $[\pi]$ electron problem, has predicted the correct order of several states of the two lowest configurations. Linnett [254] has accounted for the double bond of O_2 and the bond order of O_2^+ as 2.5. Orville-Thomas [309], has used MO theory to show that the 0–0 band length in various oxygen-containing molecules decreases with increasing bond order.

Fumi and Parr [150] have computed vertical excitation energies for the states arising from the three configurations $\pi_u^1\pi_g^2$, $\pi_u^3\pi_g^3$, and $\pi_u^2\pi_g^4$. They used LCAO–MO wave functions plus CI between states of the first and third configurations, but with neglect of overlap and empirical fitting of some parameters. Their relative energies were in fair agreement with experiment and with the more complicated results of Moffitt [280]. The $^1\Delta_u$ was predicted to lie below $^1\Sigma_u^+$, but it was not certain whether these should be bound. Gilmore [161] has drawn them as slightly stable.

Bassani, Montaldi, and Fumi [32], using the method of Fumi and Parr, have calculated vertical excitation energies of Π and Φ states of O_2^+ relative to the ground state of the ion (in the π-electron approximation). Excitation energies of unobserved states $^2\Phi_u$, $^4\Pi_g$, and $^2\Phi_g$ were indicated. The $^2\Phi_u$ state fell near the $b\ ^4\Sigma_g^-$; the other two lay far above it. The $^2\Phi_u$ state would be about 1 eV above $A\ ^2\Pi_u$, $^4\Pi_g$ several volts above $^2\Pi_u$, and $^2\Phi_g$ several volts above $^4\Pi_g$. $^2\Phi_u$ seems bound with D^e about 2.5 eV. This state as sketched by Gilmore [161] would have a binding energy of about 4.2 eV if its minimum were 1 eV above the minimum of $^2\Pi_u$. The other two unobserved states are also stable in this approximation [32].

Vanderslice et al. [387], using a valence-bond approximation and experimental data, have estimated the potentials for 12 repulsive states derived from ground state atoms. These states were slightly altered in Gilmore's figures [161] to account for configuration interaction.

b. Single configuration ab initio

Itoh and Ohno [212] have used different screening constants for the O atom and its ion (AO's for covalent and ionic structure) to calculate excitation energies (at $r = 1.207$ Å) for π-electron states. In general, their results agree with those of Moffitt [280] and Fumi and Parr [150]. A reasonable value was obtained for the separation $^3\Sigma_g^- - {}^3\Sigma_u^+$. Contour diagrams were given of individual and total orbital electron densities for the

ground state. Bader et al. [25] have reproduced Wahl's more recent calculated individual and total charge density contours for the O_2 ground state at r_e (based on nearly $H-F$ wave functions).

c. Configuration interaction ab initio

Meckler [268] has built up LCAO MO functions from a minimum basis set of Gaussian atomic functions to study the full CI for the $X\,^3\Sigma_g^-$ and $^1\Sigma_g^+$ states. The eight atomic electrons were distributed among 12 spin-orbitals arising from $2p$ atomic levels, with no $s-p$ hydridization. Though his calculations give r_0, D^0, and ω_e to within a few percent of the experimental values, large potential maxima ($\sim\frac{1}{3}\,D^0$) which peak at ~ 4 Å were calculated for both states. There is no ex-perimental evidence to support this. In all cases Meckler assumed filled $1s$ and $2s$ shells. His results are less accurate than those of Kotani et al. [236], but are given as a function of r.

Kotani et al. [236], have made very extensive calcu-lations of electronic properties of O_2 and O_2^+ at $r=1.217$ Å by the LCAO method using a minimum basis set of Slater orbitals for the all electron problem. Fifteen dimensional CI makes significant improvement in some of these properties. The relative merits of various approximate treatments (for the ground state of O_2) are compared. Properties calculated include, among others, D^e, excitation energies, quadrupole moment (Q), oscillator strengths (f), and polarizabilities. The same nine states are considered as were treated by Fumi and Parr [150], and Itoh and Ohno [212]. Kotani et al. [236] have shown that excitation of $2s$ electrons (as was done by Meckler) produces significant changes. A comparison is made of the energy levels calculated by CI with more than a dozen different approximations. A fifteen configuration calculation lowers the total energy of the ground state by 5 eV, but still gives a poor value for D^e. For $\pi_u^3\pi_g^3$ configuration the $^3\Delta_u$ state was predicted to lie between $^3\Sigma_u^+$ and $^1\Sigma_u^-$, as is tentatively found experimentally.

Schaefer and Harris [344] have calculated potential energy curves for 62 states of O_2 derived from the lowest states of O: ^3P, ^1D, ^1S. Twelve bound states were pre-dicted, including seven found experimentally, and several predicted earlier by others. Several new bound states are predicted. In the calculations, only a mini-mum STO basis set was used together with a complete "valence CI" to give the correct dissociation products. Screening parameters were used appropriate to the ^3P ground state. The $c\,^1\Sigma_u^-$ state was calculated to lie below both $C\,^3\Delta_u$ and $A\,^3\Sigma_u^+$. The new results suggest that the $^1\Sigma_u^+$ state ($^1D+{}^1S$) has a larger binding energy than $^1\Delta_u({}^1D+{}^1D)$, the reverse of the sketch by Gilmore [161]. The additional bound states are

$$^3\Sigma_u^- \;({}^3P+{}^1D)\text{ at }5.94\text{ eV},\, r_e\sim 2\text{ Å}.$$

$$^1\Pi_g({}^1D+{}^1D)\text{ at }8.13\text{ eV},\, r_e\sim 1.55\text{ Å}.$$

$$^1\Delta_g({}^3P+{}^1S)\text{ at }8.71\text{ eV},\, r_e\sim 2\text{ Å}.$$

More recent (unpublished) calculations by H. H. Michels are qualitatively the same.

2.3. Electronic Structure of O_2^{2+}

The ion O_2^{2+} has been observed only in electron impact experiments. Perhaps O_2^{2+} spectra might be observed in a hollow cathode discharge in low pressure O_2, for Carroll and Hurley [77] have observed N_2^{2+} under those circumstances. Appearance potentials for O_2^{2+} were long ago given as 54.1 eV [163] and 50.1 eV [166]. Recently, Hurley and Maslen [209] and Hurley [208] have theoretically predicted the energies, molec-ular constants, and approximate potential curves for O_2^{2+}, derived from curves of N_2. The ground state appearance potential was estimated as 35.92 eV, smaller by 15 eV than prior experimental values. Dorman and Morrison [118] have remeasured the appearance poten-tial of O_2^{2+} to be 36.2 ± 0.5 eV which lies close to the calculated value. The discrepancy between this value and earlier, higher values is not explained. Daly and Powell's [101] measured value for the appearance potential of the O_2^{2+} (X state) is about 1 volt higher than that of Dorman and Morrison; the $A\,^3\Sigma_u^+$ state energy was found to be $\geqq 4$ eV above $X\,^1\Sigma_+^-$. Hurley [208] has estimated the lifetime of the A state (O_2^{2+}) for dissocia-tion by tunneling as ~ 1 sec., and 10^{500} sec. for the X state (O_2^{2+}).

2.4. Electronic Structure of O_2^-

The molecular ion O_2^- is formed in gas discharges containing oxygen, and has been detected by mass spectrometer in H_2+O_2 at 0.1 mm pressure (A. Schmel-tekopf, private communication). It is formed also in the D layer of the upper atmosphere, and is stable in solution or in ionic lattices [97].

The ground state configuration of O_2^- is

$$KK(2\sigma_g)^2\,(2\sigma_u)^2\,(3\sigma_g)^2\,({}^1\pi_u)^4\,(1\pi_g)^3\,X\,^2\Pi_{gi}.$$
$$\quad\; b\qquad\; a\qquad\; b\qquad\; b\qquad\; a$$

The molecular ground state dissociates into ground state products $O(^3P)+O^-(^2P^0)$ which can form a total of 24 states.

The ground state dissociation energy has been crudely estimated by Bates and Massey [34], by Creighton and Lippincott [97] from a semiempirical formula using the frequency of a Raman line of KO_2, and more carefully by Mulliken [286]. By using an improved value for $EA(O_2)$ [312] one obtains $D^0(O_2^-)=4.07$ eV. This places O_2^-, $X\,^2\Pi_{gi}$ about 0.4 eV below O_2, $X\,^3\Sigma_g^-$. The dissocia-tion energy is cyclically related to several other quanti-ties by the formula $D^0(O_2)+EA(O_2)=D^0(O_2^-)+EA(O)$ where the following values have been used: $D^0(O_2)=$

$(5.116 \pm 0.002$ eV) [62], $EA(O_2) = (0.43 \pm 0.02$ eV)[7] [312], and $EA(O) = (1.478 \pm 0.002$ eV)[8] [39].

r_e for the ground state is tentatively given as 1.33 Å which is a compromise between the values 1.28 Å [2] and 1.32–1.35 Å [171], both calculated from crystal structure of KO_2, and the value 1.377 Å, estimated by the use of Badger's rule [49]. This approximate value of r_e is consistent with that expected by analogy with F_2^+ (1.3–1.4 Å). From the low-temperature fluorescence emission spectra of O_2^- in alkali halides Rolfe [336] has obtained $\omega_e'' = 1152–1163$ cm^{-1}, $\omega_e x_e'' = 8.5$ cm^{-1}, $\omega_e' = (780 \pm 100)$ cm^{-1}, $\Delta G''(\frac{1}{2}) = 1123–1145$ cm^{-1}. These results were in good agreement with $\Delta G''(\frac{1}{2}) = (1145 \pm 2)$ cm^{-1} obtained from Raman spectra in solid KO_2 [97]. Recently, the Raman spectrum of O_2^- in alkali halide crystals [194] has yielded an extrapolated value for the isolated ion: $\Delta G''(\frac{1}{2}) \sim 1090$ cm^{-1}. This value leads to $\omega_e'' \sim 1107$ cm^{-1}, $\omega_e x_e'' \sim 8–9$ cm^{-1}.

Spence and Schulz [361] and Boness and Schulz [49] have measured vibrational spacings of the ground state of O_2^- produced by scattering of electrons by gaseous O_2. They obtained $\omega_e \sim 1090$ cm^{-1}, $\omega_e x_e \sim 12$ cm^{-1}. Combining this vibrational data with $\Delta G''(\frac{1}{2})$ of Holzer et al. [194] gives compromise values $\omega_e \sim 1113$ cm^{-1}, $\omega_e x_e \sim 11.7$ cm^{-1} (uncertainties are assumed as $\omega_e \pm 25$ cm^{-1}, $\omega_e x_e \pm 4$ cm^{-1}).

There has been much speculation about a stable $^4\Sigma_g^-$ state of O_2^- which dissociates to $O(^3P) + O^-(^4P)$ [34, 68, 211, 351, 92, 286], but most likely no low-lying stable excited states exist for O^- [286, 232, S. Smith, private communication]. The fluorescence observed by Rolfe [336] has generally been assigned as $^2\Pi_{ui} \rightarrow X^2\Pi_{gi}$, but an upper state assignment as $^2\Sigma_u^-$ cannot be ruled out. Rolfe [336] had indicated that the upper state term value was 3.65 eV above the ground state of O_2^- (this was the long-wavelength limit of excitation). Hurst and Bortner [210] obtained evidence of excitation to an electronic state of O_2^- (presumably $^4\Sigma_u^-$) which lies approximately 1 eV above the ground state. Recent calculations (see below) indicate that this excited state lies somewhat higher.

The lowest-lying configurations of O_2^- which dissociate to ground-state configurations of $O + O^-$ (though perhaps not to ground-state products) are:

(a) $(3\sigma_g)^2(1\pi_u)^3(1\pi_g)^4 - {}^2\Pi_{ui}$

(b) $(3\sigma_g)^2(1\pi_u)^4(1\pi_g)^2(3\sigma_u) - {}^2\Sigma_u^+, {}^2\Sigma_u^-, {}^2\Delta_u, {}^4\Sigma_u^-$

(c) $(3\sigma_g)^2(1\pi_u)^3(1\pi_g)^3(3\sigma_u) - {}^2\Sigma_0^+(2),$
    $\quad {}^2\Sigma_g^-(2), {}^2\Delta_g, {}^2\Delta_{gi}, {}^4\Sigma_g^+, {}^2\Sigma_g^-, {}^4\Delta_{gi}$

(d) $(3\sigma_g)(1\pi_u)^4(1\pi_g)^4 - {}^2\Sigma_g^+$
    (not to ground state $O + O^-$)

Until recently the structure of the possible states of O_2^- has been largely speculative; early estimates of the relative bonding of different states were crude [34, 286]. A rough guide to these energies was provided by calculated values for analogous states of F_2^+ [144, 192]. Recent tentative results of SCF CI calculations [M. Krauss, private communication, 271a] show numerous stable states besides the ground state.

The stable states in order of increasing binding energy are: $^4\Sigma_g^-$, $^2\Sigma_g^+$, $^4\Pi_u$, $^2\Sigma_u^-$, $^2\Sigma_g^-$, $[^2\Sigma_u^+, {}^4\Sigma_g^+, {}^2\Pi_u,$ $^4\Delta_g, {}^2\Delta_u]$ $^4\Sigma_u^-$, and $X\,^2\Pi_g$. The states enclosed in brackets all have binding energies of ~ 1 eV. (Several of these states are included in fig. 2.)

2.5. Ionization Potentials, Rydberg Series, Photoionization, and Photoelectron Spectroscopy

The known ionization potentials of O_2 have been determined spectroscopically (i.e., from Rydberg series limits plus data on electronic transitions in O_2^+), by photoionization, electron impact, ion-molecule collisions, and by photoelectron (photoemission) spectroscopy. No known Rydberg series converges to the ground state of O_2^+, though the first terms of such series have been tentatively identified (see sec. 3.9, 3.10). The lowest-lying Rydberg term, expected at about 8 eV, probably $\pi_g n s \sigma_g\,^3\Pi_g$, is a dipole forbidden transition from the ground state, and remains unobserved [161]. In addition, interaction with other states causes mixing of configurations and contributes to the weakness and diffuseness of such forbidden Rydberg terms of excited O_2. Configurations $\ldots \pi_g n p \sigma_u$ and $\ldots \pi_g n p \pi_u$ do give rise to allowed Rydberg series. Broadening of auto-ionization has been discussed by Price [319]. A recent photoionization measurement of the lowest IP of O_2 by Samson and Cairns [342, 42], (12.059 ± 0.001) eV $= 97265$ cm^{-1} establishes the O_2^+ energy level scale. Samson and Cairns have given a useful summary of previous determinations of this IP by several methods.

Details of the observed Rydberg series are given in secs. 3.9 and 3.10; only a few Rydberg states have had their fine structure analyzed.

Tentative classifications of Rydberg states are given by Huber [197] and Leclercq [251]; additional classifications and related discussions are to be found in papers which give the experimental details (see also refs. [253, 125]). Even though the assignments of quantum numbers n and defects δ for the lowest terms in the various series are open to some interpretation (especially those of Yoshino and Tanaka [417]), the series limits and Rydberg formulas still properly describe the Rydberg series.

Rydberg states are known from transitions originating in the X and b states. The $\beta\,^3\Sigma_u^+$, $\alpha\,^1\Sigma_u^+$, and

---

[7] Spence and Schulz [361] and Boness and Schulz [49] discuss a number of different values for $EA(O_2)$ which are found in the literature, but state why they prefer the value of Pack and Phelps [312]. R. Celotta (unpublished results) has recently obtained a value which is virtually the same as that of Pack and Phelps.

[8] $EA(O) = 1.465 \pm 0.005$ eV was obtained by Branscomb et al. [58]. Recent experiments (unpublished) which use $EA(O)$ do not unambiguously support this value or that of Berry et al. [39]. It is desirable that this quantity be remeasured with improved accuracy.

$^3\Sigma_u^+$ Rydberg states arising from forbidden transitions have had their fine structure studied; the other observed states or series are assigned as:

$$b \; ^4\Sigma_g^-, B \; ^2\Sigma_g^- \leftarrow (3\sigma_g)(np\sigma_u) \; ^3\Sigma_u^-, (np\pi_u) \; ^3\Pi_u$$

$$c \; ^4\Sigma_u^- \leftarrow (2\sigma_u)(nd\pi_g) \; ^3\Pi_u, (ns\sigma_g) \; ^3\Sigma_u^-$$

For the $\alpha \; ^1\Sigma_u^+ - b \; ^1\Sigma_g^+$ and $\beta \; ^3\Sigma_u^+ - X \; ^3\Sigma_g^-$ transitions, $\Delta G'$ and B' from fine structure analysis are close to the values for the O_2^+, $X \; ^2\Pi_g$ state.

The electron impact method yields directly the vertical IP, not the adiabatic IP obtained by all other methods. Frost and McDowell [147] have measured by electron impact five states of O_2^+, including $^2\Pi_g$, $^4\Pi_u$, $^2\Pi_u$, $^4\Sigma_g^-$, and a new state at 21.34 eV. An O_2^+ term at this energy was confirmed experimentally by Brion [61]. This energy may represent "removal of a $\sigma_u 2s$ or $\sigma_g 2p$ electron with or without simultaneous excitation of another electron in one of the other orbits" [147]. At 22.03 eV evidence exists for a process leading to formation of O_2^+; this may be a transition to a repulsive state of O_2^+, with a minimum at 20.7 eV which is close to the Rydberg limit of 20.3 eV [147] and the limit $^1D + \; ^4S^0$.

Lichten [252] has tentatively identified a metastable state of O_2 at $\sim$ 12 eV in electron bombardment studies. The observed lifetime is $> 10^{-3}$s. Possible configuration of this state is $(\pi_u 2p)^3 (\pi_g 2p)^2 (\sigma_g R)$. McGowan and Kerwin [262] have observed four new states of O_2^+, (produced by molecule-ion collisions) at 23.9 eV, 27.9 eV, 31.3 eV, and 34.1 eV (uncertainty $\pm$ 0.2 eV).

Al-Joboury et al. [12, 11] were the first to study O_2^+ extensively by photoelectron spectroscopy (PES). More recently Turner and May [384], Turner [383] and especially Edqvist et al. [125] have extended these measurements, the latter even resolving overlapping vibrational structure of $a \; ^4\Pi_u$ and $A \; ^2\Pi_u$.

Price (see discussion by Dixon and Hull [115]) has observed a new broad feature with 1.5 eV half width at 23.7 eV in the photoelectron spectrum of O_2 with 304 Å photons. Dixon and Hull [115], on the basis of semi-empirical calculations, have assigned this feature as a new $^2\Pi_u$ state of O_2^+, the uppermost $^2\Pi_u$ state derivable from a $\pi_u^3 \pi_g^2$ configuration. It is not certain that this state is stable.

Edqvist et al. [125] have studied the PES of O_2 in the range 12–28 eV with both 584 Å and 304 Å photons. They observed vibrational levels of the $A \; ^2\Pi_u$ among the higher levels of the $a \; ^4\Pi_u$ state. The diffuse state with vertical IP of 24.0 eV corresponds to the state observed by Price.

Extensive vibrational structure was observed [125] in the following states: $X \; ^2\Pi_g$, $a \; ^4\Pi_u$, $A \; ^2\Pi_u$, $b \; ^4\Sigma_g^-$, and $B \; ^2\Sigma_g^-$. Geiger and Schröder [158] have observed many of these features (as well as some which are still unidentified) in the energy loss spectrum up to 21 eV. Additional features [125] include $a \; ^2\Pi_u$ state at 24.0 eV;

above this, $c \; ^4\Sigma_u^-$, $v = 0$–2; and at 27.4 eV, an unidentified peak in an unexplained continuum extending from 25.5 to 28 eV. The features at 23.7 and 27.4 eV had been seen earlier by McGowan and Kerwin [262].

Turner [383] observed marked broadening for $B \; ^2\Sigma_g^-$, $v > 3$. He interpreted this broadening which begins at 20.7 eV, the dissociation limit for $b \; ^4\Sigma_g^-$, as possibly due to strong interaction between the B state (which he assumes is $^4\Sigma_u^-$) and b state. Edqvist et al. [125], with slightly better resolution, see sharp structure only.

Samson [340] used photons ranging in energy from 27–66.6 eV to study the photoelectron spectrum of O_2 and found states at 23.5, 24.6, and 27.3 eV; uncertainty was estimated as $\pm$ 0.3 eV (see also McGowan and Kerwin [262]). Signal-to-noise ratio prevented resolution of possible structure above 27.3 eV. Samson speculated that the state at 23.5 eV (and possibly also the state at 24.6 eV) might arise from removal of a $\sigma_u 2s$ electron, and the state at 27.3 eV might arise from removal of a $\sigma_g 2s$ electron.

3. Electronic Spectrum of O_2 and O_2^+

O_2 is a weak light emitter because, for most of its excited states, transitions to the ground state are strongly forbidden. Since ^{16}O has zero nuclear spin, antisymmetric rotational levels of $^{16}O_2$ are missing. [9]

The $B \; ^3\Sigma_u^- - X \; ^3\Sigma_g^-$ Schumann-Runge transition dominates the spectrum of molecular oxygen. Discrete bands of this allowed transition span the region 5350–1750 Å; an even stronger dissociation continuum spans the region 1750–1300 Å. Most other O_2 transitions which have been observed under high resolution are forbidden by electric dipole selection rules and are considerably weaker than $B - X$; the exceptions are transitions below 1300 Å, mainly to Rydberg states. Between 1300 Å and 300 Å continua overlap the discrete structure. Weak $b \; ^1\Sigma_g^+ - X \; ^3\Sigma_g^-$ atmospheric bands (9970–5380 Å) and $a \; ^1\Delta_g - X \; ^3\Sigma_g^-$ IR atmospheric bands (15,800–9240 Å) have also been observed.

In contrast with O_2, the three observed transitions for O_2^+ are all electric dipole allowed: $A \; ^2\Pi_u - X \; ^2\Pi_g$ (2–), 6530–1940 Å; $b \; ^4\Sigma_g^- - a \; ^4\Pi_u$ (1–), 8530–4990 Å; and $c \; ^4\Sigma_u^- - b \; ^4\Sigma_g^-$ Hopfield bands, 2360–1940 Å. Additional states of O_2^+ known from Rydberg series and photoelectron spectroscopy enable the O_2^+ doublet and quartet states to be placed on a common energy scale.

3.1. $a \; ^1\Delta_g$ $X \; ^3\Sigma_g^-$ Infrared Atmospheric System (15,800–9240 Å)R

The $^1\Delta_g - \; ^3\Sigma_g^-$ magnetic dipole intercombination transition in O_2, predicted by Mulliken [283], was first observed by Ellis and Kneser in 1933 [126] in absorp-

[9] For example, for the $X \; ^3\Sigma_g^-$ state levels occur with $N = 1, 3, 5, \ldots$; $J = 0, 1, 2, \ldots$ all rotational levels are +. For the $B \; ^3\Sigma_u^-$ state levels occur with $N = 0, 2, 4 \ldots$; $J = 1, 2, 3, \ldots$; all rotational levels are –.

tion by liquid oxygen. The fine structure was resolved and the transition assigned as $^1\Delta_g - {}^3\Sigma_g^-$ by Herzberg (in 1934), who photographed these bands in the solar spectrum. Details of the solar 0–0 and 1–0 bands were given somewhat later by Herzberg and Herzberg [191]. The spectra were taken with a three-meter grating in first order (dispersion, 4.9 Å/mm). The observed a–X band positions and rotational constants for the a state are listed in tables 3 and 37, respectively. Rotational constants for the X state are in table 36.

The bands, inherently very weak, are characterized by $O, P, R, S,$ and Q-form branches; they showed two strong Q heads and no clear zero gap.

Relative accuracy of the observed line positions in the 0–0 band is ±0.03 cm⁻¹ for unblended lines; in 1–0, it is ±0.07 cm⁻¹. (See footnote 6(a) in ref. [191] regarding absolute accuracy.) The small difference between $F_2 - F_1$ and $F_2 - F_3$ for the ground state accounts for overlapping ^QP and ^QR branches. (See also Babcock and Herzberg [24] and sec. 8 of the microwave spectrum.)

Of nine possible branches, only one pair remained unresolved: $(^QP^QR)$. The other branches are $^SR, {}^RR, {}^RQ, {}^RQ, {}^PP, {}^PQ, {}^OP$.

The 0–0 band has been observed in the day and night airglows [165], and is weaker than might be expected because of reabsorption by the lower atmosphere. The 0–1 band was found in emission from the night sky [91, 385]. Its fine structure was resolved, but the numerical data has not been published [91].

3.2. $b\,^1\Sigma_g^+ - X\,^3\Sigma_g^-$ Atmospheric System (9970–5380Å) R

The $b\,^1\Sigma_g^+ - X\,^3\Sigma_g^-$ magnetic dipole intercombination transition consists of doublet P and R branches, i.e., $P, {}^PQ, R,$ and ^RQ branches,[10] the latter two forming a weak head. Observations of these weak, red-degraded bands date back to the work of Wollaston in 1802 and Fraunhofer in 1817. The most extensive and precise measurements of the b–X transition are by Babcock and Herzberg [24] who studied absorption in the laboratory (with air paths up to 30 m) and solar absorption by the earth's atmosphere (100 km air paths). These measurements were an extension of earlier work by Babcock and collaborators [see especially Dieke and Babcock [112] and Babcock [22] from which the transition was first identified as $^1\Sigma - {}^3\Sigma$ by Mulliken [283]. The early work led Giauque and Johnston [160] to some of the earliest identifications of isotopes ($^{16}O^{17}O, {}^{16}O^{18}O$) by spectroscopy. The only additional detailed absorption measurements are the fragmentary data on the 4–0 band by Ossenbrüggen [311]. Band origins and heads for the b–X transition are listed in tables 4 and 5, respectively; rotational constants for the X and b states are listed in tables 36 and 38, respectively.

The b–X bands were first detected in the solar spectrum[11] and later produced in the laboratory. Absorption measurements in the 1920's and 1930's, mainly by Babcock and collaborators, culminated in a definitive work by Babcock and Herzberg [24] wherein are given references to the earlier measurements. Bands of this system have also been produced in emission from a variety of sources,[12] but studies of these, with few exceptions, only provided identification of several additional band heads not seen in absorption (table 5).

Babcock and Herzberg [24] have measured the fine structure of the following absorption bands: $^{16}O_2$, 0–0, 1–0, 2–0, 3–0, 1–1, 2–1, 3–1; $^{16}O^{17}O$ and $^{16}O^{18}O$, 0–0, 1–0. The spectra were produced using a plane grating spectrograph of 30-foot focus with reciprocal dispersion of 0.88 to 0.12 Å/mm. For unblended medium intensity lines, wavelengths have been determined with an accuracy of about 0.001 Å. Combination differences for bands with $v''=0$ were in agreement to within 0.005 cm⁻¹. These measurements have provided molecular constants for the X and b states for the three isotopes studied.[13] ω_e'' was derived from $\Delta G''(\frac{1}{2})$, and the vibrational constants of Curry and Herzberg [99], with $\Delta G''(\frac{1}{2}) = 1556.3856$ believed (then) to be accurate within ±0.001 cm⁻¹. A least squares refitting by Albritton et al. [9] gives 1556.379 ± 0.006.

3.3. $b\,^1\Sigma_g^+ - a\,^1\Delta_g$ Noxon System (19,080 Å)

Noxon [301] observed emission of the Q branch of the b–a, 0–0 band at 19,080 ± 30 Å in a low pressure discharge through He containing a trace of O_2. This appears to have been the first observation of an electronic transition in a diatomic molecule which is primarily (electric) quadrupole [301]. (This system is forbidden by magnetic dipole selection rules since $\Delta\Lambda = 2$.)

3.4. $c\,^1\Sigma_u^- - X\,^3\Sigma_g^-$ Herzberg II System (4790–4490; 2715–2540 Å) R

Absorption bands of this very weak forbidden transition have been observed among the stronger $A\,^3\Sigma_u^+ - X\,^3\Sigma_g^-$ bands by Herzberg [189]. The observed band origins are listed in table 6; predicted origins are given in table 7; rotational constants for the $c\,^1\Sigma_u^-$ state are in table 39. The spectra were observed in fourth order of a 21-ft. grating spectrograph; oxygen pressure was 2.7 atm. The molecular constants for the c state were obtained by assuming the values for the ground state from the work of Babcock and Herzberg [24].

---

[11] The current and early band designations are compared: 0–0, 1–1 (A); 1–0 (B); 2–0 (α); 3–0 (α'); 4–0 (α''): 0–0, $^{16}O^{18}O$ (A'); 0–0, $^{16}O^{17}O$ (A''). The 0–0 and 1–0 bands, designated A and B, respectively, by Fraunhofer in 1817 were among the first molecular bands observed.

[12] These bands have been observed in the night airglow and aurorae, and in the laboratory in oxygen-enriched nitrogen afterglows, CO + O₂ explosions, He discharge containing a trace of O₂, glow discharge in pure O₂ at atmospheric pressure, and an r.f. electrodeless discharge. Branscomb [57] lists a number of these references; see also Chamberlain, Fan, and Meinel [82] and Herman, Herman, and Rakotoarijimy [183].

[13] Appendix C discusses molecular constants for the ground state.

---

[10] These magnetic dipole bands are always observed in almost any spectrograph of moderate size which is not evacuated. These branches are also possible for an electric quadrupole transition, but those arising from $\Delta J = \pm 2$ have not been observed.

The $c-X$ bands [with branches ^PP, ^PQ, ^RR, ^RQ] have structure similar to the $b-X$ system, but weaker by a factor 10^3, and with much greater difference $|B'-B''|$ because of the feeble binding energy of the c state. Unblended line positions are assumed uncertain by ± 0.1 cm^{-1}; numerous blended lines have considerably larger uncertainties. Long exposures resulted in 0.1 cm^{-1} displacements between iron arc calibration spectra and $c-X$ line positions.

Herzberg [189] analyzed the fine structure of six absorption bands. Degen [103] has analyzed the structure of two feeble emission bands observed in an oxygen-argon afterglow. These have been tentatively identified by Degen as the 0–7 (4491 Å) and 0–8 (4791 Å) members of the $c-X$ system. The new v' numbering, still tentative, is five units larger than that provisionally assumed by Herzberg [189]. The spectra were taken by Degen on a 3 m grating spectrograph, exposure 100 hours, dispersion 3 Å/mm. Measured rotational line positions are uncertain by 0.1 Å. The 0–7 band had been mentioned earlier by Broida and Gaydon [63] but it had not been assigned; the 4791 Å band is new.

Many features of the nightglow spectrum lie within several Angstroms of the calculated band positions [189, 103]. Broida and Gaydon [63] had observed some bands in an oxygen afterglow (4600–3600 Å) which might be fitted into this Delandres array, but only with considerable uncertainty. Some bands observed in the UV airglow suggested an increase in Herzberg's provisional v' numbering by unity, but this had only been hinted at by Chamberlain [79]. The numbering used by Degen [103] places the c state below both C and A; all three states derive from the same electron configuration. A short extrapolation of vibrational terms makes it certain that the $c\,^1\Sigma_u^-$ state dissociates to ground state atoms.

The $c-X$ transition, assumed allowed as electric dipole radiation, is only spin forbidden, and is likely so weak because it is forbidden as electric dipole radiation in the separated atoms.

3.5. $C\,^3\Delta_u-X\,^3\Sigma_g^-$ Herzberg III System (2630–2570 Å) R and High-Pressure Bands (2924–2440 Å)

Fragments of two very weak, triple-headed bands have been observed in absorption by Herzberg [189], who used a 350 meter absorbing path at 2.7 atm. pressure. These underlie the far stronger $A\,^3\Sigma_u^+\leftarrow X\,^3\Sigma_g^-$ bands. Observed $C-X$ sub-band origins are listed in table 8a; rotational constants for the $C\,^3\Delta_u$ state are in table 40.

Vibrational numbering in the C state is uncertain. Arbitrarily, Herzberg [189] assumed that the triplet observed by Herman [182], whose middle sub-band head is at 2913 Å, was the 0–0, and assigned the two fragments he (Herzberg) observed to bands 5–0 and 6–0. The only carefully determined vibrational quantum $\Delta G(5\tfrac{1}{2}) = 611.16$ cm^{-1} is for $^3\Delta_3$ components. Assign-

ment of the upper state as $^3\Delta_u$ is based on the assumed electron configuration, though the number of missing lines near the origin could not be determined. Thus, it could not be shown, unequivocally, that the upper state is not $^3\Pi_u$. ^4S, and R- and P-form branches were detected. Both odd and even J were observed in the upper state, an indication that $\Lambda > 0$.

Herzberg [189] has assumed that the $C-X$ bands are the free-gas analogue of the diffuse triplets, nearly coincident with the positions of the $A-X$ bands, as observed by Wulf [415], Finkelnburg and Steiner [141], and Finkelnburg [140]. These high-pressure bands (table 8b), first observed under pressures of 60–600 atm, had been ascribed by Finkelnburg and Steiner [141], to the collision-induced forbidden transition, $^3\Delta - {}^3\Sigma$. In a later paper Finkelnburg [140] ascribed these to vibrations of a collision complex. (See sec. 4 on condensed oxygen.)

Observation of the diffuse structure till nearly the $^3P + {}^3P$ dissociation limit [140] strongly suggests that the $^3\Delta_u$ state dissociates to ground state atoms. Experimental data is insufficient to allow a reliable potential curve to be drawn. Gilmore [161] has sketched in a fragmentary curve just below that of $A\,^3\Sigma_u^+$, following Herzberg [189]. The $C-X$ transition is forbidden only by the rule $\Delta\Lambda = 0, \pm 1$, but is extraordinarily weak, likely because it is also forbidden in the separated atoms.

For the $v'=6$ level, the triplet splitting between $^3\Delta_3$ and $^3\Delta_2$ is 145.9 cm^{-1}, indicating case a coupling. Splitting between middle and short wavelength components of the high pressure triplets is 138 cm^{-1} [141, 182]; the splitting between the middle and the long wavelength components is 118 cm^{-1}.

$B_v({}^3\Delta_2)$ is assumed a good approximation to the true B_v values. By assuming further that $B_5({}^3\Delta_3) - B_5({}^3\Delta_2) = B_6({}^3\Delta_3) - B_6({}^3\Delta_2)$, the former being unobserved, $B_5({}^3\Delta_2)$ has been approximately calculated [189].

3.6. $C\,^3\Delta_u - a\,^1\Delta_g$ Chamberlain System (4380–3700 Å) R

Twenty-seven weak bands (table 9) observed in the airglow have been tentatively assigned by Chamberlain [81] to the intercombination, electric dipole transition, $C\,^3\Delta_u - a\,^1\Delta_g$ (see table 1 of ref. [81] for a list of band heads). Identification is uncertain because of low dispersion (21 Å/mm). The quantum numbering for the upper state is based on that tentatively assumed by Herzberg [189].

3.7. $A\,^3\Sigma_u^+ - X\,^3\Sigma_g^-$ Herzberg I System (4880–2430 Å) R

Very weak absorption bands of this forbidden electric dipole transition were first observed by Herzberg [185]; additional bands were observed at longer wavelength by Herman [182]. A detailed fine structure analysis of these strongly red-degraded bands which showed no prominent heads was later given by Herzberg [187] (4th order, 21-ft. grating; absorbing paths up to 800 m-atm; 3rd

order iron lines served as calibration). This was the first $\Sigma^+ - \Sigma^-$ transition identified with like multiplicity for both states. The dominant Q-branch lines consist of six components: $^QQ_3$, $^QP_{32}$, $^QQ_1$, $^QR_{12}$, $^QR_{23} + ^QP_{21}$, and $^QQ_2$ which was observed for the strongest bands; faint branches $^SR_{21}$, $^OQ_{13}$, $^OP_{12}$, and $^OP_{23}$ were also observed in some bands [187]. Observed $A-X$ bands and rotational constants for the $A\,^3\Sigma_u^+$ state are given in tables 10 and 11, respectively. A Deslandres array of predicted band positions can be found in the paper by Herzberg [187].

Dufay [119] and others tentatively identified some bands of the UV night airglow [14] (3800–3100 Å) as members of the $A-X$ system. Finally, Chamberlain [80] definitely confirmed these identifications by fine structure assignments. Meanwhile, Broida and Gaydon [63] produced $A-X$ bands in emission from laboratory afterglows (table 11). (See also Gaydon [153].) Observation of a new progression showed that Herzberg's 1952 v' numbering [187] should be increased by unity (Herzberg's original numbering [185] was raised by 4). Barth [28, 29, 30] observed this system in oxygen and oxygen-nitrogen ("air") afterglows (4500–2500 Å) and was able to partially resolve rotational structure. Unless further revision in numbering is necessary, the last vibrational level in $A\,^3\Sigma_u^+$ before dissociation is 11.

A summary of Herzberg's fine structure analysis [187] follows. Relative wavenumbers of unblended lines are assumed accurate to ± 0.04 cm^{-1}; very weak structure at longer wavelengths is accurate to ± 0.1 cm^{-1}. Rotational constants for the A state could not be determined from combination differences because so few members of the O- and S- form branches were observed. Instead, differences $B_v' - B_o''$ and $D_v' - D_o''$ obtained from Q = branch lines were used together with precise values of B_0'' and D_0'' [24]. (For the 1–0 band only fragmentary branches were observed.)

$\Delta^2 G$ values drop drastically with v'; a polynomial of a few terms is a poor fit to the ΔG's. B_v' decreases non-linearly with v'. D_v' increases even more sharply with v'; a power series is a poor fit to this data. These complications together with the revised quantum numbering for v' lead to the following tentative formulas fitted to $v' = 1$ to 4 (see footnote to table 41):

$$B_v' = 0.91053 - 0.01416(v' + \tfrac{1}{2}) - 0.00097(v' + \tfrac{1}{2})^2$$

$$D_v' = [4.79 - 0.30(v' + \tfrac{1}{2}) + 0.10(v' + \tfrac{1}{2})^2] \times 10^{-6}$$

$$G(v') = 799.08(v' + \tfrac{1}{2}) - 12.16(v' + \tfrac{1}{2})^2 - 0.550(v' + \tfrac{1}{2})^3$$

$$T_0(v') = 35007.15 + 786.51v' - 12.985v'^2 - 0.550v'^3.$$

The short wavelength limit of these rapidly converging bands made necessary a slight revision in the dissociation energy of O_2 (but see sec. 3.8 and sec. 6 on

---

[14] Additional references to observations of $A-X$ bands in the night sky are given by Chamberlain [80], Broida and Gaydon [63], and Barth and Kaplan [30]. These include uncertain identification of bands not observed in the laboratory. (See also Babcock [23].)

dissociation energy). In sec. 4 on high pressure and condensed oxygen spectra, there is briefly discussed confusion of $A-X$ bands with certain high-pressure bands.

Triplet splitting for $A\,^3\Sigma_u^+$ shows $F_3 > F_1 > F_2$; for $X\,^3\Sigma_g^-$, beyond low N, $F_2 > F_3 > F_1$. Splitting of both states is fitted roughly by the formulas of Schlapp [346]. (See also theory of Present [318].) The positive quantity $-(2\lambda + \alpha)$ increases significantly for high v' [8 to 11], indicating increasing deviation from Hund's case b likely to case c, near dissociation. γ is virtually zero for $v' = 1$ to 6 but becomes negative thereafter.

The 11–0 band was observed till $N' = 15$. A diffuse feature where $N' = 17$ lines are expected likely indicates predissociation by rotation [187].

3.8. $B\,^3\Sigma_u^- - X\,^3\Sigma_g^-$ Schumann-Runge System (5350–1750 Å) R

The $B\,^3\Sigma_u^- - X\,^3\Sigma_g^-$ transition is the most extensively studied system of molecular oxygen, with more than 100 single-headed bands identified. These bands are red-degraded and show no prominent heads (origin-head separation is only a few cm^{-1}). The dissociation energy of O_2 ($D^0 = 41260 \pm 15$ cm^{-1}), one of the most precisely known for any diatomic molecule, is derived from the convergence limit of the upper state [62]. Band origins of this very intense system, for both emission and absorption, are listed in table 12. Rotational constants for the X and B states are given in tables 36 and 42, respectively.

Schumann, in 1903, first observed 14 discrete absorption bands of this system lying below 2000 Å, though he was not able to measure wavelengths. Absorption bands were later observed by Steubing, Bloch and Bloch, Ducleaux and Jeantet, Hopfield, and Leifson; these measurements are now of historical interest only. In 1921, Runge [338] first produced $B-X$ bands in emission by using a high-voltage arc in oxygen. A summary of the more recent measurements on this system follows.

Füchtbauer and Holm [149] observed a number of band heads absorbed by heated oxygen (2000–2300 Å, dispersion ~ 3 Å/mm); their assigned v' values should be raised by two units. Only the 8–1 band, from among their observations, has not been recorded more recently. Ossenbrüggen [311] reported fine structure of a dozen bands measured from plates taken by Füchtbauer and Holm [149]; these have been remeasured more recently (table 12).

Lochte-Holtgreven and Dieke [256] classified numerous lines, including many measured by Fesefeldt [137] from plates taken by Runge [338] with a 6.5 m grating instrument in second order. The bands (4370–3100 Å), looking like a many-lined spectrum, were emitted from a high-voltage arc in oxygen, and were characterized by low v' and high v''. ($v' = 0$, 1, 2; $v'' = 11$ to 21). P and R branch lines fell close to one another, giving the appearance of doublets. For $N \geqslant 20$, the lines split into two components, with the long

wavelength component stronger. At very high N [the highest reported was 89] the stronger component split into two, producing a triplet structure. In bands with $v' = 2$, the short wavelength component was too weak to be identified with certainty. Some of Fesefeldt's measurements on two plates differed by up to 5 cm⁻¹. Line intensities quoted by Lochte-Holtgreven and Dieke were taken from Fesefeldt [137].

Pulskamp [323] photographed weak bands of the $v'' = 0$ and 1 progressions including the first measurements of the 0–0 and 3–1 band heads (dispersion 2.76 Å/mm). Vacuum wavelengths were given for these heads and some fine structure. A discharge tube continuum was used as background source.

Curry and Herzberg [99] measured bands observed in third order of a 3 m grating spectrograph (dispersion ~1.7 Å/mm; hydrogen lamp background source). Bands measured included 1–0 to 5–0, 4–1 to 7–1. The fine structure of the 1–0 and 4–1 bands was given for the first time; these bands had been observed under low resolution by Pulskamp [323]. P and R branches were separated, but no doublet or triplet separation was observed. Improved constants for the X and B states were obtained. Sharp line positions were assumed accurate to ±0.1 cm⁻¹ (poor lines to ±0.8 cm⁻¹).

Knauss and Ballard [233] photographed absorption bands in the region 1925–1760 Å produced by a 3-m vacuum spectrograph viewing a condensed discharge through a capillary. Rotational analysis was given for bands of the (v'–0) progression with $v' = 4$ to 15. Their band origins together with those of Curry and Herzberg [99] were fitted by a formula which gave a poor prediction for the 0–0 position. Their formula representing B_r values for the B state gave too small values for B_0 and B_1. Lines of the 14–0 band were broadened; in 15–0 they were doubled, with splitting much greater than that found by Lochte-Holtgreven and Dieke [256]. Very complicated structure was observed for 16–0.[15]

Millon and Herman [278] observed several band heads in an uncondensed discharge in O_2. These were identified as 0–4 to 0–11; 1–10, 1–11. Feast [133] questioned some of the vibrational assignments. (See the discussion of Feast below.)

Lal [246], using a high-frequency discharge, produced more than two dozen bands in the region 4490–2450 Å which were attributed to the B–X transition. Details concerning these bands were never published. The many-line structure of these nearly headless bands makes identification difficult. Lal's vibrational assignments were questioned by Feast [132, 133] because of the irregular Deslandres array. Feast [132] observed bands in the same region and indicated that "the heads are so weak . . . that analysis has been made by identi-

fication of the rotational structure of each band and 'heads' that seem present with small dispersion are found, with higher dispersion to be merely due to chance overlapping of structure from several bands." Lal's bands are listed in table 30 as uncertain excluding five which appear to coincide with previous measurements.

Feast [134] has given rotational analysis for bands in the region 3100–2500 Å emitted from a high-voltage arc in oxygen. The observed bands include 1–12, 0–11, 1–11, 0–10, 1–10, 1–9, 2–9, 1–8, 2–8, 2–7. "There are too many blended lines in the region 2–10 and 0–9 to allow detailed analysis." Spin triplets were not resolved: each band showed only P and R branches. Measurements were assumed accurate to 0.2 cm⁻¹.

Garton and Feast [152] gave a preliminary report on absorption from heated oxygen and assigned vibrational quantum numbers for bands below 2500 Å. Higher J values than the data of Ossenbrüggen [311] were observed. Line positions and band origins were given in an unpublished manuscript by Feast and Garton [136]. Origins are given [152] for bands 2–10, 0–9, 3–8, 3–7, 2–6, 3–6, 4–6, 2–5, 5–6, 3–5, 4–5, 5–5, 7–5, 6–5, 5–4, 6–4, and also fine structure of yet other bands (emission and absorption) whose origins and rotational constants had been published previously.

Herczog and Wieland [181] have extended to longer wavelength the absorption studies of the B–X bands. They measured fine structure of the 1–8, 2–8, 1–7, and 2–7 bands (80 atm, 1070 °C; cell length = 20 cm).

Feast and Garton [136] have given a detailed line list of B–X bands which they observed (3100–2125 Å) in both absorption at 1900 °C and emission from a high-voltage arc. These include 0–12, 0–11, 1–11, 1–12, 1–10, 0–10, 1–9, 2–9, 1–8, 2–8, 2–7; bands not reported previously include 2–10, 0–9, 3–8, 3–7, 2–6, 3–6, 4–6, 5–6, 2–5, 3–5, and 4–5; remeasurement of bands previously observed by Ossenbrüggen [311] include 5–5, 6–5, 7–5, 5–4, and 6–4. These bands extended to high J (~59 max). (Unidentified lines, generally weak are included in the list.) Dispersion was 42 cm⁻¹/mm at 2475 Å and 36 cm⁻¹/mm at 2200 Å. Measurements were assumed accurate to 0.2 cm⁻¹ (0.01 to 0.02 Å) for sharp lines. Some lines of the band identified as 1–7 by Herczog and Wieland [181] were included here as belonging to the 3–8 band.

Durie [123] observed emission of more than 30 band heads in a water/fluorine flame (4600–2400 Å). The several new bands were subsequently reported by Rakotoarijimy, Weniger, and Grenat [324]. Durie's band heads were sharp because the low effective rotational temperature resulted in less overlap of rotational structure than is usually encountered.

Brix and Herzberg [62] have made the most precise measurements of the B–X Schumann-Runge bands with high v', and from their convergence limit, have determined a seemingly definitive value for the dissociation energy of O_2 (but see the limitation mentioned in sect. 7). The strongly red-degraded bands were photo-

---

[15] Hudson and Carter [199a] have suggested that the measurements of Knauss and Ballard [233] be increased by 0.07 Å to adjust an apparent systematic shift relative to the measurements of Curry and Herzberg [99] and more recent work of Brix and Herzberg [62]. Recent measurements by Ackerman and Biaume [3] who used the same instrument as Brix and Herzberg have verified this discrepancy in line positions.

aplied in fourth order of a 3-m vacuum spectrograph
dispersion 0.65 to 0.4 Å/mm; resolution 160,000,
xygen pressure 3 to 350 mm). A Lyman discharge
the was background source for the 50 cm long absorp-
ion tube. The region studied in detail was 1804 Å (11–0)
o 1750 Å, the limit of discrete absorption. v'–0 bands
were observed for $v'=12$ to 21. The last bound level,
$'=22$, was extrapolated. All measurements, were
made against second order iron lines as standard
wavelengths. Relative wavenumbers of unblended lines
are accurate to ± 0.05 cm^{-1}; absolute error was
± 0.2 cm^{-1}. Fine structure, band origins, and, for the B
state, vibrational quanta and rotational constants were
given.

Electric dipole selection rules allow twelve possible
branches: $P_{1,2,3}$, $R_{1,2,3}$, $^PQ_{23}$, $^PR_{13}$, $^RQ_{21}$, $^RQ_{32}$, $^RP_{31}$.
The six main branches with $\Delta J=\pm 1$ were identified
(for low N); also, some lines of the six satellite branches
($\Delta N=\pm 1$, $\Delta J=0,\pm 1$) as well as two electric dipole
forbidden branches $^TR_{31}$ and $^NP_{13}$ ($\Delta N=\pm 3$, $\Delta J=\pm 1$)
were identified. This was the first case known where
forbidden branches with $\Delta N>1$ have been observed
for an allowed ($\Sigma-\Sigma$) transition.

Near the convergence limit, the triplet splitting
was the same order of magnitude as the rotational
structure. The triplet splitting was discussed by Brix
and Herzberg [62] in terms of Schlapp's formulas [346]
and deviations therefrom. [Since then, more extensive
theory of splitting for the ground state has been given by
Tinkham and Strandberg [375] and others; see sec. 8
on microwave spectrum.] Previously, triplet splitting
had been observed only by Lochte-Holtgreven and
Dieke [256] and Knauss and Ballard [233].

For $v'\geq 16$, perturbations in structure occur accom-
panied by the appearance of extra lines and intensity
irregularities. Term values for the F_2 components of
the $B\,^3\Sigma_u^-$ state showed slight deviation from Schlapp's
formulas [346] $T_2-\sigma_0=F_2(N)=B_vN(N+1)-D_vN^2$
$(N+1)^2$. Short branches and large perturbations
limited the use of combination differences.

There remained approximately 100 weak unclassi-
fied lines just to long wavelength of the dissociation
continuum. Perturbations prevented assignment of
these lines. The perturbations indicate the presence of
another stable state dissociationing to $^3P_2+{}^1D_2$.

Bands having $v'\geq 16$ lie higher than the previously
accepted dissociation limit. $\sigma_0(22-0)$ is predicted to
lie at 57127 cm^{-1} (F_2). Some lines of 22–0 were detected,
but the quantum assignments are uncertain. A short
extrapolation beyond the origin of the 21–0 band gave
a convergence limit 57128±5 cm^{-1} which was in close
agreement with one derived from the $A\,^3\Sigma_u^--X\,^3\Sigma_g^-$
bands, provided that pairs of dissociation products
included the $^3P_2$ state. This led to $D^0(O_2)=41260\pm 15$
cm^{-1} (5.1156±0.002 eV). The magnitude of the uncer-
tainty reflects the difference between the B and A dis-
sociation limits, 15,868.6 cm^{-1}, which represents $^1D-$

$^3P_2$. This agrees with the values given by Moore [281]
to within about a cm^{-1}.

Rakotoarijimy, Weniger, and Grenat [324] have
extended observations in the UV, both in absorption
and emission, by using a high-frequency discharge in
an atmosphere of oxygen. Eight new bands were
identified in absorption (2270–1980 Å) and 28 new bands
in emission (3800–2100 Å). (Dispersion 4 Å/mm in emis-
sion; 2 Å/mm in absorption.) Details were not given,
only a Deslandres table of band origin wavelengths.

Herman, Herman, and Rakotoarijimy [183], using a
similar emission source, observed numerous bands,
and reported fine structure, rotational constants for
both states, and band origin wavelengths. Fine structure
was given for 1–21, 2–21, 2–22, 2–23, 2–24, 2–25,
3–22, 3–23, and 3–24. Origins were also given for 0–20,
3–25, 5–27, but no fine structure.

Bass and Garvin [31] have reported several absorption
heads produced following flash photolysis of NO_2.

Fitzsimmons and Bair [142] observed heads of 30
absorption bands with high v''. These high energy
states were produced in secondary processes following
photolysis of ozone. Of these bands, all but five had
previously been seen in emission; the other five had not
been observed before.

Ogawa [302], using a quartz spectrograph, photo-
graphed the absorption spectrum excited by an ac
silent discharge (dispersion 1.46 Å/mm at 2100 Å).
Seventeen bands of the $B-X$ system were identified,
several new. Rotational constants for both upper and
lower states were obtained, including several for low
v'' for which there had been no previous determination.
The primary aim was the observation of the $B-X$
system from excited vibrational levels of the ground state
and the clarification of discrepancies in rotational
constants for the B state. The observed region was
2250–1970 Å, with numerous overlapping lines in this
many-line spectrum. Resolving power was too low for
observation of electron spin splitting. Using previous
data as well as his own, Ogawa observed that the
B_v versus v plot for $B\,^3\Sigma_u^-$ showed positive curvature
for $v=0$ to 15, and was virtually straight for $v=16$ to 21.
A formula fitted to the first group of levels was given

$$B_v=0.8184-0.01238(v+\tfrac{1}{2})-3.3\times 10^{-2}(v+\tfrac{1}{2})^2$$

$$-5.7\times 10^{-6}(v+\tfrac{1}{2})^3-1.3\times 10^{-6}(v+\tfrac{1}{2})^4.$$

Ogawa and Chang [306], using a 3 m-vacuum spectro-
graph (linear reciprocal dispersion, 2.85 Å/mm), photo-
graphed 34 absorption bands in the region 2000–1770 Å.
The observed bands, half of them new, include members
of progressions with $v''=0, 1, 2, 3$. A detailed line list
is given, together with a table of band origins. For the
(v'–0) progression, the band origins differed by an
average 0.3 cm^{-1} from adjusted values of Knauss and
Ballard [233] (see footnote 15).

More than 1000 new lines belonging to absorption

bands in $v''= 1, 2$ progressions have been measured by Hudson and Carter [199a] in the region 2020–1750 Å. Their published line list spans the region 1895–1877 Å (relative accuracy ± 0.02 Å). (See also sec. 11.6.)

Ackerman and Biaume [3] have remeasured under high resolution bands 0–0 through 13–0. They used the same instrument as did Brix and Herzberg [62]. The measurements of Curry and Herzberg [99] and Brix and Herzberg [62], where they overlap Ackerman's, are in close agreement, but small differences in both sets of data are found for B_v and D_v for $v' = 12$, 13. (See table 42 footnote.)

The O_2, B–X, 0–0 transition energy and the zero point energy of the $B \, ^3\Sigma_u^-$ state have been debated (needlessly) for more than 30 years because of a misreading of the early literature. (Compare, for example refs. [162] and [175].) Improved values of both quantities have been obtained from measurements of Ackerman and Biaume [3].

3.9. Miscellaneous Absorption Transitions 1585–1140 A. Alberti, Ashby, Douglas Bands Including $\alpha \, ^1\Sigma_u^+ \leftarrow b \, ^1\Sigma_g^+$, $\alpha \, ^1\Sigma_u^+ \leftarrow X \, ^3\Sigma_g^-$ (Tanaka Progression II), $\beta \, ^3\Sigma_u^+ \leftarrow X \, ^3\Sigma_g^-$ (Tanaka Progression I), $^1\Delta_u \leftarrow a \, ^1\Delta_g$, $^1\Pi_u \leftarrow a \, ^1\Delta_g$. Ogawa-Yamawaki transition $^3\Sigma_u^+ \leftarrow X \, ^3\Sigma_g^-$.

In 1952, Tanaka [369] observed numerous absorption band heads in the region 1350–1030 Å, most of which remained unclassified (table 30d). (See also table 13h.) Alberti et al. [7] have recently measured fine structure of absorption bands in the region 1585–1195 Å. The observed bands include some involving new electronic states of O_2, as well as several bands of Tanaka's progressions I and II, now labeled β–X and α–X, respectively. (See tables 13a and 14, respectively.)

The spectra were produced by Alberti et al. in an 80-cm absorption tube by a high frequency and a pulsed discharge, and were photographed at very high dispersion (0.35–0.15 Å/mm). The sixteen bands observed included absorption from X, a, and b states; some bands were weak, but all were largely overlapped by strong oxygen continua which made observation extremely difficult. The data were fragmentary; identification of upper states and vibrational numbering was tentative.

Both α and β states, tentatively assigned as $^1\Sigma_u^+$ by Alberti et al. have B_v and ΔG values similar to those of the ground state of O_2^+, and are assumed to be members of Rydberg series. The upper states of bands originating from the $a \, ^1\Delta_g$ and $b \, ^1\Sigma_g^+$ states are possibly Rydberg states, whose series limits are an unknown state of O_2^+.

Ogawa and Yamawaki [308] have photographed forbidden absorption bands of O_2 in the region 1262–1144 Å (dispersion, 1.42 Å/mm). They remeasured the fine structure of both α–X and β–X transitions reported by Alberti et al. [7] but observed in addition, a new band at 1144.6 Å. All bands observed were double-headed, had three branches, and were violet-degraded.

Rotational perturbations were found for α, $v = 4$, $N = 7$, 9, 11 (with perturbed $B_v < 1.59$). The 1144.6 Å band, whose upper state was designated $^3\Sigma_u^+$, has a similar appearance to α–X and β–X; it is a member of a Rydberg series converging to O_2^+, $X \, ^2\Pi_g$.

Ogawa and Yamawaki [308], partly on the basis of quantum defect arguments, suggest that the β state is likely $^3\Sigma_u^+$. Tentative electron configuration of the upper states they observed are:

$$(\pi_g 2p)(3p\pi_u)\beta \, ^3\Sigma_u^+, \qquad (\delta = 0.653)$$

$$(\pi_g 2p)(3p\pi_u)\alpha \, ^1\Sigma_u^+ \qquad (\delta = 0.716)$$

$$(\pi_g 2p)(4p\pi_u) \, ^3\Sigma_u^+ \qquad (\delta = 0.675)$$

From the relative intensities in the β–X bands [308], it was concluded, that the 1292 Å band observed by Tanaka [369] is likely the 1–0 band of the β–X transition; the isotope shift observed by Tanaka (as yet unpublished) agrees with this assignment (see footnote 5, p. 1811 of ref. [308]). The β–X, 0–0 band is estimated to lie at 75,450 cm^{-1} (1325.4 Å) [308] which places it ~ 810 cm^{-1} lower than α–X, 0–0.

Though the ΔG values are irregular, Ogawa and Yamawaki roughly estimate vibrational constants:

$$\beta: \omega_e \sim 1957, \omega_e x_e \sim 19.0$$

$$\alpha: \omega_e \sim 1957, \omega_e x_e \sim 19.7.$$

Tables 13 to 18 contain successively the band positions for transitions β–X, α–X, α–b, $^3\Sigma_u^+$–X, $^1\Delta_u$–a $^1\Delta_g$, and $^1\Pi_u$–a $^1\Delta_g$. Unclassified bands are included in table 30. Rotational constants for the $\alpha \, ^1\Sigma_u^+$, $^1\Delta_u$, $^1\Pi_u$, $\beta \, ^3\Sigma_u^+$, and new $^3\Sigma_u^+$ states are given successively in tables 43 to 47.

3.10. Rydberg Series

Well established Rydberg series are known whose convergence limits are the $b \, ^4\Sigma_g^-$, $B \, ^2\Sigma_g^-$, and $c \, ^4\Sigma_u^-$ states of O_2^+. Unclassified progressions of bands exist below 1300 Å (see table 30) which likely include members of unidentified Rydberg series. Reported series with limits $a \, ^4\Pi_{ui}$ and $A \, ^2\Pi_u$ are uncertain. A vibrational progression, possibly belonging to the first term of a series converging to the ground state of O_2^+, has also been observed (table 13b). Nearly all measurements of Rydberg series in O_2 have been made with either 3-m or 6-m grazing incidence vacuum spectrographs, mainly with the use of the helium continuum as background source.

Many terms of Rydberg series have been identified in the absorption coefficient studies by Cook and Metzger [95] and Huffman et al. [204]; numerous absorption maxima in the continua (1060–580 Å) remain unclassified.

Price and Collins [320] have assigned two pairs of progressions (H, I and H', I') to separate Rydberg series converging to O_2^+, $a\,^4\Pi_u$. The two calculated limits differed by 1100 cm^{-1}; their mean was assumed to correspond to the second I.P. of O_2. It is not certain that these progressions are members of the specified Rydberg series because of their fragmentary nature and the poor agreement between the two limits. Additional progressions labeled M, N, N' provided a poor value for the energy of the $A\,^2\Pi_u$ state of O_2^+. These bands appeared as doublets, which likely were (absorption) peaks of P and R branches. Bands not reclassified in more recent work are listed as unclassified (table 30a). Possibly some of these bands defy unambiguous assignment because the early terms of Rydberg series often deviate from a Rydberg formula with roughly constant δ and because higher terms may be perturbed [253].

a. $X\,^2\Pi_g(O_2^+) \leftarrow X\,^3\Sigma_g^-(O_2)(1290-1180\ \text{Å})V$

The first I.P. of O_2 is known most precisely from photoionization measurements [342]. There are no confirmed Rydberg series converging to the ground state of O_2^+, though Tanaka [369] has tentatively identified a five-member vibrational progression of doublets in absorption (table 30c) as belonging to the first electronic term of such a series, in part, because of the similarity in vibrational constants to that of the O_2^+ ground state. The weak, violet shaded progression of doublets (separation ~ 45 cm^{-1}), showed some rotational structure. Intensity of the fourth member of this progression seemed abnormally strong and diffuse. Thus Tanaka expected a perturbation of level $v=4$ of the upper state of this Rydberg transition (its position is more than 100 cm^{-1} higher than that calculated from a formula fitted to the presumed Q heads of the other terms).

Matsunaga and Watanabe [259], studying absorption coefficients with a line source, have also tentatively fitted a series of terms (1125–1040 Å) to a Rydberg formula converging to ~ 12.1 eV. The reality of this series has not been confirmed by use of a continuum source [259]. (See also sec. 3.9 for a discussion of the band at 1144.6 Å.)

b. $b\,^4\Sigma_g^-(O_2^+) \leftarrow X\,^3\Sigma_g^-(O_2)(730-660\ \text{Å})R$

Price and Collins [320] first observed several progressions attributed to a Rydberg series converging to O_2^+, $b\,^4\Sigma_g^-$. Tanaka and Takamine [371] unscrambled some of this structure, reassigned the bands, and provided a reliable term value for O_2^+, $b\,^4\Sigma_g^-$. Namioka et al. [290] and Yoshino and Tanaka [417] have considerably extended the number of terms, including series with $v'=0$ to 4 (table 19). The bands are single headed, sharp (therefore, showing a small effect of autoionization), and red-degraded. According to Namioka [290] the likely configuration for this series is $(3\sigma_g)$ $(1\pi_u)^4(1\pi_g)^2\ np\sigma_u\,^3\Sigma_u^-$, $n=5,\ \ldots$

The band heads are fitted by

$$\sigma = 146568 - \frac{R}{(n-1.679)^2}.$$

Additional weak, diffuse, and slightly red-degraded series with $v'=0,1,2$ converge to the same limit [290, 417] (table 20); these have possible configuration $(3\sigma_g)$ $(1\pi_u)^4(1\pi_g)^2\ np\pi_u\,^3\Pi_u$, $n=4,\ \ldots$ The series limit from measured band heads is 146568 ± 2 cm^{-1}. By using an approximate correction for the origin-head separation, the origin of $b\,^4\Sigma_g^-$, $v=0$ is placed at 146556 cm^{-1}.

c. $B\,^2\Sigma_g^-(O_2^+) \leftarrow X\,^3\Sigma_g^-(O_2)$ (650–600 Å)R

Tanaka and Takamine [371] first observed members of a Rydberg series whose limit was a new state of O_2^+ at ~ 20.3 eV. Ogawa [303] and Yoshino and Tanaka [417] considerably extended this to include members with $v'=0$ to 3 (table 21). In addition to this strong series, a weak, diffuse series with the same limit was found by Yoshino and Tanaka [417] (table 22). Both strong and weak series are single headed and red degraded. Gilmore [161] assigned the new state as $^2\Sigma_g^-$; Turner and May [384] observed structure for this state in photoelectron spectroscopy, but labeled it $^4\Sigma_u^-$.

The strong series can be represented by

$$\sigma = 163702(\pm 7) - \frac{R}{(n-0.658)^2},\ n=4,\ \ldots$$

Yoshino and Tanaka [417] found an additional weak series which is unclassified (table 30e). The Rydberg states are likely

$$n p\sigma_u\,^3\Sigma_u^- \leftarrow \sigma_g 2p$$

or

$$n p\pi_u\,^3\Pi_u \leftarrow \sigma_g 2p.$$

Ogawa [303] assumed that excitation to $p\sigma$ would lead to unstable or weakly bound states and concluded that $np\pi_u\,^3\Pi_u$ was the more likely classification. The vibrational constants for the B state are $\omega_e \sim 1156$ cm^{-1}, $\omega_e x_e \sim 22$ cm^{-1} [303, 417]. A Birge-Sponer extrapolation yields $D^0 \sim 14{,}613$ cm^{-1} $[O^+(^2D^0)+O\,(^3P)]$.

d. $c\,^4\Sigma_u^-(O_2^+) \leftarrow X\,^3\Sigma_g^-(O_2)$ (595–510 Å)

LeBlanc [250b] showed that bands originally observed by Hopfield [195] and thought to belong to O_2 were really due to O_2^+, $c\,^4\Sigma_u^- \rightarrow b\,^4\Sigma_g^-$. The bands located the $v=0$ level of the upper state. Codling and Madden [89a] have observed several Rydberg series whose limits are O_2^+, $c\,^4\Sigma_u^-$, $v=0,1$, confirming the tentative vibrational numbering given by LeBlanc [250b]. The series beginning at 542.3 Å (table 23) can be reproduced by

$$\sigma = 198125(\pm 30) - \frac{R}{(n-0.159)^2},\ n=3,\ \ldots$$

The Rydberg states are likely $nd\pi_g$ (excited from $2\sigma_u$) $^3\Pi_u$ or possibly $nd\sigma_g\ ^3\Sigma_u^-$ [253]. The next series beginning at 594.3 Å is fitted by

$$\sigma = 198125 - \frac{R}{(n-0.955)^2}, n=3, \ldots$$

is likely $ns\sigma_g\ ^3\Sigma_u^-$. These tentative designations of the Rydberg states are just the reverse of that published [89b]. A weak series converging to about the same limit ($\delta \sim 0.03$) is possibly $nd\sigma, n=3, \ldots, 7$. The structure of the weak series is uncertain (table 30f).

The absorption spectra were produced using electron synchrotron radiation as a background source. The bands are broadened by autoionization. The c state has $\Delta G(\frac{1}{2}) = 1540(\pm 30)$ cm^{-1}. A $^2\Sigma$ state about 1–2 eV higher than $c\ ^4\Sigma_u^-$ is expected due to removal of a $\sigma_u 2s$ electron, but no series was found converging to such limit.

Lindholm [253, 185] has tentatively identified a number of new Rydberg transitions and reinterpreted others. (For example, consider the identification of the β state.) Some of his identifications are likely speculative because of the use of oversimplified theory of Rydberg transitions. It should be recalled that the electron configurations assigned to the various Rydberg series are tentative; varying interpretations abound because no series has been studied under high resolution.

3.11. $A\ ^2\Pi_u \to X\ ^2\Pi_g$ Second Negative System of O_2^+ (6530–1940 Å)R

The $A-X$ system of red-degraded, double-headed bands of O_2^+ has been extensively studied under low resolution. Nearly 120 vibrational transitions have been observed, but rotational analyses have been published for only eleven bands. Band origins are listed in table 24; observed band heads are listed in table 25. Rotational constants for the X and A states are given in table 48 and 50, respectively.

Recent isotopic work by Bhale and Rao [42] has established unequivocal vibrational numbering for the ground state of O_2^+, which is one unit larger than that commonly in use for 40 years (see the end of this section).

In 1914, Stark measured the positions of diffuse emission bands which he considered due to ozone (5000–2280 Å). Johnson [221] produced a number of these bands (4400–2300 Å) in an oxygen discharge, and determined that they were not due to ozone. The spectra were taken on a quartz prism spectrograph (dispersion 6 Å/mm at 2300 Å; 16 Å/mm at 3000 Å). Johnson grouped the heads in pairs (separation, 200 cm^{-1}) and arranged them in a Deslandres table. Birge (1925)[16] assigned vibrational quantum numbers to these band heads.

Ellsworth and Hopfield [127] produced additional bands in a high-voltage discharge, extending Johnson's observations down to 2180 Å. Both a 1-m concave air grating spectrograph and a $\frac{1}{2}$-m vacuum grating spectrograph were used. Bands in the region 2180–1970 Å, too weak to be measured, were thought to include progressions which would require a change in v'' numbering.

The first fine structure analysis by Stevens [365] confirmed O_2^+ as the source of these bands. The 1–7, 0–7, 1–8, and 0–8 bands were photographed in second order of a 21-ft. Rowland grating (dispersion, 1.32 Å/mm). The bands were emitted from a hollow cathode discharge, and with greater intensity from a helium discharge containing a small amount of oxygen. In an abstract of this work, Stevens used Birge's v'' numbering; in the detailed publication, he listed v'' values two units larger, based on conclusions drawn by Mulliken and by Stueckelberg, which were later shown to be incorrect. Birge's v'' numbering was used by Mulliken [284] in his massive review.

Λ-doubling was measurable only for the $F_1(^2\Pi_{1/2})$ level of the X state of O_2^+. Eight branches were observed for the A–X transition: R_1, P_1, R_2, P_2; $^SR_{21}$, $^QP_{21}$, $^QR_{12}$, and $^QP_{12}$. Q branches were too weak to be observed, since, for case b, Σ ceases being a good quantum number. ($A\ ^2\Pi_u$ is in Hund's coupling case b; $X\ ^2\Pi_g$ is in Hund's coupling case a; see footnotes to table 1). Many lines were blended. No band origins were tabulated, though line lists were given.

Some doubts had been raised by Ellsworth and Hopfield [127] and Stevens [365] about the correct v'' numbering. This was thought to be dispelled by Mulliken and Stevens [287] who observed emission from a high-frequency discharge down to 2060 Å. The region below 2180 Å included only members of the [then labeled] $(v'-0)$ progression. The recent isotopic work of Bhale and Rao [42] showed that these really belonged to the $(v'-1)$ progression.

Bozóky [52] observed bands under low resolution (quartz spectrograph, dispersion 2.5–3 Å/mm) and high resolution (6.5 m-radius concave grating spectrograph, dispersion 1.2 Å/mm). His fine structure analysis of emission from a high-frequency discharge was later extended [53], but only in the earlier paper did he list observed B_v values. Bozóky [52, 53] has given the fine structure analysis of seven bands in the region 4360–2380 Å: 0–10, 0–9, 1–6, 5–3, 6–3, 7–2, 8–2. No band origins were tabulated. Formulas for rotational constants are [53, 42]

$$A\ ^2\Pi_u: B_v = 1.0632 - 0.0206\ (v+\tfrac{1}{2})$$

$$X\ ^2\Pi_g: B_v = 1.6892 - 0.0195\ (v+\tfrac{1}{2}).$$

These have been obtained, together with the band origins, from a least squares fit to the original data by A. Lofthus (at the request of the author).

---

[16] The vibrational constants were listed by Birge in a report of the National Research Council (1926) and in the International Critical Tables (1929), and are quoted by Feast [135]. An incorrect formula is given by Ellsworth and Hopfield [127].

On a small prism spectrograph, Lal [247] photo-graphed bands emitted from a high-frequency discharge in oxygen. He mentioned numerous additional doublet bands which seemed to lie along a narrow Condon locus, but published no numerical data for these.

Feast [135], viewing an electrodeless discharge in pure oxygen, observed bands along subsidiary Condon loci which likely included some of those mentioned by Lal [247]. Feast undertook this study to reexamine O_3 emission in the region 7000–2000 Å. He found that some bands attributed by Johnson [221] to O_3 appeared to be O_2^+ or O II, and he detected no bands of O_3 in his source. (Feast used a medium quartz spectrograph; source pressure was 0.05 mm Hg. Band heads were assumed correct to ± 0.5 Å.)

Byrne [71] observed emission from a high-frequency discharge through pure oxygen, by using both a 3-m vacuum spectrograph (dispersion, 2.5 Å/mm) below 2800 Å, and a prism spectrograph (7000–2800 Å). He extended the $A–X$ system (6530–1940 Å), including $(v'–1)$ bands for v' through 23. The many-line structure at shorter wavelengths prevented positive identification of additional bands. Linton [255] observed several additional bands in a liquid-oxygen cooled discharged in oxygen and reassigned quantum numbers of others.

A study of the isotope shift in the R_1 band heads (using ^{18}O) [20, 42] has led Bhale and Rao to raise previously used v'' values by unity. Bands of the $v''=0$ progression were observed for the first time. The $A–X$ system was excited by a microwave discharge in oxygen at 0.1 mm pressure. Spectra were photographed on a 3.4 m-vacuum grating spectrograph; dispersion was 5.5 Å/mm. Vibrational constants for both states were refitted to their measurement of about 40 bands. The constants quoted in table 1 are based on a fit to the band origins; these values are compared with a fit to more than 100 bands observed by many authors (see Appendix D). The new vibrational quantum number-ing has readjusted the values of the positions of the X and A states of O_2^+. Measurements are being con-sidered [42] to obtain D^0 $(A\ ^2\Pi_u)$ directly from observa-tion of the $A–X$ system limit.

3.12. $b\ ^4\Sigma_g^- \rightarrow a\ ^4\Pi_{ui}$ First Negative System of O_2^+ (8530–4990 Å)V

The violet-degraded $b–a$ band system of O_2^+ was first observed by Schuster and by Wüllner (1877–8) near the negative pole of a discharge tube filled with oxygen. Additional low resolution observations were made by Steubing (1910). The first partial fine structure resolution was by Frerichs (1926), who divided the observed lines into two branches per band, using Hol-land's published measurements of spectra from hollow cathode emission taken by Cario. A band observed at 5900 Å by Steubing (and shown later to be the 2–2 band) was not detected by Frerichs because of overlapping rotational structure produced in the hollow cathode.

Additional band heads have been observed in high frequency discharges (low rotational temperature sources) by Mulliken and Stevens [287], Bozóky and Schmid [54], and Singh and Lal [354]. The most promi-nent heads are listed in table 27; the origins are in table 26. Rotational constants for the a and b states are given in tables 49 and 51, respectively.

Mulliken [284] assigned these bands as $^4\Sigma_g^- - ^4\Pi_u$ from the probable electronic configuration of O_2^+, and assumed the vibrational numbering of Mulliken and Stevens [287]. Fine structure analysis of this system by Nevin [291] confirmed Mulliken's assignment.

Nevin [291] used both a discharge through helium containing a small amount of oxygen (total pressure 3–4 mm; oxygen pressure ~ 0.1 mm) and a hollow cathode to produce the six bands he studied. The spectra were photographed in second order of a 21-ft grating spectro-graph (dispersion ~ 1.25 Å/mm; resolving power $\sim 180,000$). The prominent band head is formed by the $^0Q_{24}$ branch (≈ 78 cm^{-1} from the origin). Wavelength calibrations were derived from neon in the discharge and an iron arc. Absolute wavelengths were assumed correct to 0.01 Å; relative accuracy was assumed much better [291a]. Wavenumbers [17] were given to three digits beyond the decimal; use of current conversion tables would change these values in the last digit. For the 0–3 band shifts of ± 0.08 cm^{-1} between plates were not eliminated. Absolute values of wavenumbers were averaged from measurements of three plates [291c]. Lines possibly belonging to the 1–4 band were observed but not analyzed. Faint lines of unknown origin were observed near the $^0Q_{24}$ head.

The $^4\Sigma$ rotational energies have been accounted for by the theory of Budó [64].[18] The experimental fine struc-ture parameters are $\epsilon = 0.1847$ cm^{-1} and $\gamma = 0.00033$ cm^{-1} [291a]. Separations $\Delta F_{21}(J)$ and $\Delta F_{43}(J)$ for the inverted $^4\Pi$ states,[18] calculated from modified formulas originally obtained by Brandt [56], are not in complete agreement with those derived from experiment [291a]. Nevin [291a] considered this deviation due to a probable perturbation of the $^4\Pi$ state by $^4\Sigma_u^-$, $^4\Pi_u$, or $^4\Delta_u$ derived from O^+ (^2D_u) + O (^3P_g). The interval $F_4''(J)–F_1''(J)$ is about three times that of $F_3''(J)–F_2''(J)$. The perturba-tion displaces the F_4 level away from F_3, and F_2 toward F_1. No detailed study of this perturbation has been made.

Λ-doubling is very small in $^4\Pi_{5/2}$ and $^4\Pi_{3/2}$; it increases linearly with J in $^4\Pi_{1/2}$. In $^4\Pi_{-1/2}$ it increases at first, and then decreases for highest J. Λ-doubling for $^4\Pi_{1/2}$ and $^4\Pi_{-1/2}$ [65] increases systematically with v. Formulas have been derived by Budó and Kovács [65] for the Λ-doubling in a $^4\Pi$ state, intermediate in coupling between Hund's

---

[17] Unpublished wavenumbers and estimated intensities of the observed lines for the 2–0 and 0–2 bands have been deposited in the archives of the Royal Society [291b].

[18] $b\ ^4\Sigma_g^-: F_1(N+3/2), F_2(N+1/2), F_3(N-1/2), F_4(N-3/2)$

     $a\ ^4\Pi_{ui}: F_1(^4\Pi_{5/2}), F_2(^4\Pi_{3/2}), F_3(^4\Pi_{1/2}), F_4(^4\Pi_{-1/2})$

in order of increasing energy. The subscript is the value of $\Lambda + \Sigma$. $\Omega = |\Lambda + \Sigma|; J = \Omega, \Omega + 1, \ldots$.

case a and v. Comparison with Nevin's data seems adequate.

A case (a) $^4\Pi$ state gives rise to 48 branches for a $^4\Sigma_g^- - ^4\Pi_u$ transition (case (b) gives 27 branches). Since level $F_1'(N)$ is blended with $F_4'(N)$, and level $F_2'(N)$ is blended with $F_3'(N)$, the branches involving them are blended, and the number of possible branches is reduced to 40; all have been observed. The intensity distribution in these branches is in agreement with Budó's theory [64], assuming the $a\,^4\Pi_u$ state is intermediate in coupling between Hund's cases (a) and (b).

Dufay et al. [122] have produced several new emission bands (8347–6750 Å) by high-energy proton bombardment of oxygen.

Recently, Weniger [408] extended measurements of this system into the photographic infrared region. He observed emission of a dc discharge by using dispersion of 3 Å/mm (assumed precision of about ±0.07 cm^{-1} is not confirmed in the reexamination by Albritton et al. [9]). Observed bands include 0–3, 4, 5, and 1–4, 5, 6: detailed line lists were published only for 0–3 and 1–4. For the 0–3 band head, Weniger listed the Q_4 head rather than the most prominent $^0Q_{24}$ head. Λ-doubling is small (~ 0.10 cm^{-1}) for all components of $a\,^4\Pi$ except $^4\Pi_{-1/2}$, where it is several times larger. Weniger pointed out that the coupling constant A is negative, and has been misprinted by both Herzberg [186] and Rosen [337]. Kovács and Weniger [238] have used all previous measurements of Nevin and Weniger to obtain values of A for all $v \leqslant 6$ (see footnote under $a\,^4\Pi_{ui}$ in table 1 and also sec. 5).

3.13. $c\,^4\Sigma_u^- \rightarrow b\,^4\Sigma_g^-$ Hopfield System of O_2^+ (2360–1940 Å) V

In 1930, Hopfield [195] produced five single-headed, red-degraded bands in a condensed discharge in a He $+O_2$ mixture (2220–2130 Å). He assumed the progression belonged to a new system of O_2. Herzberg [186, p. 559] suggested that the lower state of this new system might be the H state, tentatively assigned as $^3\Pi$ by Price and Collins [320]. Tanaka, Jursa, and LeBlanc [370] extended Hopfield's observations (2360–1940 Å). By using a total pressure of 20 mm and O_2 pressure of 1 mm in the discharge they suppressed the stronger $A-X$, O_2^+ system which spanned the same spectral region. The appearance of the fine structure suggested a $\Sigma-\Sigma$ transition. Tentative vibrational constants were obtained by assuming the 1940.3 Å band was 0–0. Similar ΔG values for progression II of Tanaka and Takamine [371] suggested that the upper state of progression II was possibly the lower state of the Hopfield system [370].

LeBlanc [250] resolved the P and R branch fine structure for the 0–4, 0–5, and 0–6 bands; other bands had other spectra superimposed (dispersion ~ 1.5 Å/mm at 2100 Å). From the close agreement between the vibrational constants for this progression and values

obtained from fine structure on another system by Nevin [291a], the lower state was identified as $b\,^4\Sigma_g^-$ O_2^+. Assuming an allowed transition, LeBlanc assigned the upper state of the Hopfield bands as $c\,^4\Sigma_u^-$. It was then understood that the slight diffuseness of the observed lines arose from the superposition of four lines in the quartet transition.

The energy of the c state (T_0) is then [417, 370] 198098 cm^{-1} = 24.561 eV above O_2, $X\,^3\Sigma_g^-$, $v=0$. Codling and Madden [89] have recently observed new Rydberg series converging to both $v=0$ and 1 levels of the $c\,^4\Sigma_u^-$ state. For the c state $\Delta G(\tfrac{1}{2}) \approx 1540$ cm^{-1}, close to that of the ground state of O_2. The $v=0$, 1 series limits are 198125 ± 30 cm^{-1} and 199665 ± 30 cm^{-1}, respectively. These agree with the prior data to within experimental error [89].

The $c-b$ band origins and heads are given in tables 28 and 29, respectively. Rotational constants for the b and c states are listed in tables 51 and 52, respectively.

3.14. Unclassified Bands

Other sections mention bands which are unclassified or whose classification is in doubt; such bands are assembled in table 30. Bands in the same category, but not tabulated in this report, are briefly discussed below.

In an oxygen afterglow, Broida and Gaydon [63] produced a number of weak, single-headed, red-degraded bands (4835–3655 Å). Several bands did not correlate with known transitions; others could tentatively be assigned to transitions $A-X$, $c-X$, or to an otherwise unobserved transition, $A-b$. Band head positions are uncertain by several Angstroms. Unambiguous assignments to the transition $A-b$ cannot be made because the observed bands have such an irregular Franck-Condon locus.

4. $(O_2)_2$ Collision Complex or O_4, Stable Dimer of O_2. High Pressure Bands of Oxygen and Simultaneous Transitions in Compressed and Condensed Oxygen.

This brief summary of the experimental data on the spectra and physical properties of compressed and condensed molecular oxygen is an attempt to answer the question: are the high pressure bands of oxygen due to O_2? Inevitably, this leads to consideration of the possible existence of a stable dimer, O_4. For this discussion a dimer will be defined as "two molecules which interact over a period of time long compared to the time between intermolecular collisions so that the vibrational and rotational degrees of freedom cannot be treated as those of two independent particles" [234]; i.e., if two O_2 molecules are associated for a time long compared with a vibrational period characteristic of this union. A collision complex $(O_2)_2$ will be considered a similar pair of molecules whose interaction time is

ot long compared with the time between collisions more strictly, not long compared with a vibrational period characteristic of the interacting pair).[19] In the literature, there is no general agreement on the meaning of the terms dimer and complex; in addition, $(O_2)_2$ and O_4 are often used interchangeably.

While some experimental results are consistent with the stability of O_4, a stronger case can be made for a short-lived collision complex $(O_2)_2$ to account for bands observed in high pressure oxygen and the numerous simultaneous transitions which are induced (made allowed) by intermolecular forces. It is difficult to describe as a chemical entity a colliding pair with a binding energy of ≤ 600 cm^{-1} (≤ 0.008 eV) [231]. Cashion [78], using a binding energy of 82 cm^{-1}, has predicted 7 bound vibrational levels for the interacting pairs $(O_2)_2$, assuming a Lennard-Jones potential.

A dimer of O_2 was first mentioned by C. Harries and by E. Baur in 1907. It was, however, a paper by G. N. Lewis in 1924, that started serious inquiry into the stability and characteristics of an O_4 molecule. Therein, the formation of O_4 was postulated to account for the decreased paramagnetism with increased concentration of oxygen in liquid oxygen-nitrogen mixtures. Since then measurements of the spectra and physical properties of compressed and condensed oxygen have been interpreted both as supporting or denying the existence of a stable O_4 molecule. Knobler [234] has recently written "that there has been no irrefutable proof of its existence." More recently, in another thesis, Keys [231] concluded "that the formation of O_4, irrespective of its exact electronic configuration, is a reality."

Most of the literature on these topics can be traced through the cited references, especially the theses by Knobler and by Keys. Much earlier, Heller [179] had estimated a vibrational frequency and binding energy for the complex, and, in addition, had summarized the different kinds of experimental evidence indicating the existence of $(O_2)_2$ (a van der Waals complex, he called it).

The observed spectra of compressed and condensed oxygen are divided into four groups which will be discussed roughly in the following order.

(1) *3.3 μm and 6.4 μm* ; induced absorption corresponding to the O_2 ground state fundamental and first overtone.

(2) *12600–6800 Å* ; intensity proportional to pressure. Includes bands of O_2 (a–X, b–X) transitions and bands attributed to a complex.

(3) *6800–3000 Å* ; intensities of the broad, diffuse bands are roughly proportional to the square of the pressure. Simultaneous transitions in coupled O_2 molecules; e.g., $(^1\Delta_g + {}^1\Delta_g) - ({}^3\Sigma_g^- + {}^3\Sigma_g^-)$.

(4) *2900–2400 Å* ; triplet (so called high pressure) bands whose frequencies are tentatively correlated with $^3\Delta_u - {}^3\Sigma_g^-$, O_2.

Observed frequencies are slightly displaced from those of the free molecule.

O_2 has no permanent dipole moment, and consequently under normal conditions has no vibration-rotation spectrum. However, Crawford, Welsh, and Locke [96] have observed absorption corresponding to the O_2 vibrational fundamental frequency in high pressure (up to 60 atm) and liquid oxygen. Shapiro and Gush [352] have observed both the collision induced fundamental and first overtone bands in oxygen at pressures of several atmospheres. "It is significant that the perturbation is sufficient to alter the transition probabilities but has negligible effect on the vibrational frequency" [96]. Smith and Johnston [359], however, found a shoulder at 1610 cm^{-1} in the infrared spectrum of condensed oxygen; this frequency is consistent with a possible vibration in O_4. The spectral feature at 1610 cm^{-1} has a more plausible explanation, says Cairns [73, 74], who observed the infrared spectra of α and β oxygen; it is due to an O_2 vibration-translation combination band (in the solid oxygen lattice).

In liquid oxygen Ellis and Kneser [126] first observed bands (6800–3000 Å) which were attributed to simultaneous transitions (in two coupled oxygen molecules). Some of the bands, observed more recently in the gas phase under pressures of less than 10 atmospheres (path lengths > 350 m) [187, 188], were diffuse and showed no fine structure even with dispersion of 1.2 Å/mm. Several of these bands, also attributed to a complex, have been observed in the absorption spectrum of the atmosphere during the setting sun [182, 389, 120].

In a series of articles (1955 to 1964)[20] Dianov-Klokov studied the intensity variation in the absorption spectra of compressed and condensed oxygen (12600–3000 Å). The spectra included a–X and b–X bands of O_2, and bands attributed to an $(O^2)_2$ complex. Cho, Allin, and Welsh [87] have studied effects of pressure on absorption intensities in a–X and b–X bands of O_2. Both Dianov-Klokov [108] and Cho et al. [87] concluded that the pressure induced effects dominate the magnetic dipole effects above 1.5 atmospheres, and are consistent with the earlier observations in the atmosphere [182, 389, 120]. Robin [333] has observed some of the bands at pressures up to 5000 atm.

Cho, Allin, and Welsh [86] have observed simultaneous transitions $2(^1\Delta_g)-2(^3\Sigma_g^-)$, lying close to O_2, $^1\Sigma_g^+ - X\ ^3\Sigma_g^-$, in the spectrum of O_2-N_2 liquid mixtures. Landau, Allin, and Welsh [249] have observed violet-degraded bands (of simultaneous transitions) in all three forms of solid oxygen. The spectra (12600–3300 Å) were interpreted as O_2 transitions superposed on a continuous distribution of lattice frequencies. The authors deny formation of an $(O_2)_2$ complex "since simultaneous transitions are a general feature of induced absorption, particularly in condensed phases." This general feature refers to induced vibration-rotation transitions in condensed hydrogen. Whitlow and Findlay

---

[19] See the brief discussion of radiative relaxation by Arnold et al. [18].

[20] These references can be traced through ref. [108].

[412], studying emission of compressed oxygen. found the intensity variation for the simultaneous transitions to be proportional to the square of the concentration of the excited O_2 species. A similar quadratic pressure dependence in absorption has most often been interpreted as evidence for a dimer. But not all results show this dependence [234, 107].

Dianov-Klokov [109] has estimated from band widths an upper limit to the lifetime of the complex which is smaller than the (loosely defined) time between collisions at atmospheric pressure. Arnold, Browne, and Ogryzlo [17] have deduced an unbound complex from the temperature dependence of the intensity of the band at 6340 Å.

Dianov-Klokov [107] has emphasized that "all the absorption bands in the 12600–3000 Å region in liquid and condensed oxygen are basically related to intermolecular interaction," and that the spectra correspond to dipole transitions in $(O_2)_2$ complexes. Whether these are called induced dipole transitions or result from a collision complex, weak interactions are responsible. Rettschnick and Hoytink [329] explain simultaneous transitions of the complex as due to electron exchange between the two oxygen molecules during collision.

Prikhotko et al. [321] have drawn no conclusion about a dimer from their study of the spectra of solid oxygen. Jordan et al. [223] inferred that there was no O_4 in the γ-phase of solid oxygen from X-ray diffraction of single crystals. They concluded that there was no O_4 in other solid phases or in solution, because of the similar structure of $\gamma-O_2$ and $\beta-F_2$ which was inconsistent with a dimer. Cairns and Pimentel [74] have interpreted their results on the infrared spectra of solid α-oxygen as showing no evidence for O_4, stressing the uncertainty in previous identifications, Barrett, Meyer, and Wasserman [27] drew similar conclusions from their study of the crystal structure of α-oxygen. Blickensderfer and Ewing [47] have found some spectroscopic evidence for bound dimers in dilute oxygen at low temperatures. Further studies are in progress.

Finkelnburg and Steiner [141] first observed the high pressure bands of oxygen (2900–2300 Å), a long progression of diffuse triplet maxima in absorption by oxygen at pressures of 60–600 atm. Some of these are tentatively ascribed to O_2, $^3\Delta_u-X\,^3\Sigma_g^-$ [187, 188]. The bands, headless and red-degraded, did not appear at lower pressures. The convergence limit of these bands was roughly coincident with the dissociation limit of O_2. This, together with the quadratic increase of absorption with pressure, suggested that the bands originated from a collision induced forbidden transition in O_2, $^3\Delta_u \leftarrow X\,^1\Sigma_g^-$. Finkelnburg, however, later [140] interpreted these bands as arising from vibration in O_4.

Herman [182] studied the variation of absorption coefficient with pressure in the visible and UV spectra of compressed oxygen up to 30 atm. The triplet bands were shown to be independent of the $A-X$ Herzberg bands of O_2 (3000–2400 Å). The triplet bands increased in intensity with increased pressure; the $A-X$ bands of O_2 disappeared with increased pressure. These triplets were attributed to $(O_2)_2$.

Knobler [234] recently remeasured magnetic susceptibility of liquid oxygen at temperatures of 65–90 K and concluded that neither the chemical approach of Lewis nor antiferromagnetic exchange completely explained the interaction between oxygen molecules. His review of other physical properties revealed no conclusive evidence for a stable O_4 molecule.

Physical adsorption, magnetic susceptibility measurements, and the use of E.P.R. techniques by Mulay and Keys [282] and Keys [231] have provided evidence for the existence of O_4. A discussion of possible bonding in the dimer has also been given [231].

Blickensderfer and Ewing [348a, b] have observed the collision-induced simultaneous transitions in gaseous oxygen at low pressure (1–3 atm) and temperatures of 300 K and 87 K. Mechanisms of the absorption induced by binary collisions were discussed. No direct evidence for a bound state dimer was found. Krishna [243a] and Krishna and Cassen [243b] have recently developed a general theory of relative intensities for the oxygen simultaneous transitions (bimolecular induced transitions). Robinson [335] had earlier discussed enhancement of forbidden transitions by weak intermolecular interactions. Tsai and Robinson [382] have more recently calculated the intensity of one double transition and f-values for several double transitions. Tabisz et al. [368] studied intensity profiles of both single and double transitions in compressed oxygen in the near IR and visible regions. The bands were interpreted as collision (pressure)-induced electronic transitions, with no evidence for the existence of quasi-stable complexes.

In summary: Many spectral features of compressed and condensed oxygen are not found in the low pressure gas. The simultaneous transitions can be considered induced by weak intermolecular forces or due to formation of short-lived (unstable) collision complexes. The virtually unchanged infrared spectrum (wavelengths $>3\mu$) is not consistent with a dimer; but the shoulder at 1610 cm^{-1} could represent vibration in O_4. The triplet bands (2900–2400 Å) are tentatively assigned to a transition in O_2, as was done in the original work by Finkelnburg and Steiner. The quadratic pressure or concentration dependence of intensities for simultaneous transitions (12600–3000 Å) observed by some only indicates dependence on initial reactants (two bodies) but does not indicate whether or not the final product is a stable dimer. The slight displacement of band frequencies from those of low pressure O_2 indicates negligible change in electron configuration, which suggests a weak interaction between pairs of O_2 molecules.

Various physical properties provide some evidence for a stable dimer. At low temperatures it is expected that a dimer would become important when its feeble

inding energy exceeds kT. But even in studies of olid oxygen, the presence of stable dimers has not ieen unequivocally established.

5. Perturbations

Perturbations mentioned in section 3 were incidental to the discussion of the electronic-vibrational transitions. In this section, attention will be focused on several specific perturbations, even though the data may be fragmentary.

5.1. O_2, $A\,^3\Sigma_u^+$ state

In the 11-0, $A\,^3\Sigma_u^+ - X\,^3\Sigma_g^-$ band, Herzberg [187] letected a strong perturbation above $N=11$. No letails were given.

5.2. O_2, $B\,^3\Sigma_u$ state

Ackerman and Biaume [3] have implied a perturbaion of $v-5$ from a discontinuity in differences $\Delta G_{\text{exptl.}} - \Delta G_{\text{calc.}}$ obtained from their study of the $B\,^3\Sigma_u^- - X\,^3\Sigma_g^-$ fine structure. Albritton et al. [9], ising measurements of $B-X$ bands bv several auhors, have found a discontinuity at $v=5$ and 6 in plots of $\Delta^2 G$. Measured values of σ_0 (5-0] and σ_0 (6-0) are about 0.7 cm^{-1} larger and smaller respectively, than values which give a smooth plot for $\Delta^2 G$. Unpublished results of R. A. Howard and S. G. Tilford show very broad lines for the 5-0 and 6-0 $B-X$ bands. Albritton et al. consider the possibility of vibrational perturbations of levels $v=5$ and 6, perhaps originating in crossing by a repulsive potential curve derived from ground state atoms. Present accuracy of B_v values does not permit an unambiguous verification or denial that there is a vibrational perturbation [9].

For the $B-X$ transition, Brix and Herzberg [62] mentioned two perturbations: (a) In the 16-0 band a conspicuous perturbation occurs in $R(7)$ and $P(9)$, i.e., $v=16$, $J=8$. (b) Normally, $P_1 < P_2 < P_3$ and $R_1 < R_2 < R_3$, but perturbations in the 19-0 band cause lines $R_2(7)$, $R_3(7)$ to be interchanged in order; also $P_2(9)$, $P_3(9)$. This arises from perturbation of $v=19$, $J=8$.

5.3. O_2^+, $a\,^4\Pi_{ui}$ state

In his fine structure analysis of O_2^+, $b\,^4\Sigma_g^- - a\,^4\Pi_{ui}$ bands with $v''=0$, 1, 2 [291], Nevin found that Brandt's formulas [56] representing energy of a $^4\Pi$ state, indicate probable perturbation of the a state. An empirical formula was developed [291b] which fitted the rotational structure better than Brandt's formulas. According to Brandt, $F_4(J) - F_1(J)$ is about three times the separation $F_3(J) - F_2(J)$. Displacement of F_4 levels away from F_3, and F_2 levels towards F_1

was attributed by Nevin [91a] to perturbation of $a\,^4\Pi_{ui}$ by either $^4\Sigma_u^-$, $^4\Pi_u$, or $^4\Delta_u$—with dissociation products $O(^3P_g) + O^+(^2D_u)$. According to Budó and Kovács [66] the observations deviate from the theory of Brandt [56], with the two middle components lying closer than was expected (by several cm^{-1}) to the lowest energy component. A possible explanation was proposed [66] whereby the $a\,^4\Pi_u$ state is coupled by spin-orbit interaction to two $^2\Pi_u$ states, one of them not yet observed directly. Kovács [237] explained the seemingly anomalous multiplet splitting of $a\,^4\Pi_u$ as also arising from spin-spin interaction. The observed deviation from Brandt's formulas, then, being due to the joint effect of the two types of interaction (see Kovács and Weniger [238]).

The new $^2\Pi_u$ term, dissociating to $^4S_u + ^3P_g$, is estimated to lie ~ 5700 cm^{-1} above $A\,^2\Pi_u$, the other state perturbing a $^4\Pi_u$. Spin-orbit coupling constant for the new state is ~ -104 cm^{-1}.

6. Predissociation of the $B\,^3\Sigma_u^-$ state

Observed line broadening in O_2 $B-X$ bands has led to varying interpretations of predissociation of the B state. The repulsive $^3\Pi_u$ state derived from ground state atoms was assigned as the state causing predissociation, but the course of this state was ambiguous. The three types of crossings which had been used in various explanations are shown in fig. 1. Several recent theoretical papers [288, 331] provided a seemingly qualitative explanation of the line broadening as arising from the $^3\Pi_u$ state, from a single curve crossing at the right limb of the B state near $v=4$. Recent quantum mechanical calculations by Schaefer and Miller [344a] infer that the predissociation arises mainly from spin-orbit coupling which is independent of J (rather than orbit-rotation coupling which is J dependent) and may thereby involve repulsive states $^3\Pi_u$, $^1\Pi_u$, $^5\Pi_u$, and $^5\Sigma_u^-$ which all dissociate to ground-state atoms. Configuration interaction calculations show that the $^3\Pi_u$ potential curve almost certainly crosses the left limb of the B state and the $^1\Pi_u$ curve crosses the right limb of the B state. A summary will be given of the experimental and non-experimental factors affecting the interpretation of predissociation of the $B\,^3\Sigma_u^-$ state.

In 1936, Flory [143] postulated an allowed predissociation of $B\,^3\Sigma_u^-$ by a repulsive $^3\Pi_u$ state derived from ground state atoms. The predissociation was invoked to explain (1) the absence of $B-X$ emission bands with $v' > 2$, (2) broadening of $B-X$ absorption lines with $v' > 2$, (3) very weak fluorescence, disappearing at low pressure, as observed by Rasetti [327], where assumed depopulation of levels B, $v=8$, by predissociation, was reasonable, and (4) fluorescence in oxygen irradiated by 1849 Å mercury light leading to ozone formation. Feast [133] observed $B-X$ emission from bands with $v'=3$ and discounted such predissociation;

Volman [391] presented strong photochemical evidence in favor of it.

Wilkinson and Mulliken [414] obtained high resolution $B-X$ spectra which showed rotational line broadening in the 12–0 absorption band, but not in 13–0 and above. A predissociation was proposed, caused by $^3\Pi_u$ having a very shallow, broad well. crossing the left limb of the B state potential curve at 6.9 eV. It could not be established whether broad structure in bands with $v' < 12$ arose from predissociation or was due to unresolved triplets (because triplet splitting decreases at lower v').

Under lower resolution Rakotoarijimy et al. [324] observed diffuseness in $B-X$ absorption bands having $v' = 4$. Herman et al. [183] also claimed strong perturbation of $v' = 3$, 4 but not 5. It was specifically to determine whether levels of $B\ ^3\Sigma_u^-$, $v < 8$ were predissociated that Carroll [76] reexamined the absorption spectra of the $B-X$ system under high resolution. He found all lines in the 4–1 band diffuse. indicating onset of a predissociation below $v' = 4$, $N = 0$. A weaker predissociation was also observed for lines having $N \sim 25$ in $v' = 3$. He concluded that possibly $v' = 5$ was also predissociated. Reexamination of plates taken by Brix and Herzberg [62] indicated another, but weaker, predissociation peaking at $v' = 11$. Carroll [76] suggested that $^3\Pi_u$ crossed the right limb of the B state potential curve near $v = 4$, but could not determine whether B, $v = 11$ was crossed by the same state.

Lines in $B-X$ bands 2–0 and 1–0. broader than expected, were attributed by Carroll [76] to blends of fine structure components. Vanderslice et al. [387] considered this broadening more likely due to predissociation of the many levels of the B state by a nearly tangent $^3\Pi_u$ curve. Carroll further found a minimum in line broadening for B, $v = 9$, suggesting two predissociations with perhaps $^5\Sigma_u^-$ predissociating B, $v = 11$.

High temperature absorption measurements by Hudson and Carter [199a, 200] indicate that the B state is predissociated in levels $v = 3$ to 17, possibly also in $v = 2$. Myers and Bartle [289] also presume that $v = 2$ should be predissociated. Line widths measured by Hudson and Carter in $B-X$ bands 3–0 to 12–0 varied from 2.5 cm^{-1} to 0.9 cm^{-1}; for 13–0 to 17–0, line widths were ~ 0.5 cm^{-1}. Line widths for 2–0 were (0.5 ± 0.2) cm^{-1}, so predissociation was not conclusive. These results were interpreted to mean that crossing by $^3\Pi_u$ occurred between $v = 2$ and 3, on the right limb of the B state. No comment could be made about 1–0 for experimental reasons. Hudson and Carter [200] have pointed out the important role in atmospheric chemistry of predissociation of vibrational levels of the B state. (See also ref. [201].)

The predissociation is thus characterized by: (1) B, $v = 4$, lines are broadest; onset of predissociation possibly at $v = 2$; (2) broadening peaks again at $v = 8$, 11, with minimum at 9; (3) $v = 12$, sudden triplet splitting

increase. The question remains whether $v = 12$ shows triplet splitting and not apparent broadening.

Riess and Ben-Aryeh [331] and Murrell and Taylor [288] have applied the Franck-Condon principle to predissociation broadening of $B-X$ lines. They have shown that a maximum in predissociation probability occurs near curve crossing just below $v = 4$ (at r between 1.84 and 1.92 Å) and that subsidiary maxima may occur above the crossing point which do not necessarily indicate a crossing of the left limb of the B state. Tunneling is responsible for predissociation broadening below the crossing point. Franck-Condon factors for $B\ ^3\Sigma_u^- - {}^3\Pi_u$ were found to be sensitive to the form of the repulsive curve. No additional crossing of the left limb of the B state was indicated.

Child [83] has derived an analytical expression for the probability of predissociation as a function of vibrational quantum number. Analysis of a predissociation pattern can then lead to the form of the appropriate repulsive potential. The theory was applied to the $B\ ^3\Sigma_u^-$ state of O_2, using the results of Murrell and Taylor.

Ackerman and Biaume [3] have since observed line broadening for $v = 0$ to 13, incidental to their primary objective which was fine structure analysis. They were not sure that the apparent peak in broadening for the $B-X$, 11–0 band does not arise from separation of the triplets. which makes line widths difficult to measure. They cautioned against the use of photographic line widths as cross section data if the spectra have been taken mainly for fine structure analysis, but believed that their results were not in complete support of the conclusions reached by Murrell and Taylor [288].

The non-empirical calculations of Schaefer and Miller [344a] indicate that the repulsive curve deduced by Murrell and Taylor [288] and Riess and Ben-Aryeh [331] is not $^3\Pi_u$, but could be $^5\Pi_u$ or $^5\Sigma_u^-$ and still offer a partial explanation of the observed predissociation of the B state. Schaefer and Miller speculated that the $^3\Pi_u$ curve crosses the left limb of the B state near $v = 4$ and the $^1\Pi_u$ curve crosses the B state on the right, perhaps between $v = 0$ and 1. The nearly parallel calculated and RKR potential curves for the B state imply that improved wavefunctions would only lower the calculated curve.

A general conclusion drawn by Schaefer and Miller is that high-lying excited valence states are poorly described by a single electron configuration. They found that for the B state near r_e three configurations were important: $(3\sigma_g)^2(1\pi_u)^3(1\pi_g)^3$, $(3\sigma_g)(1\pi_u)^4(1\pi_g)^2(3\sigma_u)$, and $(3\sigma_g)(1\pi_u)^2(1\pi_g)^4(3\sigma_u)$. An important implication of the assumed crossing of the left limb of the B state by $^3\pi_u$ is that the $^3\Pi_u - X\ ^3\Sigma_g^-$ transition would dominate the O_2 continuum in the region 2000–1750 Å. A more reliable determination of predissociation line widths [J dependence] is necessary to resolve remaining questions concerning the predissociation of $B\ ^3\Sigma_u^-$.

7. Dissociation Energy of O_2

The dissociation energy D^0 for the ground state of O_2 is (41260 ± 15) cm^{-1}. This value is determined from (1) the convergence limit of the B $^3\Sigma_u^-$ state [62] at 57127.5 cm^{-1}, (2) the separation between dissociation limits for the B and A $^3\Sigma_u^+$ states as representing the energy $O(^1D_2)-O(^3P_2)$, and (3) the assumption from the non-crossing rule that the atomic product common to both B and A states is $O(^3P_2)$. The uncertainty takes into account the inability to rule out possible potential maxima of about 2 cm^{-1}. Details are given by Brix and Herzberg [62]; a succinct summary is given by Gaydon [154].

8. Microwave Spectrum of O_2

A summary is given below of the fine structure spectrum of $^{16}O_2$, $^{18}O_2$, $^{16}O^{18}O$, and the hyperfine structure of $^{16}O^{17}O$. The observed line frequencies are collected in tables 31–33; line widths are given in table 34. Miscellaneous data derived from the microwave spectrum are given in table 35. The magnetic resonance (Zeeman) spectrum is discussed. For details of the theoretical temperature- and pressure-dependence line widths, and the non-resonant (Debye) spectrum the reader is referred to papers by Artman and Gordon [19], Tinkham [374, 375], and papers since 1959 by M. Mizushima, and A. A. Maryott. Additional references are given in a compilation by Wacker et al. [392].

8.1. Rotational Spectrum

Through O_2 is electrically non-polar, it has a permanent magnetic moment associated with the aligned spins of two unpaired electrons. Consequently, magnetic dipole (resonance) transitions ($\Delta N = 0$, $\Delta J = \pm 1$) are allowed between the spin multiplet components of the ground state of O_2, i.e., components with the same value of N, but different values of J. The components[21] F_3 and F_1 lie close together and below F_2 by about 2 cm^{-1} (5-mm wavelength transition). Beringer, in 1946, first observed this very weak absorption without resolving F_2-F_1 and F_2-F_3 structure, and in the following year Van Vleck accounted, theoretically, for the intensity distribution of this line whose existence he had previously predicted. This line was partially resolved by Lamont (in 1948) and by Strandberg, Meng, and Ingersoll. Burkhalter et al. [69] first resolved the fine structure in the 5-mm wavelength region (60 GHz) and found deviations from the theoretical formulas of Schlapp [346], which were extensions of early theory by Kramers and Hebb. (See Brix and Herzberg [62].) The position of the 1_- line near 2.5-mm wavelength was first measured by Anderson, Johnson, and Gordy [14].

Miller and Townes [275] and Mizushima and Hill [279] revised Schlapp's formulas. Zimmerer and Mizushima [422] and West and Mizushima [411] extended these formulas, and remeasured many frequencies with high accuracy. (Table 31 also includes more recent measurements by McKnight and Gordy [265] and Wilheit and Barrett [413].)

Tinkham, in his thesis [374], and in three papers with Strandberg [375–377] has developed the most extensive theoretical treatment of the spin multiplet structure and intensities of the O_2 microwave spectrum. These papers account for the fine structure theory of the O_2 ground state [375], the magnetic field interactions (Zeeman effect) [376], and the line widths [377]. Tinkham's fine structure parameters have been recently revised by Tischer [378]. (Compare also West and Mizushima [411] and Appendix C.)

Magnetic dipole rotational transitions ($\Delta N = 1$), predicted by Tinkham [374], have been observed under high resolution by McKnight and Gordy [265][22] (12.3, 14.2, 16.3 cm^{-1}). The latter two have been identified in the solar spectrum by Gebbie et al. [157]. Additional magnetic dipole rotational transitions observed in the laboratory and the solar spectrum are included in table 33.

Miller, Javan, and Townes [274] measured the transitions in $^{16}O^{18}O$ and $^{18}O_2$. Since none of these lines showed splitting due to magnetic hyperfine structure, it was assumed that ^{18}O had zero nuclear spin [273, 274, 379], a result that has since become well established.

The hyperfine structure of $^{16}O^{17}O$ arises from magnetic dipole and electric quadrupole interactions of the ^{17}O nuclear spin with the unpaired electron spins. Miller and Townes [275] have confirmed the assignment of nuclear spin $I = \frac{5}{2}$ for ^{17}O [10, 159] by obtaining agreement between observed frequencies for $^{16}O^{17}O$ and the theoretical hyperfine spectrum calculated with the assumption that $I(^{17}O) = \frac{5}{2}$. The theory of the hyperfine structure is given by Frosch and Foley [146]. For the two parameters representing the magnetic interaction energy, the data of Miller and Townes [275] give $b = -102$ MHz, $c = 140$ MHz. (Miller and Townes also measured the fine structure of $^{16}O_2$, $^{18}O_2$, and $^{16}O^{18}O$.)

8.2. Zeeman Effect and EPR Spectrum

The Zeeman effect of O_2 was first studied in the $b-X$ system by Schmid, Budó, and Zemplen. This low resolution work was done with high magnetic fields which broke down internal coupling. An extended Zeeman theory[23] of the rotational levels of the $^{16}O_2$ ground state developed by Henry was further improved by Tinkham and Strandberg [376]. In the microwave region, Beringer and Castle first resolved lines of the magnetic

---

[21] $F_{1,2,3}$ means $J = N+1$, N, $N-1$. F_2-$F_3 = v_-$; F_2-$F_1 = v_+$. 1_- designates $N=1$, $J'-J''=1-0$; $_+$ designates $N=1$, $J'-J''=1-2$. The Pauli principle permits only odd integral values of N since the ^{16}O nucleus has zero spin.

dipole transitions between Zeeman levels of the ground vibrational state, using fields up to 9000 gauss. Some quantum numbers were assigned on the basis of Henry's theory. These observations were considerably extended by Tinkham and Strandberg [376] who observed over 200 lines and identified 40. For more than half the observed lines $\Delta J = \pm 2$. J breaks down as a good quantum number in magnetic fields of $\sim 10,000$ gauss and all ΔJ transitions then become allowed.

Hendrie and Kusch [180] also studied these Zeeman transitions and obtained total g-values for the rotational states. Bowers, Kamper, and Lustig [51] repeated Tinkham and Strandberg's measurement on 14 lines. Lines were measured with an accuracy of ± 5 ppm. Positions of absorption lines were fitted to calculated values based on the Tinkham and Strandberg theory to 2 ppm. (They also measured $^{16}O^{17}O$.)

Hill and Gordy [193], using magnetic fields of ~ 100 gauss, introduced no decoupling of internal angular momenta. Zeeman splittings were observed for lines 1_-, 3_-, and 3_+.

The electronic paramagnetic resonance (EPR) spectrum of the metastable $a\,^1\Delta_g$ state has recently been studied by Falick et al. [129] who observed the four $\Delta M_J = 1$ transitions [24] for the $J = 2$ level. Miller [277] using greater precision, observed these in addition to four $\Delta M_J = 1$ transitions for the $J = 3$ level. Measured magnetic interaction parameters are included in table 35. Miller's value of B_0 $(1.41808 \pm .00020$ cm$^{-1})$ is the same as that obtained from the $a\,^1\Delta_g - X\,^3\Sigma_g^-$ electronic spectra [191] within experimental uncertainty. (Miller's value includes the effect of electronic mass.)

Tischer [378] has observed 275 magnetic dipole transitions between Zeeman components of the fine structure terms for the $X\,^3\Sigma_g^-$ state. Paramagnetic resonance absorption between $N = 3$, $J = 4$, $M = -4$ and $N = 5$, $J = 5$, $M = -4$ levels were observed by Evenson et al. [128] using 890 GHz laser excitation (table 33). Observed zero-field energy difference between $N = 3$, $J = 3$ and $N = 5$, $J = 5$ levels is fitted slightly better by the theoretical parameters of West and Mizushima [411] than by those of Tischer [378]. Work in progress (Evenson, private communication) on 12 additional lines should lead to a consistent set of theoretical parameters which will also reproduce the rotational line frequencies. (See Appendix C.) Several lines, observed high in the earth's atmosphere, have been assigned with some uncertainty to $O_2(27.8-51$ cm$^{-1})$ [156].

9. Raman and Zeeman Effects

9.1. Raman Effect

The vibrational Raman effect has been observed in both liquid and gaseous oxygen. Rotational Raman spectra have been observed only in the gas. Among the first examples of pure vibrational transitions in a homonuclear diatomic molecule, were the observations of McLennan and McLeod (in 1928) [266] in liquid oxygen, which was irradiated with two different mercury lines. Both 1–0 and 2–0 vibrational transitions were detected (the latter smaller than the gas phase quantum by ~ 35 cm^{-1}). (Both transitions are electric dipole forbidden.) Shortly thereafter, the fundamental frequency was detected by Rasetti and others in the gas at atmospheric pressure and above. Rasetti [326] also first observed the rotational Raman spectrum. Recently, Weber and McGinnis [405] observed the vibrational and rotational Raman spectra under 5 Å/mm dispersion and obtained values for $\Delta G(\frac{1}{2})$ and B_0 in close agreement with those derived from electronic spectra. Rotational spectrograms have been published by several authors [405, 326a, c, 381, 406, 366, 328].

Bhagavantam [41], irradiating oxygen with visible light, had found that rotational structure disappeared above 30 atm pressure (no wavelengths were given). Trumpy [381], using 4046.8 Å Hg light, studied the pressure effect on rotational Raman spectra at 15, 30, and 60 atm. Surprisingly, even at 60 atm the lines were only broadened and not completely washed out. Saha [339], using about the same dispersion as Trumpy (~ 12 Å/mm), was unable to see discrete rotational structure in liquid oxygen, indicating far more broadening in the liquid than in the gas at 60 atm.

Renschler et al. [328] have measured triplet structure in the rotational Raman spectrum of O_2. Positions of lines observed at 21.29 cm^{-1}, 14.30 cm^{-1}, and 16.25 cm^{-1} are in good agreement with magnetic rotation spectra measurements (compare table 33).

Depolarization ratio for Raman scattering was determined by Cabannes and Rousset [72] to be 0.261 ± 0.010; Bhagavantam [41] had obtained $\rho < 0.3$. Recently Yoshino and Bernstein [418] obtained 0.33.

In a study of mercury light scattered by O_2 at atmospheric pressure, Rasetti [327] observed, in addition to the Raman lines, a series of doublet lines spanning the region 3980–2365 Å. This fluorescence spectrum, excited by the 1849 Å line of Hg, corresponds to elements of two branches of $B\,^3\Sigma_u^- - X\,^3\Sigma_g^-$, $8-v''$ (with $v'' = 8$ through 22). The doublet separation of 60 cm^{-1} corresponds to $F_v''(13) - F_v''(11)$. The fluorescence was not observed at 8-mm pressure, contrary to expectations. Rasetti considered these doublets to represent a possible transition between the Raman effect and fluorescence which he called "selective Raman effect" (now called Resonance Raman effect). That is, where entire branches might be expected, only Raman lines were observed whose transition probability was very high. (See Rasetti's table 2.)

Depolarization ratio for Rayleigh scattering was determined as 0.014 by Weber et al. [406], considerably lower than previous values (0.03–0.06) [314, 315, 60], presumably because of the actual isolation of the

---

[24] $\Delta N = 0, \Delta J = \pm 1; \Delta M = 0, \pm 1.$

Rayleigh line from the Raman lines. The new value represents an upper limit. The mean rate of change of polarizability with inter-nuclear distance was determined by Stansbury et al. [364] as 1.4, from the ratio of Raman to Rayleigh intensities in the gas.

9.2. Zeeman Effect in Electronic Spectra

Zeeman spectrum of the $b\,^1\Sigma_g^+ \leftarrow X\,^3\Sigma_g^-$ transition has been produced by application of magnetic fields up to 26,000 g [347]. The absorption spectrum around 600 Å includes extra lines which arise from splitting of the ground state rotational levels. Zeeman splitting was about 1 cm^{-1} for a magnetic field of 21,400 g. Lines were noticeably broadened at pressures above 10 atm. The most intense Zeeman lines lay to the red of the P and R branch lines. Zeeman lines to the violet of the ^PQ and ^RQ lines were somewhat weaker, and displaced somewhat further from the field-free lines. Maximum line sharpness and minimum displacement occurred for $N \sim 7$.

Bozóky and Schmid [55] produced measureable Zeeman splitting of lines belonging to the $b\,^4\Sigma_g^- \rightarrow a\,^4\Pi_u$, O$_2^+$ 1–0 band at 5631 Å by use of magnetic fields of 15,000 and 23,000 g. No detailed report has been published. (Zeeman effects in the microwave spectrum of the ground state are discussed in section 8.2.)

10. Potential Energy Curves

Potential energy curves for electronic states of O$_2^-$, O$_2$, and O$_2^+$ are shown in figure 2. Some of these curves have been derived from spectroscopic data by the use of the Rydberg-Klein-Rees (RKR) procedure; for these, numerical data (taken mainly from Albritton et al. [9]) are given in table 53. For several other states where data is sparse the dotted curves in figure 2 are only suggestive. For the $c\,^1\Sigma_u^-$ and $C\,^3\Delta_u$ states of O$_2$ only tentative vibrational quantum numbers can be assigned. For O$_2^-$ the approximate curves are derived from tentative ab initio quantum mechanical calculations. (See sec. 2.4.)

The curves for 12 repulsive states of O$_2$ which dissociate to ground-state atoms had been estimated semiempirically by Vanderslice et al. [387] and slightly adjusted by Gilmore [161] to account for the effects of configuration interaction. Recent configuration interaction calculations by Schaefer and Harris [344] indicate an entirely different order for these states compared with the semiempirical estimates. Schaefer and Harris found that five unobserved states of O$_2$ are likely stable; two of these had been assumed stable in prior work and were included in Gilmore's curves [161]. (See sec. 2.2c.)

The curves in Fig. 2 differ from those of Gilmore [161] as follows: (1) the $c\,^1\Sigma_u^-$ state now lies below $C\,^3\Delta_u$ because of more recent spectroscopic data; (2) the shape of the $X\,^2\Pi_g$ state of O$_2^+$ is slightly altered

because v has been increased by unity, (3) numerous approximate curves have been deleted, and (4) approximate potential curves derived from CI calculations are indicated for some stable states of O$_2^-$.

The various RKR results by different authors provide turning points that differ, in general, by no more than ±0.003 Å. The single exception has been the $B\,^3\Sigma_u^-$ state which, in all published results, shows erratic inner turning points abouve $v = 15$. RKR potential curves for O$_2$ were first calculated by Vanderslice et al. [387]. The irregularity of the left limb of the $B\,^3\Sigma_u^-$ potential curve has since been examined by others including Gilmore [161], Richards and Barrow [330], Ginter and Battino [162], and Harris et al. [172]. The scatter remained in the third decimal place in r_{min}. The possible causes of the scatter include (1) oscillations in rotational constants, (2) sensitivity of the RKR method to inaccuracies, especially in B_v values, near the dissociation limit, and (3) perturbations.

Albritton et al. [9] have recalculated the potential curve for the $B\,^3\Sigma_u^-$ state using the recent accurate data of Ackerman and Biaume [3] up to $v = 13$; the use of the data of Brix and Herzberg [62] above $v = 13$ yielded irregular r_{min}. Numerical experiments by Albritton et al. showed that monotonically varying r_{min} could be obtained by the use of adjusted B_v values lying within the experimental uncertainties of the values quoted by Brix and Herzberg. To eliminate irregularities in r_{min}, it was concluded, B_v values accurate to 0.0005 cm^{-1} would be necessary for $v > 13$. (There appears, however, to be no a priori reason why the left limb of a potential must always be monotonic (M. Krauss, private communication).)

RKR potentials have been calculated by Singh and Rai [355] for the X, a, A, and b states of O$_2^+$. A change in vibrational quantum numbering [42] voids their results for the O$_2^+$ ground state, but Asundi and Ramachandrarao [21] have recalculated the curve for the O$_2^+$ ground state with the corrected quantum numbering. Singh and Rai have commented that the A state curve appears to be approaching its convergence limit very rapidly (which suggests a possible potential maximum for this state). Albritton et al. [9] do not mention this possibility.

Potential energy curves for O$_2^{2+}$ are briefly mentioned in sec. 2.3; details can be found in references [209] and [208].

11. Transition Probability Parameters

It is not uncommon to find extensive and reliable measurements of the positions of spectral lines originating in a given state of a molecule, the analysis of the spectra being in terms of a notation which is largely agreed upon. By contrast, in the area of spectroscopy which is loosely called quantitative spectroscopy, the experimental parameters which measure transition

probabilities are not nearly so extensively studied nor so well established, and the notation used in their description is sometimes ambiguous and not standardized. The notation by a given author may vary from paper to paper.

In this section not all topics will be considered quantitatively. Measured radiative lifetimes and f-values for many transitions in O_2 and O_2^+ are summarized (table 54); the extensive measurements of f-values for the O_2, $B\,^3\Sigma_u^- - X\,^3\Sigma_g^-$ transition are summarized in table 55. Absorption coefficients for selected features in the UV are summarized in table 56; most other absorption coefficients and integrated band intensities are considered only qualitatively. Calculated Franck-Condon parameters (table 57)[25] are considered, with the reservations that results based on the Morse potential may, in some instances, be poor approximations, and that the use of the r centroid approximation for determining electronic transition moments has some limitations [214, 244]. Nearly all of the data in table 57 are from the extensive calculations of Albritton et al. [9].

For each electronic transition the radiative lifetime of the upper state is discussed together with the transition probability parameters corresponding to the transition. In general, the form of transition moments should be regarded as tentative.

In a recent review by Nicholls [298], the general concepts used in application of the Franck-Condon principle are briefly discussed, and a summary is given of recent measurements and calculations of aeronomically important transition probability parameters. Difficulties with the definition and meaning of electronic f-values (f_{el}) and electronic Einstein A coefficients for discrete spectra have been discussed by many authors, most recently by Tatum [372] and Schadee [343]. In addition to these conceptual difficulties, different conventions in the use of degeneracies lend confusion when several sets of data are compared. Wentink et al. [410] have compared the two conventions as applied to transition moments for $\Delta S = 0$ transitions only where electronic transition moment R_e (Nicholls)$= \sqrt{g'G''}R_e$ (Mulliken) where g' is the electronic degeneracy of state v', i.e. $(2-\delta_{\Lambda,0})(2S+1)$ and G'' is the number of orbitals of state v''. Values of $f_{v'v''}$ or $\tau_{v'}$ are independent of convention since these parameters involve ratios $g'/g'' = G''/G'$; but absolute values of transition moment, transition moment matrix elements, and $A_{v'v''}$ depend on the convention used.

Bates [33] assumed some years ago that $R_e(r)$ did not vary rapidly with internuclear distance for electronic transitions with $\Delta\Lambda = 0$ (labelled parallel transitions).

"The position regarding perpendicular-type transitions (i.e., $\Delta\Lambda = \pm 1$) is more uncertain" [33]. In the literature it has often been assumed that transitions with $\Delta\Lambda = \pm 1$ will have $R_e(r)$ rapidly varying. These generalizations are not rigorously based. The behavior of $R_e(r)$ has often been deduced from crude band intensities and the use of Morse based Franck-Condon factors. A brief comparison of the use of Morse and RKR potentials follows.

The Morse potential is a three parameter analytic function [186] which may represent a useful approximation, mainly for low vibrational levels of a given electronic state. For use with fragmentary data it provides a qualitative description of electronic state and transitions. When used to describe electronic transitions where $|r_e' - r_e''| \lesssim 0.1$ Å the Franck-Condon factors are often good approximations. For weak bands (those with (relatively) small Franck-Condon factors, or for electronic transitions where $|r_e' - r_e''| > 0.1$ Å then Morse based Franck-Condon factors may be unreliable. For an extreme case where $|r_e' - r_e''| \sim 0.4$ Å $(O_2, B\,^3\Sigma_u^- - X\,^3\Sigma_g^-)$ comparison between Morse and RKR results is striking [292, 310, 172, 9].

The RKR method of calculating potential curves from spectroscopic data is based on numerical integration of two phase integrals. From these integrals are obtained the turning points for a given vibrational term value.[26] The RKR potentials do not predetermine relations among molecular constants as do semiempirical potentials. However, if the vibrational term values and rotational constants are not known up to the dissociation limit then the method yields only a portion of the potential curve bounded by the known term values.

11.1. $a\,^1\Delta_g - X\,^3\Sigma_g^-$ Infrared Atmospheric System

Badger et al. [26] have measured absolute intensities of discrete absorption of the $a-X$, 0-0 (1.26 μm) and 1-0 (1.065 μm) bands at a pressure of four atmospheres. The underlying continuous absorption, proportional to pressure, is attributed to collision complex $(O_2)_2$. A radiative lifetime for the 0-0 transition of the isolated molecule was estimated as 45 minutes (see table 54); in pure oxygen at one atmosphere, it is only 9.2 minutes. Additional discussion of effects of pressure, complexes, and comparison with other measurements is given by Badger et al.; (see especially table 1 of ref. [26]).

Relative intensity ratio $I(0-0)/I(1-0)$ is estimated as $\geqslant 200$; ratio of Franck-Condon factors is about 76 [296, 9]. Integrated absorption coefficients of continua in the region of these bands exceeds those for the discrete bands above $\frac{1}{2}$ atm pressure. Badger et al. cite references to other work on a much weaker continuum underlying the 2-0 band, and a far weaker one underlying the 3-0 band.

---

[25] Franck-Condon factor: $q_{v'v''} = (v', v'')^2$; r centroid: $\bar{r}_{v'v''} = \dfrac{(v', rv'')}{(v', v'')}$; r^2 centroid $= \bar{r}_{v'v''}^2$

$= \dfrac{(v', r^2v'')}{(v', v'')}$. See ref. [244, 9]. The following phase convention was used by Albritton et al. [9] for the vibrational overlap integrals: "The sign of Ψ_r at the inner turning point was $(-1)^r$ and at the outer turning point was always positive." Integration determines the phase listed in table 57.

[26] See, e.g., [162, 330] for citations of the basic papers upon which the method is based.

Vallance Jones and Harrison [385] account for absence of the 0–0 band in twilight emission as arising from reabsorption by the lower atmosphere. "The emission rate of the 0–0 band should be about 10 times that of the 0–1 band."

Morse based Franck-Condon factors have been calculated for a small Deslandres array [168b, 296]. RKR values of Albritton et al. [9] are given in table 57.

The nine branches of this system all have comparable intensities [191], confirming the theoretical formulas of Van Vleck [388]. The intensity of the $a–X$ system in the gas phase is less than $\frac{1}{20}$ that of the $b–X$ system; in liquid oxygen the $a–X$ transition is five times stronger than the $b–X$ transition [126]. Both transitions have an absolute intensity in the liquid which is greater than in the gas. The 1–0 band in the liquid is nearly as strong as the 0–0; in the gas it is much weaker and corresponds to Franck-Condon principle expectations.

11.2. $b^1\Sigma_g^+ - X^3\Sigma_g^-$ Atmospheric System

The integrated absorption coefficient for the $b–X$, 0–0 band has recently been studied very extensively. Burch et al. [67] obtained for the integrated mass absorption coefficient a value of (4.09 ± 0.25) g^{-1} cm^2 cm^{-1}, smaller by 20 percent than the value of Wark and Mercer [398]. Burch et al. considered the effects of line broadening half-width of self-broadened oxygen lines decreased with J at one atm pressure) and line shape, and the dependence on temperature, pressure, and path length. Line positions used were from Wark and Mercer [398] who also tabulated lines for the isotopic molecules $^{16}O^{17}O$ and $^{16}O^{18}O$. The absorption coefficent of Wark and Mercer was based on solar spectra, and an assumed constant line width of 0.048 cm^{-1}. The band strength value based on extrapolation to low pressure from measurements of Cho et al. [87], primarily on induced absorption gives about the same value as that of Burch et al. (who labeled their absorption coefficient as band strength).

The A value for the 0–0 band is 0.085 cm^{-1} [67b] (table 54). The observed line strengths [67] were fitted about as well by rotational weighting functions based on experiment [85] as by theoretical weighting functions of Schalpp [345, 346] based on strictly case b coupling. Recently, Watson [403] derived weighting factors considering deviations from Hund's case b, but for O_2 these are virtually identical with Schlapp's results. Adiks and Dianov-Klokov [5] have determined the f-value for the 0–0 band (corresponding to $A = 0.082$ sec^{-1}) from a low pressure limit of the integrated absorption coefficient. No significant J-dependence was detected. Relative distribution of intensities within the band followed Schlapp's formulas [346]. Miller et al. [272] have also examined in detail the line widths and intensities of the $b–X$, 0–0 band and obtained a slightly smaller value for the Einstein A coefficient than that of Burch and Gryvnak [67]. They concluded that the theoretical Hönl-London factors of Schlapp

[346] and Watson [403] fitted their data more closely than did the empirical ones of Childs and Mecke [85].

For bands other than 0–0 the measured parameters are crude. If an estimate is made of the contribution to $\Sigma_{v''} A_{v'v''}$ by the 0–1 band (i.e., $(0.7)(.085) = .006$), the radiative lifetime (τ) for level $b^1\Sigma_g^+$, $v = 0$ is estimated as 11 seconds (table 54), which is slightly larger than earlier values [85, 398].[27]

Wallace and Hunten [397] have measured the airglow photon intensity ratio $I(0–0)/I(0–1)$ as 17 ± 2; Noxon [301] measured 20 ± 4 in the laboratory. Morse-based Franck-Condon factors [168b, 296] give 23; RKR results [9] give 14.

11.3. $b^1\Sigma_g^+ - a^1\Delta_g$ Noxon System

The absolute transition probability of the $b–a$, 0–0 transition was estimated by Noxon [301] as 1.7×10^{-3} s^{-1}.[28] The 0–0 emission band was observed superimposed on a strong continuum. Observed band width was 20 Å. In photon units of intensity, the ratio $b–a$, 0–0 to $b–X$, 0–0 was about 0.004. Noxon assumed that the Q branch represented 20 percent of the band intensity. See Noxon's paper for mention of earlier estimates of the transition probability of this electric quadrupole transition.

Morse Franck-Condon factors have been calculated by Nicholls [296]. RKR results (table 57) are from Albritton et al. [9].

11.4. $A^3\Sigma_u^+ - X^3\Sigma_g^-$ Herzberg I Transition

The $A^3\Sigma_u^+ - X^3\Sigma_g^-$ transition has a widely spread Condon locus which is characteristic of a transition dominated by a continuum $(\Sigma_{v'} q_{v'0} = 0.0138)$ [104]. Jarmain and Nicholls [219] have calculated RKR Franck-Condon factors which are slightly different than those cited by Degen et al. [104]. These differ from Morse based values [168b, 296] by as much as a factor of 3. Franck-Condon densities [219], calculated for the photodissociation continua of the $v'' = 0, 1$, and 2 progressions (2500–1500 Å), when used with the measured absorption cross sections of Ditchburn and Young [114], have led to a transition moment R_e which decreases slowly with r. This behavior was consistent with that found by Degen and Nicholls [105] who deduced their R_e (for the range $1.33 < \bar{r}_{v'v''} < 1.53$ Å) from emission band intensities and Morse based Franck-Condon factors (4880–2590 Å). (No details were published.)

Jarmain and Nicholls [219] tentatively estimated the continuum f value as 2×10^{-7}, 2 orders of magnitude

---

[27] Childs and Mecke [85] long ago obtained $A(0–0) \sim 0.13$ s^{-1}, $\tau \sim 8$ s. Wark and Mercer [398] more recently obtained $A \sim 0.106$, $\tau \sim 10$ s. (This corrects a misprint in their paper; private communication, D. Wark). van de Hulst [207] has discussed relative uncertainties in the early measurements. A critique of various determinations of $A(0–0)$ is given by Wallace and Hunten [397]. For other early measurements see, e.g., Childs [84], Mecke and Baumann [267], and Panofsky [313].

[28] Uncertainty in this transition probability is a factor of 2. The quoted numerical value, different from that given by Noxon, is based on a more recent value of A for $b–X$, 0–0 deduced by Burch and Gryvnak [67].

smaller than previously thought [114] (see discussion in ref. [219]). The possibility of over-lapping continua near the $A-X$ band convergence limit (2500 Å) may lead to an overestimate of f values in the nearby continuum.

Ditchburn and Young's [114] measured absorption cross sections in the $A-X$ continuum associated with the $v''=0$ progression (2500–1850 Å) did not obey Beer's law. The additional absorption at increasing pressure (2500–2000 Å) was ascribed to formation of O_4. Cross sections (extrapolated to zero pressure) varied from 15×10^{-24} cm^2 (1900 Å) to 3×10^{-24} cm^2 (2300 Å). The $A-X$ continuum peak was calculated to be at 1870 Å, but could not be checked experimentally because of $B-X$ overlap.

Degen [102] has measured intensities of $A-X$ bands emitted in the afterglow of a microwave discharge in an O_2-Ar mixture (3% O_2) in order to provide relative band strengths for this system. Both photographic and photoelectric measurements were made, which were calibrated against a standard tungsten strip filament lamp. From the measured intensities of more than 30 bands (estimated uncertainties were 5–20%) and the use of Morse based Franck-Condon factors and interpolated r-centroids, Degen deduced a linear decrease in transition moment with r (variation of about 20%). An approximate method was used to obtain integrated band intensities from measured rotational line intensities in these bands, which heavily overlap one another (because $\omega_e'' \sim 2\omega_e'$). Because of this complication and the dependence on somewhat unreliable $q_{v'v''}$ and r-centroids, the transition moment and band strengths are likely not very reliable (4600–2800 Å).

Degen and Nicholls [106] have made photoelectric relative intensity measurements of 36 $A-X$ bands produced in an argon-oxygen afterglow. In addition they tabulated calculated relative band strengths using transition moment $R_e(\bar{r})=$const. $\bar{r}^{-3.8}$ for the range 1.31 Å $< \bar{r} < 1.53$ Å. The band strengths were placed on an absolute scale (table 58) by Hasson et al. [174] who measured the absolute absorption coefficient for the 7–0 band. In an atlas for the $A-X$ system Degen et al. [104] include RKR Franck-Condon factors and r centroids which had been calculated by Jarmain for a large Deslandres array.

11.5. $c\ ^1\Sigma_u^- - X\ ^3\Sigma_g^-$ Herzberg II System; $C\ ^3\Delta_u - X\ ^3\Sigma_g^-$ Herzberg III System; $C\ ^3\Delta_u - a\ ^1\Delta_g$ Chamberlain System; $A\ ^3\Sigma_u^+ - b\ ^1\Sigma_g^+$ Broida-Gaydon System

Nicholls [296] has calculated Morse Franck-Condon factors for these systems. Krassovsky et al. [241] have estimated Einstein A values for $c\ ^1\Sigma_u^- - X$ and $C\ ^3\Delta_u - X$. These numbers are not tabulated in the present work. (See sec. 3.14 concerning the Broida-Gaydon bands.) The calculations pertaining to the $c\ ^1\Sigma_u^-$ state are voided by the recent drastic change in quantum numbering [103].

11.6. $B\ ^3\Sigma_u^- - X\ ^3\Sigma_g^-$ Schumann-Runge System

For the $B\ ^3\Sigma_u^- - X\ ^3\Sigma_g^-$ transition, the strongest in O_2, the absorption continuum accounts for nearly all of the transition probability, i.e., $\Sigma_{v'}q_{v'0} \sim 0.0025$ [172]. An asymmetric, broad topped dissociation continuum, peaking near 1420 Å, connects with the far weaker discrete structure at 1750 Å. Mulliken's crude theoretical estimates of f_{el} (0.03–0.55) [285] bracket the various experimentally determined values (0.14–0.26)[29] which include both continuum and discrete contributions. Kotani et al. [236], using configuration interaction wave functions have estimated f_{el} to be 0.15–0.46 from the dipole approximation, and 0.01–0.1 from the velocity approximation. Experimentally, $\Sigma f_{cont.}$ (1750–1350 Å)$=0.15\pm0.015$ [271, 164] and $\Sigma_{v'}f_{v'0} \sim 0.000255$ [4].

At the onset of discrete structure (1750 Å) the electronic transition moment R_e is already small, and the crude experimental evidence suggests that it drops by a factor 2 to 4 as r increases from 1.26 Å $< r < 1.75$ Å (1750–4300 Å). Qualitatively, R_e might be expected to decrease with increasing r since the $B-X$ transition is forbidden by electric dipole selection rules in the separated atoms. Bates [33] has stated that parallel transitions ($\Delta\Lambda=0$) should have R_e only weakly dependent on r. Nicholls [293] expects sizable r dependence for a molecular transition with large $|r_e'-r_e''|$; for $B-X$ this quantity is relatively large, 0.4 Å. These qualitative rules for estimating the behavior of transition moments are in conflict for the $B-X$ system.

(a) Photodissociation Continuum, 1750–1300 Å

The measurements of Watanabe et al. [400] indicated a possible discontinuity at ~ 1400 Å arising from an intersection of $B\ ^3\Sigma_u^-$ and an unidentified state. This has not been mentioned by subsequent authors. Bethke [40] believed that Watanabe's measurements failed to include sufficient pressure broadening for the absorption coefficients to be used in calculating f-values.

The most reliable photoelectric measurements of absorption are by Metzger and Cook [271] who used a continuum background source. A number of bands and windows (regions of weak absorption) were found (1350–1100 Å), including those observed by Tanaka [369]. (See the figures in ref. [271].) See also Huffman et al. [206]. Goldstein and Mastrup [164] have photographed the same continuum region and have obtained an integrated f-value in agreement with photoelectric measurements. This resolved a discrepancy between previous measurements where photographic results were about 20 percent higher than photoelectric.

---

[29] The early f-value determinations for $B-X$ absorption continuum are summarized by Heddle [178] and Goldstein and Mastrup [164]. Absorption coefficients at specified wavelengths (1745–1272 Å) have been measured by Huffman et al. [206], Metzger and Cook [271], and Goldstein and Mastrup [164]; these disagree by at most 20 percent. Hudson and Carter [202] have measured variation of absorption cross section with temperature (300 K to 900 K) for the region 1950–1580 Å.

The peak absorption coefficient is (390 ± 40 cm^{-1}) at about 1420 Å [271, 164, 401]. Goldstein and Mastrup caution, "The exact meaning of the (integrated) f-value reported in this paper is not clear, because the measured value might refer to several overlapping continua."

Bixon et al. [45], when remeasuring the absorption of the $B-X$ continuum, found non-smooth features. This structure in the photo-dissociation continuum is accounted for theoretically because the potential of the excited state is partly attractive.

Jarmain and Nicholls [218] have calculated Franck-Condon densities in the $B-X$ photodissociation continuum (1750–1275 Å). By using absorption coefficients measured by others, they deduced a transition moment in the continuum which connects smoothly to that for discrete structure at the dissociation limit. (The results of Marr [258], Churchill [88], Keck et al. [228] and Nicholls [294] should only be considered qualitatively.) A dip in R_e for $v' = 11$ to 16 was tentatively ascribed to predissociation of $v' = 12$ [414]. (Compare also Marr [258], Churchill [88], and Keck et al. [228].)

(b) Discrete Bands, 5000–1750 Å

Numerous measurements have been made on absorption cross sections and coefficients, integrated emission and intensities, and f-values. Franck-Condon factors have been calculated for these transitions. Results of experiment and calculation have been combined to yield values of f_{el} (for the discrete structure, $f_{v'v''}$, and $R_e(r)$ or transition moment matrix elements relevant to a moderate range of r centroids, 1.25 Å $< \bar{r}_{v'v''} < 1.75$ Å. These results are, in most instances, not quantitatively reliable because of large experimental uncertainties, and because Franck-Condon factors based on Morse functions have been used, a poor approximation for this transition. The intensity parameter measurements span nearly the entire spectral region known to this system:

Author	Ref.	Spectral region (Å)	f_{el} (crude)
Keck et al.	229	5000–3500	0.015
Biberman et al.	43	5000–3000	.1
Keck et al.	230	4700–3300	.028
Watanabe et al.	400, (230)	4000 (extrap.)	.06
Treanor and Wurster	380	3900–2650	.048
Sobolev	360	3900–2650	
Krindach et al.	242	3800–2800	
Wurster and Treanor	416	3370–3230	.035–.052
Hébert and Nicholls	177	3000–2450	
Bethke	40	2020–1750	($\Sigma f_{v'0} = 0.00029$)
Ditchburn and Heddle	113	2025–1750	
Hudson and Carter	202	1950–1580	
Ackerman et al.	4	2025–1750	($\Sigma f_{v'0} = 0.000255$)
Hasson et al.	173	2035–1945	

The absolute f-values of Ackerman et al. [4], Hudson and Carter [202], Hasson et al. [173], and Bethke [40] are the most reliable (table 55). The results of Ditchburn and Heddle [113] and Hébert and Nicholls [177] are in marked disagreement with the trends suggested by other measurements. The measurements of Ackerman et al. [4], when used with the RKR Franck-Condon factors of Harris et al. [172] or Albritton et al. [9], suggest that R_e drops by about 9 percent as $\bar{r}_{v'v''}$ decreases from 1.37–1.31 Å in going from transition 0–0 to 19–0. (The experimental uncertainty in the measurements is $\pm 20\%$.)

The value for f_{el} deduced from the $f_{v'v''}$ values of Ditchburn and Heddle [113] seemed far larger than theoretical estimates. This motivated Bethke [40] to redetermine the absorption intensities. Using a grating UV spectrometer, resolution 0.4 Å, he measured, photoelectrically, absolute integrated absorption intensities for pressure-broadened oxygen spectra in the region 2000–1750 Å. Bands with low v' showed little overlapping: bands with large v' showed significant overlap. These measurements have been extended and slightly improved by the recent results of Ackerman et al. [4]. Hudson and Carter [202] were the first to observe absorption from $v'' = 1$ and 2. (See also Hasson et al. [173].)

Pressure broadening is necessary for observation of true absorption intensity of a band. Bethke's data at low pressure [40] demonstrates that "relative absorption intensities can be grossly in error in unpressurized medium and low resolution spectra." The peak $f_{v'v''}$ is at 14–0; the peak (RKR) Franck-Condon factor [216, 172, 9] in the $v'-0$ progression is at 14–0. The $f_{v'v''}$ are given in table 55.

Wilkinson and Mulliken [414] had shown that line-broadening due to predissociation invalidated Ditchburn and Heddle's assumption of constant line breadth [113]. Heddle [178] concurred in the view that the f-values based on this assumption were unreliable. The general increase in line breadth between $v' = 2$ and 3 and between $v' = 12$ and 13 is due to both collision damping and predissociation. Based on these joint effects, Heddle estimated the line breadth due to predissociation as 0.15 cm^{-1} to 0.25 cm^{-1}. Predissociation lifetime is $2(10^{-11})$ s; radiative lifetime is $2.5(10^{-9})$ s. The probability of predissociation is $\sim$ 99 percent.

Hudson and Carter [202] found absorption coefficients decreased with increasing wavelength, and at 1750 Å, the variation with wavelength suddenly changed slope. Similar behavior was described by Marr [258].

Absolute band f-values for the $v'' = 1$, 2 progressions are given by Hudson and Carter [199a] for the region 2020–1750 Å (table 55). They are obtained from the photoelectric absorption spectrum taken at temperatures of 300, 600, and 900 K by use of a modified curve of growth technique. A nearly invariant transition moment ($\sim$ 1.5 a.u.) is deduced for the $v'' = 1$, 2 progressions; this is roughly the same as found by Marr

[258] from the data of Bethke [40]. Both Marr, and Hudson and Carter used RKR-based Franck-Condon factors of Jarmain [215, 216, also unpublished results]. These values are generally smaller than those of Harris et al. [172] and Albritton et al. [9] by as much as 50 percent for the $(v'-0)$ progression, and larger than those of Halmann and Laulicht [169].

Farmer et al. [131] have obtained f-values for the $v'=0$ progression, all larger than those of Bethke [40]; the reasons for this discrepancy are not clear.

Buttrey et al. [70] have compared measured and calculated line widths for $B-X$ shock tube emission spectra. They found that the Morse based Franch-Condon factors of Nicholls [292] were too large, and did not predict the observed discrete spectral distribution in the region 4700–3300 Å. Buttrey's results are in rough agreement with those of Krindach et al. [242c] on the magnitude of transition probabilities and the variation of R_e with r.

Halmann, in a series of papers, some with Laulicht, has measured absorption coefficients for $B-X$ bands [167, 168a, e]; in one instance [168e], agreement was found with measurements of Bethke [40]. Halmann and Laulicht [168b, d] calculated Morse-based Franck-Condon factors and r-centroids for several isotopes for the $B-X$ transition. Though the numerical values are not reliable, one qualitative feature likely is; isotopic substitution has largest effect on Franck-Condon factors for transitions which fall between Condon loci. Other possible effects on radiative properties, due to isotopic substitution, are discussed by Halmann, especially possible effect on the electronic transition moment.

Jarmain [215, 216, 217], Harris et al. [172], Halmann and Laulicht [169] and Albritton et al. [9] (table 57) have all calculated RKR-based Franck-Condon factors. These values differ from one another by as much as a factor of two. Morse-based results of Nicholls [292], Ory and Gittleman [310], and Halmann and Laulicht [168d] differ from the RKR values by as much as a factor 10^2, and are not reliable for this transition for which $\Delta r_e \sim 0.4$ Å. Though the Franck-Condon factors of Harris et al. [172], and Halmann and Laulicht [169] significantly disagreed, their r centroids were virtually the same. Halmann and Laulicht [169] deduced a transition moment, decreasing linearly with r centroid, but quite different from that given by Churchill [88]. For the 5–0 band, Halmann and Laulicht [170] have calculated RKR Franck-Condon factors as a function of J for two isotopes, and found a 10 percent drop from $N'=1$ to 21; the r centroid was virtually independent of J.

11.7. $A\,{}^2\Pi_u - X\,{}^2\Pi_g$ Second Negative System of O_2^+

Jeunehomme [220a] has measured radiative lifetimes (table 54) which were found independent of pressure (over the range 3.7–32 μ). He produced $A-X$ bands in both an interrupted discharge and modulated discharge: lifetimes based on the latter source were more accurate.

By using Morse Franck-Condon factors [409] he deduced an R_e which was linear, and having slightly positive slope $(1.2 < \bar{r}_{v'v''} < 1.4$ Å). This was in contrast to a parabolic convex upward shape obtained by Robinson and Nicholls [334] from relative emission intensity measurements. Jeunehomme believed that the Robinson and Nicholls results contained too much scatter to enable calculation of radiative lifetimes. Wentink et al. [409] also obtained a parabolic shape for R_e from a fit to Jeunehomme's lifetimes.

Morse Franck-Condon factors and r-centroids have been tabulated by Nicholls [295], Wentink et al. [409], and also for isotopic molecules, by Halmann and Laulicht [168b]. Recent isotopic work by Bhale and Rao [42] which raises the earlier v'' values by unity, will modify all the above results. Albritton et al. [8], by a comparison of calculated and observed relative intensities of $A-X$ bands, support the v'' renumbering of Bhale and Rao. RKR Franck-Condon factors employing the revised quantum numbering have been calculated by Asundi and Ramachandrarao [21] and Albritton et al. [9] (table 57).

Dalgarno and McElroy [100] have calculated mid-day dayglow intensities due to fluorescence of solar ionizing radiation. Above 120 km, their results show the $A-X$ intensity to be about three times that of the other observed transitions in O_2^+, namely $b-a$, $c-b$. They assumed that cascading from unidentified higher-lying states contributed less than 10 percent to the populations of lower-lying states.

11.8. $b\,{}^4\Sigma_g^- - a\,{}^4\Pi_u$ First Negative System of O_2^+

Rao [325] excited $b-a$ bands in four different laboratory sources: ac uncondensed and condensed discharges, dc and hollow cathode discharges. Peak intensities at the band heads were measured photographically with a Steinheil glass spectrograph. (Rao estimated the accuracy to be ±5 percent.)

Jeunehomme [220a] has measured somewhat pressure-dependent radiative lifetimes of several vibrational levels of the b state (table 54). Decay of fluorescence was interpreted as superposition of two exponentials. A possible secondary process was considered: the cascading to the b state from an unknown state having $\tau \sim 16$ μs (see discussion in ref. [220a]). Jeunehomme, using Morse Franck-Condon factors [409, 295] and graphically determined r-centroids, deduced a large curvature in the transition moment. Wentink et al. [409] from virtually the same measured lifetimes, also tentatively deduced a marked convex upward shape for the variation in transition moment. The use of RKR Franck-Condon factors and r centroids [9] would not alter the qualitative shape of the portion of R_e considered here.

Fink and Welge [139] excited O_2^+ by a modulated electron beam. Radiative lifetimes were measured b the phase shift method; this experiment was at lowe

pressure than that of Jeunehomme. Lifetimes obtained were about 10 percent larger than those of Jeunehomme; absolute error was estimated as ± 0.1 μs; relative error as ± 0.02 μs.

Dufay et al. [122] have produced $b-a$ bands emitted following high energy proton bombardment of oxygen. From the band excitation cross sections and by use of Nicholls' Franck-Condon factors [295], they deduced a linearly increasing transition moment for $1.2 < \bar{r} < 1.55$ Å. The intensity distribution is unlike that found in the more conventional spectroscopic sources for this system.

Shemansky and Vallance Jones [353] have estimated intensities of $b-a$ bands in the aurora, from lifetime measurements [220a] and Morse Franck-Condon factors and r-centroids [409].

Zare [421] has compared calculated rotational line strengths (i.e., averaged sums for each branch) with the crude relative intensities estimated by Nevin [291]. He concluded that, in general, "if electronic perturbations can be ignored, fairly reliable rotational line strengths may be calculated" in intermediate coupling without knowing all splitting parameters well (or at all). The results showed no obvious trend dependent on quantum number v, but a detailed comparison with theory requires more reliable intensity measurements.

11.9. Ionization Transitions

Nicholls [297] has calculated Morse-based Franck-Condon factors for ionization of O_2. For ionization $O_2^+ (X^2\Pi_g) - O_2(X^3\Sigma_g^-)$ the results are voided (as well as the RKR results of Jain and Sahni [213]) because of an increase of unity in the vibrational numbering [42] of the O_2^+ ground state. Asundi and Ramachandrarao [21] recalculated RKR Franck-Condon factors for the first ionization transition using the revised quantum numbering of Bhale and Rao [42]. (See the more extensive calculations by Albritton et al. [9] (table 57). See also the several values for ionization to excited states of O_2^+ by Jain and Sahni [213] for isotopes $^{16}O^{18}O$ and $^{18}O_2$). Only for the higher vibrational levels of O_2^+, A and b states, do the RKR values differ by more than 10 percent from Morse function values (compare ref. [393, 168c, 297]). Isotopic substitution for these transitions had a larger effect on the Franck-Condon factors than did the choice of potential for $v'-0$ transitions.

Early electron impact studies were crude [147, 394, 75]. Early photoelectron spectroscopy was done with 584 Å (21.2 eV) photons exclusively [148, 37, 362]. More recently Collin and Natalis [90] obtained photoelectron spectra of O_2 by use of two photons: He (584 Å, 21.2 eV) and Ne (736–744 Å doublet, 16.8–16.7 eV). For the ground state of O_2^+ a much longer vibrational progression was produced by the Ne photons than by the He photons. In addition, a second maximum in intensity distribution around $v' = 7$ was also observed with the Ne photons. The increase of photoionization cross section

with decrease in photon energy was interpreted by the authors as due to the photo-ionization process being a photon-energy dependent mixture of direct photoionization and autoionization. Edqvist et al. [125] have used He photons 584 Å and 304 Å in their study, and for the first time, resolved structure belonging to the $A^2\Pi_u$ state. They also resolved the doublet structure of the $X^2\Pi_g$ state (separation of multiplet components is 200 cm^{-1}).

Schoen [349], from early photoionization measurements on O_2, deduced that autoionization was important for the first two vibrational levels of the O_2^+ ground state. The results indicated near zero transition probabilities for these levels, in conflict with that expected for direct ionization (i.e., the Franck-Condon factors for these transitions are > 0.1).

11.10. UV Absorption Coefficients of O_2

No detailed examination of the absorption coefficients for O_2 is intended, because this has been incorporated into a comprehensive review of UV photoabsorption cross sections by Hudson [198]. Watanabe [399] had reviewed measurements made before 1958. Sullivan and Holland [367] have tabulated absorption coefficient measurements made up to 1966, for wavelengths below 3000 Å. Huffman [203], in a more recent summary of absorption cross sections, discussed discrete absorption, but tabulated only absorption of the continuum at wavelengths of solar lines below 1215 Å.

The most recent measurements (which include corrections for scattered light and pressure gradients where necessary), not always in agreement, are those of Huffman et al. [204], Cook and Metzger [95], Matsunaga and Watanabe [260], and Samson and Cairns [341]. The smallest band width used in these measurements was 0.3 Å. Observations include numerous unclassified absorption maxima. A detailed discussion of the sources of the continua (i.e., which dissociation or ionization process) is to be found in the cited references [204, 95, 260, 341].

Some highlights are discussed below. Table 56 gives a succinct summary of some special absorption features; the cited numerical values should not be regarded as definitive.

Thompson et al. [373] detected no O_2 absorption in the region 4000–2050 Å, and concluded that absorption coefficients were less than 10^{-4} cm^{-1}, their sensitivity.

The $B-X$ Schumann-Runge continuum dominates the region 1750–1300 Å, the peak absorption of this asymmetric continuum occurring near 1420 Å. Absorption by the $B-X$ transition has been discussed separately in detail (sec. 11.6).

Wilkinson and Mulliken [414] have detected a weak continuum arising from a transition to a repulsive $^3\Pi$ state by measurements in windows of the 1780–1850 Å region. The only two measurements give $k = 0.44$ cm^{-1}

at 1781 Å and $k = 0.28$ cm^{-1} at 1796 Å. The f-value of this weak continuum is estimated as 0.01.

Diffuse absorption peaks at 1293 Å, 1332 Å, and 1352 Å, detected by Tanaka [369], have also been observed in absorption coefficient measurements by Watanabe et al. [400] and Goldstein and Mastrup [164]. Tanaka has suggested that the feature at 1293 Å represents a continuum arising from products $^3P + {}^1S$; the other two features may arise from $^1D + {}^1D$ or $^3P + {}^1S$.

The region 1300–1050 Å includes complex absorption. Price and Collins [329] observed a weak continuum beginning at 1105 Å and extending to shorter wavelength.

Ogawa [304][30] has measured absorption coefficients in the region of the Lyman α-doublet (1217.8–1214.8 Å). For the doublet

λ(Å)	k(cm^{-1})
1215.72	0.278 $\}\pm 0.02$
1215.63	0.304

Measurements were made at pressures $\leqslant 6.3$ torr, and the results extrapolated to zero pressure. A 3-m vacuum spectrograph was used (dispersion (1.45–0.95)Å/mm). Ogawa [304] has summarized results of earlier measurements. Gaily [151] has measured absorption coefficients (1215.67–1212.57 Å) at 760 torr, for Lyman-α. He obtained k-values roughly twice that of Ogawa. Other windows ($k < 1$) have also been studied (1300–1000 Å) by Watanabe et al. [400], Watanabe [399], and Cook and Ching [94]. (See also measurements by Ogawa and Yamawaki [307] at the 1187–, 1271–, and 1307–Å windows).

The region of the O_2 spectrum below 1300 Å can then be loosely categorized as follows:

~ 1300 Å: air windows ($k \sim 20$ cm^{-1}).
1200–1100 Å: weak continuum ($k \sim 50$–100 cm^{-1}).
1100–1020 Å: increasing strength of dissociation continuum; complex spectrum. Rydberg series converging to X, O_2^+ should lie in this region; none have been confirmed.
1020–840 Å: intense diffuse Hopfield c–b bands of O_2^+. Rydberg series; ionization continua overlapped by dissociation continua ($k \sim 300$ cm^{-1}).
< 840 Å: sudden onset of strong continua; Rydberg series. Mainly continua, but with complicated structure down to 600 Å ($k > 300$ cm^{-1}). Absorption maximum at 800 Å; another at 500 Å.

The f-value for this region ($\lambda < 1300$ Å) is ~ 6 [245, 407, 1].[31] At 1094 Å, 1069 Å, and 1044 Å, Watanabe and

---

[30] Ogawa [304] has shown that Lyman-α wavelength does not coincide exactly with the maximum of this O_2 transmission window. This has important implications for atmospheric processes.

[31] Ladenburg et al. [245], 1100–160 Å, $f = 5.93$; Weissler and Lee [407], 1300–300 Å, $f = 6.1$; Aboud et al. [1], 909–100 Å, $f = 6.9$.

Marmo [401] observed absorption minima, with k-values somewhat pressure dependent. This was interpreted as indicating feeble but unresolved structure.

11.11. Miscellaneous (transition probability parameters)

a. O_2^+, $B\,^2\Sigma_g^-$

Doolittle et al. [117], studying photoionization of O_2 with (584–358 Å) photons, have observed possible predissociation of O_2^+, $B\,^2\Sigma_g^-$. Predissociation lifetime, short relative to the radiative lifetime which is estimated as 10^{-8} s, was assumed to explain the absence of the allowed transition $B\,^2\Sigma_g^- - A\,^2\Pi_u$.

b. O_2^-

Only crude estimates exist for the lifetime of O_2^-. Electron impact studies led Frost and McDowell [147] to estimate $\tau > 10^{-6}$ s. Conway [92] and Prasad and Craggs [317] estimated the lifetime of excited O_2^- against electron attachment of 1×10^{-9} s.

c. $(O_2)_2$

Dianov-Klokov has obtained crude estimates of the lifetime of the collision complex $(O_2)_2$. From band widths [108] he obtained a lower limit 0.3×10^{-13} s; the diffuseness of bands of the complex, hence the spacing of its energy levels, exceed the spacing of the a–X, O_2 bands which are characterized by $B_e \sim 1.44$ cm^{-1}, such that $\tau_{max} \leqslant \dfrac{1}{cB_e} \sim 2 \times 10^{-11}$ s [109].

d. Other

Smith [358] has considered the effect of autoionization on the relative intensity of vibrational peaks in photoelectron spectroscopy. Qualitative calculations are given for O_2 transitions to the O_2^+ ground state (compare ref. [90]). The striking effects of autoionization are illustrated in experiments by Branton et al. [59], who used photon energies below 21 eV (namely, the neon doublet, 736 Å and 744 Å).

Jonathan et al. [222] have observed the photoelectron spectrum of O_2, $a\,^1\Delta_g$ (to O_2^+, $X\,^2\Pi_g$). The relative intensity distribution was qualitatively different from that obtained in the PES of O_2, $X\,^3\Sigma_g$ to the same state of the ion.

Studies by Freund [145] on molecular translational spectroscopy suggest that the $^5\Pi_g$ state reported by Lichten [252] at ~ 12 eV likely has a lifetime $< 10^{-4}$ s (Lichten had assumed a lifetime of $> 10^{-3}$ s). Freund, in addition, obtained qualitative information on a repulsive $^3\Pi_u$ Rydberg state of O_2 having energy 22–23 eV.

Ogawa [305] has observed six absorption bands originating in the $a\,^1\Delta_g$ state (a new band was found at 1455.0 Å). Tentative absorption coefficients were ob-

tained (1486.0–1408.5 Å). Preliminary cross sections for excitation of excited states of O_2 have also been obtained by Konishi et al. [235].

12. Miscellaneous

(a) Bridge and Buckingham [60] have determined the depolarization ratio at one atm and 20 °C; $\rho_0 = (3.09 \pm 0.02)10^{-2}$. Polarizability is 1.598 Å^3 for 6328 Å.

(b) Molecular quadrupole moments (definitions and numerical values) have been summarized most recently by Birnbaum [44]. The various measurements for O_2 disagree by up to a factor of 10.

(c) Schnepp and Dressler [348] and Boursey et al. [50] have observed the O_2, $B-X$ transition in solid matrices.

(d) Ben-Aryeh [36] has discussed emissivity of the $B-X$ transition for optically thick systems (where there are departures from Beer's law). (See also Blake et al. [46].)

(e) Akimoto and Pitts [6] have observed O_2, $a-X$, 0–0 emission, together with simultaneous transitions in solid oxygen. The lifetime of O_2 ($^1\Delta_g$) was estimated as $< 10^{-6}$ s at liquid helium temperature.

13. Summary and Conclusion

For many electronic states of O_2 only a few vibrational levels have been studied under high resolution. Only fragmentary data exists for some states, and in some instances, the vibrational quantum numbering is uncertain. Isotopic studies can be used in principle to provide the unique quantum numbering, but the forbidden transitions of interest are inherently weak. The states which are incompletely studied include $a\,^1\Delta_g$, $c\,^1\Sigma_u^-$, $C\,^3\Delta_{ui}$, and $A\,^3\Sigma_u^+$. For study of all but the $a\,^1\Delta_g$ state very long absorption paths are necessary. A potentially strong charge transfer transition $C\,^3\Delta_u - b\,^1\Sigma_g^+$ has not been observed; a large Δr_e is a complicating factor.

The apparent irregularities above $v = 15$ in the left limb of the potential curve of the $B\,^3\Sigma_u^-$ state are still under study. Potential curves calculated with CI wavefunctions indicate that the repulsive $^3\Pi_u$ state crosses the left limb of the $B\,^3\Sigma_u^-$ state. Predissociation of the $B\,^3\Sigma_u^-$ state, primarily arising from spin-orbit coupling, likely involves more than one repulsive state. The answers to remaining questions concerning predissociation of the B state may depend on more careful examination of the J dependence of measured line widths.

Several states of O_2^+ need further study: $C\,^2\Delta_g$, $c\,^4\Sigma_u^-$, $B\,^2\Sigma_g^-$. From among these only for the $c\,^4\Sigma_u^-$ state has there been any rotational analysis. An electric dipole allowed transition $B\,^2\Sigma_g^- - A\,^2\Pi_u$ has not been observed, but this $\pi_u - \sigma_g$ transition is not inherently strong.

Pronounced changes in spin splitting are likely near the dissociation limits of states $B\,^3\Sigma_u^-$ (O_2) and $A\,^2\Pi_u$ (O_2^+); the former had been discussed some years ago.

The most reliably measured of all oxygen transitions remains $b\,^1\Sigma_g^+ - X\,^3\Sigma_g^-$, with $\Delta_2 F$'s disagreeing by at most 0.005 cm^{-1}. Recently computer least squares refitting of these measurements which were published in 1948 has demonstrated that the early graphical fitting gave too small estimates of uncertainties in B_v values and band origins.

TABLE 1. *Molecular constants, electron configurations, and*

State	T_0	T_e	M. O. Configuration $(2\sigma_g)(2\sigma_u)(3\sigma_g)(1\pi_u)(1\pi_g)(3\pi_u)$ Ry	Diss. products O+O	D^0	D^e	k_e (10^5 dyne/cm)	ω_e	$\omega_e x_e$	$\omega_e y_e$	$\omega_e z_e$	r_e (Å)
$c^4\Sigma_u^-$	198098		1 2 4 2					[1540]				
?	172000 H											
$B^2\Sigma_g^-$	163702 H	163917	1 4 2	$^3P_g + {}^2D_u$	14203	14775	6.30	(1156)	(22)			
$C^4\Delta_g$	158700 H		1 4 2	$^3P_g + {}^2D_u$	19200							
$b^4\Sigma_g^-$	146556	146759	1 4 2	$^1D_g + {}^4S_u$	20408	21002	6.75	1196.913	17.13456			1.2796516
$A^2\Pi_u$	137435	137776	2 3 2	$^3P_g + {}^4S_u$	13662	14108	3.80	898.17	13.568			1.408220
$a^4\Pi_{ui}$	129889	130161	2 3 2	$^3P_g + {}^4S_u$	21208	21723	5.05	1035.534	10.32194			1.3816042
$X^2\Pi_g$	97365	97204	2 2 2 4 1	$^3P_g + {}^4S_u$	53732	54681	17.10	1905.13	16.2818			1.117123

Rydberg series:

$c^4\Sigma_u^-(O_2^+) \leftarrow X^3\Sigma_g^-(O_2)$: $\sigma = 198125$ $-R/(n-0.159)^2$, n=3, ...(595–510 Å) ; $\sigma = 198125$ $-R/(n-0.955)^2$, n=3, ...(595–510 Å)

$B^2\Sigma_g^-(O_2^+) \leftarrow X^3\Sigma_g^-(O_2)$: $\sigma = 163602$ $-R/(n-0.658)^2$, n=4, ...(650–600 Å)

$b^4\Sigma_g^-(O_2^+) \leftarrow X^3\Sigma_g^-(O_2)$: $\sigma = 146568$ $-R/(n-1.679)^2$, n=5, ...(730–660 Å)

State	T_0	T_e	M. O. Configuration	Diss. products	D^0	D^e	k_e	ω_e	$\omega_e x_e$	$\omega_e y_e$	$\omega_e z_e$	r_e
$^1\Pi_u$	89244.9											
$^1\Delta_u$	88278.4											
$^3\Sigma_u^+$	87369.1		4 1 $np\pi_u$									
$a'\Sigma_u^+$	76262.4	76089	4 1 $np\pi_u$				17.50	(1927)	(19)			
$\beta^3\Sigma_u^+$	75450	75263	4 1 $np\pi_u$				18.05	(1957)	(19.7)			
$B^3\Sigma_u^-$	49358.15	49794.33	2 3 3	$(^3P_g + {}^1D_g)Pr$	7770	8121	2.37	709.05770	10.614080	−.059212435	−.023974994	1.6042799
$A^3\Sigma_u^+$	35007.15	35398.70	2 3 3	$^3P_g + {}^3P_g$	6253	6649	3.01	799.08	12.16	−.550		1.52153
$C^3\Delta_{ui}$	34319	34735	2 3 3	$^3P_g + {}^3P_g$	6941	7312	2.65	(750)	(14)			(~1.5)
$c^1\Sigma_u^-$	32664.1	33058.4	2 3 3	$^3P_g + {}^3P_g$	8596	8989	2.97	794.29	12.736	−0.2444	.00055	1.5174
$b^1\Sigma_g^+$	13120.9085	13195.314	2 4 2	$^3P_g + {}^3P_g$	28139	28852	9.67	1432.6661	13.9336	−.0143		1.2268431
$a^1\Delta_g$	7882.39	7918.11	2 4 2	$^3P_g + {}^3P_g$	33378	34130	10.73	(1509.3)	(12.9)			1.21569
$X^3\Sigma_g^-$	0	0	2 2 2 4 2	$^3P_g + {}^3P_g$	41260	42047	11.77	1580.1932	11.980804	.047474736	−1.2727481(−3)	1.2075358

General: (a) Where indicated, the standard deviation of each coefficient is less than 5 units in the last non-underlined or non-italicized digit. Because the coefficients are correlated. additional digits are included to minimize roundoff error. Where appropriate, an entry includes, in parentheses. the power of 10 by which it is to be multiplied.

(b) ZPE = G(0)+Y₀₀, both obtained from a low order polynomial fitted to several levels where appropriate.

(c) Values of k_e are arbitrarily given to two decimal places.

(d) Values of r_e are listed to many digits only to permit fitting for the purpose of numerically integrating the Schrödinger equation. Not all digits are significant in the least squares sense.

In the published literature to date. rotational constants for electronic states of O_2 have all been determined assuming the values for B_0 and D_0 for the ground state as given by Babcock and Herzberg [24] in 1948. A reexamination of these ground state coefficients is found in Appendix C.

State:

$X^3\Sigma_g^-$: (a) Molecular constants fitted to $v \le 21$.

(b) $\delta_e = -2.846158$ (−6).

(c) $Y_{00} = .275$.

(d) The X state deviates from pure Hund's case b with increasing J, as expected [374]. since rotational energy increases with J.

$a^1\Delta_g$: (a) Molecular constants fitted to $v \le 1$.

(b) ω_e and $\omega_e x_e$ have been estimated [191], since the $v = 1$ level is the highest observed under high resolution. Absorption from condensed oxygen includes $a-X$ bands with $v' = 2,3,4$ [86, 249].

(c) $Y_{00} = .23$.

(d) Miller [277] suggests a small correction to B_0 for the effect of electronic mass carried along by the nuclei during molecular rotation: this would alter the quoted values of B_r and r_e.

(e) Reproductions of $a-X$ spectra. ref. [191, 277].

$b^1\Sigma_g^+$: (a) Molecular constants fitted to $v \le 3$.

(b) $Y_{00} = .129$.

(c) Reproduction of $b-X$ spectra. ref. [24].

(d) $b-A$, $\sigma_H(0-0) = 5240$.

$c^1\Sigma_u^-$: (a) Bands only having $v = 0, 6-11$ have been studied; observed $c-X$ bands lie far from the 0–0 band.

(b) Misprint in value of α_r given by Degen [103] is corrected.

(b) $Y_{00} = -.84$.

(d) c state T_0 is calculated.

(e) Reproductions of $c-X$ spectra, ref. [189, 103].

$C^3\Delta_{ui}$: (a) $\Delta G(5\frac{1}{2}) = 611.16$ for $^3\Delta_3$. No other vibrational quantum is known from band origins.

(b) If the C state really lies above the c state, then because the states are isoconfigurational, it could be guessed that they have similar vibrational constants. For both states a linear Birge-Sponer extrapolation gives too high dissociation energies.

(c) For the 6–0 band $^3\Delta_3-^3\Delta_2 = 145.91$ $(A = -72.96)$.

(d) The missing lines near the origin are not uniquely established so that identification of this state as $^3\Delta_u$ follows only from electron configuration arguments. The electron configuration requires an inverted state $^3\Delta_{ui}$ [189]. The higher energy subband of the 6–0 $C-X$ band has been identified as $^3\Delta_3$ because its effective B_r is larger than for $^3\Delta_2$, implying a normal $^3\Delta$ state. The same argument is consistent with a $^3\Delta_1$ sublevel at higher energy. i.e., the electronic state is inverted.

(e) Vibrational numbering in this state is uncertain.

(f) Identification of $C-a$ bands is only tentative [81].

(g) An approximate potential curve was drawn by Gilmore [161].

(h) Reproduction of $C-X$ spectra. ref. [189].

(i) $\sigma_H(0-0)$ (high pressure bands) = 34319.

$A^3\Sigma_u^+$: (a) Molecular constants are fitted to $v \le 4$.

(b) Formula fitted to D_r's includes a term: $+0.10(v+\frac{1}{2})^2(10^{-6})$.

(c) The A state deviates from Hund's case b and approaches case c near the dissociation limit.

dissociation products for the electronic states of O_2 *and* O_2^+*

Be	αe	γe	De (10⁻⁶)	βe (10⁻⁶)	Zero pt. energy	Observed transition	System name	Spectral region (Å)		Hund's coupling case	v max. (OBS.)	References
[1.557]						c → b V	Hopfield	2360	– 1940	b	2	250, 89
					(572)					b	6	417, 125
1.287297	.02206747				594.19	b → a V	First Negative	8530	– 4990	b	7	291, 408, 250, 9
1.06297	.0205830				446.0	A → X R	Second Negative	6530	– 1940	b	23	365, 52, 53, 42, 9
1.104320	.01545646				515.41					a — b	20	291, 408, 9
1.68912	.0195769				948.7					a	20	342, 42, 365, 52, 53, 9
												89
												417, 303
												417, 290
[1.451]						← c		1230			0	7
[1.446]						← c		1245			0	7
[1.706]	[28.0]					← x		1144.6		b	0	308
						a ← b V		1585	– 1535			7
1.699	.016				(960)	a ← X V		1280	– 1195	b	4	7, 308
(1.7)	(.02)				(974)	β → X V		1295	– 1180	b	5	7, 308, 369
.818975	.0119225	-6.30472 (-4)			351.20	B → X R	Schumann–Runge	5350	– 1750	b	21	99, 62, 302, 3
.91053	.01416	-.00097	4.79	-.30	(395.83)	A → X R	Herzberg I	4880	– 2430	b	11	187, 63
						C → a R	Chamberlain (High pressure) (Herzberg III)	4380 2925 2630	– 3700 – 2440 – 2570	c	11 11 6	61 182, 141 189
					(371 est.)	C ← X R						
0.9155	.01391	-.000740	[10.5]		393.09	c → X	Herzberg II	4790–4490, 2715–2540		b	11	189, 103
						b → a	Noxon	19080				301
1.4004796	.018169303	-4.2941920 (-5)	5.356	.077	712.977	b → X R	Atmospheric	9970	– 5380	b	5	24, 9
1.4263	.0171		[4.97]		(751.66)	a → X R	IR Atmospheric	15800	– 9240		1	191
1.445622	.01593268	6.406456 (-5)			787.382					b	27	99, 24, 62, 302, 9

(d) Triplet splitting of the A state, the reverse of the splitting in the ground state, has $F_3 > F_1 > F_2$ [187]; parameter λ is negative for the A state.

(e) $Y_{00} = -.60$.

(f) T_0 is calculated.

(g) Reproduction of A–X spectra, ref. [187, 104].

$B\,{}^3\Sigma_u^-$: (a) Molecular constants are from a computer least squares fit to levels $v \leq 13$. The entire set of coefficients in addition to those tabulated includes:

$Y_{50} = 2.2067951\ (-3),\ Y_{60} = -1.5990957\ (-4)$,

$Y_{70} = 4.4274814\ (-6)$ for vibrational term values, and

$Y_{31}(\delta_e) = 1.57426\ (-6),\ Y_{41} = 6.70586\ (-6)$,

$Y_{51} = -9.35318\ (-7),\ Y_{61} = 2.90100(-8)$ for B_r values.

(b) Coefficients fitted by Ackerman and Biaume [3] were obtained graphically.

(c) Position of $v=22$, the last level before dissociation has been calculated by Brix and Herzberg [62]. Fragmentary structure of the 22–0 band was observed, but the rotational assignments are uncertain.

(d) $Y_{00} = -0.66$.

(e) Low order coefficients fitted to $v \leq 4$ are as follows:

$\omega_e = 709.309,\ \omega_e x_e = 10.6468,\ \omega_e y_e = -0.138732$; also

$B_e = 0.81902,\ \alpha_e = 1.2055\ (-2),\ \gamma_e = -5.5619\ (-4)$.

(f) Reproduction of B–X spectra, refs. [99, 233, 62, 302, 306, 76, 175].

$\beta\,{}^3\Sigma_u^+$: (a) Alberti et al. [7] identified this state as ${}^1\Sigma_u^-$; Ogawa et al. [308] consider the evidence to favor ${}^3\Sigma_u^+$.

(b) T_0 is obtained from approximate ω_e, $\omega_e x_e$ and extrapolation to $v=0$.

(c) Electron configuration and vibrational quantum assignments are tentative.

$\alpha\,{}^1\Sigma_u^+$: (a) $\Delta G(\tfrac{1}{2}) = 1889.2$.

(b) Vibrational levels are perturbed; $\omega_e x_e$ is only approximate [7].

(c) Reproduction of α–X spectra, ref. [308].

(d) α–b, $\sigma_0(0-0) = 63141.5$.

${}^3\Sigma_u^+$: (a) D_0 is abnormally large relative to that of most other states of O_2. But D_r for the β and α states are $O(10^{-5})$ [308].

(b) Reproduction of ${}^3\Sigma_u^+$–X spectra, ref. [308].

${}^1\Delta_u$: (a) Vibrational quantum numbering is tentative.

(b) $\sigma_0(0-0)\ ({}^1\Delta_u$–$a) = 80396.0$.

${}^1\Pi_u$: (a) B_0 is derived from even J levels only: odd levels are perturbed.

(b) Vibrational quantum numbering is tentative.

(c) $\sigma_0(0-0)\ ({}^1\Pi_u$–$a) = 81362.5$.

$b(O_2^+)$–$X(O_2)$ Rydberg series: Reproduction of spectra, ref. [303, 371].

$B(O_2^+)$–$X(O_2)$ Rydberg series: Reproduction of spectra, ref. [303, 417, 371].

$c(O_2^+)$–$X(O_2)$ Rydberg series: Reproduction of spectra, ref. [89a].

O_2^+

$X\,{}^2\Pi_g$: (a) Vibrational constants fitted by the author to $v \leq 10$; rotational constants fitted by Lofthus (unpublished).

(b) $Y_{00} = 0.2$.

(c) $A \approx 200$ (see Albritton et al. [9] and the early determination by Stevens [365]).

(d) For some evidence of Λ-doubling see Stevens [365].

(e) The photoionization measurements of Samson and Cairns [342] as slightly modified by the isotopic measurements on the $A\,{}^2\Pi_u$–$X\,{}^2\Pi_g$ bands of O_2^+ by Bhale and Rao [20, 42] give 97265 cm⁻¹ or 12.059 eV. Uncertainty of the photoionization measurements was stated as ± 10 cm⁻¹ = ± 0.001 eV. A large uncertainty might be attached to this value say Dibeler and Walker [111], because of partially resolved autoionized bands in this region, as observed in an ionization efficiency curve. In addition, the thermal distribution at room temperature finds a peak population for $J=8$; the unresolved rotational envelope could introduce an uncertainty of ~ 17 cm⁻¹. The photoionization measurement is assumed to correspond to the ${}^2\Pi_{1/2}$ limit. The (hypothetical) ${}^2\Pi$ state without spin-orbit splitting would be 100 cm⁻¹ higher (the separation of the doublet levels in the O_2^+ ground state is ~ 200 cm⁻¹).

Footnotes to table 1—Continued

Nicholson [299] had obtained a value for IP(O$_2$) from ionization efficiency curves which is virtually the same as that of Samson and Cairns [342].

(f) v_{max}(PES) = 20 [90]; v_{max}(spectroscopy) = 16.

(g) Reproduction of photoelectron spectra, ref. [125].

$a\ ^4\Pi_{ui}$:
(a) This term value is determined from the position of the $b\ ^4\Sigma_g^-$ as deduced from Rydberg series [417], with an approximate correction for head-origin separation, and the 0–0 band origin for transition O$_2^+$, b–a.

(b) Molecular constants fitted to $v \leqslant 6$.

(c) A ($v=0$ to 6) varies monotonically from -47.92 to -48.05 [238]. (See also [408].)

(d) $Y_{00} = 0.22$

(e) v_{max}(PES) = 20 [125]; v_{max}(spectroscopy) = 8.

$A\ ^2\Pi_u$:
(a) The term value is derived from the assumed position of the $v=0$ level of $X\ ^2\Pi_g$ state without spin splitting plus the 0–0 origin [40070 cm^{-1}] calculated from the limited number of A–X band origins (table 24). A fit to the band heads locates the 0–0 doublet at 39979 and 40179 cm^{-1}. The extrapolated band origin for 0–0 does not lie quite midway between the extrapolated doublets (heads), and though based on few data points, is based on more reliable data than the band heads.

(b) $A = 8.2$ [365]. Λ-doubling is negligible in the measurements of Stevens [365].

(c) Vibrational constants fitted by the author to $v \leqslant 8$. Rotational constants fitted by Lofthus (unpublished) and Albritton et al. [9].

(d) $Y_{00} = 0.3$

(e) v_{max}(PES) = 16 [125].

(f) A–X, σ_0(0–0) = 40070; calculated.

(g) Reproductions of O$_2^+$, A–X spectra, refs. [221, 127, 42].

$b\ ^4\Sigma_g^-$:
(a) Term value derived from limit of Rydberg series [417], assuming band origins, based on an approximate correction to observed band head positions. The original data quoted uncertainty of ± 2 cm^{-1} (± 0.0002 eV). Band head measurements would give limit 146568 cm^{-1}.

(b) Molecular constants fitted by Albritton et al. [9] to $v \leqslant 3$.

(c) $Y_{00} = 0.02$

(d) v_{max}(PES) = 6 [125].

(e) σ_0(0–0) (O$_2^+$, b–a) = 16666.74

(f) Reproduction of O$_2^+$, b–a spectra, ref. [408].

$C\ ^2\Delta_g$:
The potential curve for this state has been estimated by Gilmore [161]. Judge [224] has recently observed fluorescence following illumination (photon impact) by 630 Å radiation. With 625 Å radiation (0.15 eV difference) the fluorescence pattern changed so that Judge assumed the position of the $^2\Delta_g$ state to be determined as 19.68 to within 0.15 eV. Lindholm [253] has identified a possible Rydberg series from among the energy-loss peaks observed by Geiger and Schröder [158]; the limit is at 19.96 eV.

$B\ ^2\Sigma_g^-$:
(a) Term value derived from Rydberg series limit [417]. (Al-Joboury et al. [11] first suggested that this state might be $^4\Sigma_u^-$, by analogy with corresponding states in N$_2$).

(b) Uncertainty in $\omega_e \sim \pm 5$; uncertainty in $\omega_e x_e \sim \pm 2$ [417]. Similar values were obtained from photoelectron spectroscopy [125]. There is no rotational analysis.

(c) $r_e \sim 1.34$ Å [161].

(d) Assuming identification of this state is correct, there should exist bands for $B\ ^2\Sigma_g^- \rightarrow A\ ^2\Pi_u$ with σ(0–0) $\sim$ 26160 cm^{-1} (3821.5 Å).

(e) v_{max}(PES) = 6 [90, 125].

(unclassified)
21.3 eV: The term value is the mean of electron impact measurements by Frost and McDowell [147] and Brion [61]. Sjögren and Lindholm [357] assumed that the state at 21.3 eV is not stable, but represents an ion-molecule reaction.

$c\ ^4\Sigma_u^-$:
(a) Rydberg series limit [417] for b state plus c–b, 0–0 position as extracted by LeBlanc [250] from the reassignment of the Hopfield bands. Rydberg series of Codling and Madden [89] give closely the same limit. Molecular constants for the b state as derived by LeBlanc [250b] are not entirely compatible with those derived by Nevin [291a], but clearly belong to the same state.

(b) $\Delta G(\frac{1}{2})$ from Rydberg series is 1540 [89].

(c) v_{max}(PES) = 2 [125].

(d) Reproduction of O$_2^+$, c–b spectra, ref. [250a].

Possible new states: Features tentatively identified as new states of O$_2^+$ have been observed in electron and photon impact experiments [262, 125, 340]. They occur at the following energies (eV): 23.5–23.9 (assumed to be $^2\Pi_u$ by Edqvist et al. [125]), 24.6, 27.3–27.9, 31.3, 34.1.

*Enlarged copies of table 1 may be obtained from the author upon request.

TABLE 2. *Electronic configurations for molecular oxygen*

Molecule	Electron configuration								States
	$(1\sigma_g)$	$(1\sigma_u)$	$(2\sigma_g)$	$(2\sigma_u)$	$(3\sigma_g)$	$(1\pi_u)$	$(1\pi_g)$	$(3\sigma_u)$	
O_2^+				1	2	4	2		$c\,{}^4\Sigma_u^-,\,{}^2\Sigma_u^-,\,{}^2\Delta_u,\,{}^2\Sigma_u^+$
					1	4	2		${}^2\Sigma_g^+,\,B\,{}^2\Sigma_g^-,\,C\,{}^2\Delta_g,\,b\,{}^4\Sigma_g^-$
					2	3	2		${}^2\Pi_{ui},\,{}^2\Pi_u,\,A\,{}^2\Pi_u,\,{}^2\Phi_{ui},\,a\,{}^4\Pi_{ui}$
					2	4	1		$X\,{}^2\Pi_g$
O_2					1	4	2	1	${}^1\Sigma_u^+,\,{}^1\Sigma_u^-,\,{}^1\Delta_u,\,{}^3\Sigma_u^+,\,{}^3\Sigma_u^-(2),\,{}^3\Delta_u,\,{}^5\Sigma_u^-$
					2	4	1	1	${}^1\Pi_u,\,{}^3\Pi_u$
					2	3	3		${}^1\Sigma_u^+,\,c\,{}^1\Sigma_u^-,\,{}^1\Delta_u,\,A\,{}^3\Sigma_u^+,\,B\,{}^3\Sigma_u^-,\,C\,{}^3\Delta_{ui}$
	2	2	2	2	2	4	2		$X\,{}^3\Sigma_g^-,\,a\,{}^1\Delta_g,\,b\,{}^1\Sigma_g^+$

$O({}^3P_g)+O({}^3P_g)$: $b\,{}^1\Sigma_g^+,{}^1\Sigma_g^+,\,c\,{}^1\Sigma_u^-,{}^1\Pi_g,{}^1\Pi_u,\,a\,{}^1\Delta_g,\,A\,{}^3\Sigma_u^+,{}^3\Sigma_u^+,X\,{}^3\Sigma_g^-,{}^3\Pi_g,{}^3\Pi_u,\,C\,{}^3\Delta_{ui},{}^5\Sigma_g^+(2),{}^5\Sigma_u^-,{}^5\Pi_g,{}^5\Pi_u,{}^5\Delta_g$
(The 2411, ${}^3\Pi_u$ state is repulsive. and predissociates $B\,{}^3\Sigma_u^-$.)

The 1421, ${}^1\Sigma_u^+$, ${}^1\Delta_u$ states are slightly bound, but not observed spectroscopically.

For O_2^+, the $C\,{}^2\Delta_g$ state is known from possible Rydberg series and fluorescence. (See footnotes to table 1.)

For O_2^- see sect. 2.4.

TABLE 3. *Band origins of the* a ${}^1\Delta_g$—X ${}^3\Sigma_g^-$ *atmospheric IR system (R)*

λ_0(Å)	σ_0(cm^{-1})	$v'-v''$	Ref.
(15800)	6327	0-1	385
12683.0	7882.39	0-0	191
10674.1	9365.89	1-0	191
(9240)	10820	2-0	86

0-1 band head observed in twilight emission by Vallance Jones and Harrison [385].

0-0, 1-0 band origins from high resolution measurements by Herzberg and Herzberg [191].

2-0 band head from liquid oxygen absorption measurements of Cho, Allin, and Welsh [86].

2-0,3-0,4-0 bands observed in solid oxygen by Landau, Allin,and Welsh [249]. These positions are shifted to higher wavenumber by ~110 cm^{-1}, relative to estimated gas phase positions. (See also Ellis and Kneser [126].)

TABLE 4. *Band origins of the* b ${}^1\Sigma_g^+$—X ${}^3\Sigma_g^-$ *atmospheric syst*

Isotope	λ_0 (Å)	σ_0 (cm^{-1})	$v'-v$
${}^{16}O_2$	7708.41	12969.2821	1-1
	7619.33	13120.9085	0-0
	6968.63	14346.076	2-1
	6882.47	14525.6609	1-0
	6369.80	15694.74	3-1
	6286.61	15902.4174	2-0
	5795.13	17251.0922	3-0
	5383.49	[a](13571.13)	4-0

Data from Babcock and Herzberg [24]; refitted using least squares by Albritton et al. [9].

[a] Obtained from fragmentary data by Ossenbrüggen [311].

| ${}^{16}O^{17}O$ | 7618.71 | 13121.978 | 0-0 |
| | 6891.67 | 14506.26 | 1-0 |

Data from Babcock and Herzberg [24].

| ${}^{16}O^{18}O$ | 7618.12 | 13122.986 | 0-0 |
| | 6899.96 | 14488.84 | 1-0 |

Data from Babcock and Herzberg [24].

TABLE 5. *Band heads of the* b $^1\Sigma_g^+ - X\ ^3\Sigma_g^-$ *atmospheric system (R)*

λ_H (Å)	σ_H (cm^{-1})	$v'-v''$	Ref.
(9970)	10027	0–2	240
(8803)	11357	2–3	196, 184
8697.8	11494.0	1–2	196, 184
(8623)	11594	0–1	226, 270
8103	12338	5–5	183
7987	12517	4–4	183
7879.17	12688.20	3–3	196, 184
7779.03	12851.54	2–2	196, 184
7683.85	13010.73	1–1	196, 184
7593.73	13165.14	0–0	196, 184
7240	13808	5–4	183
7141	14000	4–3	183
7043	14195	3 2	103
6953	14378	2–1	183
6867.2	14558	1–0	98
6276.6	15928	2–0	98

Presence of the 0–2 band in the night sky has been suggested by Dufay [121]; Krassovsky [240], using higher dispersion did not observe it. Findlay [138], did observe it in an afterglow from an oxygen discharge. Many bands (showing some rotational structure) were observed in CO-O_2 explosions by Hornbeck and Hopfield [196] and Herman et al. [184]. Most intense were 0–0 and 1–1. Herman et al. [183] produced many bands in a high frequency discharge through O_2 at atmospheric pressure. Some band head positions differed from earlier observations [196] by up to 5 Å. Curcio et al. [98] observed two bands in absorption by the earth's atmosphere. Observed wavelength of 0–2, 2–3, and 0–1 bands are uncertain; so are the identifications. A band head at 8597.8 Å has been identified as 0–1 [196, 184, 183], but lies far from its predicted position. The wavelength $\sim$ 8645 Å given by Kaplan [226] and Meinel [270] for the band labeled by them as 0–1 corresponds to the origin of that band; the head position given above was derived from this value.

TABLE 6. *Band origins of the* c $^1\Sigma_u^- - X\ ^3\Sigma_g^-$ *Herzberg II system (R)*

λ_0 (Å)	σ_0 (cm^{-1})	$v'-v''$
	(a) emission	
4791.4	20864.7	0–8
4491.5	22258.3	0–7

Data from Degen [103].

	(b) absorption	
2714.5	36828.75	6–0
2672.3	37409.55	7–0
2634.0	37954.11	8–0
2599.2	38461.30	9–0
2568.0	38929.70	10–0
2540.0	39357.80	11–0

Data of Herzberg [189].

Tentative v' values used are those of Degen [103], and are an increase of 5 over those provisionally used by Herzberg [189].

The broad Condon locus for this system results in weakening of the bands at longer wavelengths.

TABLE 7. *Calculated band origin wavelengths (Å) of the* c $^1\Sigma_u^- - X\ ^3\Sigma_g^-$ *Herzberg II system*

$v' \backslash v''$	0	1	2	3	4	5	6	7	8	9	10	11	12
0	3060.6	3213.7	3380.3	3562.0	3761.2	3980.3	4222.4	<u>4491.3</u>	<u>4791.5</u>	5128.8	5510.3	5945.2	6445.1
1	2990.3	3136.3	3294.7	3467.2	3655.6	3862.2	4089.7	4341.5	4621.4	4934.4	5286.5	5685.5	6141.0
2	2925.5	3065.1	3216.2	3380.4	3559.2	3754.8	3969.5	4206.2	4468.5	4760.4	5087.4	5455.8	5873.9
3	2865.8	2999.7	3144.3	3301.0	3471.3	3657.1	3860.5	4084.0	4330.8	4604.5	4909.7	5251.9	5638.2
4	2811.0	2939.6	3078.4	3228.4	3391.1	3568.2	3761.6	3973.5	4206.7	4464.5	4750.8	5070.6	5429.8
5	2760.6	2884.6	3018.1	3162.1	3318.1	3487.5	3671.9	3873.6	4094.9	4338.8	4608.7	4909.0	5245.0
6	2714.5	2834.2	2963.0	3101.8	3251.7	3414.2	3590.8	3783.4	3994.2	4225.9	4481.6	4765.0	5080.9
7	2672.3	2788.3	2912.9	3046.9	3191.4	3347.8	3517.4	3702.0	3903.6	4124.6	4367.8	4636.7	4935.2
8	2634.0	2746.6	2867.4	2997.1	3136.9	3287.8	3451.3	3628.8	3822.4	4034.0	4266.3	4522.4	4806.0
9	2599.2	2708.9	2826.2	2952.2	3087.7	3233.9	3391.9	3563.2	3749.6	3953.1	4175.9	4421.0	4691.6
10	2568.0	2674.9	2789.3	2911.9	3043.7	3185.6	3338.8	3504.7	3684.9	3881.2	4095.8	4331.3	4590.7
11	2540.0	2644.6	2756.4	2876.1	3004.5	3142.7	3291.7	3452.9	3627.7	3817.7	4025.2	4252.4	4502.2

Bands enclosed in the rectangle are those observed by Herzberg [189] in absorption. Underlined entries are those from afterglow emission studies by Degen [103], from whose publication this table was taken.

TABLE 8. (a) Band origins of the $C\,^3\Delta_u - X\,^3\Sigma^-$ Herzberg III system (R)

λ_0 (Å)	σ_0 (cm⁻¹)	$v'-v''$
2578.62	38768.79	6-0 $\left\{\begin{array}{l}F_3 \\ F_2\end{array}\right.$
2588.36	38622.88	
2619.93	38157.63	5-0 F_3

Data from Herzberg [189]. Vibrational quantum numbering is uncertain.

(b) Band heads of diffuse high-pressure bands (R)

2924	34190	
2913	34319	0-0
2904	34425	
2855	35016	
2842	35176	1-0
2832	35300	
2795	35768	
2783.9	35910	2-0
2769.1	36022	
2739.8	36488	
2729.9	36621	3-0
2720.7	36744	
2689.8	37166	
2679.3	37312	4-0
2671.6	37420	
2642.7	37829	
2632.7	37973	5-0
2626	38068	
2598.8	38408	
2590.3	38594	6-0
2582.4	38712	
2559.9	39052	
2553.5	39150	7-0
2537	39305	
2525.4	39596	
2517	39718	8-0
2510	39821	
2497.4	40030	
2488.7	40169	9-0
2482	40278	
2472.5	40433	
2465.1	40554	10-0
2456.5	40696	
....	....	11-0
2440	ª 40971	

Data from Herman [182] and (a) Finkelnburg and Steiner [141]. The quantum assignments by Herzberg [189] are tentative. These bandless absorption maxima were first observed by Finkelnburg and Steiner [141] in oxygen at pressures from 60-600 atm; path lengths were 0.2-2.6 m. These bands have not been observed at low pressures (below 1 atm). More recent measurements by Herman [182] extended this system to longer wavelength. Herman observed that these triplets increased in strength with increased pressure, while the $A-X$ bands which they overlap, disappeared. The center absorption maxima (strongest) correlated closely with the wavelengths of the $A-X$ bands. Herman observed, in addition, feeble structure in the region 2990–3017 Å, and around 3050 Å. "The spacing and weakness of this structure," said Herman, "made it impossible to tell whether this was a continuation of these triplets."

TABLE 9. Possible $^3\Delta_v \rightarrow {}^1\Delta_g$ bands

λ_H (Å)	$v'-v''$	Tentative identification
4378	5-5	$^3\Delta_1$
4326	5-5	$^3\Delta_3$
4317	3-4	$^3\Delta_3$
4244	4-4	$^3\Delta_1$
4240	6-5	$^3\Delta_2$
4221	4-4	$^3\Delta_2$
4215	6-5	$^3\Delta_3$
4135	1-2	$^3\Delta_1$
4127	5-4	$^3\Delta_1$
4114	3-3	$^0\Delta_1$
4107	5-4 / 1-2	$^3\Delta_2$ / $^3\Delta_2$
4090	3-3	$^3\Delta_2$
4086	5-4 / 1-2	$^3\Delta_3$ / $^3\Delta_3$
4071	3-3	$^3\Delta_3$
4031	6-4	$^3\Delta_1$
4009	6-4	$^3\Delta_2$
3985	6-4	$^3\Delta_3$
3887	3-2	$^3\Delta_3$
3866	3-2	$^3\Delta_2$
3861	5-3	$^3\Delta_3$
3844	3-2	$^3\Delta_3$
3813	6-3	$^3\Delta_1$
3792	6-3	$^3\Delta_2$
3771	6-3	$^3\Delta_3$
3698	5-2	$^3\Delta_1$

Data from Chamberlain [81]. Quantum numbering is tentative.

TABLE 10. Band origins of the $A\,^3\Sigma_u^+ - X\,^3\Sigma_g^-$ Herzberg I System

σ_0	$v'-v''$	σ_0	$v'-v''$
(35007.15)	0-0	39138.54	6-0
35780.06	1-0	39681.29	7-0
36523.85	2-0	40166.80	8-0
37234.84	3-0	40584.67	9-0
37910.23	4-0	40920.45	10-0
38546.26	5-0	41153.94	11-0

Data from Herzberg [187]; v' values are larger by unity than those used by Herzberg (see Broida and Gaydon [63]). 0-0 band position is calculated. The 1-0 band position is derived from relatively fragmentary data.

TABLE 11. *Band heads of the A–X system observed in emission (R)*

λ_H (Å)	σ_H (cm^{-1})	I	$v'-v''$	Ref.	λ_H (Å)	σ_H (cm^{-1})	I	$v'-v''$	Ref.
4880	20486	2	0–10		3292	30368	4	4–5	
4577	21835	5	0–9		3285	30433	7	2–4	
4421.9	22608.3	4	1–9	30	3257.1	30693.8	4	7–6	30
4309	23201	7	0–8		3225.0	30998.9	2	5–5	30
4281.1	23352.1	2	2–9	30	3211	31134	10	3–4	
4274.4	23388.8	2	4–10	30	3142	31818	7	4–4	
4170	23974	6	1–8		3080	32458	....	5–4	
4064	24599	5	0–7		3066	32606	5	3–3	
4044*	24721	2	2–8	30	3026	33037	3	6–4	
4041.2	24738.4	2	4–9	30	3002	33301	5	4–3	
3938	25386	7	1–7		2945	33946	5	5–3	
3842.2	25435.1	2	3–8	30	2931	34108	1	3–2	
3840	26034	5	0–6		2895	34532	6	6–3	
3829	26109	8	2–7		2873	34797	2	4–2	
3771.2	26509.5	2	7–9	30	2850	35077	5	7–3	
3737.7	26746.6	4	5–8	30	2820	35451	3	5–2	
3734	26773	8	1–6		2775	36025	3	6–2	
3726.1	26829.9	2	3–7	30	2734	36566	5	7–2	
3657*	27337	2	6–8	30	2696	37081	4	8–2	
3634.6	27505.3	2	4–7	30					
					2667	37484	2	9–2	
3633	27518	8	2–6		2644	37810	1	10–2	
3552.5	28141.4	4	5–7	30	2622	38127	3	7–1	
3542	28225	8	{3–6 {1–5		2588	38628	2	8–1	
3479.3	28733.6	4	6–7	30	2563	39005	1	9–1	
3459*	28902	2	4–6	30					
3453	28952	8	2–5						
3414.7	29276.4	4	7–7	30					
3370	29665	10	3–5						
3366.5	29695.7	2	1–4	30					
3315.7	30151.0	2	6–6	30					

Band head wavelengths are from Broida and Gaydon [63] unless otherwise indicated. Experimental band positions are uncertain by 2–5 angstroms. Band origins are given for observations of Barth and Kaplan [30]. These were calculated by a formula of Herzberg [187]. Laboratory afterglow intensities are from Broida and Gaydon supplemented by those of Barth and Kaplan.

*Means wavelength from Broida and Gaydon and intensity from Barth and Kaplan. Numerous additional bands have been attributed to this system. with only quantum assignments suggested but no wavelengths reported. See refs. [29, 80, 102].

TABLE 12. Band origins of the B $^3\Sigma_u^-$—X $^3\Sigma_g^-$ Schumann-Runge system (R)

(a) emission

λ₀ (Å)	σ₀ (cm⁻¹)	v'—v''	Ref	λ₀ (Å)	σ₀ (cm⁻¹)	v'—v''	Ref.	λ₀ (Å)	σ₀ (cm⁻¹)	v'—v''	Ref.
5345.61	18701.74	5–27	183	3500.0	28563.5	2–16	256	2527.6	39551.1	3–8	136
5332.1	18749.1	2–25	183	3433.4	29117	1–15	324	2521.9	39641	1–7	324
5155.7	19390.6	3–25	183	3370.1	29664.6	0–14	256	2488.7	40170	4–8	324
5064.8	19738.6	2–24	183	3356.8	29781.7	2–15	256	2480.4	40304.6	2–7	134, 395
4905.3	20380.4	3–24	183	3293.7	30352	1–14	324	2478H	40343	0–6	278
4816.8	20754.9	2–23	183	3232.9	30923.0	0–13	256	2441.5	40945.9	3–7	136
4672.4	21396.3	3–23	183	3223.0	31018	2–14	324	2405.1	41566	4–7	324
4586.6	21796.5	2–22	183	3162.5	31611	1–13	324	2396.1	41722.3	2–6	136
4503.5	22198.7	1–21	183	3104.3	32204.4	0–12	256	2391H	41811	0–5	278
4455.6	22437.4	3–22	183	3039.4	32892.2	1–12	134	2371.4	42156	5–7	324
4422.9	22603.3	0–20	183	2983.4	33508.9	0–11	134	2359.8	42363.6	3–6	136
4372.6	22863.3	2–21	256	2979.0	33559	2–12	324	2331H	42887	0–4	278
4292.4	23290.6	1–20	256	2923.4	34197.3	1–11	134	2325.8	42982.4	4–6	136
4214.7	23719.8	0–19	256	2869.8	34835.7	0–10	134	2316.1	43162.6	2–5	136
4173.2	23955.9	2–20	256	2867.6	34862	2–11	324	2294.3	43572.4	5–6	136
4095.9	24407.8	1–19	256	2814.3	35522.7	1–10	134	2282.2	43804.1	3–5	136
4021.1	24861.6	0–18	256	2762.7	36185.7	0–9	136	2265.0	44136	6–6	324
3987.3	25072.4	2–19	256	2762.5	36188.3	2–10	136	2250.5	44420.5	4–5	136
3912.8	25549.8	1–18	256	2711.2	36872.8	1–9	134	2221.0	45011.2	5–5	136
3841.1	26026.7	0–17	256	2663.2	37537.9	2–9	134	2193.6	45573.3	6–5	136
								2178.6	45887	4–4	324
3742.2	26714.6	1–17	256	2661.8	37557	0–8	324				
3673.2	27216.2	0–16	256	2618.6	38177	3–9	324	2168.1	46108.3	7–5	136
3651.2	27380	2–17	324	2613.9	38245.2	1–8	134	2151.0	46476.0	5–4	136
3583.0	27901.6	1–16	256	2569.3	38910.1	2–8	134	2144.5	46616	8–5	324
3516.6	28428.7	0–15	256	2567H	38944	0–7	278	2125.2	47040	6–4	324
								2101.3	47574	7–4	324
								2079.2	48080	8–4	324

Herman, Herman and Rakotoarijimy [183]. Fine structure is given for 1–21; 2–22, 23, 24, 25; 3–22, 23, 24. For some of these bands only moderate to high N values were observed (11 to 50). Wavelengths of band origins are included for 0–20, 3–25, 5–27, though no fine structure was published. Calculated positions of additional long-wavelength bands have also been given.

Lochte-Holtgreven and Dieke [256] observed no low-J lines for bands 2–15 and 2–16. For 0–11 they observed structure only for high J values [3061–3128 Å].

Rakotoarijimy, Weniger, Grenat [324] give only a Deslandres table of band orgin wavelengths, but no fine structure.

Feast [134].

Millon and Herman [278] list band heads only. Feast [133] lists possible alternative quantum assignments for several bands.

Feast and Garton [136].

Waelbroeck and Bauer [395] resolved rotational structure in the 2–7 band in an especially intense source of the B–X bands in emission. The 0–9 band has also been measured by Hebért and Nicholls [176]; measured line positions differ by several cm⁻¹ from the more extensive measurements of Feast and Garton [136]. Many bands which have been observed under low resolution (40 Å/mm) in an auroral spectrogram have been attributed to O_2. B–X. These identifications by Vegard and Kvifte [390], with many bands assigned $v'' > 20$, are uncertain.

TABLE 12. *Band origins of the* B $^3\Sigma_u^-$ — X $^3\Sigma_g^-$ *Schumann-Runge system* (R) — Continued

(b) absorption

λ_0 (Å)	σ_0 (cm^{-1})	$v'-v''$	Ref.	λ_0 (Å)	σ_0 (cm^{-1})	$v'-v''$	Ref.	λ_0 (Å)	σ_0 (cm^{-1})	$v'-v''$	Ref.
4671.73	21399.36	3–23	142	2282.2	43804.1	3–5	136	1924.5	51962.0	10–2	306
4586.16	21798.63	2–22	142	2250.5	44420.5	4–5	136	1924.19	51969.81	4–0	3
4502.98	22201.29	1–21	142	2220.8	45014.1	5–5	302	1919.37	52100.4	7–1	99
4455.02	22440.34	3–22	142	2193.5	45574.7	6–5	302	1910.2	52350.2	11–2	306
4372.19	22865.41	2–21	142	2178.7	45885	4–4	302	1902.54	52561.39	5–0	3
4292.08	23292.18	1–20	142	2168.1	46108.8	7–5	302	1901.1	52600.0	8–1	306
4214.80	23719.24	0–19	142	2150.9	46476.9	5–4	302	1897.7	52695.1	12–2	306
4172.99	23956.88	2–20	142	2144.9	46608.4	8–5	302	1887.0	52995.5	13–2	306
4095.67	24409.14	1–19	142	2125.3	47038.0	6–4	302	1884.5	53065.3	9–1	306
4021.82	24857.34	0–18	142	2123.6	47074.0	9–5	302	1882.43	53122.79	6–0	3
3987.36	25072.16	2–19	142	2110.2	47373.0	4–3	302	1877.9	53250.9	14–2	306
3912.72	25550.43	1–18	142	2104.4	47504.7	10–5	302	1869.4	53494.0	10–1	306
3841.02	26027.37	0–17	142	2101.4	47572.6	7–4	302	1863.72	53656.27	7–0	3
3742.11	26715.30	1–17	142	2084.3	47963.2	5–3	302	1855.9	53882.8	11–1	306
3723.74	26847.09	3–18	142	2079.6	48071.8	8–4	302	1846.51	54156.28	8–0	3
3673.07	27217.43	0–16	142	2060.2	48524.0	6–3	302	1844.1	54228.4	12–1	306
3582.39	27906.36	1–16	142	2059.6	48537.3	9–4	302	1833.9	54529.7	13–1	306
3568.96	28011.37	3–17	142	2041.6	48966.2	10–4	302	1830.76	54622.17	9–0	3
3516.11	28432.39	0–15	142	2037.7	49059.2	7–3	302	1825.3	54704.0	14–1	306
3499.30	28568.97	2–16	142	2033.64	49157.10	2–1	76	1818.4	54993.8	15–1	306
3369.98	29665.25	0–14	142	2025.5	49355.1	11–4	302	1816.50	55050.90	10–0	3
3356.81	29781.63	2–15	142	2025.36	49358.15	0–0	3	1808.4	55297.1	17–1	306
3232.85	30923.53	0–13	142	2020.6	49473.6	5–2	302	1805.1	55398.1	18–1	306
3223.11	31016.98	2–14	142	2017.2	49558.0	8–3	302	1803.79	55438.90	11–0	3
3162.40	31612.40	1–13	142	2007.46	49798.09	3–1	76	1792.61	55 84.57	12–0	3
3157.40	31662.46	3–14	142	1999.0	50023.8	9–3	302	1782.99	56085.47	13–0	3
3104.31	32203.93	0–12	142	1998.6	50034.2	6–2	302	1774.92	56340.47	14–0	62
3097.54	32274.32	2–13	142	1998.17	50045.68	1–0	3	1768.33	56550.54	15–0	62
3039.76	32887.77	1–12	142	1983.60	50413.34	4–1	99	1763.06	56719.50	16–0	62
2983.50	33507.90	0–11	142	1982.0	50453.5	10–3	302	1758.94	56852.41	17–0	62
2613.9	38245.8	1–8	181	1977.6	50567.1	7–2	306	1755.79	56954.54	18–0	62
2569.2	38911.2	2–8	181	1971.97	50710.83	2–0	3	1753.46	57030.18	19–0	62
2521.9	39640.6	1–7	181	1967.0	50840.1	11–3	306	1751.84	57082.83	20–0	62
2480.3	40306.0	2–7	181	1960.58	51005.26	5–1	99	1750.86	57114.77	21–0	62
2441.5	40945.9	3–7	136	1958.2	51067.0	8–2	306	(1750.5)	57127	22–0	62
2396.1	41722.3	2–6	136	1953.7	51185.4	12–3	306				
2359.8	42363.6	3–6	136	1947.33	51352.26	3–0	3				
2325.8	42982.4	4–6	136	1940.5	51533.8	9–2	306				
2316.1	43162.6	2–5	136	1939.25	51566.4	6–1	99				
2294.3	43572.4	5–6	136	1924.8	51953	15–3	31				

Herczog and Wieland [181]: $p=80$ atm, $T=1070$ °C. Rotational constants of Curry and Herzberg [99] were used.

Feast and Garton [136].

Ogawa [302]. Many bands observed by Ogawa had previously been reported by Rakotoarijimy, Weniger, and Grenat [324] and Feast and Garton [136].

Ogawa and Chang [306].

Fitzsimmons and Bair [142] observed numerous *band heads* (which are included in this table of origins) of vibrationally excited oxygen produced by secondary processes in flash photolysis of ozone. High *J* values were populated. Some of these had been produced earlier by the same photolysis by McGrath and Norrish [263]. New bands include 3–18, 1–16, 3–17, 3–14, 2–13. In addition, bands were observed at wavelengths longer than 4670 Å; these are tentatively

identified as 6–28, 4–27, 5–28, 6–29. More recently weak bands 0–17 and 1–17 were detected in flash photolysis of ozone [264], but no wavelengths were given. Head origin separation for these bands is about 1 cm^{-1}.

Carroll [76] observed three band heads.

Bass and Garvin [31] observed several band heads following photolysis of NO$_2$.

Ackerman and Biaume [3]. These extensive new measurements supersede the earlier work of Curry and Herzberg [99] and Knauss and Ballard [233].

Origin of the 22–0 band is predicted by a short extrapolation. Only fragments of this band, the last before dissociation, were observed by Brix and Herzberg [62].

TABLE 13. *Bands of the* $\beta\,^3\Sigma_u^+ \leftarrow X\,^3\Sigma_g^-$ *system* (V)

Origins [a]		
σ_0 (cm^{-1})	$v'-v''$	Ref.
79228	2-0	37
81072	3-0	37

Band heads [b]					
n	λ_H (A)	σ_H (cm^{-1})	I	$v'-v''$	ΔG
3	1293.31	77321.0	2	1-0	
Q	1292.52	77368.2	2		
					1868.7
	1262.97	79189.7	3	2-0	
	1262.14	79230.5	3		
					1841.7
	1234.09	81031.4	4	3-0	
	1233.43	81074.7	4		
	1205.38	82961.4	9	(4-0)	
	1204.54	83019.2	9		
	1182.32	84579.5	2	5-0	
	1181.64	84628.1	2		

[a] Data of Alberti et al. [37]. Bands labeled 2-0 and 3-0 had previously been observed by Tanaka [369] under low resolution (his progression *I*). Alberti et al. did not observe the 1292.5 Å band, but Ogawa and Yamawaki [308], did and gave reasons why this band was difficult to detect under high resolution. v' numbering is that of Ogawa and Yamawaki, which is one higher than that of Alberti et al. Rotational structure was diffuse and only partially resolved.

[b] Data of Tanaka [369]. These appear to belong to one term in a $X\,^2\Pi_g\ (O_2^+) \leftarrow X\,^3\Sigma_g^-$ Rydberg series. v' numbering of Ogawa and Yamawaki [308] is one unit higher than that originally suggested by Tanaka [369] and assumed by Alberti et al. [37]. Tanaka expected a strong predissociation of $v'=4$; the intensity for the band labeled 4-0 is irregular with respect to other bands in the progression; the band position is about 150 cm^{-1} larger than the expected position, so identification is uncertain.

TABLE 14. *Bands of the* $\alpha\,^1\Sigma_u^+ \leftarrow X\,^3\Sigma_g^-$ *system* (V)

λ_H (Å)	σ_0 (cm^{-1})	$v'-v''$
1279.5	78151.3	1-0
1250.0	80002	2-0
1222.1	81822.7	3-0
1196.4	83599.6	4-0

Data from Alberti et al. [7]. Misprints of 4-0 line positions and band origin have been corrected by Ogawa and Yamawaki [308]. The 2-0 band is diffuse; the others are sharp. The 0-0 band position ~ 1300 Å is overlapped by a strong continuum. Some of these bands had previously been observed under low resolution by Tanaka [369] (his progression II), but had not been identified. Observed bands are weak.

TABLE 15. *Bands of the* $\alpha\,^1\Sigma_u^+ \leftarrow b\,^1\Sigma_g^+$ *system* (V)

λ_H (Å)	σ_0 (cm^{-1})	$v'-v''$
1583.9	63141.5	0-0
1571.9	63625.9	1-1
1537.9	65031.0	1-0

Data from Alberti et al. [7]. The 1-0 band appears diffuse because of overlapping P and R branches; rotational structure of the other two is sharp.

TABLE 16. *Bands of the* $^3\Sigma_u^+ \leftarrow X\,^3\Sigma_g^-$ *transition*

λ_H (Å)	σ_0 (cm^{-1})	$v'-v''$
1144.6	87369.1	0-0

Data of Ogawa and Yamawaki [308].

TABLE 17. *Bands of the* $^1\Delta_u \leftarrow a\,^1\Delta_g$ *transition*

λ_H (Å)	σ_0 (cm^{-1})	$v'-v''$
1243.8	80396.0	0-0

Data from Alberti et al. [7]. Sharp rotational structure; strong P, R branches, but weak, head-forming Q branch. The upper state is likely ungerade, because the transition is strong.

TABLE 18. *Bands of the* $^1\Pi_u \leftarrow a\,^1\Delta_g$ *transition*

λ_H (Å)	σ_0 (cm^{-1})	$v'-v''$
1229.0	81362.5	0-0

Data from Alberti et al. [7]. Strong, only partially resolved P, Q, R branches. The upper state is perturbed.

TABLE 19. *Strong Rydberg series* b $^3\Sigma_u^-(O_2^+)$ ← X $^3\Sigma_g^-$ (O₂)

(0–0) band series

n	$\lambda(\text{Å})$[a]	I	$\sigma(\text{cm}^{-1})$	n^*	$\Delta G_{1/2}$
5	732.222	10	136 571	3.3131	1174
6	710.613	9	140 724	4.3333	1165
7	700.713	7	142 712	5.3347	1157
8	695.292	6	143 825	6.3247	1167
9	691.931	5	144 523	7.326	1170
10	689.696	5	144 992	8.344	1162
11	688.212	6	145 304	9.318	1164
12	687.133	7	145 532	10.29	1165
13	686.317	4	145 705	11.28	1162
14	685.678	4	145 841	12.29	1162
15	685.198	4	145 943	13.25	1162
16	684.838	7	146 020	14.15	1162
17	684.492	2	146 094	15.22	1167
18	684.211	3	146 154	16.3	1163
19	683.988	2	146 202	17.3	1161
20	683.805	2	146 241	18.3	1162
21	683.651	1	146 273	19.3	1163
22	683.520	1	146 301	20.3	1163
23	683.408	1	146 326	21.3	1163
24	683.312	0	146 346	22.2	1166
25	683.217	0	146 366	23.3	1161
26	683.139	0	146 383	24.4	1162
27	683.076	0	146 397	25.3	1162
28	683.011	0	146 410	26.4	1162
29	682.961	00	146 421	27.4	1163
30	682.906	00	146 433	28.5	
31	682.863	00	146 442	29.6	
∞	682.277±0.009		146 568±2		1162

(1–0) band series — $\Delta G_{3/2}$

n	$\lambda(\text{Å})$	I	$\sigma(\text{cm}^{-1})$	n^*	$\Delta G_{3/2}$
5	725.977	10	137 745	3.3152	1132
6	704.778	10	141 889	4.3343	1158
7	695.078	6	143 869	5.3310	1123
8	689.695	5	144 992	6.3305	1125
9	686.375	4	145 693	7.339	1122
10	684.211	3	146 154	8.343	1126
11	682.743	5	146 468	9.324	1128
12	681.676	6	146 697	10.31	1126
13	680.888	3	146 867	11.28	1134
14	680.260	4	147 003	12.28	1128
15	679.789	5	147 105	13.25	1130
16	679.433	3	147 182	14.15	1131
17	679.066	1	147 261	15.30	1128
18	678.809	1	147 317	16.3	1127
19	678.595	1	147 363	17.3	1130
20	678.412	1	147 403	18.3	1129
21	678.259	1	147 436	19.3	1130
22	678.131	1	147 464	20.3	1128
23	678.018	1	147 489	21.3	1128
24	677.911	0	147 512	22.4	1123
25	677.844	0	147 527	23.2	1126
26	677.760	0	147 545	24.3	1128
27	677.694	0	147 559	25.3	
28	677.635	00	147 572	26.3	
29	677.581	00	147 584	27.4	
∞	676.911±0.014		147 730±3		1128

(2–0) band series — $\Delta G_{5/2}$

n	$\lambda(\text{Å})$[a]	I	$\sigma(\text{cm}^{-1})$	n^*	$\Delta G_{5/2}$
5	720.063	7	138 877	3.3158	1096
6	699.071	3	143 047	4.3458	1131
7	689.695	5	144 992	5.3279	1086
8	684.384	0	146 117	6.3280	1092
9	681.130	3	146 815	7.330	1095
10	678.981	1	147 280	8.339	1096
11	677.525	2	147 596	9.327	1092
12	676.485	4	147 823	10.30	1089
13	675.673	2	148 001	11.32	1093
14	675.076	3	148 131	12.29	1095
15	674.606	4	148 235	13.27	1095
16	674.250	3	148 313	14.20	1101
17	673.905	1	148 389	15.31	1088
18	673.653	0	148 444	16.30	1093
19	673.431	0	148 493	17.4	
20	673.258	1	148 532	18.4	
21	673.102	1	148 566	19.4	
22	672.983	0	148 592	20.3	
23	672.872	0	148 617	21.3	
24	672.789	00	148 635	22.2	
25	672.707	00	148 653	23.2	
26	672.619	00	148 673	24.4	
∞	671.781±0.014		148 858±3		1090

(3–0) band series — $\Delta G_{7/2}$

n	$\lambda(\text{Å})$	I	$\sigma(\text{cm}^{-1})$	n^*	$\Delta G_{7/2}$
5	714.425	4	139 973	3.3168	1066
6	693.585	1	144 178	4.3612	
7	684.568	2	146 078	5.3250	1069
8	679.307	1	147 209	6.3290	1056
9	676.086	1	147 910	7.338	
10	673.963	1	148 376	8.355	
11	672.547	2	148 688	9.334	1060
12	671.538	3	148 912	10.29	1058
13	670.716	1	149 094	11.34	1054
14	670.127	1	149 226	12.33	1067
15	669.659	1	149 330	13.32	
16	669.281	0	149 414	14.34	
17	668.999	0	149 477	15.26	
18	668.733	0	149 537	16.3	
∞	666.898±0.027		149 948±6		1060

(4–0) band series

n	$\lambda(\text{Å})$	I	$\sigma(\text{cm}^{-1})$	n^*
5	709.026	0	141 039	3.3178
6				
7	679.593	0	147 147	5.331
8	674.466	0	148 265	6.326
9				
10				
11	667.790	0	149 748	9.332
12	666.801	0	149 970	10.28
13	666.011	0	150 148	11.30
14	665.367	0	150 293	12.39
∞	662.217±0.035		151 008±8	

[a] Estimated average error of the measurement is 0.007 Å for data in tables 19–22.
Data from Yoshino and Tanaka [417]. Series limit based on approximated band origins is 146556 cm⁻¹.

TABLE 20. *Weak Rydberg series* b $^4\Sigma_g^-(O_2^+) \leftarrow$ X $^3\Sigma_g^-(O_2)$

n	$\lambda(\text{Å})$	I	$\sigma(\text{cm}^{-1})$	n^*	$\Delta G_{1/2}$
(0–0) band series					
5	727.634	0	137 432	3.465	1150
6	708.483	0	141 147	4.497	1114
7	699.409	3	142 978	5.525	1096
8	694.845	3	143 917	6.428	1257
9	691.415	1	144 631	7.518	1169
10	689.366	1	145 061	8.520	1141
11	688.053	1	145 338	9.426	1165
12	686.955	2	145 570	10.46	1163
13	686.157	1	145 739	11.47	1165
14	685.521	1	145 874	12.53	1163
15	685.006	3	145 984	13.65	1150
16	684.719	2	146 045	14.43	1164
17	684.384	0	146 117	15.52	1163
∞	682.27 ± 0.10		146 570 ± 20		1160
(1–0) b band series					$\Delta G_{3/2}$
5	721.593	0	138 582	3.463	1154
6	702.931	2	142 261	4.478	1174
7	694.087	1	144 074	5.476	1133
8	688.830	1	145 174	6.547	1055
9	685.873	1	145 800	7.533	1103
10	683.988	2	146 202	8.463	
11	682.582	0	146 503	9.442	1140
12	681.510	1	146 733	10.47	1128
13	680.719	0	146 904	11.49	1140
14	680.102	0	147 037	12.55	1130
15	679.652	1	147 134	13.53	1131
16	679.307	1	147 209	14.46	1130
17	678.981	1	147 280	15.55	
∞	676.91 ± 0.09		147 730 ± 20		1130
(2–0) band series					
5	715.634	0	139 736	3.467	
6	697.179	0	143 435	4.495	
7	688.673	0	145 207	5.477	
8	683.857	0	146 229	6.453	
9	680.719	0	146 904	7.480	
10					
11	677.309	00	147 643	9.479	
12	676.311	0	147 861	10.45	
13	675.474	00	148 044	11.57	
14	674.914	00	148 167	12.54	
15	674.466	00	148 265	13.53	
16	674.130	00	148 339	14.45	
∞	671.77 ± 0.09		148 860 ± 20		

Data from Yoshino and Tanaka [417].

TABLE 21. *Strong Rydberg series* B $^2\Sigma_g^-(O_2^+)\leftarrow X^3\Sigma_g^-(O_2)$

n	$\lambda(\text{Å})$	I	$\sigma(\text{cm}^{-1})$	n^*	$\Delta G_{1/2}$	n	$\lambda(\text{Å})$	I	$\sigma(\text{cm}^{-1})$	n^*	$\Delta G_{/2}$
	(0–0) band series						(2–0) band series				$\Delta G_{5/2}$
4	(702.6)		142 329		1102	4	(692.1)		144 488		
5	651.349	6	153 528	3.284	1140	5	642.096	5	155 740	3.290	1014
6	633.903	6	157 753	4.295	1120	6	625.225	4	159 943	4.297	1040
7	625.797	6	159 796	5.310	1114	7	617.351	7	161 982	5.303	1029
8	621.308	3	160 951	6.315	1106	8	613.007	3	163 130	6.311	1028
9	618.622	4	161 650	7.312	1110	9	610.370	4	163 835	7.317	1019
10	616.867	4	162 110	8.301	1117	10	608.637	4	164 302	8.325	1025
11	615.596	5	162 444	9.339	1103	11	607.464	4	164 619	9.310	1023
12	614.742	5	162 670	10.31	1108	12	606.597	3	164 854	10.32	1023
13	614.070	1	162 848	11.33	1109	13	605.954	2	165 029	11.32	1020
14	613.567	2	162 981	12.34	1108	14	605.473	2	165 160	12.31	1028
15	613.182	3	163 084	13.32	1109	15	605.073	2	165 269	13.35	1018
16	612.879	3	163 164	14.28	1112	16	604.771	1	165 352	14.35	1017
17	612.642	4	163 228	15.20	1110	17	604.524	1	165 420	15.36	1010
18	612.392	1	163 294	16.4	1106	18	604.325	1	165 474	16.3	
19	612.234	2	163 336	17.3	1105	19	604.170	0	165 516	17.3	
20	612.085	2	163 376	18.3	1106	∞	602.827±0.015		165 885±4		1022
21	611.959	1	163 410	19.4							
22	611.848	1	163 439	20.4			(3–0) band series				
23	611.749	0	163 466	21.5							
24	611.667	0	163 488	22.6		5	637.941	3	156 754	3.288	
∞	610.866±0.025		163 702±7		1109	6	621.184	1	160 983	4.304	
						7	613.454	2	163 011	5.307	
	(1–0) band series				$\Delta G_{3/2}$	8	609.170	3	164 158	6.318	
						9	606.598	3	164 854	7.311	
4	(697.2)		143 431			10	604.863	2	165 327	8.333	
5	646.547	8	154 668	3.289	1072	11	603.710	1	165 642	9.315	
6	629.435	7	158 873	4.299	1070	12	602.856	1	165 877	10.32	
7	621.467	6	160 910	5.303	1072	13	602.234	1	166 049	11.31	
8	617.069	6	162 057	6.316	1073	14	601.730	1	166 188	12.35	
9	614.402	6	162 760	7.314	1075	15	601.360	0	166 287	13.33	
10	612.645	4	163 227	8.322	1075	16	601.072	3	166 369	14.29	
11	611.445	4	163 547	9.317	1072	17	600.853	0	166 430	15.17	
12	610.581	4	163 778	10.31	1076	∞	599.136±0.018		166 907±5		
13	609.917	3	163 957	11.33	1072						
14	609.425	4	164 089	12.33	1071						
15	609.039	4	164 193	13.32	1076						
16	608.733	3	164 276	14.31	1076						
17	608.502	1	164 338	15.23	1082						
18	608.271	1	164 400	16.3	1074						
19	608.121	0	164 441	17.2	1075						
20	607.969	0	164 482	18.3							
∞	606.756±0.011		164 811±3		1074						

Data from Yoshino and Tanaka [417]. Gilmore [161] assigned the O_2^+ state which is the series limit as most likely $^2\Sigma_g^-$. $n=4$ terms observed by Tanaka and Takamine [371].

TABLE 22. *Weak Rydberg series* $B\,^2\Sigma_{\bar{g}}$ $(O_2^+)\!\leftarrow\! X\,^3\Sigma_{\bar{g}}$ (O_2)

n	$\lambda(\text{Å})$	I	$\sigma(\text{cm}^{-1})$	n^*	$\Delta G_{1/2}$
		(0–0) band series			
7	624.877	0	160 031	5.471	1087
8					
9	618.482	1	161 686	7.386	1110
10	616.680	0	162 159	8.443	1101
11	615.462	0	162 480	9.491	1110
12	614.623	1	162 701	10.49	1112
13	613.956	1	162 878	11.57	1113
∞	610.87±0.12		163 700±30		1110

		(1–0) band series			$\Delta G_{3/2}$
7	620.665	1	161 118	5.452	1113
8	616.680	0	162 159	6.434	1069
9	614.265	1	162 796	7.383	1080
10	612.519	0	163 260	8.416	1079
11	611.286	0	163 590	9.484	1058
12	610.453	0	163 813	10.49	1089
13	609.791	1	163 991	11.58	1075
14	609.286	1	164 126	12.67	1079
15	608.908	0	164 228	13.74	1068
∞	606.76±0.11		164 810±30		1080

		(2–0) band series			$\Delta G_{5/2}$
7	616.406	2	162 231	5.475	969
8	612.642	4	163 228	6.418	1035
9	610.217	1	163 876	7.378	1026
10	608.498	1	164 339	8.407	
11	607.357	0	164 648	9.391	1036
12	606.423	0	164 902	10.53	
13	605.818	0	165 066	11.45	
14	605.310	00	165 205	12.64	
15	604.976	00	165 296	13.57	
∞	602.81±0.07		165 890±20		1010

		(3–0) band series			
7	612.746	1	163 200	5.443	
8	608.781	1	164 263	6.446	
9	606.423	0	164 902	7.403	
10					
11	603.559	00	165 684	9.483	
∞	599.16±0.07		166 900±20		

Data from Yoshino and Tanaka [417].

TABLE 23. Strong Rydberg series $c\,^4\Sigma_u^-(O_2^+) \leftarrow X\,^3\Sigma_g^-(O_2)$

(0–0) Band series			(1–0) Band series		
n	$\lambda(\text{Å})$	$\sigma(\text{cm}^{-1})$	n^*	n	$\lambda(\text{Å})$	$\sigma(\text{cm}^{-1})$	n^*

$^3\Pi \leftarrow {}^3\Sigma$ Transitions

n	$\lambda(\text{Å})$	$\sigma(\text{cm}^{-1})$	n^*	n	$\lambda(\text{Å})$	$\sigma(\text{cm}^{-1})$	n^*
4	542.28($\pm$0.1)	184 410	2.828	4	537.88($\pm$0.1)	185 920	2.825
5	524.68($\pm$0.1)	190 590	3.817	5	520.42($\pm$0.1)	192 150	3.822
6	517.13($\pm$0.05)	193 375	4.807	6	513.02($\pm$0.1)	194 920	4.81
7	513.02($\pm$0.1)	194 920	5.86	7	509.08($\pm$0.05)	196 433	5.83
8	510.79($\pm$0.05)	195 775	6.83	8	506.78($\pm$0.05)	197 324	6.85
9	509.23($\pm$0.05)	196 375	7.92	9	505.25($\pm$0.05)	197 922	7.93
10	508.32($\pm$0.05)	196 726	8.86	10	504.30($\pm$0.05)	198 295	8.95
11	507.63($\pm$0.05)	196 994	9.85	∞		199 665($\pm$30)	
12	507.14($\pm$0.05)	197 184	10.80				
∞		198 125($\pm$30)					

$^3\Sigma \leftarrow {}^3\Sigma$ Transitions

n	$\lambda(\text{Å})$	$\sigma(\text{cm}^{-1})$	n^*	n	$\lambda(\text{Å})$	$\sigma(\text{cm}^{-1})$	n^*
3	594.32($\pm$0.2)	168 260	1.917	3	589.04($\pm$0.2)	169 770	1.916
4	537.24($\pm$0.1)	186 140	3.026	4	532.89($\pm$0.1)	187 660	3.023
5	522.46($\pm$0.1)	191 400	4.040	5	518.29($\pm$0.05)	192 942	4.040
6	515.95($\pm$0.05)	193 817	5.047	6	511.92($\pm$0.05)	195 343	5.045
7	512.49($\pm$0.05)	195 126	6.05	∞		199 665($\pm$30)	
8	510.40($\pm$0.05)	195 925	7.06				
∞		198 125($\pm$30)					

Data from Codling and Madden [89]. Π series fitted by $\sigma = 198125 - \dfrac{R}{(n-1.159)^2}$; Σ series fitted by $\sigma = 198125 - \dfrac{R}{(n-0.96)^2}$.

TABLE 24. Band origins of the $A\,^2\Pi_u - X\,^2\Pi_g$ system of O_2^+

$\sigma_0(\text{cm}^{-1})$	$v'\ v''$	$\sigma_0(\text{cm}^{-1})$	$v'\ v''$
22809.3	0–10	30193.6	1–6
24388.5	0–9	38633.3	5–3
26001.1	0–8	39368.6	6–3
26872.4	1–8	41884.5	7–2
27645.4	0–7	42565.4	8–2
28517.3	1–7		

These band origins are published for the first time, having been obtained by a least squares fit to the data of Stevens [365] and Bozóky [52, 53] by A. Lofthus. Both Stevens and Bozóky published detailed line lists and rotational constants but not band origins.

TABLE 25. Band heads of the A²Πu—X²Πg system of O₂⁺ (R)

λH (Å)	σH (cm⁻¹)	I	v'-v''	Ref.	λH (Å)	σH (cm⁻¹)	I	v'-v''	Ref.
R2 6531.8	15305		0-15	71.255	4238.0	23589	0	1-10	135
R1					—	—			
—	—		1-15	237	4219.1	23695	0	3-11	221
6102.9	16381				4182.2	23904			71
—	—		4-16	71	4115.8	24290	8	0-9	221
5729.1	17450				4082.4	24488	8		
5678.3	17606		1-14	287	4092.0	24431		2-10	71
—	—				4059.9	24624			
5498.4	18182		0-13	287	—	—		4-11	71
5443.0	18367				4050.1	24684			
5364.2	18637		4-15	71	3972.0	25169		1-9	71
5308.6	18832				3943.6	25350			
—	—		3-14	71.135	3959.4	25249	6	5-11	221
5142.9	19439	3			3929.0	25446	7		
5154.8	19394		5-15	71	3959.4	25249	6	3-10	221
5102	19595	3		135	3929.0	25446	7		
5086.3	19655		0-12	287	3859.5	25903	8	0-8	221
5035.1	19855				3830.5	26099	8		
4877.6	20496		1-12	287	—	—		2-9	52
4826.3	20714				3814	26211			
—	—		3-13	71	3733.9	26774	8	1-8	221
4783.8	20898				3706.6	26971	8		
4803	20815	3	5-14	135	3727.5	26820	8	3-9	221
4760	21002				3700.5	27016	8		135
4720.8	21177		0-11	287	3653.0	27367	2	8-11	135
4678.6	21368				—	—			
—	—		2-12	71	3629.8	27542	8	0-7	221
4636.5	21562				3603.7	27741	7		
—	—		6-14	52	3620.1	27616	2	2-8	221
4599	21739				3594.5	27812	2		
4536.3	22038		*1-11	71	3567.7	28021	4	9-11	135
4495.9	22236				3541.9	28225	4		
—	—		*3-12	71	3517.7	28420	8	1-7	221
4466.5	22383				3494.2	28611	7		
4403.0	22705	4	0-10	221	—	—		10-11	135
4363.3	22912			127	3465.9	28844	1		
4368	22887		2-11	52	3421.2	29221	8	0-6	221
4331	23081				3397.8	29422	8		
4351.0	22977		4-12	71	3416.2	29264	2	2-7	221
4313.4	23177				3393.1	29463	4		
4348	22992		6-13	52	3351	29837	3	7-9	52.135
4311	23189				3330	30023			
4271.8	23403		*11-15	71	3334.2	29984		5-8	135
4237.0	23595				3312.7	30178			

TABLE 25. *Band heads of the* A $^2\Pi_u$–X $^2\Pi_g$ *system of* O$_2^+$ (R)—Continued

λ_H (Å)	σ_H (cm⁻¹)	I	$v'-v''$	Ref.	λ_H (Å)	σ_H (cm⁻¹)	I	$v'-v''$	Ref.
3322.6	30088	6	3–7	221	2839.7	35205	9	3–4	221
3300.3	30292	6			2823.7	35404	8		
3322.6	30088	6	1–6	221	2821.0	35438		8–6	255
3300.3	30292	6			2806.1	35626	3		221
3277	30504		8–9	52, 135	2776.7	36003	7	4–4	221
3257	30699	3			2761.9	36196	7		
—	—		11–10	135	2763.0	36182		2–3	247
3225.8	30991				2749.1	36365			
3231.2	30939	8	0–5	221	2720.0	36754	7	5–4	221
3210.8	31136	8			2705.3	36954	7		
3231.2	30939	8	2–6	221	2703.2	36982	2	3–3	255
3210.8	31136	8			2688.5	37184	2		221
—	—		7–8	135	2691.5	37143	1	8–5	135
3160.7	31629				2677.8	37333	1		
—	—	5	5–7	221, 255	2666.5	37491	4	6–4	221
3141.0	31820	5			2652.3	37692	4		
3148.1	31756		3–6	255	2646.7	37772	6	4–3	221
3127.9	31961				2632.7	37973	6		
3143.4	31803		1–5	247	2630.7	38001		2–2	247
3123.2	32009	5		221	2617.3	38196			
3113.6	32108	2	8–8	135	2617.3	38196		7–4	247
3095	32301	2			2602.6	38412			
3088.7	32367	5	6–7	135	2602.9	38407	4	10–5	135
3070.0	32564	5			2588.9	38615	4		
3071.3	32550		4–6	247	2594.3	38535	8	5–3	221
3052.5	32750				2581.0	38733	8		
3062.8	32640	8	2–5	221	2577.6	38784		3–2	247
3043.6	32846	8			2564.0	38990			
3022.8	33072	2	7–7	135	2562.5	39013	2	11–5	135
3005.0	33268	2			2548.1	39233			71, 255
2987.5	33463	8	3–5	221	2545.5	39273	7	6–3	221
2970.0	33660	7			2532.8	39470	6		
2980.0	33547		1–4	255	2526.8	39564		4–2	247, 221
2962.0	33751	4		221	2513.8	39768	3		
2937.1	34038	2	6–6	221	2500.6	39978	6	7–3	221
—	—				2488.3	40176	6		
2919.8	34239	8	4–5	221	2478.0	40343	4	5–2	221
2901.9	34450	7			2465.8	40543	2		
2907.1	34388	5	2–4	221	2458.6	40661	1	8–3	221
2890.3	34588	7			2446.9	40856	1		
2877.3	34745	3	7–6	135	2433.5	41081	3	6–2	221
2860.0	34955	3			2421.8	41279	2		
2854	35025		5–5	52	2392.6	41783	3	7–2	221
—	—				2381.0	41986	3		

TABLE 25. *Band heads of the* $A\,^2\Pi_u - X\,^2\Pi_g$ *system of* O_2^+ (R) — Continued

$\lambda_H(\text{Å})$	$\sigma_H(\text{cm}^{-1})$	I	$v'-v''$	Ref.	$\lambda_H(\text{Å})$	$\sigma_H(\text{cm}^{-1})$	I	$v'-v''$	Ref.
— 2371.8	— 42149		10-3	71	— 2097.1	— 47671		10-0	42
2354.3 2343.3	42462 42662	1 1	8-2	221	2090.3 2080.8	47824 48042		14-1	287
2330.3 2318.4	42900 43120	 1	6-1	247,221	— 2071.5	— 48260		11-0	42
2317.9 2307.2	43129 43329		9-2	127	2068.3 2059.7	48334 48536		15-1	287
2291.1 2280.5	43634 43837		7-1	127	— 2046.4	— 48850		12 0	42
2284.9 2274.6	43753 43950		10-2	127	2048.1 2039.8	48810 49009		16-1	71
— 2246.2	— 44506		8-1	127	— 2024.3	— 49385		13-0	42
2252.8 2243.5	44375 44559		11-2	287	2029.9 2022.0	49248 49440		17-1	71
2223.6 2213.0	44958 45174		9-1	127	2013.7 2005.9	49644 49837		18-1	71
— 2187.9	— 45692		13-2	71	— 1991.5	— 50213		19-1	71
— 2183.2	— 45789		10-1	127	1985 1977	50378 50582		20-1	71
2164.0 2155.3	46197 46383		11-1	287	— 1966	— 50865		21-1	71
2138.6 2128.4	46745 46969		12-1	287	— 1956	— 51125		22-1	71
— 2125.8	— 47026		9-0	42	— 1942	— 51493		23-1	71
2112.2 2103.7	47329 47520		13-1	287					

Data from Johnson [221], Ellsworth and Hopfield [127], Mulliken nd Stevens [287], Bozóky [52], Lal [247], Feast [135], Byrne [71], md Linton [255]. Band head measurements by different authors sometimes disagree by more than 1Å. Blending has also led to more than one possible quantum assignment for some bands. The v'' quantum numbering, one unit larger than that in general use, has recently been unequivocally determined from isotopic measurements on the A–X bands by Bhale and Rao[42].

Johnson [221]: Wavelengths assumed correct; his wavenumbers are not always consistent with these wavelengths.

Ellsworth and Hopfield [127]: For bands below 2300Å, vacuum wavelengths were published. For wavelengths above 2300Å, air wavelengths were published. In the above table air wavelengths are given above 2000Å.

Feast [135]: Mislabeled a band at 4218.3Å as the R_1 head of the 0–10 band. Johnson [221] had previously observed a head at 4219.1Å, the R_2 head of 3–11, which is likely the same feature. Feast used roughly the same intensity scale as Johnson, with a maximum of 9.

Byrne [71]: Vacuum wavelengths observed below 2000Å and listed above. Many-line structure in this region. An asterisk (*) indicates weak band and uncertain identification. Koval et al. [239], using high-energy electron bombardment of oxygen, produced some bands of this system. The pair of heads at 4772.5, 4725.0Å do not belong to the 5–13 transition as they had assumed. The band at 3160.7Å is possibly the R_2 head of the 5–7 band. Emission intensities measured photoelectrically by Robinson and Nicholls [334] are not much different from eye estimates given in the table.

The possibility of misidentifications can not be excluded. Comparison of the observed band positions with those calculated from the band head coefficients in Appendix D indicate two likely misidentification:

R_2, 1–12	20527 (calc);	20496 (obs.)	Ref. [71, 225]
R_1, 0–15	15506 (calc);	15541 (obs.)	Ref. [287]

TABLE 26. *Band origins of the* $b\,^4\Sigma_g^-\!-a\,^4\Pi_{ui}$ *First Negative system of* O_2^+ *(V)*

σ_0 (cm^{-1})	$v'-v''$	Ref.
11799.81	0–5	408
12053.09	1–6	408
12733.12	0–4	408
12963.91	1–5	408
13683.99	0–3	291c
13895.34	1–4	408
14657.67	0–2	291b
15651.82	0–1	291a
16666.74	0–0	291a
17829.34	1–0	291a
18957.77	2–0	291b

Data from Nevin [291a, b], Nevin and Murphy [291c], and Weniger [408]. Weniger's value for the 0–3 origin is 0.82 cm^{-1} larger than Nevin's value.

TABLE 27. *Band heads of the* $b\,^4\Sigma_g^-\!-a\,^4\Pi_{ui}$ *First Negative system of* O_2^+ *(V)*

λ_H (Å)	σ_H (cm^{-1})	I	$v'-v''$	Ref.
8527.1	11724		0–5	408
8347.3	11977		1–6	408
8240	12133		2–7	122
8110	12327		3–8	122
7899.7	12655		0–4	408
7757.8	12887		1–5	408
7700	12983		2–6	122
7650	13068		3–7	122
7347.7	13606		0–3	287
7235.0	13818		1–4	408
7150	13982		2–5	122
6856.3	14581		0–2	287
6770	14767		1–3	130
(6684)	14957		2–4	130
6419.2	15574	10	0–1	287
6351.1	15741	10	1–2	54
6291.9	15889	6	2–3	354
6232.7	16040	3	3–4	354
6177.2	16184	3	4–5	354
6026.4	16589	10	0–0	287
5973.5	16736	10	1–1	54
5925.7	16871	9	2–2	54
5883.5	16992	8	3–3	54
5847.4	17097	2	4–4	54
5814.4	17194	1	5–5	354
5631.9	17751	10	1–0	287
5597.6	17860	10	2–1	54
5566.7	17959	6	3–2	54
5540.8	18043	2	4–3	54
5520.9	18108	2	5–4	354
5295.7	18878	9	2–0	287
5274.7	18953	10	3–1	54
5259.2	19009	6	4–2	354
5251.2	19038	10	5–3	354
5241.0	19075	8	6–4	354
5234.7	19098	9	7–5	354
5005.6	19972	2	3–0	287
4998.6	20000	2	4–1	354
4992.6	20024	2	5–2	354

Data from Mulliken and Stevens [287], Bozoky and Schmid [54], Singh and Lal [543], Fan [130], Dufay et al. [122], and Weniger [408]. Intensities are from Singh and Lal. The most prominent heads (listed above) occur in the branch $^OQ_{24}$; at longer wavelength is a weaker head in branch $^SP_{24}$. Numerous other bands observed in aurorae have been attributed to this system by Vegard [390], but the identifications are uncertain. The band observed by Fan [130] at 6684Å is uncertain (excitation by high-energy electrons). A band at 7891.1Å, labeled 0–4 by Mulliken and Stevens [287], is possibly the $^SP_{24}$ head, or is misidentified. Bands labeled 1–3 (6756 Å) and 2–4 (6750 Å) by Dufay et al. [122], are misidentified (excitation by high-energy protons). Among a number of unclassified bands (table 30i) Bozóky [52] observed what can now be identified as 2–2, 4–3, 4–2, 5–3, and 7–5 bands of the $b-a$ system of O_2^+.

TABLE 28. *Band origins of the* c $^4\Sigma_u^-$ → b $^4\Sigma_g^-$ *system of* O⁺₂

σ_0 (cm⁻¹)	$v'-v''$
45080.3(4)	0-6
46071.5(3)	0-5
47097.1(1)	0-4

Data of LeBlanc [250]. The fine structure is given only in his thesis [250a].

LeBlanc's calculated iron line positions differed from the established wavelengths in the third decimal place. The rotational line positions were given to three decimal places in cm⁻¹ (one too many, even assuming that the band lines were as accurately known as the calibration standards). Kayser's tables were used for conversion to wavenumbers (these differ at ~ 2100 Å by ~ .006 cm⁻¹ from the Meggers tables). So the band positions [250a] are uncertain in the first or second decimal place in cm⁻¹. The last digit listed by LeBlanc is given in parentheses to focus attention on the uncertainty of his values.

TABLE 29. *Band heads of the* c $^4\Sigma_u^-$ → b $^4\Sigma_g^-$ *system of* O₂⁺ (V)

λ_H (Å)	σ_H (cm⁻¹)	I	$v'-v''$
2363.1	42317	0.02	0-9
2314.8	43200	0.17	0-8
2266.4	44123	0.50	0-7
2218.3	45080	0.90	0-6
2170.6	46070	0.66	0-5
2123.4	47094	0.46	0-4
2076.6	48156	0.37	0-3
2030.5	49249	0.25	0-2
1985.0	50378	0.17	0-1
1940.3	51538	0.15	0-0

Data of Tanaka, Jursa, and LeBlanc [370] who measured vacuum wavelengths. Intensities are densitometer readings on a logarithimic scale.

TABLE 30. *Miscellaneous unclassified bands*

(a)

	λ (Å)	σ (cm⁻¹)	I		λ (Å)	σ (cm⁻¹)	I		λ (Å)	σ (cm⁻¹)	I
H	1003.7	99630	3	*M'*	933.3	107150	8	*N*	826.0	121064	8
	993.0	100700	8		924.5	108170	9		819.9	121963	8
	983.1	101720	10		916.3	109130	8		814.1	122830	7
	972.6	102820	8		909.2	109990	6		808.6	123670	4
H'	985.8	101440	4	*I*	853.2	117200	3	*P*	810.8	123330	10
	975.3	102530	8		845.9	118212	5		802.1	124670	8
	965.4	103580	10		839.0	119195	6		793.9	125960	6
	956.1	104590	7		832.3	120145	4		786.1	127210	4
M	957.2	104470	8	*I'*	843.9	118500	2	*Q*	714.7	139924	2
	947.9	105500	10		836.6	119530	4				
	938.9	106510	9		829.6	120540	5	*W*	697.8	143300	5
	930.6	107460	7		823.0	121510	3				
	922.8	108360	3		816.6	122460	1				

Data from Price and Collins [320] who arranged the absorption bands in the above progressions; uncertainty attends their assignments as members of Rydberg series. Those bands reclassified as members of now well-established Rydberg series are not included in the above. (See also section 3.10 and ref. [251, 253, 125].

(b) Unclassified progressions observed in absorption

	I				II				III				IV		
λ(Å)	I	σ(cm⁻¹)	Δσ	λ(Å)	I	σ(cm⁻¹)	Δσ	λ(Å)	I	σ(cm⁻¹)	Δσ	λ(Å)	I	σ(cm⁻¹)	Δσ
893.8	4	111 882		856.1	1	116 809		756.0	1	132 275		754.5	3	132 538	
			1 061				1 102				828				867
885.4	5	112 943		848.1	2	117 911		751.3	2	133 103		749.6	3	133 404	
			1 017				1 052				820				859
877.5	4	113 960		840.6	2	118 963		746.7	1	133 923		744.8	1	134 264	
			983				1 013				812				835
870.0	1	114 943		833.5	1	119 976		742.2	1	134 735		740.2	1	135 099	
			892				987				803				
863.3	1	115 835		826.7	1	120 963		737.8	1	135 538					

Data of Tanaka and Takamine [371]. These are non-Rydberg progressions.

TABLE 30. *Miscellaneous unclassified bands* — Continued

(c)

λ(Å)	σ(cm⁻¹)	I
1250.51	79967.7	2
1250.21	79998.7	2
1222.58	81794.2	2
1222.01	81832.4	2
1169.14	83602.3	3
1172.08	85318.4	7
1171.35	85371.6	7
1148.62	87061.0	2

Violet shaded doublets observed in absorption by Tanaka [369] labeled by Tanaka as progression II. It is not certain whether these are vibrational members of the first term in a Rydberg series whose limit is the first I. P. of O_2.

(d)

λ(Å)	σ(cm⁻¹)	I	Dissociation products
1349	74130	9	$^3P + {}^1S$ or $^1D + {}^1D$
1334	74960	7	$^3P + {}^1S$ or $^1D + {}^1D$
1290	77520	6	$^3P + {}^1S$

Maxima in absorption continua observed by Tanaka [369]; tentative designations are included.

λ(Å)	σ(cm⁻¹)	I	λ(Å)	σ(cm⁻¹)	I	λ(Å)	σ(cm⁻¹)	I
1268.81	78814.0	1	1125.60	88841.5	4	1090.63	91690.1	5
1268.08	78859.4	1	1125.34	88862.0	5	1089.82	91758.3	3
			1124.68	88914.2	4	1089.46	91788.6	4
1244.26	80369.2	10	1123.62	88998.1	3	1088.68	91854.4	4
1243.49	80419.0	10	1123.08	89040.9	6	1088.38	91879.7	5
			1122.78	89064.6	3			
1207.50	82815.7	9				1084.51	92207.5	4
1206.75	82867.2	9	1122.34	89099.6	5	1083.67	92279.0	4
1205.38	82961.4	9	1121.94	89131.3	5	1083.44	92298.6	5
			1120.98	89207.7	5	1082.29	92396.7	6
1172.08	85318.4	7	1120.76	89225.2	5			
1171.35	85371.6	7				1067.22	93701.4	8
			1116.78	89543.2	3	1066.85	93733.9	8
1164.23	85893.7	9	1115.87	89616.2	4	1066.09	93800.7	8
1163.87	85920.2	10	1115.10	89678.1	5	1065.78	93828.0	8
1162.98	85986.0	8	1113.89	89775.5	3	1064.93	93902.9	8
1162.44	86025.9	8	1112.98	89848.9	3	1064.68	93924.9	8
1161.72	86079.3	9	1112.29	89904.6	2			
1161.47	86097.8	5				1050.17	95222.7	6
			1106.36	90386.5	4	1049.86	95250.8	8
1154.36	86628.1	6	1106.13	90405.3	5	1048.91	95337.1	7
1154.06	86650.6	10	1105.00	90497.7	3	1048.64	95361.6	6
1153.20	86715.2	8	1104.41	90546.1	4	1047.60	95456.3	6
1152.98	86731.8	6	1103.95	90583.8	5	1047.41	95473.6	6
1151.67	86830.4	7	1103.64	90609.3	4			
1151.46	86846.3	6				1032.70	96833.5	5
			1102.59	90695.5	4	1031.35	96960.3	5
1136.41	87996.4	5	1102.37	90713.6	5			
1136.09	88021.2	5	1101.74	90765.5	4			
1135.13	88095.6	5	1100.34	90881.0	4			
1134.74	88125.9	5						

Absorption bands observed by Tanaka [369]. The groupings are his; most bands are violet degraded.

TABLE 30 (e). *Bands in the region below 600 Å*

m [a]	λ(Å)	I	σ (cm^{-1})
9	594.95	1	168 080
10	594.13	1	168 310
11	593.47	0	168 500
12	593.00	0	168 630
13	592.64	0	168 740
14	592.36	00	168 820
15	592.15	00	168 880
∞			169 350$\pm$40

[a] m is a running number proportional to n, the principal quantum number.

Data from Yoshino and Tanaka [417]. Weak, diffuse bands. Uncertain classification whose Rydberg series limit falls between vibrational levels of state $B\,^2\Sigma_g^-$. It is not certain whether this limit identifies a new state of O_2^+.

TABLE 30(f). *"Weak series"*

Probable n	λ(Å)	σ(cm^{-1})
3	537.41($\pm$0.1)	186 080
4		
5	516.10($\pm$0.05)	193 761
5	512.62($\pm$0.05)	195 076
7	510.48($\pm$0.05)	195 894

Data from Codling and Madden [89]. This series is only crudely fitted by

$$\sigma = 198125 - \frac{R}{(n+0.03)^2}, \; n=3 \text{ to } 7$$

Interpretation of the series is uncertain.

TABLE 30 (g). *Unclassified absorption bands observed by Alberti et al*

λ_H(Å)	σ_H(cm^{-1})
1486.5	67 272
1481.5	67 499
1442.7	69 314

Data of Alberti et al. [7]. Strong violet shaded bands. Probably absorption from $a\,^1\Delta_g$, but not conclusive. Diffuse; no rotational structure observed.

(h)

λ_H (Å)	σ_H (cm^{-1})
1265.6	79 014
1262.6	79 202

Data of Alberti et al. [7]. Strong heads; diffuse, open rotational structure, violet shaded. Possibly absorption from $a\,^1\Delta_g$ or $b\,^1\Sigma_g^-$. The kinetic absorption spectroscopy observations of Donovan et al. [116] support the assignment of the $a\,^1\Delta_g$ state as the lower state of bands in table 30 (g), (h).

TABLE 30(i). *Unidentified violet-degraded band heads observed with $b-a(1-)$, O_2^+*

λ_H (Å)	σ_H (cm^{-1})	λ_H (Å)	σ_H (cm^{-1})
6337.4	15 775	5853.5	17 079
6325.4	15 805	5835.1	17 133
5961.7	16 769	5834.4	17 135
5952.5	16 795	5824.9	17 163
5941.2	16 827	5588.2	17 890
5922.5	16 880	5579.4	17 918
5915.2	16 901	5570.7	17 946
5904.7	16 931	5557.1	17 990
5895.3	16 958	5553.1	18 003
5876.6	17 012	5548.8	18 017
5873.5	17 021	5532.2	18 071
5863.1	17 051	5267.0	18 981

Data of Bozóky [52].

TABLE 30(j). *Unidentified band heads among double-headed A–X system of O_2^-*

λ (Å)	σ (cm^{-1})	I	Ref.
5736.1	17 429		71
4399.6	22 723		127
4199.2	23 807	1	
3997.3	25 010	4	
3950.6	25 305	6	
2952.5	33 860	5	
2895.6	34 525	8	
2881.8	34 690	6	
2376.4	42 068	1	

Red-degraded bands. Mainly data of Johnson [221]; also data of Byrne [71] and Ellsworth and Hopfield [127].

TABLE 30 (k). *Unclassified band heads (emission) (R)*

λ(Å)	σ(cm^{-1})	λ(Å)	σ(cm^{-1})
4487.7	22 277	3543.6	28 212
4384.0	22 804	3352.0	29 824
4307.7	23 208	3286.8	30 416
4296.2	23 270	3219.1	31 056
4144.8	24 120	3099.7	32 252
4123.6	24 244	3095.9	32 291
4116.6	24 285	2790.3	35 828
4063.1	24 605	2733.3	36 575
3779.4	26 452	2678.2	37 327
3693.7	27 065	2451.7	40 776
3569.8	28 005		

Data of Lal (1948) [246]. Band heads were observed in a low pressure, high-frequency discharge [246]. Though attributed to the $B\,^3\Sigma_u^- - X\,^3\Sigma_g^-$ transition, the bands produce an irregular Deslandres array. Some heads may be due to clustering of overlapping lines of different bands [132].

TABLE 30 (I). *New band progression of O_2 in the 830–900 Å region*

v' [a]	λ(Å)	I	σ(cm^{-1})	$\Delta G_{r+1/2}$	Remark
0	902.59	3	110 792		Sharp
				1064	
1	894.01	5	111 856		Diffuse [b]
				1062	
2	885.60	7	112 918		Diffuse [b]
				1011	
3	877.74	8	113 929		Sharp
				1004	
4	870.07	7	114 933		Diffuse
				988	
5	862.66	6	115 921		Sharp
				972	
6	855.48	5	116 893		Diffuse
				948	
7	848.60	4	117 841		Sharp
				941	
8	841.88	3	118 782		Diffuse
				914	
9	835.45	2	119 696		Diffuse (?) [b]

[a] This is a running number and does not necessarily indicate the correct vibration quantum number.

[b] Overlapped.

Red-degraded bands observed together with Rydberg progressions by Huffman et al. [205]. These bands may originate from a $^1\Delta_g$ or b $^1\Sigma_g^+$.

TABLE 31. *Observed fine structure (microwave) frequencies for O_2 (MHz)*

Isotope	N	ν_-	Ref.	ν_+	Ref.
$^{16}O_2$	1	118750.343	265	56264.772	411, 265
	3	62486.255	422, 265	58446.590	422, 265
	5	60306.044	422	59590.978	422
	7	59164.215	422	60434.776	422
	9	58323.885	422	61150.570	422
	11	57611.4 ± 0.2	279	61800.169	411
	13	56968.180	411	62411.223	411
	15	56363.393	411	62996.6 ± 0.2	279
	17	55783.819	411	63568.520	422
	19	55221.372	411	64127.777	411
	21	54671.145	411	64678.2 ± 0.2	279
	23	54129.4 ± 0.4	279	65224.120	422
	25	53599.4 ± 0.8	279	65764.744	411
	27	(53070)	225		

Quoted uncertainty is ±0.010 MHz unless otherwise indicated. (See also Wilheit and Barrett [413]). For the 23$_+$ line, uncertainty may be 0.2 MHz. 1$_+$ and 3$_+$ lines are mean values.

Data from Zimmerer and Mizushima [422], West and Mizushima [411], Mizushima and Hill [279], McKnight and Gordy [265], and Kahan [225]. Kahan observed atmospheric absorption of solar radiation.

$^{18}O_2$	3			58900	109
	5	59875	109	59810	109
	7	58965	109		

Data from Miller, Javan, and Townes [274]. Uncertainty is ±2 MHz.

$^{16}O^{18}O$	3			58650	
	4			59220	
	5			59685	
	6	59540			
	7	59075			
	8	58670			

Data from Miller, Javan, and Townes [274]. Uncertainty is ±2 M Miller and Townes [275] have assumed that the theoretical frequen for the $^{18}O_2$ and $^{16}O^{18}O$ transitions are more accurate than the expe mental values.

TABLE 32. *Magnetic hyperfine structure lines*

Isotope	N	F'	F''	ν-	F'	F''	ν+
$^{16}O^{17}O$	4	11/2	9/2	a (60250)			
					11/2	13/2	59250
					13/2	15/2	59398
	5				5/2	7/2	59359
					7/2	9/2	59431
					9/2	11/2	b (59519)
		13/2	11/2	60130	11/2	13/2	59627
		15/2	13/2	59989	13/2	15/2	59748
					15/2	17/2	59889
	6				7/2	9/2	59790
		11/2	9/2	59737	9/2	11/2	59864
		13/2	11/2	59638	11/2	13/2	59956
		15/2	13/2	59519	13/2	15/2	60060
		17/2	15/2	59385	15/2	17/2	c (60179)
	6	11/2	9/2	59322	9/2	11/2	d (60172)
		9/2	7/2	59390	11/2	13/2	e (60251)

a measured 60240–60250.

b no experimental wavelength given for this line.

c no experimental wavelength given for this line.

d measured two lines 60170–60180.

e observed strong feature, no frequency given.

Data from Miller and Townes [275]. (   ) = calculated, assuming magnetic hyperfine structure constants $b = -102$ MHz, $c = 140$ MHz, for $^{16}O_2$.

TABLE 33. *Magnetic dipole rotational spectrum of* O_2

$J'-J''$	$N'-N''$	ν (MHz)	σ (cm^{-1})	Ref.
2–1 b	3–1	368499.02 ± 0.21	12.29	265
2–2 a	3–1	424763.80 ± .20	14.17	265, 157
3–1 b	3–1	430985.28 ± .20	14.38	265
3–2 b	3–1	487250.05 ± .21	16.25	265, 157
4–4	5–3		25.80	257
5–3 c	5–3	775770 ± 10	25.88	128
5–4	5–3		27.80	257
6–5	7–5		35.40	257
6–6	7–5		37.39	157
7–6 d	7–5		39.24	157
8–8	9–7		48.95	257
9–8 e	9–7		51.00	257
10–9	11–9		58.36	155
10–10	11–9		60.47	155
14–14	15–13		83.45	257
16–16	17–15		95.00	257
20–20	21–19		115.70	257

a Direct measurement.

b Inferred from rotation measurement and fine structure measurement.

c Inferred from laser measurement and EPR measurement.

d Gebbie et al. [155] obtained 39.35 cm^{-1}.

e Gebbie et al. [155] obtained 50.88 cm^{-1}.

Data from McKnight and Gordy [265], Evenson et al. [128], Gebbie et al. [157, 155], MacQueen et al. [257], and Eddy et al. [124].

TABLE 34. *Line widths* $\left(\dfrac{\Delta\nu}{p}\right)$ *in MHz/mmHg*

(a) 300 K

N	Transition	
	−	+
1	(1.97)(a)	1.78
3	1.85	1.72
5	1.75	1.66
7	1.73	1.62
9	1.69	1.57
11	1.63	1.53
13	1.54	1.48
15	1.49	1.35
17	1.48	1.42
19	1.47	1.37
21	1.40	1.37
23	(1.49)(b)	(1.26)(b)
25	....	....

Data of Battaglia and Cattani [35] supplemented by data of (a) Hill and Gordy [193], and (b) Anderson, Smith, and Gordy [16]. Recent measurements by Zimmerer and Mizushima [422], and Stafford and Tolbert [363] also show decreasing line widths with increasing N. Earlier measurements by Artman and Gordon [19] had line widths nearly independent of rotational state (~ 1.97). Artman examined various line broadening theories, concluding that Van der Waals and exchange interactions were primarily responsible for the line widths. Currently, no theory of line broadening accounts for the experimental results. $\dfrac{\Delta\nu}{p}$ is half-width at half-peak absorption; sometimes this is given in units of cm^{-1}/atm.

TABLE 34. *Line widths* $\left(\dfrac{\Delta\nu}{\text{p}}\right)$ *in MHz/mmHg* — Continued

(b) 193 K

Line	$\dfrac{\Delta\nu}{\text{p}}$
1—	4.7

Data from Anderson, Johnson, and Gordy [14].

(c) 90 K

Line	$\dfrac{\Delta\nu}{\text{p}}$
1—	5.80
7—	2.01
9—	1.94
1+	5.63
3+	5.77
5+	5.22

Data from Hill and Gordy [193].

(d) Line widths for magnetic resonance lines

Transition			$\dfrac{\Delta\nu}{\text{p}}$	
N	J	M	300 K	78 K
1	1	0 ←— 1	2.35 ± 0.10	6.13 ± 0.3
1	2	2 ← 1	2.20 ± .10	6.00 ± .2
1	2	1 ← 0	....	5.92 ± .3
1	2	0 ← 1	2.23 ± 0.14	6.20 ± .1
3	2	−1 ← 0	....	5.93 ± .3
3	4	0 ←— 1	2.00 ± 0.10	5.70 ± .3
5	4	−1 ← 0	....	6.0 ± .5
5	6	0 ←— 1	....	5.5 ± .3

Data of Tinkham and Strandberg [377].

TABLE 35. *Miscellaneous constants derived from the microwave spectrum*[1,2]

(a) Zeeman constants (ppm)

$\dfrac{g_s'}{g_s} - 1$	$\dfrac{g_L}{g_s}$	$\dfrac{g_N}{g_s}$
−147 ± 10	1405 ± 15	−63 ± 6

Data from Bowers et al. [51]. Compare also Hendrie and Kusch [180], Tinkham and Strandberg [376, 377], and comments by Kayama and Baird [227].

g_s: Spectroscopic splitting factor for free electron spin (free electron spin magnetic moment).

g_s': In O_2, unpaired electron spin moment.

g_N: Molecular rotational magnetic moment (sometimes labeled g_r or g_K).

g_L: Molecular electronic oribital moment (also labeled g_p). No standard notation exists for these quantities.

(b) $Q(^{16}O_2) = 0.04(10^{-16})$ cm^2

This value of the quadrupole moment is from Anderson et al. [15]. It is based on a theory of Mizushima and an arbitrary assumption about one of the parameters.

(c) $eqQ(^{16}O^{17}O) = 2.7$ MHz

The value of the quadrupole coupling constant is from Miller [273].

(d) For the a $^1\Delta_g$ state.

$g_N = (-1.234 \pm .025)10^{-4}$

$g_L = 0.999866 \pm .000010$

Q(electronic quadrupole moment) $= (-3.19 \pm 0.65)10^{-25}$ esu-cm·

Data from Miller [277]. See Miller's table 2 for additional observed and derived constants.

[1] Bowers et al. [51] did not state the numerical value of g_s that they assumed. Kayama and Baird [227] indicated that Tinkham and Strandberg [376, 377] had used −2.00229. The current value is −2.002319 which was assumed by Kayama and Baird, however, without corrections, in their treatment of the true spin-orbit interaction Hamiltonian which they used instead of the isotropic form AL·S used by Tinkham and Strandberg. The true spin-orbit interaction mixes $^1\Sigma_g^+$ with the ground state. Preliminary ab initio calculations by Pritchard et al. [322] imply that spin-orbit effects "contribute 75 percent to the observed [λ] splittings."

[2] Parameters for the fine-structure Hamiltonian have been discussed by Wilheit and Barrett [413], McKnight and Gordy [265], Tischer [378], and West and Mizushima [411].

TABLE 36. *Rotational constants for the* X $^3\Sigma_g^-$ *state*.

	v	$B_v(\text{cm}^{-1})$	$D_v(10^{-6}\text{ cm}^{-1})$
$^{16}O_2$	0	1.43768	5.02
	1	1.4220	4.8
	2	1.4068	3.6
	3	1.3886	4.7
	4	1.3743	3.8
	5	1.3590	3.5
	6	1.350	....
	7	1.329	....
	8	1.316	....
	9	1.298	....
	10	1.282	....
	11	1.269	4.79
	12	1.250	4.79
	13	1.235	4.79
	14	1.221	4.79
	15	1.202	4.79
	16	1.186	4.79
	17	1.171	4.79
	18	1.156	4.79
	19	1.139	4.79
	20	1.121	4.79
	21	1.104	4.79
	22	1.091	4.9
	23	1.075	(7)
	24	1.055	(6)
	25	(1.033)	
$^{16}O^{17}O$	0	1.3958	
$^{16}O^{18}O$	0	1.3579	

$v = 0$, 1: data from Babcock and Herzberg [24], refitted using least squares by Albritton et al. [9] (see Appendix C).

$v = 2$–5: data from Ogawa [302]. B_4 and B_5 of Feast and Garton [136] are ~ 0.003 cm^{-1} larger. Albritton et al. [9] found that the fourth decimal place of B_v values of Ogawa was only suggestive.

$v = 6$: data from Feast and Garton [136].

$v = 7$–11: data from Feast [134].

$v = 12$–21: data from Lochte-Holtgreven and Dieake [256]. For $v = 21$ data of Herman et al. [183] are for high N only.

$v = 22$–25: data from Herman et al. [183]. No data for low N for $v = 24$, 25; only fragmentary data for the latter. For $v = 23$ the quoted value is the mean of two determinations which differ by 0.014 cm^{-1}. Isotopic B_v values are from Babcock and Herzberg [24].

TABLE 37. *Rotational constants for the* a $^1\Delta_g$ *state*

v	B_v	D_v (10^{-6})
0	1.41774	4.97
1	1.4006	....

Data from Herzberg and Herzberg [191], adjusted by use of B_0 and D_0 values for the X state (discussed in Appendix C).

TABLE 38. *Rotational constants for the* b $^1\Sigma_g^+$ *state*

Isotope	v	B_v	D_v (10^{-6})
$^{16}O_2$	0	1.391382	5.486
	1	1.373135	5.588
	2	1.354785	5.651
	3	1.33646	5.95
	4	1.321	
$^{16}O^{17}O$	0	1.3520	
	1	1.3331	
$^{16}O^{18}O$	0	1.3141(2)	5.05
	1	1.2974(0)	

Data from Babcock and Herzberg [24], refitted using least squares by Albritton et al. [9] to data on $^{16}O_2$. Refitting changed B_v's in the fifth decimal place. Fragmentary data on the $b-X$, 4–0 band [which gives B_4] is from Ossenbrüggen [311]. Isotopic data is from Babcock and Herzberg [24]; the fifth decimal place is suggestive, since the data have not been refitted by least squares.

TABLE 39. *Rotational constants for the* c $^1\Sigma_u^-$ *state*

v	B_v	D_v(10^{-6})	Ref.
0	0.9084	(7.4 ± 2)	103
1	....	....	....
2	....	....	....
3	....	....	....
4	....	....	....
5	....	....	....
6	0.7935	10.5	
7	0.7695	9.7	
8	0.7440	(9.5)	
9	0.7167	(9.5)	189
10	0.6882	9.5	
11	0.6573	(9.5)	

Data from Herzberg [189] and Degen [103]. D_v values for $v=8$, 9, 11 are assumed equal to that for $v=10$ [189]. Herzberg assumed that the D_v values were uncertain by ±10 percent. Tentative v numbering of Degen has been assumed.

TABLE 40. *Rotational constants for the* C $^3\Delta_u$ *state*

	v	B_v
$^3\Delta_3$	5	0.8233
$^3\Delta_2$	5	^{a}(.8177)
$^3\Delta_3$	6	.7971
$^3\Delta_2$	6	.7915

^{a} B_5 ($^3\Delta_2$) is calculated (see discussion, sect. 3.5).

Data of Herzberg [189]. Difference $B_6(^3\Delta_3)-B_6(^3\Delta_2)$ is real [189]. Vibrational numbering is tentative.

TABLE 41. *Rotational constants for the* A $^3\Sigma_u^+$ *state*

v	B_v	D_v(10^{-6})
0	(0.90321)	(4.67)
1	0.8880	(4.5)
2	.8686	(4.7)
3	.84905	5.0
4	.82717	5.4
5	.80336	6.2
6	.77640	8.4
7	.74465	10.4
8	.70633	12.9
9	.65805	18.2
10	.59346	31.2
11	.4969	165.

Data from Herzberg [187]. Vibrational quantum numbering is that of Broida and Gaydon [63], and is one unit larger than that of Herzberg. The 11–0 band shows a strong perturbation for $N>7$. B_0, D_0 have been calculated, for the 0 level was not observed under high resolution. D_1, D_2 are of low accuracy because bands with low v' are extremely faint. B_v values decrease and D_v values increase at an increased pace as the convergence limit is approached [187]. B_{11} is determined from low N values only. Q-branches were used for determining $(B'_v-B''_0)$ and $(D'_v-D''_0)$ for the $A-X$ bands. The tabulated B_v and D_v differ from those cited by Herzberg [187]; the assumed ground state constants are $B_0=1.43768$ and $D_0=5.02(10^{-6})$. Appendix C discusses the revised ground state constants.

TABLE 42. *Rotational constants for the* B $^3\Sigma_u^-$ *state*

v	B_v	D_v (10^{-6})
0	0.8127	5.06
1	.8001	6.61
2	.7852	5.10
3	.7699	4.54
4	.7537	3.56
5	.7372	5.71
6	.7194	5.71
7	.6997	6.96
8	.6771	6.71
9	.6538	7.21
10	.6270	9.75
11	.5980	9.31
12	.5640	14.16
13	.5269	23.91
14	.4836	21.2
15	.4399	25.7
16	.3953	34.3
17	.347	45
18	.296	152
19	.258	49
20	.207	76
21	.159	105

$v=0-13$, data of Ackerman and Biaume [3].
$v=14-21$, data of Brix and Herzberg [62].
Brix and Herzberg obtained $v=12$, $B=0.5625$, $D=13(10^{-6})$
$v=13$, $B=0.5247$, $D=16.8(10^{-6})$
Ackerman and Biaume have compared their measurements to earlier values of Knauss and Ballard [233], Curry and Herzberg [99], Brix and Herzberg [62], Ogawa [302], Ogawa and Chang [306].

TABLE 43. *Rotational constants for the $\beta\ ^3\Sigma_u^+$ state*

v	B_r (cm^{-1})
2	1.65
3	1.63

Crude B_r values from Alberti et al. [7]. Quantum numbering is that suggested by Ogawa and Yamawaki [308], who fitted longer branches, including many blended lines, by using both B_r and D_r.

TABLE 44. *Rotational constants for the $\alpha\ ^1\Sigma_u^+$ state*

v	D_v (cm^{-1})
0	1.691
1	1.675
2	1.640
3	1.633
4	1.59

Data from Alberti et al. [7]. Ogawa and Yamawaki [308] obtained slightly different values by fitting longer branches with both B_v and D_v, but many blends were included. D_v's varied irregularly with v [308].

TABLE 45. *Rotational constants for the $^3\Sigma_u^+$ state*

v	B_v (cm^{-1})	D_v (10^{-6} cm^{-1})
0	1.706	2.80

Data of Ogawa and Yamawaki [308].

TABLE 46. *Rotational constants for the $^1\Delta_u$ state*

v	B_v (cm^{-1})
0	1.446

Data from Alberti et al. [7].

TABLE 47. *Rotational constants for the $^1\Pi_u$ state*

v	B_v (cm^{-1})
0	1.451

Data from Alberti et al. [7].

TABLE 48. *Rotational constants for the X $^2\Pi_g$ state of O_2^+*

v	B_r	Ref.	A_r
0	....		(200.81)
1	....		(199.99)
2	1.643	52	199.03
3	1.622	52	198.38
4	....		(197.55)
5	....		(196.74)
6	1.563	53	196.14
7	1.540	365	195.30
8	1.522	365	194.46
9	1.504	53	193.46
10	1.484	53	192.58

Data from Stevens [365] and Bozóky [52–3] was refitted on a computer using the method of least squares. These values obtained by A. Lofthus differ slightly from the values obtained graphically in the original references. D (calc) $\sim 5.3(10^{-6})$. Vibrational quantum number, that of Bhale and Rao [42], is one unit larger than that assumed in the original references.

A_r values are from Albritton et al. [9] who refitted the data of Stevens and of Bozóky. The values in parenthesis have been calculated from $A_r = 201.212 - 0.8136\ (v+\tfrac{1}{2})$.

TABLE 49. *Rotational constants for the a $^4\Pi_{ui}$ state of O_2^+*

v	B_r	D_r (10^{-6})
0	1.09681	4.83
1	1.08099	4.73
2	1.06531	4.64
3	1.05027	5.04
4	1.033	
5	1.017	
6	0.999	

$v=0, 1, 2$—Nevin [291b].
$v=3$—Nevin and Murphy [291c], who list uncertainties
$$B_3 = \pm 0.00002$$
$$D_3 = \pm 0.04 \times 10^{-6}$$
$v=4, 5, 6$—Weniger [408]. For $v=3$ he has $B_3=1.047$, $A_v=-47.94$. D_r were only estimated to be $O(10^{-6})$.

TABLE 50. *Rotational constants for the A $^2\Pi_u$ state of O_2^+*

v	B_r	Ref.
0	1.053	365
1	1.031	365
2	....	
3	....	
4	....	
5	0.953	52
6	0.928	52
7	0.910	52
8	0.885	52

Data from Stevens [365] and Bozóky [52] was refitted by A. Lofthus; the values obtained graphically in the original references differ slightly from those cited above. D (calc) $\sim 6.0 \times (10^{-6})$.

TABLE 51. *Rotational constants for the* b $^4\Sigma_g^-$ *state of* O_2^+

v	B_v	D_v (10^{-6})
0	1.27626	5.91
1	1.25420	6.07
2	1.23213	6.28

Data from Nevin [291b]. Probable error $B \sim \pm 0.00005$; probable error $D \sim \pm 0.09 \times 10^{-6}$.

Spin fine-structure constants for this state are also given by Nevin, using the theory of Budo [64].

3	....	....
4	1.181	....
5	1.158	....
6	1.135	....

Data of Le Blanc [250b].

TABLE 52. *Rotational constants for the* c $^4\Sigma_u^-$ *state of* O_2^+

v	B_v	D_v
0	1.557	(10^{-6})

Data from Le Blanc [250]. Only the order of magnitude of D_0 is given.

TABLE 53. *RKR potentials for electronic states of* O_2 *and* O_2^+

Most of the RKR potentials are taken from the work of Albritton et al. [9]. The data for the $a\ ^1\Delta_g$ state is extrapolated after $v=1$. The data for the $A\ ^3\Sigma_u^+$ state is based on the work of Degen et al. [104]. For the A state, $v=0$ is not known experimentally from high resolution measurements and $v=1$ is known only from fragmentary branches. For vibrational levels which are underlined the potentials have been extrapolated. The data taken from Albritton et al. [9] has been rounded; the tabulated numbers are given to one digit beyond the last significant digit as determined from the experimental data.

v	V (cm^{-1})	$T_e + V$ (eV)	r_{min} (Å)	r_{max} (Å)
		$O_2\ X\ ^3\Sigma_g^-$		
-0.50	0.0	0.	1.2075358	
-0.25	394.5748	.049	1.1726052	1.2457931
0.00	787.3818	.098	1.1590417	1.2626908
0.50	1568.5332	.194	1.1406952	1.2877294
1.00	2343.7613	.291	1.1272513	1.3078976
1.50	3113.0972	.386	1.1163265	1.3255800
2.00	3876.57	.481	1.10700	1.34170
2.50	4634.21	.575	1.09880	1.35672
3.00	5386.03	.668	1.09146	1.37093
3.50	6132.07	.760	1.08478	1.38451
4.00	6872.34	.852	1.07864	1.39759
4.50	7606.86	.943	1.07296	1.41025
5.00	8335.65	1.033	1.06767	1.42257
5.50	9058.73	1.123	1.06271	1.43460
6.00	9776.11	1.212	1.0580	1.4464
6.50	10487.80	1.300	1.0536	1.4580

TABLE 53. *RKR potentials for electronic states of* O_2 *and* O_2^+ — Con.

v	V (cm^{-1})	$T_e + V$ (eV)	r_{min} (Å)	r_{max} (Å)
7.00	11193.80	1.388	1.0494	1.4693
7.50	11894.14	1.475	1.0454	1.4806
8.00	12588.82	1.561	1.0417	1.4917
8.50	13277.83	1.646	1.0380	1.5027
9.00	13961.18	1.731	1.0346	1.5136
9.50	14638.87	1.815	1.0312	1.5244
10.00	15310.91	1.898	1.0280	1.5351
10.50	15977.28	1.981	1.0250	1.5457
11.00	16637.98	2.063	1.0220	1.5563
11.50	17293.00	2.144	1.0191	1.5669
12.00	17942.34	2.225	1.0164	1.5774
12.50	18585.98	2.304	1.0137	1.5879
13.00	19223.91	2.383	1.0112	1.5984
13.50	19856.12	2.462	1.0087	1.6089
14.00	20482.58	2.540	1.0063	1.6194
14.50	21103.29	2.616	1.0039	1.6299
15.00	21718.21	2.693	1.0017	1.6403
15.50	22327.33	2.768	0.9995	1.6509
16.00	22930.61	2.843	0.9974	1.6614
16.50	23528.05	2.917	0.9953	1.6719
17.00	24119.60	2.990	0.9933	1.6825
17.50	24705.24	3.063	0.9913	1.6931
18.00	25284.93	3.135	0.9894	1.7038
18.50	25858.64	3.206	0.9876	1.7145
19.00	26426.33	3.276	0.9858	1.7253
19.50	26987.98	3.346	0.9841	1.7361
20.00	27543.52	3.415	0.9824	1.7470
20.50	28092.94	3.483	0.9807	1.7580
21.00	28636.17	3.550	0.9791	1.7691
21.50	29173.18	3.617	0.9776	1.7802
22.00	29703.92	3.683	0.9761	1.7915

v	V (cm^{-1})	$T_e + V$ (eV)	r_{min} (Å)	r_{max} (Å)
		$O_2\ a\ ^1\Delta_g$		
-0.50	0.0	0.982	1.2156449	
-0.25	376.7521	1.028	1.17999	1.25489
0.00	751.658	1.075	1.16619	1.27228
0.50	1496.633	1.167	1.14757	1.29814
1.00	2235.158	1.259	1.13396	1.31904
1.50	2967.233	1.350	1.12293	1.33742
2.00	3692.86	1.440	1.11353	1.35422
2.50	4412.03	1.529	1.10528	1.36933
3.00	5124.76	1.617	1.0979	1.3848

v	V (cm^{-1})	$T_e + V$ (eV)	r_{min} (Å)	r_{max} (Å)
		$O_2\ b\ ^1\Sigma_g^+$		
-0.50	0.0	1.636	1.2268431	
-0.25	357.4241	1.680	1.190331	1.267217
0.00	712.9766	1.724	1.176241	1.285186
0.50	1418.8469	1.812	1.157272	1.311972
1.00	2117.7290	1.899	1.143442	1.333696
1.50	2809.6121	1.984	1.132251	1.352859
2.00	3494.4855	2.069	1.122734	1.370428
2.50	4172.3385	2.153	1.114398	1.386898
3.00	4843.1603	2.237	1.106952	1.402561

TABLE 53.   *RKR potentials for electronic states of* O_2 *and* O_2^+ — Con.

v	V (cm⁻¹)	$T_e + V$ (eV)	r_{min} (Å)	r_{max} (Å)
		O_2 A $^3\Sigma_u^+$		
−0.50	0.0	4.389	1.52153	
−0.25	....	....	....	
0.00	395.8	4.438	1.454	1.600
0.50	785.6	4.486	1.429	1.638
1.00	1168.7	4.534	1.411	1.668
1.50	1544.7	4.580	1.397	1.696
2.00	1912.5	4.626	1.385	1.722
2.50	2272.1	4.671	1.375	1.748
3.00	2623.5	4.714	1.366	1.772
3.50	2966.1	4.757	1.357	1.797
4.00	3298.9	4.798	1.350	1.822
4.50	3621.8	4.838	1.343	1.846
5.00	3934.9	4.877	1.337	1.872
5.50	4237.3	4.914	1.332	1.897
6.00	4527.2	4.950	1.326	1.925
6.50	4804.8	4.985	1.322	1.953
7.00	5070.0	5.018	1.317	1.982
7.50	5321.2	5.047	1.313	2.014
8.00	5555.6	5.078	1.310	2.050
8.50	5772.9	5.105	1.306	2.089
9.00	5973.4	5.130	1.304	2.131
9.50	6154.0	5.152	1.301	2.182
10.00	6309.1	5.171	1.298	2.245
10.50	6438.7	5.187	1.297	2.323
11.00	6542.6	5.200	1.297	2.423
		O_2 B $^3\Sigma_u^-$		
−0.50	0.0	6.174	1.6042799	
−0.25	175.9373	6.196	1.5526332	1.6618190
0.00	351.204	6.217	1.53266	1.68771
0.50	697.700	6.260	1.50589	1.72668
1.00	1038.736	6.303	1.48649	1.75876
1.50	1374.200	6.344	1.47090	1.78749
2.00	1703.961	6.385	1.45776	1.81426
2.50	2027.872	6.425	1.44634	1.83979
3.00	2345.774	6.465	1.43623	1.86450
3.50	2657.493	6.503	1.42714	1.88869
4.00	2962.845	6.541	1.41889	1.91257
4.50	3261.631	6.578	1.41132	1.93631
5.00	3553.643	6.614	1.40434	1.96005
5.50	3838.654	6.650	1.39786	1.98393
6.00	4118.425	6.684	1.39181	2.00806
6.50	4386.700	6.718	1.38615	2.03258
7.00	4649.207	6.750	1.38084	2.05761
7.50	4903.657	6.782	1.37586	2.08329
8.00	5149.746	6.812	1.37117	2.10976
8.50	5387.153	6.842	1.36677	2.13720
9.00	5615.548	6.870	1.36264	2.16578
9.50	5834.589	6.897	1.35878	2.19571
10.00	6043.932	6.923	1.35518	2.22722
10.50	6243.235	6.948	1.35184	2.26056
11.00	6432.167	6.971	1.34876	2.29602
11.50	6610.416	6.993	1.34592	2.33395

v	V (cm⁻¹)	$T_e + V$ (eV)	r_{min} (Å)	r_{max} (Å)
12.00	6777.701	7.014	1.34332	2.37471
12.50	6933.801	7.033	1.34097	2.41874
13.00	7078.535	7.051	1.33883	2.46652
13.50	7211.822	7.068	1.33690	2.51859
14.00	7333.678	7.083	1.33515	2.57557
		O_2^+ X $^2\Pi_g$		
−0.50	0.0	12.052	1.1171227	
−0.25	475.46	12.111	1.0853699	1.1520296
0.00	948.69	12.157	1.07307	1.16750
0.50	1889.04	12.286	1.05646	1.19048
1.00	2821.26	12.402	1.04431	1.20904
1.50	3745.33	12.516	1.03445	1.22536
2.00	4661.26	12.630	1.02604	1.24028
2.50	5569.05	12.742	1.01867	1.25422
3.00	6468.70	12.854	1.01206	1.26744
3.50	7360.21	12.964	1.00606	1.28010
4.00	8243.57	13.074	1.00055	1.29233
4.50	9118.80	13.182	0.99546	1.30420
5.00	9985.89	13.290	0.99071	1.31577
5.50	10844.83	13.396	0.98626	1.32710
6.00	11695.64	13.502	0.98207	1.33823
6.50	12538.30	13.606	0.97811	1.34918
7.00	13372.82	13.710	0.97436	1.35999
7.50	14199.20	13.812	0.97079	1.37067
8.00	15017.44	13.914	0.96738	1.38125
8.50	15827.54	14.014	0.96413	1.39174
9.00	16629.50	14.114	0.96101	1.40216
9.50	17423.32	14.212	0.95801	1.41252
10.00	18208.99	14.310	0.95513	1.42282
10.50	18986.53	14.406	0.95235	1.43309
11.00	19755.92	14.501	0.94968	1.44333
11.50	20517.18	14.596	0.94709	1.45355
12.00	21270.29	14.689	0.94459	1.46375
		O_2^+ a $^4\Pi_{ui}$		
−0.50	0.0	16.138	1.3816042	
−0.25	258.4628	16.170	1.3387259	1.4291889
0.00	515.411	16.202	1.32223	1.45041
0.50	1025.437	16.265	1.30007	1.48208
1.00	1530.301	16.328	1.28395	1.50781
1.50	2030.005	16.390	1.27093	1.53052
2.00	2524.547	16.451	1.25987	1.55135
2.50	3013.929	16.512	1.25019	1.57089
3.00	3498.150	16.572	1.24156	1.58948
3.50	3977.209	16.631	1.23374	1.60735
4.00	4451.11	16.690	1.22660	1.6246
4.50	4919.85	16.748	1.22001	1.6415
5.00	5383.42	16.805	1.21391	1.6579
5.50	5841.84	16.862	1.20811	1.6741
6.00	6295.09	16.919	1.20268	1.6900
6.50	6743.19	16.974	1.19777	1.7057
7.00	7186.12	17.029	1.19329	1.7213

TABLE 53.   *RKR potentials for electronic states of* O_2 *and* O_2^+ — Con.

v	V (cm^{-1})	$T_e + V$ (eV)	r_{min} (Å)	r_{max} (Å)
		O_2^+ A $^2\Pi_u$		
− 0.50	0.0	17.082	1.4082204	
− 0.25	223.9937	17.110	1.3627045	1.4599662
0.00	445.99	17.138	1.34550	1.48344
0.50	884.90	17.192	1.32265	1.51895
1.00	1317.03	17.246	1.30623	1.54820
1.50	1742.37	17.298	1.29308	1.57434
2.00	2160.92	17.350	1.28202	1.59857
2.50	2572.70	17.401	1.27240	1.62153
3.00	2977.69	17.451	1.26388	1.64359
3.50	3375.89	17.501	1.25621	1.66498
4.00	3767.31	17.549	1.24923	1.68587
4.50	4151.95	17.597	1.24281	1.70640
5.00	4529.80	17.644	1.23688	1.72666
5.50	4900.87	17.690	1.23135	1.74673
6.00	5265.16	17.735	1.22618	1.76666
6.50	5622.66	17.779	1.22132	1.78652
7.00	5973.37	17.823	1.21672	1.80634
7.50	6317.31	17.865	1.21237	1.82617
8.00	6654.46	17.907	1.20822	1.84604
8.50	6984.82	17.948	1.20427	1.86599
9.00	7308.40	17.988	1.20048	1.88604
		O_2^+ b $^4\Sigma_g^-$		
− 0.50	0.0	18.196	1.2796516	
− 0.25	298.1764	18.233	1.2400818	1.3242684
0.00	594.192	18.270	1.225006	1.344421
0.50	1179.798	18.342	1.204882	1.374788
1.00	1756.836	18.414	1.190329	1.399706
1.50	2325.307	18.484	1.178624	1.421904
2.00	2885.211	18.554	1.168714	1.442435
2.50	3436.547	18.622	1.160065	1.461838
3.00	3979.32	18.689	1.15236	1.48043
3.50	4513.52	18.756	1.14539	1.49843
4.00	5039.15	18.821	1.13902	1.51599
4.50	5556.22	18.885	1.13313	1.53319
5.00	6064.72	18.948	1.12766	1.55014
5.50	6564.65	19.010	1.12254	1.56690
6.00	7056.02	19.071	1.11773	1.58351
6.50	7538.82	19.131	1.11318	1.60003
7.00	8013.05	19.189	1.10886	1.61649

PAUL H. KRUPENIE

TABLE 54. *Lifetimes, Einstein coefficients, and oscillator strengths*

Molecule	Transition	Band	$\tau(s)$	$A_{v'}\ (s^{-1})$	$A_{v'v''}\ (s^{-1})$	Absorption f-value	Ref.
O_2	$a\ ^1\Delta_g - X\ ^3\Sigma_g^-$	0–0	$3.88(10^3)$		$2.58(10^{-4})$	$4.15(10^{-12})$	26
	$b\ ^1\Sigma_g^+ - X\ ^3\Sigma_g^-$	0–0			0.085	$2.47(10^{-10})$	67b
		1–0			(0.0069)		84
		2–0			$(0.1636 \pm .0040)10^{-3}$		356
		1–1			$0.0704 \pm .0042$		356
	$b\ ^1\Sigma_g^+ - a\ ^1\Delta_g$	0–0			$1.5(10^{-3})$		301
	$A\ ^3\Sigma_u^+ - X\ ^3\Sigma_g^-$		$(1-10^3)$				28,420,241,419
		7–0				$1.24(10^{-10})$	174
	$c\ ^1\Sigma_u^- - X\ ^3\Sigma_g^-$			$\sim 10^{-4}$			241
			$> 10^{-3}$				420
	$C\ ^3\Delta_u - X\ ^3\Sigma_g^-$			$\leq 10^{-5}$			241
			$> 10^{-3}$				420
	$B\ ^3\Sigma_u^- - X\ ^3\Sigma_g^-$						(see table 55)
O_2^+	$a\ ^4\Pi_u$		$> 10^{-3}$ (est.)				386,13
	$A\ ^2\Pi_u$	$v=0$	$677(10^{-9})$				
		1	$679(10^{-9})$				
		2	$679(10^{-9})$				
		3	$666(10^{-9})$				
		4	$671(10^{-9})$				
		5	$680(10^{-9})$				
		6	$675(10^{-9})$				
		7	$676(10^{-9})$				220a
	$A\ ^2\Pi_u - X\ ^2\Pi_g$	4–4				$(3.66 \pm .18)10^{-4}$	220a
	$b\ ^4\Sigma_g^-$	$v=0$	$(1.12 \pm .04)10^{-6}$				220a
		1	$(1.10 \pm .05)10^{-6}$				
		2	$(1.22 \pm .04)10^{-6}$				
	$b\ ^4\Sigma_g^- - a\ ^4\Pi_u$	0–0				0.00102	220a

O_2

a–X: Other estimates of transition probability lie within ± 50 percent of the cited value. Badger et al. [26] discuss the pressure dependence of the reciprocal lifetime of the $a\ ^1\Delta_g$ state. (Radiative half life is ~ 0.69 times the cited value.)

b–X: (a) Relative transition probabilities as estimated years ago by Childs [84] would give $A_{11} = 0.068$.

(b) "The probability of the entire electronic transition is equal to 0.0878 ± 0.0053 sec^{-1}" according to Sitnik and Khlystov [356]. This value is approximate.

b–a: Noxon's original estimate [301] of $2.5(10^{-3})$ s^{-1} was based on b–X, 0–0, A-value being 0.143. Uncertainty is a factor of 2.

A–X: (a) Total f-value in the continuum below 2500 Å is estimated as $2(10^{-7})$ [219].

(b) Estimates of the lifetime for the A state range from 10^{-4}s to 10^3s.

(c) f-value for the A–X transition in compressed oxygen is estimated as $\sim 10^{-9}$ [110].

(d) f_{70} is absolute, not relative. Uncertainty is ± 15 percent.

c–X, C–X: Only crude estimates are available.

B–X: (a) See table 55 for a list of band f-values.

(b) $\sum_{v'=2}^{17} f_{v'0} = 2.5(10^{-4})$, but this means little since the continuum so dominates the discrete structure. See sect. 11.6 for a discussion of the B–X continuum (1750–1300 Å).

O_2^+

$A\ ^2\Pi_u$: Uncertainty in lifetime are $\pm 5(10^{-9})$s [220a].

A–X: (a) 4–4 band f-value is calculated [220a].

(b) Fink and Welge [139], from measurements on several A–X bands, obtained $\tau(A\ ^2\Pi_u) - (7.1 \pm 0.6)10^{-7}$s.

$b\ ^4\Sigma_g^-$: All lifetimes are based on data exrapolated to zero pressure.

b–a: f-value for the 0–0 band is calculated (and based on Morse function Franck-Condon factors) [220a]. Vance [386] has estimated b–a lifetime as $< 10^{-6}$s, within an order of magnitude of that estimated from f_{00}. (See Ref. [13] on lifetime.)

TABLE 55. *Absolute f-values for the* O_2 $B\,^3\Sigma_u^- - X\,^3\Sigma_g^-$ *bands*

v'	v''		
	0	1	2
0	3.45 10		
1	3.90–9		
2	2.38–8	5.35–7	
3	9.90–8	2.08–6	
4	3.21–7	6.15–6	
5	8.52–7	1.53–5	
6	1.91–6	3.15–5	2.13–4
7	3.81–6	5.78–5	3.39–4
8	6.68–6	9.40–5	5.46–4
9	1.06–5	1.38–4	9.87–4
10	1.57–5	1.91–4	1.03–3
11	2.09–5	2.38–4	1.04–3
12	2.53–5	2.73–4	1.22–3
13	2.88–5	2.93–4	1.04–3
14	3.03–5	2.95–4	
15	2.92–5	2.77–4	
16	2.59–5	2.42–4	
17	2.23–5	2.01–4	
18	1.83–5		
19	1.44–5		

Data of Ackerman et al. [4] for $v''=0$ and 1 progressions; data of
Hudson and Carter [199a] for $v''=2$ progression. Estimated uncer-
tainty in these measurements is ± 20 percent. Compare also data of
Bethke [10], Halmann and Laulicht [168e], and Hasson et al. [173] which
are in agreement within experimental error (estimated as 10–30%).
However, Bethke's value for the 3–0 band (7.4–8) differs considerably
from that of Ackermann et al. Data of Farmer et al. [131] are discrep-
ant. (Notation: 3.45–8 means 3.45 (10^{-8}), etc.)

TABLE 56. *UV absorption; some special features*

$\lambda(\text{Å})$	$k(\text{cm}^{-1})$	Ref.	Comments
4000–2050	$< 10^{-4}$	373	
1750–1300	390 (peak)		$B-X$ Schumann-Runge continuum.
1800–1400			Peak at 1420 Å. Weak $^3\Pi_u$
1796	0.28	414	(repulsive) $- X\,^3\Sigma_g^-$
1781	0.44		continuum. (f-value for this region estimated as 0.01.)
1352	185		
1332	55		
1293	20		
1244	1200	369, 400	
1205	430	271	
1153	200		
1215.7	0.28		Windows, regions of
1187.1	0.20		minimum absorption.
1166.8	0.29		
1157.0	0.44	271	
1142.8	0.31		
1126.9	0.62		
1108.3	0.20		

Table 57. Franck-Condon integrals.

Franck-Condon integrals are taken from the extensive calculations of Albritton et al.
[9]; these include calculations for unobserved transitions. For the O_2 $A^3\Sigma_u^+-X^3\Sigma_g^-$
transition data from Degen et al. [104] are placed at the end of the table.

$$O_2\ a^1\Delta_g - X^3\Sigma_g^-\ \text{Infrared atmospheric system}$$

v' v"	σ_o	$q_{v'v"}$	$\lambda_o^{(vac)}$	$q_{v'v"}\sigma_o^3$	$q_{v'v"}\sigma_o^4$	$\bar{r}$	$\overline{r^2}$	phase
0, 0	7882.39	9.869−1	12686.51	4.833+11	3.810+15	1.217	1.482	+
1	6326.01	1.297−2	15807.75	3.284+ 9	2.077+13	1.547	2.289	+
2	4793.20	1.260−4	20862.88	1.388+ 7	6.652+10	1.555	2.487	+
1, 0	9365.89	1.303−2	10677.04	1.071+10	1.003+14	0.902	0.713	−
1	7809.51	9.586−1	12804.90	4.566+11	3.566+15	1.227	1.510	+
2	6276.70	2.791−2	15931.93	6.903+ 9	4.333+13	1.547	2.295	+
3	4767.24	4.296−4	20976.49	4.655+ 7	2.219+11	1.568	2.518	+
4	3280.93	1.735−6	30479.12	6.126+ 4	2.010+ 8	2.079	3.782	+
2, 0	10823.59	6.794−5	9239.08	8.615+ 7	9.325+11	0.198	−0.782	+
1	9267.21	2.814−2	10790.73	2.240+10	2.076+14	0.928	0.772	−
2	7734.40	9.258−1	12929.25	4.284+11	3.313+15	1.238	1.539	+
3	6224.94	4.497−2	16064.41	1.085+10	6.752+13	1.547	2.302	+
4	4738.63	9.802−4	21103.12	1.043+ 8	4.942+11	1.581	2.547	+
5	3275.32	6.073−6	30531.37	2.134+ 5	6.989+ 8	2.008	3.622	+
3, 1	10699.11	2.591−4	9346.57	3.173+ 8	3.394+12	0.302	−0.571	+
2	9166.30	4.548−2	10909.53	3.502+10	3.210+14	0.953	0.832	−
3	7656.84	8.881−1	13060.22	3.987+11	3.053+15	1.248	1.568	+
4	6170.53	6.423−2	16206.05	1.509+10	9.312+13	1.548	2.311	+
5	4707.22	1.867−3	21243.96	1.948+ 8	9.168+11	1.592	2.575	+
6	3266.76	1.652−5	30611.33	5.759+ 5	1.881+ 9	1.957	3.510	+

THE CALCULATED ARRAY EXTENDED THROUGH (3,21). Q LESS THAN 1.0−6 HAVE BEEN OMITTED.

$$O_2\ b^1\Sigma_g^+-X^3\Sigma_g^-\ \text{Red atmospheric system}$$

v' v"	σ_o	$q_{v'v"}$	$\lambda_o^{(vac)}$	$q_{v'v"}\sigma_o^3$	$q_{v'v"}\sigma_o^4$	$\bar{r}$	$\overline{r^2}$	phase
0, 0	13120.91	9.308−1	7621.42	2.103+12	2.759+16	1.222	1.495	+
1	11564.53	6.660−2	8647.13	1.030+11	1.191+15	1.370	1.857	+
2	10031.72	2.523−3	9968.38	2.547+ 9	2.555+13	1.464	2.131	+
3	8522.26	5.648−5	11733.98	3.496+ 7	2.979+11	1.573	2.444	+
1, 0	14525.66	6.647−2	6884.37	2.037+11	2.959+15	1.089	1.169	−
1	12969.28	7.928−1	7710.53	1.729+12	2.243+16	1.233	1.524	+
2	11436.47	1.322−1	8743.95	1.977+11	2.261+15	1.378	1.880	+
3	9927.01	8.284−3	10073.53	8.104+ 9	8.045+13	1.471	2.151	+
4	8440.71	2.736−4	11847.35	1.645+ 8	1.388+12	1.574	2.453	+
5	6977.39	6.417−6	14332.01	2.180+ 6	1.521+10	1.636	2.672	+
2, 0	15902.42	2.639−3	6288.35	1.061+10	1.688+14	0.919	0.785	+
1	14346.04	1.315−1	6970.57	3.883+11	5.571+15	1.106	1.210	−
2	12813.23	6.527−1	7804.43	1.373+12	1.759+16	1.243	1.554	+
3	11303.77	1.943−1	8846.61	2.807+11	3.172+15	1.386	1.905	+
4	9817.46	1.802−2	10185.93	1.705+10	1.674+14	1.478	2.172	+
5	8354.15	8.232−4	11970.10	4.799+ 8	4.010+12	1.577	2.464	+
6	6913.69	2.512−5	14464.05	8.301+ 6	5.739+10	1.643	2.690	+
3, 0	17251.09	6.911−5	5796.74	3.548+ 8	6.121+12	0.656	0.240	−
1	15694.71	8.753−3	6371.57	3.384+10	5.311+14	0.947	0.846	+
2	14161.90	1.924−1	7061.20	5.463+11	7.737+15	1.123	1.252	−
3	12652.44	5.144−1	7903.61	1.042+12	1.318+16	1.253	1.583	+
4	11166.14	2.499−1	8955.65	3.479+11	3.885+15	1.394	1.930	+
5	9702.82	3.240−2	10306.28	2.960+10	2.872+14	1.485	2.194	+
6	8262.37	1.968−3	12103.07	1.110+ 9	9.172+12	1.581	2.477	+
7	6844.67	7.617−5	14609.91	2.442+ 7	1.672+11	1.640	2.708	+
8	5449.66	2.025−6	18349.77	3.277+ 5	1.786+ 9	1.728	2.959	+

THE CALCULATED ARRAY EXTENDED THROUGH (3,21). Q LESS THAN 1.0−6 HAVE BEEN OMITTED.

Table 57. Franck-Condon integrals--continued

O_2 $B^3\Sigma_u^- - X^3\Sigma_g^-$ Schumann-Runge system

v' v''	σ_0	$q_{v'v''}$	$\lambda_0^{(vac)}$	$q_{v'v''}\sigma_0^3$	$q_{v'v''}\sigma_0^4$	$\bar{r}$	$\overline{r^2}$	phase
0, 2	46268.90	1.303-6	2161.28	1.290+ 8	5.970+12	1.404	1.974	+
3	44759.43	1.173-5	2234.17	1.052+ 9	4.710+13	1.420	2.017	+
4	43273.13	7.582-5	2310.90	6.144+ 9	2.659+14	1.435	2.061	+
5	41809.81	3.741-4	2391.78	2.734+10	1.143+15	1.451	2.106	+
6	40369.36	1.465-3	2477.13	9.638+10	3.891+15	1.467	2.153	+
7	38951.66	4.676-3	2567.29	2.763+11	1.076+16	1.484	2.202	+
8	37556.65	1.239-2	2662.64	6.563+11	2.465+16	1.500	2.252	+
9	36184.29	2.763-2	2763.63	1.309+12	4.736+16	1.518	2.305	+
10	34834.56	5.240-2	2870.71	2.215+12	7.715+16	1.536	2.360	+
11	33507.49	8.514-2	2984.41	3.203+12	1.073+17	1.554	2.416	+
12	32203.12	1.192-1	3105.29	3.981+12	1.282+17	1.573	2.476	+
13	30921.55	1.443-1	3233.99	4.266+12	1.319+17	1.593	2.538	+
14	29662.88	1.514-1	3371.22	3.951+12	1.172+17	1.614	2.604	+
15	28427.26	1.378-1	3517.75	3.164+12	8.996+16	1.635	2.673	+
16	27214.85	1.087-1	3674.46	2.190+12	5.960+16	1.657	2.746	+
17	26025.87	7.417-2	3842.33	1.307+12	3.403+16	1.680	2.823	+
18	24860.54	4.370-2	4022.44	6.714+11	1.669+16	1.705	2.905	+
19	23719.13	2.213-2	4216.01	2.953+11	7.005+15	1.731	2.993	+
20	22601.94	9.585-3	4424.40	1.107+11	2.501+15	1.758	3.088	+
21	21509.30	3.525-3	4649.15	3.508+10	7.546+14	1.787	3.191	+
1, 2	46956.43	1.234-5	2129.63	1.277+ 9	5.999+13	1.397	1.955	-
3	45446.97	9.847-5	2200.37	9.243+ 9	4.201+14	1.412	1.997	-
4	43960.66	5.557-4	2274.76	4.721+10	2.075+15	1.428	2.040	-
5	42497.35	2.352-3	2353.09	1.805+11	7.672+15	1.443	2.084	-
6	41056.89	7.732-3	2435.64	5.351+11	2.197+16	1.459	2.129	-
7	39639.19	2.013-2	2522.76	1.254+12	4.969+16	1.475	2.176	-
8	38244.18	4.189-2	2614.78	2.343+12	8.961+16	1.491	2.225	-
9	36871.82	6.967-2	2712.10	3.493+12	1.288+17	1.508	2.276	-
10	35522.09	9.140-2	2815.15	4.097+12	1.455+17	1.526	2.328	-
11	34195.02	9.128-2	2924.40	3.650+12	1.248+17	1.543	2.382	-
12	32890.66	6.350-2	3040.38	2.259+12	7.431+16	1.561	2.437	-
13	31609.08	2.328-2	3163.65	7.352+11	2.324+16	1.579	2.490	-
14	30350.41	3.441-4	3294.85	9.619+ 9	2.919+14	1.566	2.427	-
15	29114.79	1.553-2	3434.68	3.833+11	1.116+16	1.629	2.656	+
16	27902.38	6.165-2	3583.92	1.339+12	3.737+16	1.647	2.715	+
17	26713.40	1.087-1	3743.44	2.072+12	5.534+16	1.669	2.786	+
18	25548.07	1.284-1	3914.19	2.142+12	5.472+16	1.692	2.863	+
19	24406.66	1.144-1	4097.24	1.664+12	4.061+16	1.716	2.945	+
20	23289.47	8.062-2	4293.78	1.018+12	2.372+16	1.742	3.034	+
21	22196.83	4.589-2	4505.15	5.018+11	1.114+16	1.770	3.130	+
2, 1	49154.46	5.300-6	2034.40	6.294+ 8	3.094+13	1.376	1.896	+
2	47621.65	6.008-5	2099.88	6.488+ 9	3.090+14	1.391	1.936	+
3	46112.19	4.245-4	2168.62	4.162+10	1.919+15	1.406	1.977	+
4	44625.89	2.087-3	2240.85	1.855+11	8.277+15	1.421	2.019	+
5	43162.57	7.540-3	2316.82	6.063+11	2.617+16	1.436	2.062	+
6	41722.11	2.057-2	2396.81	1.494+12	6.235+16	1.451	2.107	+
7	40304.42	4.280-2	2481.12	2.802+12	1.129+17	1.467	2.152	+
8	38909.41	6.724-2	2570.07	3.961+12	1.541+17	1.483	2.199	+
9	37537.04	7.696-2	2664.04	4.070+12	1.528+17	1.499	2.248	+
10	36187.31	5.824-2	2763.40	2.760+12	9.987+16	1.516	2.297	+
11	34860.24	2.124-2	2868.60	8.997+11	3.136+16	1.531	2.343	+
12	33555.88	5.507-5	2980.10	2.081+ 9	6.982+13	1.476	2.115	+
13	32274.31	1.853-2	3098.44	6.230+11	2.011+16	1.576	2.486	-
14	31015.64	5.696-2	3224.18	1.699+12	5.271+16	1.593	2.537	-
15	29780.01	6.930-2	3357.96	1.830+12	5.450+16	1.611	2.596	-

Table 57. Franck-Condon integrals--continued

O_2 $B^3\Sigma_u^- - X^3\Sigma_g^-$ Schumann-Runge system

v' v"	σ_o	$q_{v'v"}$	$\lambda_o^{(vac)}$	$q_{v'v"}\sigma_o^3$	$q_{v'v"}\sigma_o^4$	$\bar{r}$	$\bar{r^2}$	phase
2,16	28567.61	3.928-2	3500.47	9.157+11	2.616+16	1.630	2.655	−
17	27378.62	3.934-3	3652.49	8.073+10	2.210+15	1.641	2.682	−
18	26213.29	1.018-2	3814.86	1.834+11	4.807+15	1.688	2.854	+
19	25071.89	5.989-2	3988.53	9.439+11	2.366+16	1.705	2.910	+
20	23954.70	1.111-1	4174.55	1.527+12	3.659+16	1.729	2.990	+
21	22862.05	1.257-1	4374.06	1.502+12	3.434+16	1.755	3.078	+
3, 1	49796.27	1.979-5	2008.18	2.443+ 9	1.216+14	1.370	1.880	−
2	48263.47	2.013-4	2071.96	2.263+10	1.092+15	1.385	1.919	−
3	46754.00	1.258-3	2138.85	1.286+11	6.013+15	1.399	1.959	−
4	45267.70	5.375-3	2209.08	4.986+11	2.257+16	1.414	2.000	−
5	43804.38	1.646-2	2282.88	1.384+12	6.061+16	1.429	2.042	−
6	42363.93	3.677-2	2360.50	2.795+12	1.184+17	1.444	2.085	−
7	40946.23	5.929-2	2442.23	4.070+12	1.667+17	1.459	2.129	−
8	39551.22	6.571-2	2528.37	4.066+12	1.608+17	1.475	2.174	−
9	38178.86	4.331-2	2619.25	2.410+12	9.203+16	1.490	2.220	−
10	36829.13	9.417-3	2715.24	4.704+11	1.732+16	1.504	2.258	−
11	35502.06	2.395-3	2816.74	1.072+11	3.805+15	1.536	2.368	+
12	34197.69	3.150-2	2924.17	1.260+12	4.308+16	1.546	2.391	+
13	32916.12	5.446-2	3038.02	1.942+12	6.393+16	1.562	2.441	+
14	31657.45	3.492-2	3158.81	1.108+12	3.508+16	1.579	2.492	+
15	30421.83	2.823-3	3287.11	7.948+10	2.418+15	1.587	2.508	+
16	29209.42	1.221-2	3423.55	3.042+11	8.885+15	1.628	2.657	−
17	28020.44	5.283-2	3568.82	1.162+12	3.257+16	1.644	2.706	−
18	26855.11	6.233-2	3723.69	1.207+12	3.242+16	1.664	2.769	−
19	25713.70	2.540-2	3888.98	4.319+11	1.111+16	1.683	2.829	−
20	24596.51	2.017-5	4065.62	3.001+ 8	7.382+12	1.984	4.041	+
21	23503.87	3.218-2	4254.62	4.178+11	9.821+15	1.745	3.050	+
4, 0	51969.72	2.881-6	1924.20	4.044+ 8	2.102+13	1.351	1.826	+
1	50413.34	5.726-5	1983.60	7.337+ 9	3.699+14	1.365	1.864	+
2	48880.54	5.232-4	2045.80	6.110+10	2.987+15	1.379	1.902	+
3	47371.08	2.893-3	2110.99	3.075+11	1.457+16	1.393	1.941	+
4	45884.77	1.070-2	2179.37	1.034+12	4.745+16	1.407	1.982	+
5	44421.45	2.756-2	2251.17	2.416+12	1.073+17	1.422	2.023	+
6	42981.00	4.941-2	2326.61	3.924+12	1.686+17	1.437	2.065	+
7	41563.30	5.894-2	2405.97	4.232+12	1.759+17	1.452	2.107	+
8	40168.29	4.031-2	2489.53	2.612+12	1.049+17	1.467	2.150	+
9	38795.93	8.393-3	2577.59	4.901+11	1.901+16	1.479	2.185	+
10	37446.20	2.916-3	2670.50	1.531+11	5.734+15	1.509	2.284	−
11	36119.13	3.091-2	2768.62	1.456+12	5.260+16	1.519	2.309	−
12	34814.77	4.503-2	2872.34	1.900+12	6.615+16	1.535	2.355	−
13	33533.19	1.900-2	2982.12	7.165+11	2.403+16	1.550	2.399	−
14	32274.52	1.902-4	3098.42	6.393+ 9	2.063+14	1.622	2.664	+
15	31038.90	2.620-2	3221.76	7.836+11	2.432+16	1.594	2.544	+
16	29826.49	4.910-2	3352.72	1.303+12	3.886+16	1.611	2.595	+
17	28637.51	2.392-2	3491.92	5.618+11	1.609+16	1.627	2.645	+
18	27472.18	2.859-5	3640.05	5.928+ 8	1.629+13	1.840	3.479	−
19	26330.77	2.924-2	3797.84	5.338+11	1.406+16	1.680	2.827	−
20	25213.58	6.313-2	3966.12	1.012+12	2.551+16	1.699	2.889	−
21	24120.94	4.079-2	4145.78	5.725+11	1.381+16	1.720	2.955	−
5, 0	52560.52	P 7.576-6	1902.57	1.100+ 9	5.782+13	1.345	1.811	−
1	51004.14	P 1.371-4	1960.63	1.819+10	9.278+14	1.359	1.849	−
2	49471.33	P 1.126-3	2021.37	1.364+11	6.747+15	1.373	1.886	−
3	47961.87	P 5.506-3	2084.99	6.075+11	2.914+16	1.387	1.925	−
4	46475.57	P 1.758-2	2151.67	1.765+12	8.204+16	1.401	1.965	−
5	45012.25	P 3.768-2	2221.62	3.436+12	1.547+17	1.416	2.005	−

Table 57. Franck-Condon integrals--continued

$$O_2 \; B^3\Sigma_u^- - X^3\Sigma_g^- \; \text{Schumann-Runge system}$$

v' v''	σ_o	$q_{v'v''}$	$\lambda_o^{(vac)}$	$q_{v'v''}\sigma_o^3$	$q_{v'v''}\sigma_o^4$	$\bar{r}$	$\bar{r^2}$	phase
5, 6	43571.80	P 5.278-2	2295.06	4.366+12	1.902+17	1.430	2.046	−
7	42154.10	P 4.298-2	2372.25	3.220+12	1.357+17	1.445	2.086	−
8	40759.09	P 1.283-2	2453.44	8.685+11	3.540+16	1.458	2.123	−
9	39386.72	P 7.930-4	2538.93	4.845+10	1.908+15	1.492	2.239	+
10	38037.00	P 2.408-2	2629.02	1.325+12	5.040+16	1.495	2.236	+
11	36709.93	P 3.928-2	2724.06	1.943+12	7.134+16	1.509	2.279	+
12	35405.56	P 1.579-2	2824.42	7.006+11	2.481+16	1.524	2.318	+
13	34123.99	P 6.553-4	2930.49	2.604+10	8.886+14	1.568	2.478	−
14	32865.32	P 2.667-2	3042.72	9.467+11	3.111+16	1.565	2.452	−
15	31629.70	P 3.844-2	3161.59	1.216+12	3.848+16	1.581	2.498	−
16	30417.29	P 9.388-3	3287.60	2.642+11	8.036;15	1.594	2.535	−
17	29228.30	P 5.262-3	3421.34	1.314+11	3.840+15	1.633	2.674	+
18	28062.98	P 3.970-2	3563.41	8.773+11	2.462+16	1.644	2.704	+
19	26921.57	P 3.805-2	3714.49	7.424+11	1.998+16	1.661	2.759	+
20	25804.38	P 3.340-3	3875.31	5.740+10	1.481+15	1.667	2.766	+
21	24711.73	P 1.609-2	4046.66	2.428+11	6.001+15	1.719	2.961	−
6, 0	53123.30	P 1.711-5	1882.41	2.565+ 9	1.362+14	1.340	1.798	+
1	51566.92	P 2.826-4	1939.23	3.874+10	1.998+15	1.354	1.834	+
2	50034.12	P 2.090-3	1998.64	2.618+11	1.310+16	1.368	1.872	+
3	48524.66	P 9.032-3	2060.81	1.032+12	5.008+16	1.382	1.910	+
4	47038.35	P 2.481-2	2125.93	2.582+12	1.214+17	1.396	1.949	+
5	45575.03	P 4.367-2	2194.18	4.133+12	1.884+17	1.410	1.988	+
6	44134.58	P 4.591-2	2265.80	3.947+12	1.742+17	1.424	2.027	+
7	42716.88	P 2.182-2	2341.00	1.701+12	7.265+16	1.438	2.065	+
8	41321.87	P 3.507-4	2420.03	2.474+10	1.022+15	1.434	2.038	+
9	39949.51	P 1.395-2	2503.16	8.896+11	3.554+16	1.473	2.172	−
10	38599.78	P 3.470-2	2590.69	1.996+12	7.703+16	1.486	2.210	−
11	37272.71	P 1.896-2	2682.93	9.820+11	3.660+16	1.500	2.248	−
12	35968.35	P 1.153-5	2780.22	5.366+ 8	1.930+13	1.683	2.931	+
13	34686.77	P 2.070-2	2882.94	8.638+11	2.996+16	1.539	2.372	+
14	33428.10	P 3.298-2	2991.50	1.232+12	4.118+16	1.554	2.414	+
15	32192.48	P 6.965-3	3106.32	2.323+11	7.480+15	1.565	2.445	+
16	30980.07	P 6.669-3	3227.88	1.983+11	6.143+15	1.601	2.568	−
17	29791.09	P 3.556-2	3356.71	9.401+11	2.801+16	1.613	2.601	−
18	28625.76	P 2.279-2	3493.36	5.346+11	1.530+16	1.628	2.647	−
19	27484.35	P 6.201-5	3638.43	1.287+ 9	3.538+13	1.783	3.251	+
20	26367.16	P 2.848-2	3792.60	5.221+11	1.377+16	1.679	2.821	+
21	25274.52	P 4.287-2	3956.55	6.921+11	1.749+16	1.696	2.877	+
7, 0	53656.09	3.402-5	1863.72	5.254+ 9	2.819+14	1.335	1.785	−
1	52099.71	5.141-4	1919.40	7.270+10	3.788+15	1.349	1.821	−
2	50566.90	3.432-3	1977.58	4.437+11	2.244+16	1.363	1.858	−
3	49057.44	1.311-2	2038.43	1.548+12	7.594+16	1.377	1.896	−
4	47571.13	3.084-2	2102.12	3.320+12	1.579+17	1.390	1.934	−
5	46107.82	4.388-2	2168.83	4.301+12	1.983+17	1.404	1.972	−
6	44667.36	3.255-2	2238.77	2.901+12	1.296+17	1.418	2.010	−
7	43249.66	6.024-3	2312.16	4.874+11	2.108+16	1.429	2.040	−
8	41854.65	3.883-3	2389.22	2.847+11	1.191+16	1.454	2.119	+
9	40482.29	2.672-2	2470.22	1.773+12	7.175+16	1.465	2.147	+
10	39132.56	2.477-2	2555.42	1.484+12	5.808+16	1.478	2.185	+
11	37805.49	1.646-3	2645.12	8.895+10	3.363+15	1.484	2.192	+
12	36501.13	1.149-2	2739.64	5.589+11	2.040+16	1.516	2.303	−
13	35219.56	2.986-2	2839.33	1.305+12	4.595+16	1.529	2.339	−
14	33960.89	9.879-3	2944.56	3.869+11	1.314+16	1.542	2.373	−
15	32725.26	3.412-3	3055.74	1.196+11	3.913+15	1.576	2.492	+
16	31512.85	2.905-2	3173.31	9.092+11	2.865+16	1.585	2.512	+

PAUL H. KRUPENIE

Table 57. Franck-Condon integrals--continued

$$O_2 \; B^3\Sigma_u^- - X^3\Sigma_g^- \text{ Schumann-Runge system}$$

v' v''	σ_0	$q_{v'v''}$	$\lambda_0^{(vac)}$	$q_{v'v''}\sigma_0^3$	$q_{v'v''}\sigma_0^4$	$\bar{r}$	$\overline{r^2}$	phase
7,17	30323.87	1.910-2	3297.73	5.326+11	1.615+16	1.599	2.554	+
18	29158.54	2.712-4	3429.53	6.724+ 9	1.961+14	1.677	2.846	-
19	28017.13	2.661-2	3569.24	5.853+11	1.640+16	1.646	2.711	-
20	26899.95	2.968-2	3717.48	5.777+11	1.554+16	1.662	2.759	-
21	25807.30	8.707-4	3874.87	1.497+10	3.862+14	1.647	2.686	-
8, 0	54156.63	6.054-5	1846.50	9.616+ 9	5.208+14	1.331	1.773	+
1	52600.25	8.401-4	1901.13	1.223+11	6.431+15	1.345	1.809	+
2	51067.44	5.073-3	1958.19	6.756+11	3.450+16	1.358	1.845	+
3	49557.98	1.715-2	2017.84	2.088+12	1.035+17	1.372	1.882	+
4	48071.67	3.441-2	2080.23	3.823+12	1.838+17	1.385	1.920	+
5	46608.36	3.877-2	2145.54	3.925+12	1.829+17	1.399	1.957	+
6	45167.90	1.826-2	2213.96	1.682+12	7.598+16	1.412	1.993	+
7	43750.20	9.514-5	2285.70	7.967+ 9	3.486+14	1.395	1.918	+
8	42355.19	1.391-2	2360.99	1.057+12	4.477+16	1.445	2.091	-
9	40982.83	2.748-2	2440.05	1.892+12	7.754+16	1.458	2.126	-
10	39633.10	8.768-3	2523.14	5.458+11	2.163+16	1.470	2.158	-
11	38306.03	2.581-3	2610.56	1.451+11	5.558+15	1.499	2.254	+
12	37001.67	2.385-2	2702.58	1.208+12	4.471+16	1.507	2.272	+
13	35720.09	1.625-2	2799.55	7.405+11	2.645+16	1.520	2.308	+
14	34461.42	1.529-4	2901.80	6.257+ 9	2.156+14	1.588	2.558	-
15	33225.80	2.062-2	3009.71	7.564+11	2.513+16	1.560	2.434	-
16	32013.39	2.095-2	3123.69	6.874+11	2.201+16	1.573	2.474	-
17	30824.41	8.690-5	3244.18	2.545+ 9	7.845+13	1.512	2.219	-
18	29659.08	1.948-2	3371.65	5.081+11	1.507+16	1.617	2.618	+
19	28517.67	2.541-2	3506.60	5.894+11	1.681+16	1.631	2.660	+
20	27400.48	6.319-4	3649.57	1.300+10	3.562+14	1.615	2.578	+
21	26307.84	1.971-2	3801.15	3.589+11	9.441+15	1.681	2.830	-
9, 0	54622.43	9.751-5	1830.75	1.589+10	8.680+14	1.327	1.762	-
1	53066.05	1.247-3	1884.44	1.864+11	9.889+15	1.340	1.798	-
2	51533.24	6.837-3	1940.50	9.357+11	4.822+16	1.354	1.834	-
3	50023.78	2.050-2	1999.05	2.566+12	1.283+17	1.367	1.870	-
4	48537.47	3.494-2	2060.26	3.995+12	1.939+17	1.381	1.907	-
5	47074.16	3.033-2	2124.31	3.164+12	1.490+17	1.394	1.943	-
6	45633.70	7.361-3	2191.36	6.995+11	3.192+16	1.406	1.975	-
7	44216.00	2.176-3	2261.63	1.881+11	8.318+15	1.430	2.049	+
8	42820.99	2.106-2	2335.30	1.654+12	7.082+16	1.439	2.072	+
9	41448.63	1.874-2	2412.63	1.335+12	5.532+16	1.452	2.106	+
10	40098.90	4.568-4	2493.83	2.945+10	1.181+15	1.449	2.083	+
11	38771.83	1.248-2	2579.19	7.274+11	2.820+16	1.487	2.213	-
12	37467.47	2.162-2	2668.98	1.137+12	4.260+16	1.499	2.247	-
13	36185.90	2.303-3	2763.51	1.091+11	3.949+15	1.506	2.259	-
14	34927.23	9.561-3	2863.10	4.074+11	1.423+16	1.538	2.369	+
15	33691.60	2.279-2	2968.10	8.716+11	2.936+16	1.550	2.402	+
16	32479.19	3.042-3	3078.89	1.042+11	3.385+15	1.557	2.417	+
17	31290.21	9.800-3	3195.89	3.002+11	9.394+15	1.593	2.541	-
18	30124.88	2.439-2	3319.51	6.669+11	2.009+16	1.605	2.576	-
19	28983.47	2.819-3	3450.24	6.863+10	1.989+15	1.610	2.581	-
20	27866.29	1.209-2	3588.57	2.616+11	7.290+15	1.652	2.735	+
21	26773.64	2.710-2	3735.02	5.202+11	1.393+16	1.665	2.773	+
10, 0	55050.81	1.431-4	1816.50	2.388+10	1.315+15	1.323	1.752	+
1	53494.43	1.695-3	1869.35	2.595+11	1.388+16	1.337	1.788	+
2	51961.62	8.477-3	1924.50	1.189+12	6.179+16	1.350	1.823	+
3	50452.16	2.260-2	1982.08	2.902+12	1.464+17	1.363	1.859	+
4	48965.86	3.264-2	2042.24	3.832+12	1.876+17	1.377	1.895	+
5	47502.54	2.108-2	2105.15	2.260+12	1.073+17	1.390	1.930	+

Table 57. Franck-Condon integrals--continued

O_2 $B^3\Sigma_u^- - X^3\Sigma_g^-$ Schumann-Runge system

v' v"	σ_o	$q_{v'v"}$	$\lambda_o^{(vac)}$	$q_{v'v"}\sigma_o^3$	$q_{v'v"}\sigma_o^4$	$\bar{r}$	$\bar{r^2}$	phase
10, 6	46062.09	1.519-3	2170.98	1.485+11	6.839+15	1.398	1.949	+
7	44644.39	7.537-3	2239.92	6.707+11	2.994+16	1.422	2.023	-
8	43249.38	2.177-2	2312.17	1.761+12	7.617+16	1.434	2.055	-
9	41877.01	8.458-3	2387.94	6.211+11	2.601+16	1.445	2.086	-
10	40527.29	1.628-3	2467.47	1.083+11	4.391+15	1.473	2.178	+
11	39200.21	1.853-2	2551.01	1.116+12	4.375+16	1.480	2.191	+
12	37895.85	1.097-2	2638.81	5.972+11	2.263+16	1.492	2.223	+
13	36614.28	8.241-4	2731.18	4.045+10	1.481+15	1.529	2.350	-
14	35355.61	1.821-2	2828.40	8.048+11	2.845+16	1.529	2.338	-
15	34119.98	1.076-2	2930.83	4.274+11	1.458+16	1.541	2.371	-
16	32907.58	1.405-3	3038.81	5.005+10	1.647+15	1.578	2.503	+
17	31718.59	2.012-2	3152.73	6.421+11	2.037+16	1.581	2.501	+
18	30553.27	8.941-3	3272.97	2.550+11	7.791+15	1.593	2.533	+
19	29411.86	3.449-3	3399.99	8.776+10	2.581+15	1.631	2.669	-
20	28294.67	2.323-2	3534.24	5.262+11	1.489+16	1.638	2.684	-
21	27202.02	6.200-3	3676.20	1.248+11	3.394+15	1.648	2.707	-
11, 0	55439.05	1.924-4	1803.78	3.279+10	1.818+15	1.320	1.744	-
1	53882.67	2.123-3	1855.88	3.321+11	1.789+16	1.333	1.778	-
2	52349.86	9.733-3	1910.22	1.396+12	7.310+16	1.346	1.814	-
3	50840.40	2.318-2	1966.94	3.046+12	1.549+17	1.360	1.849	-
4	49354.09	2.832-2	2026.18	3.405+12	1.680+17	1.373	1.885	-
5	47890.78	1.299-2	2088.08	1.426+12	6.831+16	1.385	1.918	-
7	45032.62	1.211-2	2220.61	1.106+12	4.981+16	1.416	2.008	+
8	43637.61	1.756-2	2291.60	1.459+12	6.369+16	1.429	2.041	+
9	42265.25	1.968-3	2366.01	1.486+11	6.281+15	1.437	2.058	+
10	40915.52	6.765-3	2444.06	4.633+11	1.896+16	1.463	2.142	-
11	39588.45	1.708-2	2525.99	1.060+12	4.196+16	1.474	2.172	-
12	38284.09	2.544-3	2612.05	1.427+11	5.465+15	1.482	2.189	-
13	37002.52	6.706-3	2702.52	3.397+11	1.257+16	1.511	2.286	-
14	35743.84	1.671-2	2797.68	7.633+11	2.728+16	1.522	2.315	+
15	34508.22	1.400-3	2897.86	5.754+10	1.986+15	1.525	2.315	+
16	33295.81	9.526-3	3003.38	3.516+11	1.171+16	1.561	2.439	-
17	32106.83	1.579-2	3114.60	5.225+11	1.677+16	1.572	2.471	-
18	30941.50	1.107-4	3231.90	3.280+ 9	1.015+14	1.527	2.279	-
19	29800.09	1.450-2	3355.69	3.836+11	1.143+16	1.614	2.609	+
20	28682.90	1.315-2	3486.40	3.103+11	8.900+15	1.627	2.643	+
21	27590.26	7.435-4	3624.47	1.561+10	4.308+14	1.684	2.856	+
12, 0	55784.58	2.377-4	1792.61	4.126+10	2.302+15	1.317	1.736	+
1	54228.20	2.458-3	1844.06	3.919+11	2.125+16	1.330	1.770	+
2	52695.40	1.041-2	1897.70	1.523+12	8.023+16	1.343	1.805	+
3	51185.94	2.229-2	1953.66	2.989+12	1.530+17	1.356	1.840	+
4	49699.63	2.305-2	2012.09	2.830+12	1.406+17	1.370	1.875	+
5	48236.31	7.040-3	2073.13	7.901+11	3.811+16	1.381	1.907	+
6	46795.86	9.564-4	2136.94	9.800+10	4.586+15	1.404	1.978	-
7	45378.16	1.407-2	2203.70	1.315+12	5.966+16	1.412	1.995	-
8	43983.15	1.170-2	2273.60	9.953+11	4.378+16	1.424	2.028	-
9	42610.79	1.015-5	2346.82	7.853+ 8	3.346+13	1.341	1.706	-
10	41261.06	1.068-2	2423.59	7.505+11	3.096+16	1.457	2.124	+
11	39933.99	1.153-2	2504.13	7.340+11	2.931+16	1.469	2.156	+
13	37348.05	1.145-2	2677.52	5.965+11	2.228+16	1.504	2.263	-
14	36089.38	9.696-3	2770.90	4.557+11	1.645+16	1.515	2.293	-
15	34853.76	4.485-4	2869.13	1.899+10	6.619+14	1.559	2.447	+
16	33641.35	1.406-2	2972.53	5.353+11	1.801+16	1.553	2.412	+
17	32452.37	6.219-3	3081.44	2.125+11	6.897+15	1.563	2.439	+
18	31287.04	3.129-3	3196.21	9.583+10	2.998+15	1.597	2.559	-

Table 57.　Franck-Condon integrals--continued

$$O_2 \; B^3\Sigma_u^- - X^3\Sigma_g^- \; \text{Schumann-Runge system}$$

v' v''	σ_0	$q_{v'v''}$	$\lambda_0^{(vac)}$	$q_{v'v''}\sigma_0^3$	$q_{v'v''}\sigma_0^4$	$\bar{r}$	$\overline{r^2}$	phase
12,19	30145.63	1.613-2	3317.23	4.420+11	1.332+16	1.605	2.577	−
20	29028.44	2.021-3	3444.90	4.943+10	1.435+15	1.609	2.577	−
21	27935.80	9.203-3	3579.64	2.006+11	5.605+15	1.650	2.728	+
13, 0	56085.41	2.701-4	1783.00	4.766+10	2.673+15	1.314	1.729	−
1	54529.04	2.638-3	1833.88	4.277+11	2.332+16	1.328	1.763	−
2	52996.23	1.040-2	1886.93	1.548+12	8.202+16	1.341	1.798	−
3	51486.77	2.020-2	1942.25	2.756+12	1.419+17	1.354	1.833	−
4	50000.46	1.776-2	1999.98	2.220+12	1.110+17	1.367	1.867	−
5	48537.14	3.306-3	2060.28	3.780+11	1.835+16	1.378	1.895	−
6	47096.69	2.611-3	2123.29	2.728+11	1.285+16	1.398	1.958	+
7	45678.99	1.352-2	2189.19	1.288+12	5.885+16	1.409	1.985	+
8	44283.98	6.607-3	2258.15	5.738+11	2.541+16	1.420	2.015	+
9	42911.62	7.408-4	2330.37	5.854+10	2.512+15	1.447	2.104	−
10	41561.89	1.160-2	2406.05	8.328+11	3.461+16	1.453	2.111	−
11	40234.82	5.998-3	2485.41	3.907+11	1.572+16	1.464	2.140	−
12	38930.46	1.245-3	2568.68	7.346+10	2.860+15	1.492	2.236	+
13	37648.88	1.200-2	2656.12	6.404+11	2.411+16	1.498	2.246	+
14	36390.21	3.605-3	2747.99	1.737+11	6.321+15	1.508	2.269	+
15	35154.59	3.607-3	2844.58	1.567+11	5.508+15	1.537	2.368	−
16	33942.18	1.225-2	2946.19	4.791+11	1.626+16	1.546	2.391	−
17	32753.20	7.873-4	3053.14	2.766+10	9.060+14	1.546	2.375	−
18	31587.87	8.314-3	3165.77	2.620+11	8.277+15	1.586	2.519	+
19	30446.46	9.930-3	3284.45	2.803+11	8.533+15	1.597	2.549	+
20	29329.27	3.204-4	3409.56	8.084+ 9	2.371+14	1.658	2.775	−
21	28236.63	1.365-2	3541.50	3.072+11	8.674+15	1.640	2.692	−

THE CALCULATED ARRAY EXTENDED THROUGH (13,21). Q LESS THAN 1.0-6 HAVE BEEN OMITTED.

$$O_2^+ \; X^2\Pi_g - O_2 \; X^3\Sigma_g^- \; \text{Ionization system}$$

v' v''	σ_0	$q_{v'v''}$	$\lambda_0^{(vac)}$	$q_{v'v''}\sigma_0^3$	$q_{v'v''}\sigma_0^4$	$\bar{r}$	$\overline{r^2}$	phase
0, 0	97365.00	1.884-1	1027.06	1.739+14	1.693+19	1.166	1.360	+
1	95808.62	2.710-1	1043.75	2.384+14	2.284+19	1.141	1.302	−
2	94275.81	2.292-1	1060.72	1.921+14	1.811+19	1.119	1.251	+
3	92766.35	1.495-1	1077.98	1.194+14	1.107+19	1.098	1.206	−
4	91280.04	8.364-2	1095.53	6.361+13	5.806+18	1.080	1.165	+
5	89816.73	4.232-2	1113.38	3.066+13	2.754+18	1.063	1.128	−
6	88376.27	2.000-2	1131.53	1.381+13	1.220+18	1.046	1.093	+
7	86958.58	9.017-3	1149.97	5.929+12	5.156+17	1.031	1.062	−
8	85563.57	3.932-3	1168.72	2.463+12	2.108+17	1.017	1.033	+
9	84191.20	1.676-3	1187.77	1.000+12	8.423+16	1.004	1.005	−
10	82841.47	7.041-4	1207.13	4.003+11	3.316+16	0.991	0.980	+
11	81514.40	2.931-4	1226.78	1.587+11	1.294+16	0.979	0.956	−
12	80210.04	1.215-4	1246.73	6.270+10	5.029+15	0.968	0.933	+
13	78928.47	5.040-5	1266.97	2.478+10	1.956+15	0.957	0.912	−
14	77669.80	2.099-5	1287.50	9.834+ 9	7.638+14	0.947	0.893	+
15	76434.17	8.806-6	1308.31	3.932+ 9	3.005+14	0.937	0.874	−
16	75221.77	3.734-6	1329.40	1.589+ 9	1.195+14	0.928	0.857	+
17	74032.78	1.605-6	1350.75	6.511+ 8	4.820+13	0.919	0.841	−
1, 0	99237.57	3.645-1	1007.68	3.563+14	3.536+19	1.196	1.430	+
1	97681.19	8.139-2	1023.74	7.585+13	7.409+18	1.163	1.351	−
2	96148.38	5.385-3	1040.06	4.787+12	4.602+17	1.168	1.377	−
3	94638.92	8.398-2	1056.65	7.118+13	6.737+18	1.128	1.273	+
4	93152.61	1.337-1	1073.51	1.081+14	1.007+19	1.106	1.222	−
5	91689.30	1.246-1	1090.64	9.603+13	8.805+18	1.086	1.179	+
6	90248.84	8.953-2	1108.05	6.581+13	5.939+18	1.068	1.140	−

Table 57. Franck-Condon integrals--continued

$$O_2^+ \; X^2\Pi_g - O_2 \; X^3\Sigma_g^- \; \text{Ionization system}$$

v' v''	σ_o	$q_{v'v''}$	$\lambda_o^{(vac)}$	$q_{v'v''}\sigma_o^3$	$q_{v'v''}\sigma_o^4$	$\bar{r}$	$\overline{r^2}$	phase
7	88831.14	5.515−2	1125.73	3.866+13	3.434+18	1.052	1.106	+
8	87436.13	3.073−2	1143.69	2.054+13	1.796+18	1.037	1.073	+
9	86063.77	1.598−2	1161.93	1.019+13	8.768+17	1.023	1.044	+
10	84714.04	7.920−3	1180.44	4.815+12	4.079+17	1.009	1.016	−
11	83386.97	3.794−3	1199.23	2.200+12	1.834+17	0.997	0.991	+
12	82082.61	1.775−3	1218.28	9.816+11	8.057+16	0.985	0.967	−
13	80801.04	8.175−4	1237.61	4.313+11	3.485+16	0.973	0.944	+
14	79542.37	3.731−4	1257.19	1.878+11	1.493+16	0.962	0.923	−
15	78306.74	1.696−4	1277.03	8.144+10	6.377+15	0.952	0.903	+
16	77094.33	7.715−5	1297.11	3.535+10	2.725+15	0.942	0.885	−
17	75905.35	3.525−5	1317.43	1.542+10	1.170+15	0.933	0.867	+
18	74740.02	1.624−5	1337.97	6.780+ 9	5.067+14	0.925	0.852	−
19	73598.61	7.565−6	1358.72	3.016+ 9	2.220+14	0.917	0.837	+
20	72481.43	3.574−6	1379.66	1.361+ 9	9.865+13	0.910	0.824	−
21	71388.78	1.717−6	1400.78	6.246+ 8	4.459+13	0.903	0.812	+
2, 0	101077.57	2.901−1	989.34	2.995+14	3.028+19	1.229	1.510	+
1	99521.19	4.502−2	1004.81	4.438+13	4.416+18	1.212	1.473	+
2	97988.38	1.659−1	1020.53	1.561+14	1.530+19	1.174	1.378	−
3	96478.92	5.231−2	1036.50	4.698+13	4.532+18	1.143	1.304	+
4	94992.61	6.789−4	1052.71	5.819+11	5.528+16	1.195	1.459	+
5	93529.30	4.470−2	1069.18	3.657+13	3.420+18	1.115	1.246	−
6	92088.84	8.982−2	1085.91	7.015+13	6.460+18	1.093	1.195	+
7	90671.15	9.816−2	1102.89	7.317+13	6.634+18	1.074	1.155	−
8	89276.14	8.056−2	1120.12	5.733+13	5.118+18	1.058	1.118	+
9	87903.77	5.584−2	1137.61	3.793+13	3.334+18	1.043	1.086	−
10	86554.04	3.466−2	1155.35	2.247+13	1.945+18	1.028	1.055	+
11	85226.97	1.993−2	1173.34	1.234+13	1.052+18	1.015	1.028	−
12	83922.61	1.086−2	1191.57	6.419+12	5.387+17	1.002	1.002	+
13	82641.04	5.692−3	1210.05	3.213+12	2.655+17	0.990	0.978	−
14	81382.37	2.903−3	1228.77	1.565+12	1.273+17	0.979	0.955	+
2,15	80146.74	1.453−3	1247.71	7.481+11	5.996+16	0.968	0.934	−
16	78934.34	7.190−4	1266.88	3.536+11	2.791+16	0.958	0.914	+
17	77745.35	3.536−4	1286.25	1.661+11	1.292+16	0.948	0.895	−
18	76580.02	1.737−4	1305.02	7.000+10	5.973+15	0.939	0.878	+
19	75438.62	8.556−5	1325.58	3.673+10	2.771+15	0.930	0.862	−
20	74321.43	4.243−5	1345.51	1.742+10	1.294+15	0.922	0.847	+
21	73228.78	2.124−5	1365.58	8.340+ 9	6.108+14	0.915	0.834	−
3, 0	102885.01	1.227−1	971.96	1.337+14	1.375+19	1.266	1.602	+
1	101328.63	2.602−1	986.89	2.707+14	2.743+19	1.238	1.533	+
2	99795.82	1.529−2	1002.05	1.520+13	1.516+18	1.182	1.386	−
3	98286.36	7.426−2	1017.44	7.051+13	6.930+18	1.185	1.408	−
4	96800.05	1.092−1	1033.06	9.903+13	9.586+18	1.154	1.331	+
5	95336.74	3.006−2	1048.91	2.605+13	2.483+18	1.125	1.259	−
6	93896.28	7.590−4	1065.00	6.283+11	5.900+16	1.173	1.407	−
7	92478.59	3.233−2	1081.33	2.557+13	2.365+18	1.102	1.219	−
8	91083.57	6.789−2	1097.89	5.130+13	4.673+18	1.081	1.171	−
9	89711.21	7.938−2	1114.69	5.731+13	5.142+18	1.064	1.132	+
10	88361.48	7.016−2	1131.72	4.840+13	4.277+18	1.048	1.098	−
11	87034.41	5.246−2	1148.97	3.458+13	3.010+18	1.034	1.068	+
12	85730.05	3.512−2	1166.45	2.213+13	1.897+18	1.020	1.039	−
13	84448.48	2.177−2	1184.15	1.311+13	1.107+18	1.007	1.013	+
14	83189.81	1.277−2	1202.07	7.352+12	6.116+17	0.995	0.989	−
15	81954.18	7.199−3	1220.19	3.963+12	3.248+17	0.984	0.966	+
16	80741.78	3.945−3	1238.52	2.076+12	1.677+17	0.973	0.945	−
17	79552.79	2.120−3	1257.03	1.067+12	8.490+16	0.963	0.925	+

Table 57.　Franck-Condon integrals--continued

$$O_2^+ \; X^2\Pi_g - O_2 \; X^3\Sigma_g^- \text{ Ionization system}$$

v' v"	σ_o	$q_{v'v''}$	$\lambda_o^{(vac)}$	$q_{v'v''}\sigma_o^3$	$q_{v'v''}\sigma_o^4$	$\bar{r}$	$\overline{r^2}$	phase
18	78387.46	1.125-3	1275.71	5.417+11	4.246+16	0.954	0.906	−
19	77246.06	5.927-4	1294.56	2.732+11	2.110+16	0.944	0.889	+
20	76128.87	3.117-4	1313.56	1.375+11	1.047+16	0.936	0.873	−
21	75036.22	1.642-4	1332.69	6.937+10	5.205+15	0.928	0.858	+
4, 0	104659.88	2.977-2	955.48	3.413+13	3.572+18	1.310	1.714	+
1	103103.50	2.349-1	969.90	2.575+14	2.655+19	1.274	1.623	+
2	101570.70	1.139-1	984.54	1.193+14	1.212+19	1.250	1.566	+
3	100061.24	9.524-2	999.39	9.542+13	9.547+18	1.204	1.447	−
4	98574.93	4.733-3	1014.46	4.533+12	4.469+17	1.224	1.516	−
5	97111.61	8.316-2	1029.74	7.616+13	7.396+18	1.163	1.355	+
6	95671.16	7.360-2	1045.25	6.445+13	6.166+18	1.135	1.288	−
7	94253.46	1.558-2	1060.97	1.304+13	1.229+18	1.106	1.216	+
8	92858.45	1.645-3	1076.91	1.317+12	1.223+17	1.138	1.316	+
9	91486.09	2.743-2	1093.06	2.101+13	1.922+18	1.090	1.193	−
10	90136.36	5.529-2	1109.43	4.049+13	3.649+18	1.071	1.148	+
11	88809.29	6.608-2	1126.01	4.628+13	4.110+18	1.054	1.112	−
12	87504.93	6.093-2	1142.79	4.082+13	3.572+18	1.040	1.080	+
13	86223.35	4.797-2	1159.78	3.075+13	2.651+18	1.026	1.051	−
14	84964.68	3.397-2	1176.96	2.084+13	1.770+18	1.013	1.025	+
15	83729.06	2.234-2	1194.33	1.311+13	1.098+18	1.001	1.000	−
16	82516.65	1.392-2	1211.88	7.820+12	6.453+17	0.990	0.977	+
17	81327.67	8.343-3	1229.59	4.488+12	3.650+17	0.979	0.956	−
18	80162.34	4.863-3	1247.47	2.505+12	2.008+17	0.969	0.936	+
19	79020.93	2.780-3	1265.49	1.372+12	1.084+17	0.959	0.917	−
20	77903.74	1.569-3	1283.63	7.419+11	5.780+16	0.950	0.900	+
21	76811.10	8.794-4	1301.90	3.985+11	3.061+16	0.942	0.883	−
5, 0	106402.20	4.145-3	939.83	4.993+12	5.313+17	1.364	1.855	+
1	104845.82	8.906-2	953.78	1.026+14	1.076+19	1.318	1.735	+
2	103313.01	2.675-1	967.93	2.949+14	3.047+19	1.283	1.646	+
3	101803.55	1.719-2	982.28	1.814+13	1.847+18	1.279	1.650	+
5, 4	100317.24	1.286-1	996.84	1.298+14	1.302+19	1.215	1.475	−
5	98853.93	1.231-2	1011.59	1.189+13	1.175+18	1.163	1.339	+
6	97413.47	2.940-2	1026.55	2.718+13	2.648+18	1.177	1.391	+
7	95995.77	7.688-2	1041.71	6.801+13	6.528+18	1.144	1.309	−
8	94600.76	4.789-2	1057.07	4.055+13	3.836+18	1.119	1.248	+
9	93228.40	6.952-3	1072.63	5.633+12	5.252+17	1.087	1.170	−
10	91878.67	3.029-3	1088.39	2.349+12	2.158+17	1.114	1.256	−
11	90551.60	2.503-2	1104.34	1.858+13	1.683+18	1.079	1.169	+
12	89247.24	4.701-2	1120.48	3.341+13	2.982+18	1.061	1.127	−
13	87965.67	5.620-2	1136.81	3.826+13	3.365+18	1.046	1.093	+
14	86707.00	5.315-2	1153.31	3.465+13	3.004+18	1.032	1.064	−
15	85471.37	4.344-2	1169.98	2.712+13	2.318+18	1.019	1.037	+
16	84258.96	3.216-2	1186.82	1.924+13	1.621+18	1.006	1.012	−
17	83069.98	2.220-2	1203.80	1.272+13	1.057+18	0.995	0.989	+
18	81904.65	1.456-2	1220.93	8.001+12	6.553+17	0.984	0.967	−
19	80763.24	9.206-3	1238.19	4.850+12	3.917+17	0.974	0.947	+
20	79646.05	5.666-3	1255.56	2.863+12	2.280+17	0.965	0.928	−
21	78553.41	3.423-3	1273.02	1.659+12	1.303+17	0.956	0.911	+
6, 0	108111.94	3.103-4	924.97	3.922+11	4.240+16	1.436	2.049	+
1	106555.56	1.676-2	938.48	2.028+13	2.161+18	1.372	1.878	+
2	105022.76	1.587-1	952.17	1.838+14	1.930+19	1.326	1.757	+
3	103513.30	2.278-1	966.06	2.527+14	2.616+19	1.293	1.673	+
4	102026.99	2.891-3	980.13	3.071+12	3.133+17	1.162	1.303	−
5	100563.67	9.942-2	994.39	1.011+14	1.017+19	1.225	1.503	−
6	99123.22	5.299-2	1008.84	5.161+13	5.116+18	1.184	1.397	+

Table 57. Franck-Condon integrals--continued

$$O_2^+ \ X^2\Pi_g - O_2 \ X^3\Sigma_g^- \ \text{Ionization system}$$

v' v''	σ_o	$q_{v'v''}$	$\lambda_o^{(vac)}$	$q_{v'v''}\sigma_o^3$	$q_{v'v''}\sigma_o^4$	$\bar{r}$	$\overline{r^2}$	phase
7	97705.52	1.163-3	1023.48	1.085+12	1.060+17	1.247	1.590	+
8	96310.51	4.788-2	1038.31	4.277+13	4.119+18	1.154	1.334	−
9	94938.15	6.304-2	1053.32	5.394+13	5.121+18	1.127	1.269	+
10	93588.42	2.959-2	1068.51	2.425+13	2.270+18	1.103	1.212	−
11	92261.35	2.400-3	1083.88	1.885+12	1.739+17	1.063	1.111	+
12	90956.99	4.571-3	1099.42	3.440+12	3.129+17	1.097	1.215	+
13	89675.41	2.344-2	1115.13	1.690+13	1.516+18	1.069	1.147	−
14	88416.74	4.090-2	1131.01	2.827+13	2.500+18	1.052	1.108	+
15	87181.12	4.849-2	1147.04	3.213+13	2.801+18	1.038	1.077	−
16	85968.71	4.662-2	1163.21	2.962+13	2.547+18	1.024	1.049	+
17	84779.73	3.924-2	1179.53	2.391+13	2.027+18	1.012	1.024	−
18	83614.40	3.014-2	1195.97	1.762+13	1.473+18	1.001	1.000	+
19	82472.99	2.169-2	1212.52	1.217+13	1.004+18	0.990	0.978	−
20	81355.80	1.489-2	1229.17	8.016+12	6.522+17	0.980	0.958	+
21	80263.16	9.867-3	1245.90	5.102+12	4.095+17	0.970	0.939	−
7, 0	109789.13	1.030-5	910.84	1.364+10	1.497+15	1.548	2.369	+
1	108232.75	1.547-3	923.94	1.961+12	2.123+17	1.446	2.078	+
2	106699.94	3.960-2	937.21	4.811+13	5.133+18	1.381	1.902	+
3	105190.48	2.182-1	950.66	2.540+14	2.672+19	1.335	1.780	+
4	103704.17	1.540-1	964.28	1.717+14	1.781+19	1.304	1.706	+
5	102240.86	3.746-2	978.08	4.004+13	4.094+18	1.233	1.511	−
6	100800.40	4.841-2	992.06	4.958+13	4.997+18	1.239	1.541	−
7	99382.71	8.046-2	1006.21	7.897+13	7.849+18	1.194	1.425	+
8	97987.70	7.866-3	1020.54	7.401+12	7.252+17	1.144	1.291	−
9	96615.33	1.586-2	1035.03	1.430+13	1.382+18	1.169	1.374	−
10	95265.60	5.355-2	1049.70	4.630+13	4.411+18	1.135	1.290	+
11	93938.53	4.755-2	1064.53	3.942+13	3.703+18	1.112	1.234	−
12	92634.17	1.722-2	1079.51	1.368+13	1.268+18	1.088	1.178	+
13	91352.60	4.557-4	1094.66	3.474+11	3.174+16	1.016	0.988	−
14	90093.93	5.953-3	1109.95	4.353+12	3.922+17	1.083	1.183	−
7,15	88858.30	2.202-2	1125.39	1.545+13	1.373+18	1.060	1.127	+
16	87645.90	3.597-2	1140.96	2.422+13	2.123+18	1.044	1.092	−
17	86456.91	4.221-2	1156.65	2.728+13	2.358+18	1.030	1.062	+
18	85291.58	4.109-2	1172.45	2.550+13	2.175+18	1.018	1.036	−
19	84150.18	3.545-2	1188.35	2.112+13	1.778+18	1.006	1.012	−
20	83032.99	2.813-2	1204.34	1.610+13	1.337+18	0.996	0.990	−
21	81940.34	2.101-2	1220.40	1.156+13	9.470+17	0.986	0.970	+
8, 1	109877.37	5.809-5	910.11	7.707+10	8.468+15	1.564	2.417	+
2	108344.56	4.414-3	922.98	5.614+12	6.083+17	1.456	2.108	+
3	106835.10	7.151-2	936.02	8.720+13	9.316+18	1.390	1.927	+
4	105348.80	2.554-1	949.23	2.986+14	3.145+19	1.343	1.805	+
5	103885.48	8.112-2	962.60	9.094+13	9.448+18	1.320	1.752	+
6	102445.02	7.985-2	976.13	8.585+13	8.795+18	1.249	1.555	−
7	101027.33	1.106-2	989.83	1.140+13	1.152+18	1.268	1.625	−
8	99632.32	7.903-2	1003.69	7.816+13	7.787+18	1.204	1.450	+
9	98259.95	3.194-2	1017.71	3.030+13	2.978+18	1.166	1.353	−
10	96910.23	5.764-4	1031.88	5.246+11	5.084+16	1.260	1.633	−
11	95583.15	3.086-2	1046.21	2.695+13	2.576+18	1.145	1.315	+
12	94278.79	4.995-2	1060.68	4.185+13	3.946+18	1.119	1.253	−
13	92997.22	3.374-2	1075.30	2.714+13	2.524+18	1.098	1.202	+
14	91738.55	9.375-3	1090.05	7.238+12	6.640+17	1.073	1.144	−
16	89290.52	6.966-3	1119.94	4.959+12	4.428+17	1.072	1.158	+
17	88101.53	2.050-2	1135.05	1.402+13	1.235+18	1.052	1.110	−
18	86936.20	3.174-2	1150.27	2.085+13	1.813+18	1.037	1.077	+
19	85794.80	3.692-2	1165.57	2.331+13	2.000+18	1.024	1.049	−

Table 57. Franck-Condon integrals--continued

$$O_2^+ \; X^2\Pi_g - O_2 \; X^3\Sigma_g^- \text{ Ionization system}$$

v' v''	σ_o	$q_{v'v''}$	$\lambda_o^{(vac)}$	$q_{v'v''}\sigma_o^3$	$q_{v'v''}\sigma_o^4$	$\bar{r}$	$\overline{r^2}$	phase
20	84677.61	3.634-2	1180.95	2.206+13	1.868+18	1.012	1.025	+
21	83584.96	3.206-2	1196.39	1.872+13	1.565+18	1.002	1.002	−
9, 2	109956.62	1.834-4	909.45	2.438+11	2.680+16	1.582	2.469	+
3	108447.16	9.474-3	922.11	1.208+13	1.310+18	1.467	2.139	+
4	106960.85	1.094-1	934.92	1.339+14	1.432+19	1.399	1.952	+
5	105497.54	2.669-1	947.89	3.134+14	3.307+19	1.353	1.832	+
6	104057.08	2.931-2	961.01	3.303+13	3.437+18	1.349	1.837	+
7	102639.39	1.055-1	974.28	1.141+14	1.171+19	1.260	1.585	−
8	101244.37	4.893-5	987.71	5.078+10	5.141+15	0.580	−0.390	+
9	99872.01	5.675-2	1001.28	5.653+13	5.646+18	1.214	1.478	+
10	98522.28	5.296-2	1015.00	5.065+13	4.990+18	1.177	1.382	−
11	97195.21	4.726-3	1028.86	4.339+12	4.218+17	1.125	1.244	+
12	95890.85	1.008-2	1042.85	8.892+12	8.526+17	1.161	1.359	+
13	94609.28	3.836-2	1056.98	3.249+13	3.074+18	1.128	1.274	−
14	93350.61	4.191-2	1071.23	3.409+13	3.182+18	1.105	1.221	+
15	92114.98	2.289-2	1085.60	1.789+13	1.648+18	1.085	1.172	−
16	90902.58	4.740-3	1100.08	3.560+12	3.236+17	1.058	1.108	+
17	89713.59	2.510-4	1114.66	1.813+11	1.626+16	1.144	1.350	+
18	88548.26	7.519-3	1129.33	5.220+12	4.623+17	1.063	1.137	−
19	87406.86	1.883-2	1144.07	1.257+13	1.099+18	1.045	1.094	+
20	86289.67	2.796-2	1158.89	1.796+13	1.550+18	1.031	1.064	−
21	85197.02	3.233-2	1173.75	1.999+13	1.703+18	1.019	1.038	+
10, 3	110026.65	4.264-4	908.87	5.679+11	6.249+16	1.600	2.525	+
4	108540.35	1.700-2	921.32	2.174+13	2.360+18	1.477	2.171	+
5	107077.03	1.496-1	933.91	1.837+14	1.967+19	1.408	1.979	+
6	105636.58	2.564-1	946.64	3.023+14	3.193+19	1.363	1.861	+
7	104218.88	3.951-3	959.52	4.473+12	4.661+17	1.450	2.141	+
8	102823.87	1.082-1	972.54	1.176+14	1.209+19	1.270	1.612	−
9	101451.50	1.061-2	985.69	1.108+13	1.124+18	1.195	1.405	+
10	100101.78	2.923-2	998.98	2.932+13	2.935+18	1.228	1.516	+
10,11	98774.71	6.001-2	1012.41	5.783+13	5.712+18	1.186	1.406	−
12	97470.34	1.998-2	1025.95	1.850+13	1.804+18	1.150	1.315	+
13	96188.77	4.087-4	1039.62	3.637+11	3.499+16	1.259	1.635	+
14	94930.10	2.113-2	1053.41	1.808+13	1.716+18	1.138	1.299	−
15	93694.48	3.888-2	1067.30	3.198+13	2.996+18	1.113	1.239	+
16	92482.07	3.293-2	1081.29	2.605+13	2.409+18	1.093	1.192	−
17	91293.08	1.507-2	1095.37	1.146+13	1.047+10	1.073	1.145	+
18	90127.76	2.200-3	1109.54	1.611+12	1.452+17	1.041	1.066	−
19	88986.35	7.158-4	1123.77	5.044+11	4.488+16	1.101	1.236	−
20	87869.16	7.613-3	1138.06	5.165+12	4.538+17	1.055	1.120	+
21	86776.51	1.700-2	1152.39	1.111+13	9.641+17	1.038	1.081	−

THE CALCULATED ARRAY EXTENDED THROUGH (10,21). Q LESS THAN 1.0-6 HAVE BEEN OMITTED.

$$O_2^+ \; a^4\Pi_u - O_2 \; X^3\Sigma_g^- \text{ Ionization system}$$

v' v''	σ_o	$q_{v'v''}$	$\lambda_o^{(vac)}$	$q_{v'v''}\sigma_o^3$	$q_{v'v''}\sigma_o^4$	$\bar{r}$	$\overline{r^2}$	phase
0, 0	129889.26	9.684-3	769.89	2.122+13	2.756+18	1.291	1.669	+
1	128332.88	5.387-2	779.22	1.139+14	1.461+19	1.314	1.728	+
2	126800.07	1.377-1	788.64	2.808+14	3.560+19	1.338	1.791	+
3	125290.61	2.150-1	798.14	4.230+14	5.299+19	1.363	1.858	+
4	123804.30	2.299-1	807.73	4.363+14	5.401+19	1.389	1.928	+
5	122340.99	1.788-1	817.39	3.273+14	4.005+19	1.416	2.004	+
6	120900.53	1.048-1	827.13	1.852+14	2.240+19	1.444	2.084	+
7	119482.84	4.744-2	836.94	8.091+13	9.668+18	1.474	2.170	+
8	118087.83	1.681-2	846.83	2.767+13	3.268+18	1.505	2.263	+
9	116715.46	4.701-3	856.78	7.474+12	8.723+17	1.538	2.363	+

Table 57. Franck-Condon integrals--continued

$O_2^+ \, a^4\Pi_u - O_2 \, X^3\Sigma_g^-$ Ionization system

v' v"	σ_o	$q_{v'v''}$	$\lambda_o^{(vac)}$	$q_{v'v''}\sigma_o^3$	$q_{v'v''}\sigma_o^4$	$\bar{r}$	$\overline{r^2}$	phase
1 0	115365.73	1.042-3	866.81	1.600+12	1.846+17	1.573	2.471	+
1	114038.66	1.828-4	876.90	2.712+11	3.092+16	1.611	2.590	+
2	112734.30	2.526-5	887.04	3.619+10	4.080+15	1.652	2.721	+
3	111452.73	2.716-6	897.24	3.760+ 9	4.190+14	1.696	2.868	+
1, 0	130904.15	3.548-2	763.92	7.959+13	1.042+19	1.276	1.630	−
1	129347.77	1.231-1	773.11	2.664+14	3.446+19	1.298	1.686	−
2	127814.96	1.580-1	782.38	3.299+14	4.216+19	1.321	1.744	−
3	126305.50	7.392-2	791.73	1.489+14	1.881+19	1.343	1.802	−
4	124819.19	6.013-4	801.16	1.169+12	1.460+17	1.335	1.751	−
5	123355.88	5.251-2	810.66	9.855+13	1.216+19	1.400	1.965	+
6	121915.42	1.515-1	820.24	2.745+14	3.347+19	1.426	2.034	+
7	120497.73	1.787-1	829.89	3.126+14	3.767+19	1.454	2.113	+
8	119102.72	1.291-1	839.61	2.182+14	2.598+19	1.483	2.199	+
9	117730.35	6.484-2	849.40	1.058+14	1.246+19	1.514	2.292	+
10	116380.62	2.391-2	859.25	3.769+13	4.386+18	1.547	2.392	+
11	115053.55	6.655-3	869.16	1.014+13	1.166+18	1.583	2.502	+
12	113749.19	1.416-3	879.13	2.084+12	2.371+17	1.620	2.621	+
13	112467.62	2.310-4	889.14	3.286+11	3.696+16	1.661	2.754	+
14	111208.95	2.869-5	899.21	3.946+10	4.389+15	1.706	2.902	+
15	109973.32	2.671-6	909.31	3.553+ 9	3.907+14	1.756	3.073	+
2, 0	131898.40	7.118-2	758.16	1.633+14	2.154+19	1.262	1.594	+
1	130342.02	1.416-1	767.21	3.136+14	4.087+19	1.283	1.646	+
2	128809.21	6.096-2	776.34	1.303+14	1.678+19	1.303	1.697	+
3	127299.75	2.155-3	785.55	4.446+12	5.660+17	1.347	1.829	−
4	125813.44	8.255-2	794.83	1.644+14	2.068+19	1.355	1.837	−
5	124350.13	9.545-2	804.18	1.835+14	2.282+19	1.378	1.897	−
6	122909.67	1.351-2	813.61	2.509+13	3.083+18	1.397	1.944	−
7	121491.97	2.319-2	823.10	4.159+13	5.053+18	1.440	2.080	+
8	120096.96	1.220-1	832.66	2.114+14	2.539+19	1.464	2.145	+
9	118724.60	1.679-1	842.28	2.809+14	3.335+19	1.493	2.229	+
10	117374.87	1.269-1	851.97	2.052+14	2.408+19	1.524	2.322	+
11	116047.80	6.321-2	861.71	9.879+13	1.146+19	1.557	2.422	+
12	114743.44	2.233-2	871.51	3.373+13	3.870+18	1.592	2.532	+
13	113461.87	5.784-3	881.35	8.448+12	9.585+17	1.630	2.653	+
14	112203.20	1.115-3	891.24	1.574+12	1.767+17	1.671	2.787	+
15	110967.57	1.598-4	901.16	2.183+11	2.423+16	1.716	2.938	+
16	109755.16	1.682-5	911.12	2.224+10	2.441+15	1.767	3.111	+
17	108566.18	1.267-6	921.10	1.621+ 9	1.759+14	1.825	3.316	+
3, 0	132872.00	1.039-1	752.60	2.437+14	3.238+19	1.249	1.560	−
1	131315.62	1.031-1	761.52	2.335+14	3.067+19	1.268	1.608	−
2	129782.81	1.416-3	770.52	3.096+12	4.017+17	1.271	1.599	−
3	128273.35	6.255-2	779.58	1.320+14	1.693+19	1.315	1.732	+
4	126787.04	7.024-2	788.72	1.431+14	1.815+19	1.336	1.783	+
5	125323.73	2.454-4	797.93	4.830+11	6.053+16	1.298	1.625	+
6	123883.27	6.122-2	807.21	1.164+14	1.442+19	1.390	1.934	−
3, 7	122465.58	8.813-2	816.56	1.619+14	1.982+19	1.413	1.995	−
8	121070.57	1.253-2	825.97	2.223+13	2.692+18	1.432	2.041	−
9	119698.20	2.519-2	835.44	4.320+13	5.171+18	1.479	2.194	+
10	118348.47	1.241-1	844.96	2.057+14	2.435+19	1.504	2.263	+
11	117021.40	1.612-1	854.55	2.583+14	3.023+19	1.534	2.353	+
12	115717.04	1.135-1	864.18	1.758+14	2.034+19	1.567	2.454	+
13	114435.47	5.179-2	873.86	7.760+13	8.881+18	1.602	2.565	+
14	113176.80	1.646-2	883.57	2.386+13	2.701+18	1.640	2.686	+
15	111941.17	3.759-3	893.33	5.272+12	5.902+17	1.681	2.822	+
16	110728.77	6.221-4	903.11	8.445+11	9.351+16	1.727	2.974	+

Table 57. Franck-Condon integrals--continued

$$O_2^+\ a^4\Pi_u - O_2\ X^3\Sigma_g^-\ \text{Ionization system}$$

v' v"	σ_o	$q_{v'v"}$	$\lambda_o^{(vac)}$	$q_{v'v"}\sigma_o^3$	$q_{v'v"}\sigma_o^4$	$\bar{r}$	$\overline{r^2}$	phase
17	109539.78	7.398-5	912.91	9.724+10	1.065+16	1.778	3.150	+
18	108374.45	6.161-6	922.73	7.843+ 9	8.499+14	1.837	3.361	+
4, 0	133824.96	1.237-1	747.25	2.965+14	3.968+19	1.236	1.528	+
1	132268.58	4.696-2	756.04	1.087+14	1.437+19	1.254	1.570	+
2	130735.77	1.926-2	764.90	4.305+13	5.628+18	1.282	1.647	−
3	129226.31	7.697-2	773.84	1.661+14	2.146+19	1.299	1.686	−
4	127740.00	3.438-3	782.84	7.167+12	9.155+17	1.307	1.694	−
5	126276.69	5.071-2	791.91	1.021+14	1.289+19	1.348	1.820	+
6	124836.23	5.880-2	801.05	1.144+14	1.428+19	1.368	1.870	+
7	123418.53	7.736-5	810.25	1.454+11	1.795+16	1.527	2.431	−
8	122023.52	6.607-2	819.51	1.200+14	1.465+19	1.425	2.033	−
9	120651.16	7.427-2	828.84	1.304+14	1.574+19	1.449	2.097	−
10	119301.43	3.603-3	838.21	6.118+12	7.298+17	1.457	2.103	−
11	117974.36	4.367-2	847.64	7.170+13	8.458+18	1.517	2.307	+
12	116670.00	1.401-1	857.12	2.224+14	2.595+19	1.545	2.388	+
13	115388.43	1.517-1	866.64	2.330+14	2.689+19	1.577	2.487	+
14	114129.76	9.222-2	876.20	1.371+14	1.565+19	1.612	2.598	+
15	112894.13	3.642-2	885.79	5.240+13	5.916+18	1.650	2.720	!
16	111681.72	9.905-3	895.40	1.380+13	1.541+18	1.692	2.857	+
17	110492.74	1.895-3	905.04	2.557+12	2.825+17	1.737	3.012	+
18	109327.41	2.545-4	914.68	3.326+11	3.636+16	1.789	3.191	+
19	108186.01	2.340-5	924.33	2.963+10	3.205+15	1.849	3.407	+
20	107068.82	1.396-6	933.98	1.714+ 9	1.835+14	1.923	3.679	+
5, 0	134757.27	1.278-1	742.08	3.128+14	4.215+19	1.224	1.498	−
1	133200.89	9.046-3	750.75	2.138+13	2.848+18	1.237	1.526	−
2	131668.08	5.747-2	759.48	1.312+14	1.727+19	1.266	1.603	+
3	130158.62	3.149-2	768.29	6.945+13	9.039+18	1.282	1.641	+
4	128672.32	2.009-2	777.17	4.280+13	5.508+18	1.313	1.728	−
5	127209.00	6.100-2	786.11	1.256+14	1.597+19	1.329	1.766	−
6	125768.55	1.052-4	795.11	2.092+11	2.632+16	1.251	1.465	−
7	124350.85	5.826-2	804.18	1.120+14	1.393+19	1.381	1.908	+
8	122955.84	3.921-2	813.30	7.289+13	8.963+18	1.400	1.958	+
9	121583.47	5.860-3	822.48	1.053+13	1.280+18	1.448	2.111	−
10	120233.75	7.905-2	831.71	1.374+14	1.652+19	1.461	2.135	−
11	118906.68	5.067-2	841.00	8.518+13	1.013+19	1.485	2.201	−
12	117602.31	7.023-4	850.32	1.142+12	1.343+17	1.581	2.550	!
13	116320.74	7.772-2	859.69	1.223+14	1.423+19	1.557	2.428	+
14	115062.07	1.555-1	869.10	2.369+14	2.726+19	1.588	2.523	+
15	113826.45	1.325-1	878.53	1.954+14	2.224+19	1.623	2.633	+
16	112614.04	6.626-2	887.99	9.463+13	1.066+19	1.661	2.756	+
17	111425.05	2.164-2	897.46	2.993+13	3.335+18	1.703	2.894	+
18	110259.73	4.801-3	906.95	6.435+12	7.096+17	1.749	3.051	+
19	109118.32	7.280-4	916.44	9.459+11	1.032+17	1.801	3.234	+
20	108001.13	7.376-5	925.92	9.292+10	1.004+16	1.862	3.455	+
21	106908.48	4.720-6	935.38	5.767+ 9	6.166+14	1.938	3.738	+
6, 0	135668.94	1.190-1	737.09	2.971+14	4.031+19	1.212	1.469	+
1	134112.56	3.868-4	745.64	9.330+11	1.251+17	1.261	1.616	−
2	132579.75	6.876-2	754.26	1.602+14	2.124+19	1.252	1.567	−
3	131070.29	8.683-4	762.95	1.955+12	2.563+17	1.246	1.529	−
4	129583.99	5.577-2	771.70	1.214+14	1.573+19	1.295	1.678	+
5	128120.67	1.182-2	780.51	2.486+13	3.185+18	1.308	1.705	+
6	126680.22	3.507-2	789.39	7.130+13	9.032+18	1.343	1.806	−
7	125262.52	4.096-2	798.32	8.050+13	1.008+19	1.360	1.846	−
8	123867.51	5.262-3	807.31	*****+12	1.239+18	1.403	1.983	+
9	122495.14	6.584-2	816.36	1.210+14	1.482+19	1.414	1.999	+

Table 57. Franck-Condon integrals--continued

$O_2^+ a^4\Pi_u - O_2 X^3\Sigma_g^-$ Ionization system

v' v"	σ_o	$q_{v'v"}$	$\lambda_o(vac)$	$q_{v'v"}\sigma_o^3$	$q_{v'v"}\sigma_o^4$	$\bar{r}$	$\bar{r^2}$	phase
10	121145.42	1.459-2	825.45	2.594+13	3.142+18	1.430	2.037	+
11	119818.35	2.702-2	834.60	4.649+13	5.570+18	1.476	2.185	-
12	118513.98	8.328-2	843.78	1.386+14	1.643+19	1.498	2.243	-
13	117232.41	2.012-2	853.01	3.241+13	3.799+18	1.519	2.297	-
14	115973.74	1.867-2	862.26	2.912+13	3.378+18	1.575	2.492	ı
15	114738.12	1.202-1	871.55	1.815+14	2.083+19	1.600	2.561	+
16	113525.71	1.570-1	880.86	2.297+14	2.607+19	1.634	2.669	+
17	112336.72	1.023-1	890.18	1.451+14	1.630+19	1.672	2.793	+
18	111171.40	4.059-2	899.51	5.577+13	6.200+18	1.714	2.932	+
19	110029.99	1.049-2	908.84	1.397+13	1.538+18	1.760	3.091	+
20	108912.80	1.798-3	918.17	2.323+12	2.530+17	1.813	3.278	+
21	107820.16	2.004-4	927.47	2.512+11	2.709+16	1.876	3.505	+

THE CALCULATED ARRAY EXTENDED THROUGH (6,21). Q LESS THAN 1.0-6 HAVE BEEN OMITTED.

$O_2^+ A^2\Pi_u - O_2 X^3\Sigma_g^-$ Ionization system

v' v"	σ_o	$q_{v'v"}$	$\lambda_o(vac)$	$q_{v'v"}\sigma_o^3$	$q_{v'v"}\sigma_o^4$	$\bar{r}$	$\bar{r^2}$	phase
0, 0	137434.51	2.881-3	727.62	7.480+12	1.028+18	1.299	1.690	+
1	135878.13	1.994-2	735.95	5.001+13	6.796+18	1.321	1.747	+
2	134345.32	6.475-2	744.35	1.570+14	2.109+19	1.344	1.806	+
3	132835.86	1.315-1	752.81	3.083+14	4.096+19	1.367	1.869	+
4	131349.56	1.880-1	761.33	4.261+14	5.597+19	1.391	1.934	+
5	129886.24	2.017-1	769.90	4.420+14	5.741+19	1.415	2.003	+
6	128445.78	1.691-1	778.54	3.584+14	4.604+19	1.440	2.074	+
7	127028.09	1.140-1	787.23	2.336+14	2.967+19	1.466	2.149	+
8	125633.08	6.296-2	795.97	1.248+14	1.568+19	1.492	2.226	+
9	124260.71	2.893-2	804.76	5.550+13	6.897+18	1.520	2.308	+
10	122910.98	1.117-2	813.60	2.074+13	2.550+18	1.548	2.393	+
11	121583.91	3.654-3	822.48	6.568+12	7.986+17	1.576	2.482	+
12	120279.55	1.017-3	831.40	1.771+12	2.130+17	1.606	2.576	+
13	118997.98	2.418-4	840.35	4.074+11	4.848+16	1.636	2.675	+
14	117739.31	4.907-5	849.33	8.009+10	9.429+15	1.668	2.779	+
15	116503.68	8.492-6	858.34	1.343+10	1.564+15	1.701	2.890	+
16	115291.28	1.247-6	867.37	1.911+ 9	2.204+14	1.736	3.008	+
1, 0	138305.54	1.225-2	723.04	3.241+13	4.483+18	1.287	1.658	-
1	136749.16	6.015-2	731.27	1.538+14	2.103+19	1.308	1.712	-
2	135216.36	1.238-1	739.56	3.061+14	4.139+19	1.330	1.769	-
3	133706.90	1.305-1	747.91	3.120+14	4.171+19	1.352	1.828	-
4	132220.59	6.178-2	756.31	1.428+14	1.888+19	1.375	1.888	-
5	130757.27	2.467-3	764.78	5.516+12	7.213+17	1.390	1.918	-
6	129316.82	2.648-2	773.30	5.727+13	7.406+18	1.428	2.044	+
7	127899.12	1.029-1	781.87	2.153+14	2.754+19	1.452	2.108	+
8	126504.11	1.530-1	790.49	3.096+14	3.917+19	1.477	2.182	+
9	125131.75	1.435-1	799.16	2.811+14	3.517+19	1.503	2.259	+
10	123782.02	9.808-2	807.87	1.860+14	2.302+19	1.530	2.340	+
11	122454.95	5.210-2	816.63	9.567+13	1.172+19	1.558	2.426	+
12	121150.59	2.226-2	825.42	3.958+13	4.795+18	1.587	2.515	+
13	119869.01	7.805-3	834.24	1.344+13	1.611+18	1.616	2.609	+
14	118610.34	2.274-3	843.10	3.794+12	4.500+17	1.647	2.708	+
15	117374.72	5.539-4	851.97	8.957+11	1.051+17	1.678	2.813	+
16	116162.31	1.132-4	860.86	1.774+11	2.060+16	1.712	2.925	+
17	114973.33	1.936-5	869.77	2.942+10	3.383+15	1.746	3.044	+
18	113808.00	2.760-6	878.67	4.068+ 9	4.629+14	1.783	3.173	+
2, 0	139149.44	2.862-2	718.65	7.712+13	1.073+19	1.275	1.628	+
1	137593.06	9.634-2	726.78	2.510+14	3.453+19	1.296	1.680	+
2	136060.25	1.116-1	734.97	2.812+14	3.826+19	1.317	1.734	+
3	134550.79	3.666-2	743.21	8.930+13	1.202+19	1.337	1.786	+

Table 57. Franck-Condon integrals--continued

$$O_2^+ \; A^2\Pi_u - O_2 \; X^3\Sigma_g^- \;\; \text{Ionization system}$$

v' v''	σ_o	$q_{v'v''}$	$\lambda_o^{(vac)}$	$q_{v'v''}\sigma_o^3$	$q_{v'v''}\sigma_o^4$	$\bar{r}$	$\overline{r^2}$	phase
4	133064.49	2.476-3	751.52	5.834+12	7.764+17	1.374	1.900	−
5	131601.17	6.328-2	759.87	1.442+14	1.898+19	1.388	1.927	−
6	130160.72	9.248-2	768.28	2.039+14	2.654+19	1.410	1.988	−
7	128743.02	3.667-2	776.74	7.826+13	1.007+19	1.433	2.050	−
8	127348.01	2.535-4	785.25	5.236+11	6.668+16	1.500	2.298	+
9	125975.64	4.796-2	793.80	9.588+13	1.208+19	1.489	2.221	+
10	124625.92	1.199-1	802.40	2.321+14	2.893+19	1.514	2.294	+
11	123298.85	1.427-1	811.04	2.676+14	3.299+19	1.541	2.375	+
12	121994.48	1.120-1	819.71	2.034+14	2.482+19	1.569	2.460	+
13	120712.91	6.493-2	828.41	1.142+14	1.379+19	1.597	2.549	+
14	119454.24	2.930-2	837.14	4.994+13	5.966+18	1.627	2.644	+
15	118218.62	1.060-2	845.89	1.752+13	2.071+18	1.657	2.743	+
16	117006.21	3.127-3	854.66	5.009+12	5.861+17	1.689	2.849	+
17	115817.22	7.583-4	863.43	1.178+12	1.364+17	1.722	2.961	+
18	114651.90	1.516-4	872.20	2.285+11	2.620+16	1.757	3.081	+
2,19	113510.49	2.493-5	880.98	3.646+10	4.138+15	1.794	3.212	+
20	112393.30	3.356-6	889.73	4.765+ 9	5.355+14	1.833	3.352	+
3, 0	139966.20	4.882-2	714.46	1.339+14	1.873+19	1.264	1.600	−
1	138409.82	1.075-1	722.49	2.851+14	3.946+19	1.284	1.650	−
2	136877.02	5.506-2	730.58	1.412+14	1.933+19	1.304	1.699	−
3	135367.56	2.367-4	738.73	5.872+11	7.949+16	1.365	1.899	+
4	133881.25	5.528-2	746.93	1.326+14	1.776+19	1.351	1.827	+
5	132417.93	6.716-2	755.19	1.559+14	2.065+19	1.372	1.882	+
6	130977.48	6.697-3	763.49	1.505+13	1.971+18	1.389	1.922	+
7	129559.78	2.380-2	771.84	5.176+13	6.706+18	1.424	2.033	−
8	128164.77	8.066-2	780.25	1.698+14	2.176+19	1.446	2.092	−
9	126792.41	5.523-2	788.69	1.126+14	1.427+19	1.470	2.158	−
10	125442.68	2.642-3	797.18	5.216+12	6.542+17	1.484	2.186	−
11	124115.61	2.637-2	805.70	5.042+13	6.258+18	1.528	2.340	+
12	122811.25	9.945-2	814.26	1.842+14	2.262+19	1.553	2.412	+
13	121529.67	1.371-1	822.84	2.460+14	2.990+19	1.580	2.496	+
14	120271.00	1.160-1	831.46	2.017+14	2.426+19	1.608	2.585	+
15	119035.38	6.994-2	840.09	1.180+14	1.404+19	1.638	2.680	+
16	117822.97	3.212-2	848.73	5.254+13	6.191+18	1.668	2.780	+
17	116633.99	1.162-2	857.38	1.844+13	2.151+18	1.700	2.886	+
18	115468.66	3.375-3	866.04	5.195+12	5.999+17	1.733	2.999	+
19	114327.25	7.931-4	874.68	1.185+12	1.355+17	1.768	3.120	+
20	113210.06	1.510-4	883.31	2.190+11	2.480+16	1.805	3.252	+
21	112117.42	2.321-5	891.92	3.271+10	3.667+15	1.844	3.395	+
4, 0	140755.83	6.815-2	710.45	1.901+14	2.675+19	1.254	1.573	+
1	139199.45	9.191-2	718.39	2.479+14	3.451+19	1.273	1.621	+
2	137666.64	1.014-2	726.39	2.645+13	3.642+18	1.290	1.658	+
3	136157.18	2.866-2	734.44	7.234+13	9.849+18	1.318	1.741	−
4	134670.88	6.449-2	742.55	1.575+14	2.121+19	1.337	1.788	−
5	133207.56	7.455-3	750.71	1.762+13	2.347+18	1.353	1.024	−
6	131767.10	2.558-2	758.92	5.852+13	7.711+18	1.387	1.926	+
7	130349.41	6.578-2	767.17	1.457+14	1.899+19	1.407	1.979	+
8	128954.40	1.673-2	775.47	3.587+13	4.626+18	1.427	2.031	+
9	127582.03	1.090-2	783.81	2.264+13	2.888+18	1.462	2.147	−
10	126232.30	6.926-2	792.19	1.393+14	1.758+19	1.483	2.200	−
11	124905.23	5.999-2	800.61	1.169+14	1.460+19	1.507	2.268	−
12	123600.87	5.785-3	809.06	1.092+13	1.350+18	1.525	2.315	−
13	122319.30	1.944-2	817.53	3.557+13	4.351+18	1.568	2.464	+
14	121060.63	9.102-2	826.03	1.615+14	1.955+19	1.592	2.536	+
15	119825.00	1.333-1	834.55	2.293+14	2.747+19	1.620	2.624	+

Table 57. Franck-Condon integrals--continued

$$O_2^+ \; A^2\Pi_u - O_2 \; X^3\Sigma_g^- \;\; \text{Ionization system}$$

v' v"	σ_o	$q_{v'v"}$	$\lambda_o^{(vac)}$	$q_{v'v"}\sigma_o^3$	$q_{v'v"}\sigma_o^4$	$\bar{r}$	$\bar{r^2}$	phase
16	118612.60	1.152-1	843.08	1.923+14	2.281+19	1.649	2.718	+
17	117423.61	6.962-2	851.62	1.127+14	1.324+19	1.679	2.818	+
18	116258.28	3.155-2	860.15	4.957+13	5.763+18	1.711	2.925	+
19	115116.88	1.110-2	868.68	1.694+13	1.950+18	1.744	3.039	+
20	113999.69	3.092-3	877.19	4.581+12	5.223+17	1.779	3.161	+
21	112907.04	6.853-4	885.68	9.864+11	1.114+17	1.816	3.294	+
5, 0	141518.32	8.280-2	706.62	2.347+14	3.321+19	1.244	1.549	−
1	139961.94	6.171-2	714.48	1.692+14	2.368+19	1.263	1.593	−
2	138429.13	8.015-4	722.39	2.126+12	2.943+17	1.302	1.713	+
3	136919.67	5.625-2	730.36	1.444+14	1.977+19	1.306	1.706	+
4	135433.37	2.444-2	738.37	6.073+13	8.224+18	1.323	1.748	+
5	133970.05	1.013-2	746.44	2.435+13	3.262+18	1.354	1.841	−
6	132529.59	5.675-2	754.55	1.321+14	1.751+19	1.371	1.880	−
7	131111.90	1.339-2	762.71	3.017+13	3.956+18	1.389	1.924	−
8	129716.89	1.606-2	770.91	3.505+13	4.547+18	1.423	2.030	+
5, 9	128344.52	6.062-2	779.15	1.282+14	1.645+19	1.443	2.081	+
10	126994.79	1.966-2	787.43	4.026+13	5.112+18	1.463	2.136	+
11	125667.72	7.805-3	795.75	1.549+13	1.946+18	1.501	2.263	−
12	124363.36	6.413-2	804.09	1.233+14	1.534+19	1.520	2.312	−
13	123081.79	5.857-2	812.47	1.092+14	1.344+19	1.544	2.383	−
14	121823.12	5.752-3	820.86	1.040+13	1.267+18	1.563	2.429	−
15	120587.49	1.959-2	829.27	3.435+13	4.143+18	1.607	2.591	+
16	119375.09	9.131-2	837.70	1.553+14	1.854+19	1.632	2.666	+
17	118186.10	1.320-1	846.12	2.179+14	2.575+19	1.661	2.759	+
18	117020.77	1.117-1	854.55	1.790+14	2.095+19	1.691	2.859	+
19	115879.37	6.549-2	862.97	1.019+14	1.181+19	1.723	2.966	+
20	114762.18	2.848-2	871.37	4.304+13	4.940+18	1.756	3.080	+
21	113669.53	9.507-3	879.74	1.396+13	1.587+18	1.791	3.204	+
6, 0	142253.67	9.086-2	702.97	2.616+14	3.721+19	1.235	1.525	+
1	140697.29	3.142-2	710.75	8.752+13	1.231+19	1.252	1.566	+
2	139164.49	1.654-2	718.57	4.457+13	6.203+18	1.277	1.635	−
3	137655.03	5.141-2	726.45	1.341+14	1.846+19	1.294	1.674	−
4	136168.72	3.352-4	734.38	8.463+11	1.152+17	1.282	1.609	−
5	134705.40	4.180-2	742.36	1.022+14	1.376+19	1.339	1.793	+
6	133264.95	2.579-2	750.39	6.103+13	8.134+18	1.356	1.837	+
7	131847.25	6.633-3	758.45	1.520+13	2.004+18	1.390	1.941	−
8	130452.24	5.117-2	766.56	1.136+14	1.482+19	1.406	1.976	−
9	129079.88	1.322-2	774.71	2.843+13	3.669+18	1.424	2.022	−
10	127730.15	1.474-2	782.90	3.071+13	3.922+18	1.459	2.134	+
11	126403.08	5.705-2	791.12	1.152+14	1.456+19	1.479	2.187	+
12	125098.72	1.747-2	799.37	3.420+13	4.279+18	1.499	2.242	+
13	123817.14	8.908-3	807.64	1.691+13	2.094+18	1.538	2.376	−
14	122558.47	6.374-2	815.94	1.173+14	1.438+19	1.558	2.429	−
15	121322.85	5.368-2	824.25	9.585+13	1.163+19	1.583	2.502	−
16	120110.44	3.427-3	832.57	5.938+12	7.132+17	1.597	2.532	−
17	118921.46	2.479-2	840.89	4.169+13	4.958+18	1.648	2.722	+
18	117756.13	9.776-2	849.21	1.596+14	1.880+19	1.674	2.803	+
19	116614.72	1.320-1	857.53	2.093+14	2.441+19	1.703	2.902	+
20	115497.53	1.057-1	865.82	1.628+14	1.881+19	1.735	3.009	+
21	114404.89	5.844-2	874.09	8.750+13	1.001+19	1.768	3.124	+
7, 0	142961.89	9.233-2	699.49	2.698+14	3.857+19	1.226	1.503	−
1	141405.51	1.026-2	707.19	2.902+13	4.104+18	1.241	1.537	−
2	139872.70	3.650-2	714.94	9.989+13	1.397+19	1.266	1.605	+
3	138363.24	2.700-2	722.73	7.151+13	9.895+18	1.283	1.643	+
4	136876.94	1.034-2	730.58	2.652+13	3.630+18	1.311	1.724	−

PAUL H. KRUPENIE

Table 57. Franck-Condon integrals--continued

$$O_2^+ \ A^2\Pi_u - O_2 \ X^3\Sigma_g^- \text{ Ionization system}$$

v' v''	σ_0	$q_{v'v''}$	$\lambda_0(vac)$	$q_{v'v''}\sigma_0^3$	$q_{v'v''}\sigma_0^4$	$\bar{r}$	$\overline{r^2}$	phase
5	135413.62	4.310-2	738.48	1.070+14	1.449+19	1.326	1.758	-
6	133973.17	2.789-4	746.42	6.707+11	8.985+16	1.308	1.666	-
7	132555.47	3.799-2	754.40	8.848+13	1.173+19	1.372	1.884	+
8	131160.46	2.170-2	762.42	4.896+13	6.421+18	1.390	1.928	+
9	129788.09	7.813-3	770.49	1.708+13	2.217+18	1.424	2.036	-
10	128438.37	4.793-2	778.58	1.015+14	1.304+19	1.441	2.076	-
11	127111.30	9.602-3	786.71	1.972+13	2.507+18	1.459	2.119	-
12	125806.93	1.770-2	794.87	3.524+13	4.433+18	1.495	2.241	+
13	124525.36	5.433-2	803.05	1.049+14	1.306+19	1.515	2.296	+
14	123266.69	1.236-2	811.25	2.316+13	2.854+18	1.535	2.349	+
15	122031.07	1.323-2	819.46	2.403+13	2.933+18	1.575	2.490	-
16	120818.66	6.576-2	827.69	1.160+14	1.401+19	1.597	2.551	-
17	119629.67	4.579-2	835.91	7.839+13	9.378+18	1.622	2.626	-
18	118464.35	7.466-4	844.14	1.241+12	1.470+17	1.614	2.561	-
19	117322.94	3.510-2	852.35	5.668+13	6.650+18	1.689	2.859	+
7,20	116205.75	1.084-1	860.54	1.700+14	1.976+19	1.717	2.949	+
21	115113.11	1.316-1	868.71	2.007+14	2.311+19	1.748	3.055	+
8, 0	143642.97	8.838-2	696.17	2.620+14	3.763+19	1.218	1.483	+
1	142086.59	8.423-4	703.80	2.416+12	3.433+17	1.223	1.482	+
2	140553.79	4.701-2	711.47	1.305+14	1.835+19	1.256	1.579	-
3	139044.33	6.193-3	719.19	1.665+13	2.315+18	1.270	1.606	-
4	137558.02	3.051-2	726.97	7.940+13	1.092+19	1.298	1.686	+
5	136094.70	1.938-2	734.78	4.884+13	6.647+18	1.314	1.723	+
6	134654.25	1.214-2	742.64	2.964+13	3.992+18	1.343	1.810	-
7	133236.55	3.642-2	750.55	8.614+13	1.148+19	1.359	1.845	-
8	131841.54	3.926-5	758.49	8.998+10	1.186+16	1.495	2.346	+
9	130469.18	3.825-2	766.47	8.495+13	1.108+19	1.406	1.978	+
10	129119.45	1.518-2	774.48	3.267+13	4.218+18	1.424	2.022	+
11	127792.38	1.192-2	782.52	2.487+13	3.179+18	1.458	2.133	-
12	126488.02	4.486-2	790.59	9.078+13	1.148+19	1.477	2.180	-
13	125206.44	4.814-3	798.68	9.449+12	1.183+18	1.491	2.211	-
14	123947.77	2.378-2	806.79	4.528+13	5.612+18	1.531	2.350	+
15	122712.15	5.058-2	814.92	9.347+13	1.147+19	1.553	2.410	+
16	121499.74	6.252-3	823.05	1.121+13	1.362+18	1.570	2.451	+
17	120310.76	2.101-2	831.18	3.658+13	4.401+18	1.614	2.611	-
18	119145.43	6.776-2	839.31	1.146+14	1.366+19	1.637	2.679	-
19	118004.02	3.490-2	847.43	5.735+13	6.768+18	1.661	2.755	-
20	116886.83	2.723-4	855.53	4.348+11	5.082+16	1.773	3.213	+
21	115794.19	5.121-2	863.60	7.950+13	9.206+18	1.732	3.005	+

THE CALCULATED ARRAY EXTENDED THROUGH (8,21). Q LESS THAN 1.0-6 HAVE BEEN OMITTED.

$$O_2^+ \ b^4\Sigma_g^- - O_2 \ X^3\Sigma_g^- \text{ Ionization system}$$

v' v''	σ_0	$q_{v'v''}$	$\lambda_0(vac)$	$q_{v'v''}\sigma_0^3$	$q_{v'v''}\sigma_0^4$	$\bar{r}$	$\overline{r^2}$	phase
0, 0	146556.00	4.081-1	682.33	1.285+15	1.883+20	1.246	1.555	+
1	144999.62	3.772-1	689.66	1.150+15	1.667+20	1.293	1.673	+
2	143466.81	1.618-1	697.03	4.779+14	6.856+19	1.340	1.794	+
3	141957.35	4.330-2	704.44	1.239+14	1.758+19	1.386	1.919	+
4	140471.04	8.227-3	711.89	2.280+13	3.203+18	1.431	2.045	+
5	139007.73	1.188-3	719.38	3.191+12	4.435+17	1.476	2.172	+
6	137567.27	1.360-4	726.92	3.539+11	4.869+16	1.519	2.301	+
7	136149.58	1.271-5	734.49	3.207+10	4.367+15	1.561	2.430	+
1, 0	147718.64	3.363-1	676.96	1.084+15	1.601+20	1.211	1.467	-
1	146162.26	2.446-3	684.17	7.638+12	1.116+18	1.261	1.632	+

Table 57. Franck-Condon integrals--continued

$$O_2^+ \; b^4\Sigma_g^- - O_2 \; X^3\Sigma_g^- \;\; \text{Ionization system}$$

v' v''	σ_o	$q_{v'v''}$	$\lambda_o^{(vac)}$	$q_{v'v''}\sigma_o^3$	$q_{v'v''}\sigma_o^4$	$\bar{r}$	$\overline{r^2}$	phase
2	144629.46	2.331−1	691.42	7.051+14	1.020+20	1.305	1.705	+
3	143120.00	2.624−1	698.71	7.693+14	1.101+20	1.351	1.824	+
4	141633.69	1.227−1	706.05	3.486+14	4.938+19	1.396	1.947	+
5	140170.37	3.487−2	713.42	9.604+13	1.346+19	1.440	2.071	+
6	138729.92	6.949−3	720.83	1.856+13	2.574+18	1.484	2.197	+
7	137312.22	1.044−3	728.27	2.702+12	3.711+17	1.527	2.325	+
8	135917.21	1.240−4	735.74	3.113+11	4.231+16	1.568	2.453	+
9	134544.85	1.178−5	743.25	2.870+10	3.861+15	1.612	2.592	+
2, 0	148847.02	1.636−1	671.83	5.397+14	8.033+19	1.177	1.384	+
1	147290.64	1.678−1	678.93	5.363+14	7.900+19	1.225	1.503	−
2	145757.83	8.214−2	686.07	2.543+14	3.707+19	1.270	1.608	−
3	144248.37	4.793−2	693.25	1.438+14	2.075+19	1.317	1.743	+
4	142762.06	2.320−1	700.47	6.751+14	9.638+19	1.361	1.855	+
5	141298.75	1.960−1	707.72	5.529+14	7.813+19	1.406	1.976	+
6	139858.29	8.278−2	715.01	2.265+14	3.167+19	1.450	2.099	+
7	138440.60	2.250−2	722.33	5.971+13	8.266+18	1.492	2.224	+
8	137045.59	4.388−3	729.68	1.129+13	1.548+18	1.535	2.351	+
9	135673.22	6.554−4	737.06	1.637+12	2.220+17	1.576	2.478	+
10	134323.49	7.678−5	744.47	1.861+11	2.500+16	1.619	2.614	+
11	132996.42	7.298−6	751.90	1.717+10	2.283+15	1.660	2.749	+
3, 0	149941.12	6.228−2	666.93	2.099+14	3.148+19	1.144	1.307	−
1	148384.74	2.095−1	673.92	6.843+14	1.015+20	1.191	1.420	+
2	146851.94	1.709−2	680.96	5.412+13	7.947+18	1.239	1.551	−
3	145342.48	1.612−1	688.03	4.948+14	7.191+19	1.283	1.646	−
4	143856.17	2.505−3	695.14	7.456+12	1.073+18	1.326	1.716	−
5	142392.85	1.208−1	702.28	3.487+14	4.965+19	1.372	1.888	+
6	140952.40	2.180−1	709.46	6.105+14	8.606+19	1.417	2.007	+
7	139534.70	1.405−1	716.67	3.816+14	5.324+19	1.460	2.129	+
8	138139.69	5.223−2	723.91	1.377+14	1.902+19	1.502	2.252	+
9	136767.33	1.318−2	731.17	3.371+13	4.611+18	1.543	2.378	+
10	135417.60	2.462−3	738.46	6.113+12	8.278+17	1.584	2.504	+
11	134090.53	3.538−4	745.77	8.529+11	1.144+17	1.626	2.638	+
12	132786.17	4.022−5	753.09	9.416+10	1.250+16	1.669	2.777	+
13	131504.59	3.779−6	760.43	8.593+ 9	1.130+15	1.705	2.901	+

THE CALCULATED ARRAY EXTENDED THROUGH (3,21). Q LESS THAN 1.0−6 HAVE BEEN OMITTED.

$$O_2 \; b^1\Sigma_g^+ - a^1\Delta_g \;\; \text{Noxon system}$$
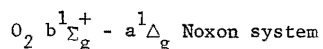
v' v''	σ_o	$q_{v'v''}$	$\lambda_o^{(vac)}$	$q_{v'v''}\sigma_o^3$	$q_{v'v''}\sigma_o^4$	$\bar{r}$	$\overline{r^2}$	phase
0, 0	5238.52	9.770−1	19089.37	1.404+11	7.357+14	1.227	1.506	+
1	3755.02	2.283−2	26631.03	1.209+ 9	4.538+12	1.483	2.136	+
2	2297.32	2.136−4	43529.02	2.589+ 6	5.948+ 9	1.625	2.632	+
1, 0	6643.27	2.267−2	15052.83	6.648+ 9	4.416+13	0.985	0.910	−
1	5159.77	9.290−1	19380.71	1.270+11	6.585+14	1.238	1.537	+
2	3702.07	4.760−2	27011.91	2.415+ 9	8.941+12	1.488	2.156	+
3	2270.17	7.217−4	44049.56	8.444+ 6	1.917+10	1.630	2.648	+
2, 0	8020.03	3.628−4	12468.79	1.871+ 8	1.501+12	0.673	0.243	+
1	6536.53	4.694−2	15298.64	1.311+10	8.569+13	1.004	0.955	−
2	5078.83	8.768−1	19689.59	1.149+11	5.833+14	1.250	1.569	+
3	3646.93	7.430−2	27420.35	3.604+ 9	1.314+13	1.494	2.177	+
3, 0	9368.70	4.426−6	10673.84	3.639+ 6	3.410+10	0.154	−0.735	−
1	7885.20	1.213−3	12681.98	5.946+ 8	4.689+12	0.707	0.310	+
2	6427.50	7.266−2	15558.14	1.929+10	1.240+14	1.023	1.001	−
3	4995.60	8.202−1	20017.61	1.022+11	5.108+14	1.261	1.601	+

THE CALCULATED ARRAY EXTENDED THROUGH (3, 3). Q LESS THAN 1.0−6 HAVE BEEN OMITTED.

Table 57. Franck-Condon integrals--continued

$$O_2^+ X^2\Pi_g - O_2 a^1\Delta_g \text{ Ionization system}$$

v'	v''	σ_o	$q_{v'v''}$	$\lambda_o^{(vac)}$	$q_{v'v''}\sigma_o^3$	$q_{v'v''}\sigma_o^4$	$\bar{r}$	$\overline{r^2}$	phase
0,	0	89482.61	1.422-1	1117.54	1.019+14	9.117+18	1.169	1.368	+
	1	87999.11	2.371-1	1136.38	1.616+14	1.422+19	1.146	1.315	−
	2	86541.41	2.286-1	1155.52	1.482+14	1.282+19	1.126	1.267	+
	3	85109.51	1.681-1	1174.96	1.036+14	8.819+18	1.107	1.225	−
1,	0	91355.18	3.211-1	1094.63	2.448+14	2.236+19	1.198	1.435	+
	1	89871.68	1.260-1	1112.70	9.144+13	8.218+18	1.170	1.368	−
	2	88413.98	1.091-3	1131.04	7.541+11	6.667+16	1.109	1.202	+
	3	86982.08	4.228-2	1149.66	2.783+13	2.420+18	1.137	1.296	+
2,	0	93195.18	3.078-1	1073.02	2.491+14	2.322+19	1.228	1.509	+
	1	91711.68	6.883-3	1090.37	5.310+12	4.870+17	1.226	1.515	+
	2	90253.98	1.400-1	1107.98	1.030+14	9.292+18	1.181	1.395	−
	3	88822.08	9.267-2	1125.85	6.494+13	5.768+18	1.155	1.332	+
3,	0	95002.62	1.637-1	1052.60	1.404+14	1.333+19	1.263	1.593	+
	1	93519.12	1.880-1	1069.30	1.537+14	1.438+19	1.238	1.535	+
	2	92061.42	6.226-2	1086.23	4.858+13	4.472+18	1.202	1.441	−
	3	90629.52	2.133-2	1103.39	1.588+13	1.439+18	1.198	1.442	−
4,	0	96777.49	5.301-2	1033.30	4.804+13	4.649+18	1.301	1.690	+
	1	95293.99	2.548-1	1049.38	2.205+14	2.101+19	1.271	1.616	+
	2	93836.29	3.162-2	1065.69	2.613+13	2.452+18	1.256	1.585	+
	3	92404.39	1.303-1	1082.20	1.028+14	9.501+18	1.214	1.473	−
5,	0	98519.81	1.077-2	1015.02	1.030+13	1.015+18	1.345	1.804	+
	1	97036.31	1.395-1	1030.54	1.275+14	1.237+19	1.309	1.712	+
	2	95578.61	2.162-1	1046.26	1.888+14	1.804+19	1.280	1.641	+
	3	94146.71	4.544-3	1062.17	3.792+12	3.570+17	1.204	1.425	−
6,	0	100229.55	1.367-3	997.71	1.376+12	1.379+17	1.396	1.943	+
	1	98746.05	4.043-2	1012.70	3.893+13	3.844+18	1.353	1.826	+
	2	97288.35	2.121-1	1027.87	1.953+14	1.900+19	1.317	1.735	+
	3	95856.45	1.160-1	1043.23	1.022+14	9.796+18	1.292	1.674	+
7,	0	101906.74	1.037-4	981.29	1.097+11	1.118+16	1.460	2.122	+
	1	100423.24	6.651-3	995.78	6.736+12	6.765+17	1.405	1.967	+
	2	98965.54	8.746-2	1010.45	8.477+13	8.389+18	1.361	1.850	+
	3	97533.64	2.389-1	1025.29	2.216+14	2.162+19	1.326	1.760	+
8,	0	103551.36	4.254-6	965.70	4.724+ 9	4.891+14	1.548	2.375	+
	1	102067.86	6.141-4	979.74	6.530+11	6.665+16	1.470	2.150	+
	2	100610.16	1.844-2	993.94	1.878+13	1.889+18	1.414	1.992	+
	3	99178.26	1.422-1	1008.28	1.388+14	1.376+19	1.370	1.874	+
9,	1	103679.92	2.913-5	964.51	3.247+10	3.366+15	1.560	2.412	+
	2	102222.22	2.046-3	978.26	2.186+12	2.234+17	1.480	2.179	+
	3	100790.32	3.824-2	992.16	3.915+13	3.946+18	1.423	2.018	+
10,	2	103801.71	1.108-4	963.38	1.239+11	1.287+16	1.572	2.449	+
	3	102369.81	5.053-3	976.85	5.421+12	5.549+17	1.490	2.209	+

THE CALCULATED ARRAY EXTENDED THROUGH (10, 3). Q LESS THAN 1.0-6 HAVE BEEN OMITTED.

$$O_2^+ a^4\Pi_u - O_2 a^1\Delta_g \text{ Ionization system}$$

v'	v''	σ_o	$q_{v'v''}$	$\lambda_o^{(vac)}$	$q_{v'v''}\sigma_o^3$	$q_{v'v''}\sigma_o^4$	$\bar{r}$	$\overline{r^2}$	phase
0,	0	122006.87	1.655-2	819.63	3.006+13	3.667+18	1.297	1.685	+
	1	120523.37	8.313-2	829.72	1.455+14	1.754+19	1.322	1.749	+
	2	119065.67	1.879-1	839.87	3.171+14	3.776+19	1.348	1.817	+
	3	117633.77	2.529-1	850.10	4.116+14	4.841+19	1.375	1.890	+
1,	0	123021.76	5.369-2	812.86	9.995+13	1.230+19	1.281	1.642	−
	1	121538.26	1.553-1	822.79	2.788+14	3.389+19	1.304	1.700	−
	2	120080.56	1.466-1	832.77	2.538+14	3.048+19	1.327	1.761	−
	3	118648.66	2.946-2	842.83	4.921+13	5.839+18	1.348	1.813	−
2,	0	124016.01	9.649-2	806.35	1.840+14	2.282+19	1.265	1.602	+
	1	122532.51	1.428-1	816.11	2.626+14	3.218+19	1.287	1.655	+

Table 57. Franck-Condon integrals--continued

$$O_2^+ a^4\Pi_u - O_2 a^1\Delta_g \text{ Ionization system}$$

v'	v''	σ_o	$q_{v'v''}$	$\lambda_o^{(vac)}$	$q_{v'v''}\sigma_o^3$	$q_{v'v''}\sigma_o^4$	$\bar{r}$	$\overline{r^2}$	phase
	2	121074.81	2.465-2	825.94	4.376+13	5.298+18	1.305	1.698	+
	3	119642.91	3.130-2	835.82	5.360+13	6.412+18	1.342	1.805	-
3,	0	124989.61	1.275-1	800.07	2.489+14	3.111+19	1.251	1.565	-
	1	123506.11	7.749-2	809.68	1.460+14	1.803+19	1.270	1.611	-
	2	122048.41	5.823-3	819.35	1.059+13	1.292+18	1.307	1.719	+
	3	120616.51	9.317-2	829.07	1.635+14	1.972+19	1.319	1.741	+
4,	0	125942.57	1.387-1	794.01	2.770+14	3.489+19	1.237	1.530	+
	1	124459.07	2.046-2	803.48	3.944+13	4.909+18	1.253	1.565	+
	2	123001.37	5.155-2	813.00	9.593+13	1.180+19	1.282	1.646	-
	3	121569.47	5.406-2	822.58	9.713+13	1.181+19	1.300	1.687	-
5,	0	126874.88	1.319-1	788.18	2.694+14	3.418+19	1.224	1.498	-
	1	125391.38	7.754-5	797.50	1.529+11	1.917+16	1.157	1.265	-
	2	123933.68	7.632-2	806.88	1.453+14	1.801+19	1.266	1.603	+
	3	122501.78	4.632-3	816.31	8.515+12	1.043+18	1.272	1.607	+
6,	0	127786.55	1.139-1	782.56	2.377+14	3.037+19	1.212	1.467	+
	1	126303.05	1.055-2	791.75	2.126+13	2.686+18	1.238	1.538	-
	2	124845.35	5.993-2	800.99	1.166+14	1.456+19	1.251	1.563	-
	3	123413.45	8.380-3	810.28	1.575+13	1.944+18	1.284	1.655	+

THE CALCULATED ARRAY EXTENDED THROUGH (6, 3). Q LESS THAN 1.0-6 HAVE BEEN OMITTED.

$$O_2^+ A^2\Pi_u - O_2 a^1\Delta_g \text{ Ionization system}$$

v'	v''	σ_o	$q_{v'v''}$	$\lambda_o^{(vac)}$	$q_{v'v''}\sigma_o^3$	$q_{v'v''}\sigma_o^4$	$\bar{r}$	$\overline{r^2}$	phase
0,	0	129552.12	5.255-3	771.89	1.143+13	1.480+18	1.306	1.708	+
	1	128068.62	3.341-2	780.83	7.018+13	8.988+18	1.329	1.768	+
	2	126610.92	9.816-2	789.82	1.992+14	2.523+19	1.353	1.832	+
	3	125179.02	1.772-1	798.86	3.476+14	4.351+19	1.378	1.900	+
1,	0	130423.15	2.018-2	766.73	4.477+13	5.839+18	1.293	1.672	-
	1	128939.65	8.649-2	775.56	1.854+14	2.391+19	1.315	1.729	-
	2	127481.95	1.465-1	784.42	3.036+14	3.870+19	1.338	1.790	-
	3	126050.05	1.114-1	793.34	2.230+14	2.811+19	1.361	1.851	-
2,	0	131267.05	4.296-2	761.81	9.718+13	1.276+19	1.280	1.639	+
	1	129783.55	1.185-1	770.51	2.591+14	3.363+19	1.301	1.693	+
	2	128325.85	9.558-2	779.27	2.020+14	2.592+19	1.323	1.748	+
	3	126893.95	7.990-3	788.06	1.633+13	2.072+18	1.339	1.785	+
3,	0	132083.81	6.732-2	757.09	1.551+14	2.049+19	1.268	1.608	-
	1	130600.31	1.118-1	765.69	2.491+14	3.253+19	1.288	1.659	-
	2	129142.61	2.602-2	774.34	5.604+13	7.237+18	1.307	1.704	-
	3	127710.71	1.698-2	783.02	3.536+13	4.516+18	1.339	1.798	+
4,	0	132873.44	8.697-2	752.60	2.040+14	2.711+19	1.256	1.579	+
	1	131389.94	7.840-2	761.09	1.778+14	2.336+19	1.276	1.627	+
	2	129932.24	1.735-5	769.63	3.805+10	4.944+15	1.127	1.099	+
	3	128500.34	5.927-2	778.21	1.257+14	1.616+19	1.322	1.749	-
5,	0	133635.93	9.840-2	748.30	2.348+14	3.138+19	1.246	1.552	-
	1	132152.43	4.022-2	756.70	9.282+13	1.227+19	1.264	1.595	-
	2	130694.73	1.474-2	765.14	3.291+13	4.301+18	1.292	1.673	+
	3	129262.83	6.137-2	773.62	1.326+14	1.713+19	1.308	1.711	+
6,	0	134371.28	1.012-1	744.21	2.455+14	3.298+19	1.236	1.527	+
	1	132887.78	1.276-2	752.52	2.995+13	3.980+18	1.251	1.561	+
	2	131430.08	3.064-2	760.86	0.999+13	1.183+19	1.278	1.635	-
	3	129998.18	3.189-2	769.24	7.006+13	9.108+18	1.295	1.674	-
7,	0	135079.50	9.683-2	740.31	2.386+14	3.224+19	1.226	1.504	-
	1	133596.00	8.613-4	748.53	2.054+12	2.744+17	1.228	1.493	-

Table 57. Franck-Condon integrals--continued

O_2^+ $A^2\Pi_u$ - O_2 $a^1\Delta_g$ Ionization system

v' v"	σ_o	$q_{v'v"}$	λ_o(vac)	$q_{v'v"}\sigma_o^3$	$q_{v'v"}\sigma_o^4$	$\bar{r}$	$\overline{r^2}$	phas
2	132138.30	5.266-2	756.78	1.215+14	1.605+19	1.266	1.605	+
3	130706.40	6.045-3	765.07	1.350+13	1.764+18	1.278	1.626	+
8, 0	135760.58	8.772-2	736.59	2.195+14	2.980+19	1.217	1.482	+
1	134277.08	1.860-3	744.73	4.503+12	6.046+17	1.248	1.568	-
2	132819.38	4.927-2	752.90	1.154+14	1.533+19	1.256	1.577	-
3	131387.48	4.970-4	761.11	1.127+12	1.481+17	1.307	1.733	+

THE CALCULATED ARRAY EXTENDED THROUGH (8, 3). Q LESS THAN 1.0-6 HAVE BEEN OMITTED.

O_2^+ $b^4\Sigma_g^-$ - O_2 $a^1\Delta_g$ Ionization system

v' v"	σ_o	$q_{v'v"}$	λ_o(vac)	$q_{v'v"}\sigma_o^3$	$q_{v'v"}\sigma_o^4$	$\bar{r}$	$\overline{r^2}$	phas
0, 0	138673.61	5.030-1	721.12	1.341+15	1.860+20	1.252	1.568	+
1	137190.11	3.600-1	728.92	9.296+14	1.275+20	1.305	1.703	+
2	135732.41	1.131-1	736.74	2.829+14	3.840+19	1.360	1.847	+
3	134300.51	2.095-2	744.60	5.076+13	6.817+18	1.416	1.999	+
1, 0	139836.25	3.190-1	715.12	8.722+14	1.220+20	1.210	1.463	-
1	138352.75	4.260-2	722.79	1.128+14	1.561+19	1.267	1.618	+
2	136895.05	3.267-1	730.49	8.380+14	1.147+20	1.317	1.736	+
3	135463.15	2.283-1	738.21	5.675+14	7.687+19	1.371	1.877	+
2, 0	140964.63	1.240-1	709.40	3.474+14	4.896+19	1.170	1.367	+
1	139481.13	2.400-1	716.94	6.514+14	9.086+19	1.223	1.499	-
2	138023.43	1.989-2	724.52	5.229+13	7.217+18	1.269	1.591	-
3	136591.53	1.627-1	732.11	4.145+14	5.662+19	1.329	1.773	+
3, 0	142058.73	3.900-2	703.93	1.118+14	1.588+19	1.133	1.279	-
1	140575.23	1.993-1	711.36	5.536+14	7.782+19	1.184	1.402	+
2	139117.53	8.429-2	718.82	2.269+14	3.157+19	1.239	1.542	-
3	137685.63	1.147-1	726.29	2.994+14	4.122+19	1.286	1.649	-

THE CALCULATED ARRAY EXTENDED THROUGH (3, 3). Q LESS THAN 1.0-6 HAVE BEEN OMITTED.

O_2^+ $X^2\Pi_g$ - O_2 $b^1\Sigma_g^+$ Ionization system

v' v"	σ_o	$q_{v'v"}$	λ_o(vac)	$q_{v'v"}\sigma_o^3$	$q_{v'v"}\sigma_o^4$	$\bar{r}$	$\overline{r^2}$	phas
0, 0	84244.09	9.354-2	1187.03	5.592+13	4.711+18	1.174	1.378	+
1	82839.34	1.869-1	1207.16	1.062+14	8.799+18	1.153	1.331	-
2	81462.58	2.125-1	1227.56	1.149+14	9.358+18	1.135	1.288	+
3	80113.91	1.820-1	1248.22	9.357+13	7.496+18	1.118	1.249	-
1, 0	86116.66	2.571-1	1161.22	1.642+14	1.414+19	1.200	1.441	+
1	84711.91	1.724-1	1180.47	1.048+14	8.878+18	1.177	1.386	-
2	83335.15	2.645-2	1199.97	1.531+13	1.276+18	1.153	1.325	+
3	81986.47	6.019-3	1219.71	3.317+12	2.720+17	1.154	1.342	+
2, 0	87956.66	3.087-1	1136.92	2.101+14	1.848+19	1.229	1.510	+
1	86551.91	5.965-3	1155.38	3.867+12	3.347+17	1.188	1.400	-
2	85175.15	7.773-2	1174.05	4.803+13	4.091+18	1.189	1.415	-
3	83826.48	1.183-1	1192.94	6.969+13	5.842+18	1.166	1.359	+
3, 0	89764.10	2.131-1	1114.03	1.542+14	1.384+19	1.260	1.586	+
1	88359.35	8.947-2	1131.74	6.172+13	5.454+18	1.240	1.541	+
2	86982.59	1.209-1	1149.66	7.954+13	6.919+18	1.211	1.466	
3	85633.92	1.412-3	1167.76	8.870+11	7.595+16	1.152	1.298	+
4, 0	91538.98	9.372-2	1092.43	7.189+13	6.580+18	1.293	1.671	+
1	90134.22	2.315-1	1109.46	1.696+14	1.528+19	1.269	1.611	+
2	88757.47	1.061-3	1126.67	7.422+11	6.587+16	1.185	1.364	-
3	87408.79	1.016-1	1144.05	6.789+13	5.934+18	1.222	1.496	-

Table 57. Franck-Condon integrals--continued

$O_2^+ X^2\Pi_g - O_2 b^1\Sigma_g^+$ Ionization system

v' v"	σ_o	$q_{v'v"}$	$\lambda_o^{(vac)}$	$q_{v'v"}\bar{\nu}_o^3$	$q_{v'v"}\bar{\nu}_o^4$	$\bar{r}$	$\bar{r^2}$	phase
5, 0	93281.29	2.747-2	1072.03	2.230+13	2.080+18	1.330	1.766	+
1	91876.54	1.967-1	1088.42	1.525+14	1.401+19	1.302	1.694	+
2	90499.78	1.065-1	1104.97	7.897+13	7.147+18	1.280	1.642	+
3	89151.10	6.719-2	1121.69	4.761+13	4.244+18	1.245	1.546	-
6, 0	94991.04	5.463-3	1052.73	4.683+12	4.448+17	1.371	1.875	+
1	93586.28	8.844-2	1068.53	7.249+13	6.784+18	1.338	1.789	+
2	92209.53	2.219-1	1084.49	1.740+14	1.604+19	1.311	1.719	+
3	90860.85	1.128-2	1100.58	8.463+12	7.690+17	1.305	1.716	+
7, 0	96668.22	7.354-4	1034.47	6.643+11	6.422+16	1.417	2.003	+
1	95263.47	2.403-2	1049.72	2.077+13	1.979+18	1.379	1.899	+
2	93886.71	1.590-1	1065.11	1.316+14	1.236+19	1.347	1.813	+
3	92538.04	1.643-1	1080.64	1.302+14	1.205+19	1.321	1.748	+
8, 0	98312.84	6.570-5	1017.16	6.243+10	6.138+15	1.471	2.156	+
1	96908.09	4.121-3	1031.91	3.751+12	3.635+17	1.426	2.028	+
2	95531.33	5.921-2	1046.78	5.162+13	4.932+18	1.388	1.924	+
3	94182.66	2.063-1	1061.77	1.723+14	1.623+19	1.356	1.839	+
9, 0	99924.90	3.742-6	1000.75	3.733+ 9	3.730+14	1.537	2.348	+
1	98520.15	4.477-4	1015.02	4.201+11	4.218+16	1.481	2.183	ɪ
2	97143.39	1.288-2	1029.41	1.180+13	1.147+18	1.435	2.054	+
3	95794.72	1.070-1	1043.90	9.405+13	9.010+18	1.397	1.949	+
10, 1	100099.64	2.994-5	999.00	3.003+10	3.006+15	1.546	2.378	+
2	98722.89	1.689-3	1012.94	1.625+12	1.604+17	1.490	2.211	+
3	97374.21	2.950-2	1026.97	2.724+13	2.652+18	1.444	2.080	+

THE CALCULATED ARRAY EXTENDED THROUGH (10, 3). Q LESS THAN 1.0-6 HAVE BEEN OMITTED.

$O_2^+ a^4\Pi_u - O_2 b^1\Sigma_g^+$ Ionization system

| v' v"	σ_o	$q_{v'v"}$	$\lambda_o^{(vac)}$	$q_{v'v"}\bar{\nu}_o^3$	$q_{v'v"}\bar{\nu}_o^4$	$\bar{r}$	$\bar{r^2}$	phase
0, 0	116768.35	3.150-2	856.40	5.015+13	5.856+18	1.305	1.706	+
1	115363.60	1.351-1	866.83	2.074+14	2.393+19	1.332	1.775	+
2	113986.84	2.534-1	877.29	3.753+14	4.278+19	1.360	1.851	+
3	112638.17	2.735-1	887.80	3.909+14	4.403+19	1.391	1.934	+
1, 0	117783.24	8.660-2	849.02	1.415+14	1.667+19	1.286	1.656	-
1	116378.49	1.873-1	859.27	2.953+14	3.436+19	1.310	1.718	-
2	115001.73	1.010-1	869.55	1.536+14	1.767+19	1.334	1.779	-
3	113653.06	2.093-6	879.87	3.072+ 9	3.492+14	0.079	-2.410	-
2, 0	118777.49	1.341-1	841.91	2.248+14	2.670+19	1.269	1.611	+
1	117372.74	1.199-1	851.99	1.938+14	2.275+19	1.290	1.664	+
2	115995.98	7.002-5	862.10	1.093+11	1.268+16	1.142	1.165	+
3	114647.30	9.678-2	872.24	1.458+14	1.672+19	1.348	1.818	-
3, 0	119751.09	1.549-1	835.06	2.660+14	3.186+19	1.253	1.569	-
1	118346.34	3.588-2	844.98	5.947+13	7.038+18	1.270	1.610	-
2	116969.58	4.593-2	854.92	7.350+13	8.598+18	1.304	1.704	+
3	115620.91	8.418-2	864.89	1.301+14	1.504+19	1.323	1.748	+
4, 0	120704.05	1.491-1	828.47	2.623+14	3.166+19	1.237	1.531	+
1	119299.30	6.876-4	838.23	1.168+12	1.393+17	1.219	1.459	+
2	117922.54	8.712-2	848.01	1.429+14	1.685+19	1.283	1.647	-
3	116573.87	9.857-3	857.83	1.561+13	1.820+18	1.292	1.659	-
5, 0	121636.36	1.269-1	822.12	2.284+14	2.778+19	1.223	1.496	-
1	120231.61	1.163-2	831.73	2.021+13	2.430+18	1.253	1.576	+
2	118854.85	6.867-2	841.36	1.153+14	1.370+19	1.265	1.598	+
3	117506.18	9.445-3	851.02	1.532+13	1.801+18	1.303	1.707	-
6, 0	122548.03	9.896-2	816.01	1.821+14	2.232+19	1.210	1.463	+

Table 57.　Franck-Condon integrals--continued

$$O_2^+\ a^4\Pi_u - O_2\ b^1\Sigma_g^+\ \text{Ionization system}$$

v' v"	σ_o	$q_{v'v"}$	$\lambda_o^{(vac)}$	$q_{v'v"}\sigma_o^3$	$q_{v'v"}\sigma_o^4$	$\bar{r}$	$\bar{r^2}$	phase
1	121143.28	4.014-2	825.47	7.137+13	8.646+18	1.234	1.525	−
2	119766.53	2.764-2	834.96	4.747+13	5.686+18	1.247	1.550	−
3	118417.85	4.703-2	844.47	7.810+13	9.249+18	1.277	1.633	+

THE CALCULATED ARRAY EXTENDED THROUGH (6, 3). Q LESS THAN 1.0-6 HAVE BEEN OMITTED.

$$O_2^+\ A^2\Pi_u - O_2\ b^1\Sigma_g^+\ \text{Ionization system}$$

v' v"	σ_o	$q_{v'v"}$	$\lambda_o^{(vac)}$	$q_{v'v"}\sigma_o^3$	$q_{v'v"}\sigma_o^4$	$\bar{r}$	$\bar{r^2}$	phase
0, 0	124313.60	1.086-2	804.42	2.087+13	2.594+18	1.315	1.730	+
1	122908.85	6.045-2	813.61	1.122+14	1.379+19	1.340	1.796	+
2	121532.09	1.524-1	822.83	2.736+14	3.325+19	1.366	1.866	+
3	120183.42	2.309-1	832.06	4.008+14	4.817+19	1.393	1.942	+
1, 0	125184.64	3.638-2	798.82	7.136+13	8.933+18	1.299	1.689	−
1	123779.88	1.259-1	807.89	2.388+14	2.955+19	1.323	1.750	−
2	122403.13	1.552-1	816.97	2.846+14	3.484+19	1.347	1.814	−
3	121054.45	6.219-2	826.08	1.103+14	1.335+19	1.371	1.877	−
2, 0	126028.53	6.836-2	793.47	1.368+14	1.725+19	1.285	1.652	+
1	124623.78	1.370-1	802.42	2.651+14	3.304+19	1.307	1.708	+
2	123247.03	5.517-2	811.38	1.033+14	1.273+19	1.328	1.762	+
3	121898.35	4.466-3	820.36	8.089+12	9.860+17	1.374	1.900	−
3, 0	126845.30	9.560-2	788.36	1.951+14	2.475+19	1.271	1.617	−
1	125440.54	9.882-2	797.19	1.951+14	2.447+19	1.292	1.669	−
2	124063.79	1.291-3	806.04	2.466+12	3.059+17	1.289	1.641	−
3	122715.11	6.306-2	814.90	1.165+14	1.430+19	1.344	1.808	+
4, 0	127634.92	1.113-1	783.48	2.314+14	2.954+19	1.259	1.585	+
1	126230.17	4.817-2	792.20	9.688+13	1.223+19	1.277	1.630	+
2	124853.41	1.572-2	800.94	3.060+13	3.820+18	1.310	1.720	−
3	123504.74	7.420-2	809.69	1.398+14	1.726+19	1.326	1.758	−
5, 0	128397.41	1.145-1	778.83	2.424+14	3.112+19	1.247	1.556	−
1	126992.66	1.274-2	787.45	2.609+13	3.313+18	1.262	1.588	−
2	125615.90	4.821-2	796.08	9.556+13	1.200+19	1.293	1.672	+
3	124267.23	3.443-2	804.72	6.606+13	8.210+18	1.309	1.711	+
6, 0	129132.77	1.079-1	774.40	2.322+14	2.999+19	1.236	1.528	+
1	127728.01	1.686-4	782.91	3.514+11	4.488+16	1.203	1.403	+
2	126351.26	6.175-2	791.44	1.246+14	1.574+19	1.279	1.635	−
3	125002.58	3.413-3	799.98	6.666+12	8.332+17	1.284	1.636	−
7, 0	129840.98	9.523-2	770.17	2.084+14	2.707+19	1.226	1.503	−
1	128436.23	4.949-3	778.60	1.048+13	1.347+18	1.255	1.583	+
2	127059.48	5.215-2	787.03	1.070+14	1.359+19	1.266	1.602	+
3	125710.80	3.594-3	795.48	7.140+12	8.976+17	1.304	1.711	−
8, 0	130522.07	8.010-2	766.15	1.781+14	2.325+19	1.216	1.479	+
1	129117.31	1.785-2	774.49	3.842+13	4.961+18	1.240	1.541	−
2	127740.56	3.181-2	782.84	6.631+13	8.470+18	1.254	1.570	−
3	126391.88	2.095-2	791.19	4.231+13	5.347+18	1.282	1.647	+

THE CALCULATED ARRAY EXTENDED THROUGH (8, 3). Q LESS THAN 1.0-6 HAVE BEEN OMITTED.

$$O_2^+\ b^4\Sigma_g^- - O_2\ b^1\Sigma_g^+\ \text{Ionization system}$$

v' v"	σ_o	$q_{v'v"}$	$\lambda_o^{(vac)}$	$q_{v'v"}\sigma_o^3$	$q_{v'v"}\sigma_o^4$	$\bar{r}$	$\bar{r^2}$	phase
0, 0	133435.09	6.347-1	749.43	1.508+15	2.012+20	1.258	1.585	+
1	132030.34	3.013-1	757.40	6.935+14	9.156+19	1.324	1.750	+
2	130653.58	5.762-2	765.38	1.285+14	1.679+19	1.394	1.937	+
3	129304.91	5.940-3	773.37	1.284+13	1.660+18	1.467	2.143	+
1, 0	134597.74	2.686-1	742.95	6.550+14	8.817+19	1.204	1.449	−

Table 57. Franck-Condon integrals--continued

$$O_2^+ \; b^4\Sigma_g^- - O_2 \; b^1\Sigma_g^+ \text{ Ionization system}$$

v'	v''	σ_o	$q_{v'v''}$	$\lambda_o^{(vac)}$	$q_{v'v''}\sigma_o^3$	$q_{v'v''}\sigma_o^4$	$\bar{r}$	$\overline{r^2}$	phase
	1	133192.98	1.781-1	750.79	4.208+14	5.605+19	1.274	1.630	+
	2	131816.23	3.855-1	758.63	8.831+14	1.164+20	1.335	1.784	+
	3	130467.55	1.428-1	766.47	3.171+14	4.137+19	1.404	1.967	+
2,	0	135726.11	7.417-2	736.78	1.854+14	2.517+19	1.155	1.329	+
	1	134321.36	2.961-1	744.48	7.176+14	9.639+19	1.218	1.485	-
	2	132944.60	1.283-2	752.19	3.014+13	4.007+18	1.303	1.733	+
	3	131595.93	3.314-1	759.90	7.553+14	9.939+19	1.348	1.820	+
3,	0	136820.22	1.749-2	730.89	4.480+13	6.129+18	1.111	1.226	-
	1	135415.46	1.505-1	738.47	3.738+14	5.062+19	1.169	1.364	+
	2	134038.71	2.075-1	746.05	4.996+14	6.697+19	1.233	1.526	-
	3	132690.03	1.534-2	753.64	3.583+13	4.755+18	1.274	1.592	-

THE CALCULATED ARRAY EXTENDED THROUGH (3, 3). Q LESS THAN 1.0-6 HAVE BEEN OMITTED.

$$O_2^+ \; X^2\Pi_g - O_2 \; B^3\Sigma_u^- \text{ Recombination system}$$

v'	v''	σ_o	$q_{v'v''}$	$\lambda_o^{(vac)}$	$q_{v'v''}\sigma_o^3$	$q_{v'v''}\sigma_o^4$	$\bar{r}$	$\overline{r^2}$	phase
1,	13	43152.15	1.048-6	2317.38	8.423+ 7	3.635+12	1.282	1.644	-
2,	8	46920.94	1.904-6	2131.24	1.967+ 8	9.228+12	1.306	1.706	+
	9	46455.14	3.499-6	2152.61	3.508+ 8	1.630+13	1.303	1.698	-
	10	46026.76	5.791-6	2172.65	5.646+ 8	2.599+13	1.300	1.691	+
	11	45638.52	8.667-6	2191.13	8.239+ 8	3.760+13	1.297	1.684	-
	12	45292.99	1.176-5	2207.85	1.093+ 9	4.951+13	1.295	1.678	+
	13	44992.15	1.451-5	2222.61	1.321+ 9	5.944+13	1.293	1.673	-
3,	5	50324.49	P 1.907-6	1987.10	2.430+ 8	1.223+13	1.328	1.766	-
	6	49761.70	P 4.770-6	2009.58	5.878+ 8	2.925+13	1.324	1.756	+
	7	49228.92	1.042-5	2031.33	1.243+ 9	6.119+13	1.321	1.746	-
	8	48728.38	2.020-5	2052.19	2.337+ 9	1.139+14	1.317	1.737	+
	9	48262.58	3.512-5	2072.00	3.948+ 9	1.906+14	1.314	1.729	-
	10	47834.20	5.521-5	2090.56	6.042+ 9	2.890+14	1.311	1.721	+
	11	47445.96	7.881-5	2107.66	8.417+ 9	3.994+14	1.309	1.714	-
	12	47100.42	1.025-4	2123.12	1.071+10	5.045+14	1.307	1.708	+
	13	46799.59	1.217-4	2136.77	1.248+10	5.839+14	1.304	1.703	-
4,	3	53307.23	1.875-6	1875.92	2.840+ 8	1.514+13	1.349	1.822	-
	4	52690.16	6.252-6	1897.89	9.145+ 8	4.818+13	1.345	1.810	+
	5	52099.36	P 1.710-5	1919.41	2.418+ 9	1.260+14	1.341	1.799	-
	6	51536.58	P 3.989-5	1940.37	5.460+ 9	2.814+14	1.337	1.788	+
	7	51003.80	8.144-5	1960.64	1.080+10	5.511+14	1.333	1.778	-
	8	50503.26	1.480-4	1980.07	1.906+10	9.626+14	1.329	1.768	+
	9	50037.46	2.420-4	1998.50	3.032+10	1.517+15	1.326	1.760	-
	10	49609.07	3.592-4	2015.76	4.385+10	2.175+15	1.323	1.752	+
	11	49220.84	4.862-4	2031.66	5.797+10	2.854+15	1.321	1.745	-
	12	48875.30	6.026-4	2046.02	7.036+10	3.439+15	1.318	1.738	+
	13	48574.47	6.858-4	2058.69	7.860+10	3.818+15	1.316	1.733	-
5,	2	55691.36	3.677-6	1795.61	6.350+ 8	3.537+13	1.367	1.870	+
	3	55049.54	1.470-5	1816.55	2.451+ 9	1.349+14	1.362	1.857	-
	4	54432.47	4.520-5	1837.14	7.290+ 9	3.968+14	1.357	1.844	+
	5	53841.67	P 1.142-4	1857.30	1.782+10	9.596+14	1.353	1.832	-
	6	53278.89	P 2.466-4	1876.92	3.729+10	1.987+15	1.349	1.821	+
	7	52746.11	4.669-4	1895.87	6.851+10	3.614+15	1.345	1.810	-
	8	52245.57	7.889-4	1914.04	1.125+11	5.878+15	1.341	1.800	+
	9	51779.77	1.204-3	1931.26	1.671+11	8.655+15	1.338	1.791	-

PAUL H. KRUPENIE

Table 57. Franck-Condon integrals--continued

$$O_2^+ \; X^2\Pi_g - O_2 \; B^3\Sigma_u^- \text{ Recombination system}$$

v' v''	σ_o	$q_{v'v''}$	$\lambda_o^{(vac)}$	$q_{v'v''}\sigma_o^3$	$q_{v'v''}\sigma_o^4$	$\bar{r}$	$\overline{r^2}$	phase
10	51351.39	1.673-3	1947.37	2.266+11	1.164+16	1.335	1.783	+
11	50963.15	2.131-3	1962.20	2.821+11	1.438+16	1.332	1.775	-
12	50617.61	2.499-3	1975.60	3.241+11	1.641+16	1.330	1.769	+
13	50316.78	2.707-3	1987.41	3.448+11	1.735+16	1.328	1.763	-
6, 1	58066.33	4.618-6	1722.17	9.041+ 8	5.250+13	1.385	1.921	-
2	57401.10	2.469-5	1742.13	4.669+ 9	2.680+14	1.380	1.906	+
3	56759.29	9.014-5	1761.83	1.648+10	9.356+14	1.375	1.892	-
4	56142.22	2.535-4	1781.19	4.486+10	2.519+15	1.370	1.878	+
5	55551.42	P 5.862-4	1800.13	1.005+11	5.582+15	1.366	1.866	-
6	54988.64	P 1.160-3	1818.56	1.929+11	1.061+16	1.361	1.854	+
7	54455.86	2.017-3	1836.35	3.258+11	1.774+16	1.357	1.843	-
8	53955.32	3.137-3	1853.38	4.927+11	2.659+16	1.353	1.833	+
9	53489.52	4.419-3	1869.53	6.762+11	3.617+16	1.350	1.823	-
10	53061.13	5.689-3	1884.62	8.499+11	4.510+16	1.347	1.815	+
11	52672.90	6.744-3	1898.51	9.855+11	5.191+16	1.344	1.807	-
12	52327.36	7.402-3	1911.05	1.060+12	5.549+16	1.341	1.800	+
13	52026.53	7.554-3	1922.10	1.064+12	5.535+16	1.339	1.794	-
7, 0	60431.05	2.922-6	1654.78	6.449+ 8	3.897+13	1.405	1.975	+
1	59743.51	2.769-5	1673.82	5.904+ 9	3.527+14	1.399	1.958	-
2	59078.29	1.338-4	1692.67	2.760+10	1.630+15	1.393	1.942	+
7, 3	58436.48	4.419-4	1711.26	8.817+10	5.152+15	1.388	1.927	-
4	57819.41	1.124-3	1729.52	2.172+11	1.256+16	1.383	1.913	+
5	57228.61	P 2.351-3	1747.38	4.406+11	2.522+16	1.378	1.900	-
6	56665.83	P 4.211-3	1764.73	7.662+11	4.342+16	1.374	1.888	+
7	56133.04	6.633-3	1781.48	1.173+12	6.585+16	1.370	1.876	-
8	55632.50	9.357-3	1797.51	1.611+12	8.963+16	1.366	1.866	+
9	55166.70	1.198-2	1812.69	2.011+12	1.109+17	1.362	1.856	-
10	54738.32	1.406-2	1826.87	2.306+12	1.262+17	1.359	1.847	+
11	54350.08	1.526-2	1839.92	2.449+12	1.331+17	1.356	1.839	-
12	54004.55	1.541-2	1851.70	2.428+12	1.311+17	1.353	1.831	+
13	53703.71	1.458-2	1862.07	2.259+12	1.213+17	1.351	1.825	-
8, 0	62075.67	1.622-5	1610.94	3.880+ 9	2.409+14	1.419	2.014	+
1	61388.14	1.375-4	1628.98	3.181+10	1.952+15	1.413	1.997	-
2	60722.91	5.940-4	1646.82	1.330+11	8.076+15	1.407	1.980	+
3	60081.10	1.751-3	1664.42	3.798+11	2.282+16	1.401	1.964	-
4	59464.03	3.972-3	1681.69	8.352+11	4.966+16	1.396	1.949	+
5	58873.23	P 7.402-3	1698.56	1.510+12	8.892+16	1.391	1.936	-
6	58310.45	P 1.180-2	1714.96	2.339+12	1.364+17	1.386	1.922	+
7	57777.66	1.651-2	1730.77	3.184+12	1.840+17	1.382	1.910	-
8	57277.13	2.068-2	1745.90	3.885+12	2.225+17	1.378	1.899	+
9	56811.32	2.349-2	1760.21	4.307+12	2.447+17	1.374	1.889	-
10	56382.94	2.448-2	1773.59	4.388+12	2.474+17	1.371	1.879	+
11	55994.70	2.364-2	1785.88	4.150+12	2.324+17	1.368	1.870	-
12	55649.17	2.133-2	1796.97	3.675+12	2.045+17	1.365	1.863	+
13	55348.34	1.813-2	1806.74	3.074+12	1.701+17	1.362	1.856	-
9, 0	63687.73	7.635-5	1570.16	1.972+10	1.256+15	1.433	2.055	+
1	63000.19	5.716-4	1587.30	1.429+11	9.004+15	1.427	2.036	-
2	62334.97	2.176-3	1604.24	5.271+11	3.285+16	1.420	2.019	+
3	61693.15	5.637-3	1620.93	1.323+12	8.165+16	1.415	2.002	-
4	61076.08	1.120-2	1637.30	2.550+12	1.558+17	1.409	1.986	+
5	60485.29	P 1.819-2	1653.29	4.025+12	2.434+17	1.404	1.972	-
6	59922.50	P 2.515-2	1668.82	5.411+12	3.242+17	1.399	1.958	+
7	59389.72	3.036-2	1683.79	6.360+12	3.777+17	1.394	1.945	-
8	58889.18	3.258-2	1698.10	6.654+12	3.919+17	1.390	1.933	+
9	58423.38	3.149-2	1711.64	6.280+12	3.669+17	1.386	1.922	-

Table 57. Franck-Condon integrals--continued

$$O_2^+ \ X^2\Pi_g - O_2 \ B^3\Sigma_u^- \text{ Recombination system}$$
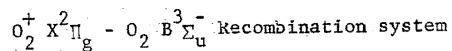
v' v"	σ_0	$q_{v'v"}$	λ_0 (vac)	$q_{v'v"}\sigma_0^3$	$q_{v'v"}\sigma_0^4$	$\bar{r}$	$\overline{r^2}$	phase
10	57995.00	2.770-2	1724.29	5.404+12	3.134+17	1.383	1.911	+
11	57606.76	2.240-2	1735.91	4.282+12	2.467+17	1.379	1.902	-
12	57261.22	1.682-2	1746.38	3.157+12	1.808+17	1.376	1.894	+
13	56960.39	1.184-2	1755.61	2.188+12	1.247+17	1.374	1.886	-
10, 0	65267.22	3.076-4	1532.16	8.553+10	5.582+15	1.448	2.097	+
1	64579.69	2.003-3	1548.47	5.394+11	3.483+16	1.441	2.077	-
2	63914.46	6.599-3	1564.59	1.723+12	1.101+17	1.434	2.058	+
3	63272.65	1.470-2	1580.46	3.724+12	2.356+17	1.428	2.041	-
4	62655.58	2.492-2	1596.03	6.128+12	3.840+17	1.422	2.024	+
5	62064.78	P 3.419-2	1611.22	8.174+12	5.073+17	1.417	2.008	-
6	61502.00	P 3.940-2	1625.96	9.165+12	5.637+17	1.412	1.994	+
7	60969.22	3.895-2	1640.17	8.827+12	5.382+17	1.407	1.980	-
8	60468.68	3.342-2	1653.75	7.390+12	4.468+17	1.402	1.967	+
9	60002.88	2.499-2	1666.59	5.400+12	3.240+17	1.398	1.954	-
10	59574.49	1.624-2	1678.57	3.433+12	2.045+17	1.394	1.943	+
11	59186.26	9.046-3	1689.58	1.875+12	1.110+17	1.390	1.932	-
12	58840.72	4.194-3	1699.50	8.545+11	5.028+16	1.386	1.920	+
13	58539.89	1.510-3	1708.24	3.030+11	1.774+16	1.382	1.906	-

THE CALCULATED ARRAY EXTENDED THROUGH (10,13). Q LESS THAN 1.0-6 HAVE BEEN OMITTED.

$$O_2^+ \ a^4\Pi_u - O_2 \ B^3\Sigma_u^- \text{ Recombination system}$$
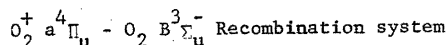
v' v"	σ_0	$q_{v'v"}$	λ_0 (vac)	$q_{v'v"}\sigma_0^3$	$q_{v'v"}\sigma_0^4$	$\bar{r}$	$\overline{r^2}$	phase
0, 0	80531.18	6.639-3	1241.75	3.467+12	2.792+17	1.493	2.230	+
1	79843.64	2.475-2	1252.45	1.260+13	1.006+18	1.474	2.175	-
2	79178.42	5.071-2	1262.97	2.517+13	1.993+18	1.457	2.126	+
3	78536.61	7.616-2	1273.29	3.689+13	2.897+18	1.442	2.080	-
4	77919.54	9.420-2	1283.38	4.457+13	3.473+18	1.427	2.039	+
5	77328.74	P 1.022-1	1293.18	4.724+13	3.653+18	1.414	2.001	-
6	76765.96	P 1.008-1	1302.66	4.562+13	3.502+18	1.402	1.966	+
7	76233.17	9.285-2	1311.76	4.113+13	3.136+18	1.391	1.935	-
8	75732.63	8.105-2	1320.44	3.520+13	2.666+18	1.381	1.906	+
9	75266.83	6.786-2	1328.61	2.894+13	2.178+18	1.371	1.880	-
10	74838.45	5.497-2	1336.21	2.304+13	1.724+18	1.363	1.857	+
11	74450.21	4.335-2	1343.18	1.789+13	1.332+18	1.355	1.836	-
12	74104.68	3.344-2	1349.44	1.361+13	1.008+18	1.349	1.818	+
13	73803.85	2.531-2	1354.94	1.018+13	7.510+17	1.343	1.802	-
1, 0	81546.07	4.396-2	1226.30	2.384+13	1.944+18	1.520	2.311	+
1	80858.53	1.050-1	1236.73	5.548+13	4.486+18	1.500	2.250	-
2	80193.31	1.310-1	1246.99	6.755+13	5.417+18	1.481	2.194	+
3	79551.50	1.109-1	1257.05	5.583+13	4.442+18	1.464	2.142	-
4	78934.43	6.818-2	1266.87	3.353+13	2.647+18	1.448	2.094	+
5	78343.63	P 2.903-2	1276.43	1.396+13	1.094+18	1.432	2.047	-
6	77780.85	P 6.265-3	1285.66	2.948+12	2.293+17	1.414	1.992	+
7	77248.06	1.925-6	1294.53	8.871+ 8	6.853+13	1.915	3.848	+
8	76747.52	4.332-3	1302.97	1.958+12	1.503+17	1.410	1.998	-
9	76281.72	1.272-2	1310.93	5.644+12	4.306+17	1.396	1.953	+
10	75853.34	2.054-2	1318.33	8.963+12	6.799+17	1.386	1.923	-
11	75465.10	2.554-2	1325.12	1.097+13	8.282+17	1.377	1.898	+
12	75119.57	2.725-2	1331.21	1.155+13	8.677+17	1.370	1.877	-
13	74818.74	2.621-2	1336.56	1.098+13	8.212+17	1.364	1.860	+
2, 0	82540.31	1.292-1	1211.53	7.267+13	5.999+18	1.548	2.399	+
1	81852.78	1.604-1	1221.71	8.799+13	7.202+18		2.328	-

Table 57.   Franck-Condon integrals--continued

$O_2^+ \; a^4\Pi_u - O_2 \; B^3\Sigma_u^-$ Recombination system

v' v"	σ_o	$q_{v'v"}$	$\lambda_o^{(vac)}$	$q_{v'v"}\sigma_o^3$	$q_{v'v"}\sigma_o^4$	$\bar{r}$	$\bar{r^2}$	phase
2	81187.56	7.969-2	1231.72	4.264+13	3.462+18	1.504	2.260	+
3	80545.74	1.093-2	1241.53	5.712+12	4.601+17	1.478	2.176	-
4	79928.67	3.342-3	1251.12	1.707+12	1.364+17	1.494	2.247	-
5	79337.87	P 2.854-2	1260.43	1.425+13	1.131+18	1.464	2.148	+
6	78775.09	P 4.963-2	1269.44	2.426+13	1.911+18	1.448	2.098	-
7	78242.31	5.253-2	1278.08	2.516+13	1.969+18	1.434	2.057	+
8	77741.77	4.145-2	1286.31	1.947+13	1.514+18	1.421	2.020	-
9	77275.97	2.587-2	1294.06	1.194+13	9.226+17	1.410	1.986	+
10	76847.59	1.271-2	1301.28	5.766+12	4.431+17	1.399	1.954	-
11	76459.35	4.511-3	1307.88	2.016+12	1.541+17	1.388	1.919	+
12	76113.81	8.253-4	1313.82	3.639+11	2.770+16	1.372	1.865	-
3, 0	83513.92	2.226-1	1197.41	1.297+14	1.083+19	1.579	2.494	+
1	82826.38	8.767-2	1207.34	4.981+13	4.126+18	1.552	2.406	-
2	82161.16	1.496-6	1217.12	8.296+ 8	6.816+13	2.852	7.290	-
3	81519.35	4.305-2	1226.70	2.332+13	1.901+18	1.521	2.318	+
4	80902.27	7.258-2	1236.06	3.843+13	3.109+18	1.500	2.249	-
5	80311.48	P 4.897-2	1245.15	2.536+13	2.037+18	1.481	2.190	+
6	79748.69	P 1.440-2	1253.94	7.304+12	5.825+17	1.460	2.127	-
7	79215.91	1.433-4	1262.37	7.123+10	5.643+15	1.362	1.777	+
8	78715.37	5.756-3	1270.40	2.807+12	2.210+17	1.457	2.133	+
9	78249.57	1.780-2	1277.96	8.528+12	6.673+17	1.439	2.075	-
10	77821.19	2.609-2	1285.00	1.230+13	9.570+17	1.427	2.038	+
11	77432.95	2.773-2	1291.44	1.287+13	9.968+17	1.417	2.008	-
12	77087.41	2.440-2	1297.23	1.118+13	8.615+17	1.408	1.984	+
13	76786.58	1.894-2	1302.31	8.576+12	6.585+17	1.401	1.962	-
4, 0	84466.87	2.498-1	1183.90	1.505+14	1.272+19	1.612	2.599	+
1	83779.34	1.287-3	1193.61	7.567+11	6.339+16	1.533	2.310	-
2	83114.12	7.547-2	1203.16	4.333+13	3.601+18	1.569	2.463	-
3	82472.30	7.769-2	1212.53	4.358+13	3.594+18	1.542	2.377	+
4	81855.23	1.284-2	1221.67	7.044+12	5.766+17	1.512	2.277	-
5	81264.44	P 4.466-3	1230.55	2.396+12	1.947+17	1.532	2.362	-
6	80701.65	P 3.260-2	1239.13	1.713+13	1.383+18	1.499	2.250	+
7	80168.87	4.549-2	1247.37	2.344+13	1.879+18	1.481	2.193	-
8	79668.33	3.427-2	1255.20	1.733+13	1.381+18	1.465	2.144	+
9	79202.53	1.569-2	1262.59	7.795+12	6.174+17	1.450	2.097	-
10	78774.15	3.383-3	1269.45	1.654+12	1.303+17	1.430	2.033	+
12	78040.37	1.977-3	1281.39	9.394+11	7.331+16	1.446	2.106	-
13	77739.54	5.184-3	1286.35	2.436+12	1.893+17	1.431	2.055	+
5, 0	85399.19	1.920-1	1170.97	1.196+14	1.021+19	1.648	2.715	+
1	84711.66	6.270-2	1180.47	3.811+13	3.228+18	1.630	2.661	+
2	84046.43	9.950-2	1189.82	5.907+13	4.965+18	1.594	2.541	-
3	83404.62	1.391-3	1198.97	8.069+11	6.730+16	1.517	2.262	+
4	82787.55	3.777-2	1207.91	2.143+13	1.774+18	1.561	2.443	+
5	82196.75	P 6.128-2	1216.59	3.403+13	2.797+18	1.536	2.358	+
6	81633.97	P 2.739-2	1224.98	1.490+13	1.216+18	1.512	2.282	+
7	81101.19	1.274-3	1233.03	6.798+11	5.513+16	1.461	2.103	-
8	80600.65	5.974-3	1240.69	3.128+12	2.521+17	1.508	2.287	-
9	80134.84	2.121-2	1247.90	1.091+13	8.746+17	1.485	2.208	+
10	79706.46	2.842-2	1254.60	1.439+13	1.147+18	1.470	2.162	-
11	79318.23	2.512-2	1260.74	1.254+13	9.943+17	1.458	2.125	+
12	78972.69	1.703-2	1266.26	8.385+12	6.622+17	1.447	2.092	-
13	78671.86	9.383-3	1271.10	4.569+12	3.594+17	1.438	2.063	+
6, 0	86310.86	1.035-1	1158.60	6.654+13	5.743+18	1.687	2.845	+
1	85623.33	1.827-1	1167.91	1.147+14	9.822+18	1.662	2.763	+
2	84958.10	9.066-3	1177.05	5.559+12	4.723+17	1.605	2.559	-

Table 57. Franck-Condon integrals--continued

$$O_2^+ \; a^4\Pi_u - O_2 \; B^3\Sigma_u^- \text{ Recombination system}$$

v' v''	σ_0	$q_{v'v''}$	$\lambda_0^{(vac)}$	$q_{v'v''}\sigma_0^3$	$q_{v'v''}\sigma_0^4$	$\bar{r}$	$\overline{r^2}$	phase
3	84316.29	6.425−2	1186.01	3.851+13	3.247+18	1.613	2.605	−
4	83699.22	6.196−2	1194.75	3.633+13	3.041+18	1.581	2.496	+
5	83108.42	P 2.538−3	1203.25	1.457+12	1.211+17	1.523	2.289	−
6	82545.64	P 1.748−2	1211.45	9.832+12	8.116+17	1.559	2.438	−
7	82012.86	4.328−2	1219.32	2.387+13	1.958+18	1.533	2.350	+
8	81512.32	3.417−2	1226.81	1.851+13	1.508+18	1.513	2.286	−
9	81046.52	1.180−2	1233.86	6.280+12	5.090+17	1.492	2.218	+
10	80618.13	5.182−4	1240.42	2.715+11	2.189+16	1.432	2.007	−
11	80229.90	2.181−3	1246.42	1.126+12	9.038+16	1.507	2.287	−
12	79884.36	8.236−3	1251.81	4.199+12	3.354+17	1.483	2.204	+
13	79583.53	1.235−2	1256.54	6.223+12	4.953+17	1.470	2.166	−

THE CALCULATED ARRAY EXTENDED THROUGH (6,13). Q LESS THAN 1.0−6 HAVE BEEN OMITTED.

$$O_2^+ \; A^2\Pi_u - X^2\Pi_g \text{ Second negative system}$$

v' v''	σ_0	$q_{v'v''}$	$\lambda_0^{(vac)}$	$q_{v'v''}\sigma_0^3$	$q_{v'v''}\sigma_0^4$	$\bar{r}$	$\overline{r^2}$	phase
0, 0	40069.51	1.648−6	2495.66	1.060+ 8	4.247+12	1.244	1.548	+
1	38196.94	3.099−5	2618.01	1.727+ 9	6.597+13	1.259	1.586	+
2	36356.94	2.763−4	2750.51	1.328+10	4.828+14	1.274	1.625	+
3	34549.50	1.554−3	2894.40	6.408+10	2.214+15	1.290	1.665	+
4	32774.63	6.183−3	3051.14	2.177+11	7.134+15	1.306	1.708	+
5	31032.31	1.852−2	3222.45	5.534+11	1.717+16	1.323	1.752	+
6	29322.57	4.338−2	3410.51	1.094+12	3.207+16	1.341	1.798	+
7	27645.38	8.151−2	3617.24	1.722+12	4.761+16	1.359	1.847	+
8	26000.76	1.251−1	3846.04	2.198+12	5.716+16	1.377	1.898	+
9	24388.70	1.587−1	4100.26	2.302+12	5.615+16	1.397	1.951	+
10	22809.21	1.681−1	4384.19	1.994+12	4.549+16	1.417	2.008	+
1, 0	40940.54	1.315−5	2442.57	9.024+ 8	3.695+13	1.237	1.531	−
1	39067.98	2.147−4	2559.64	1.280+10	5.002+14	1.251	1.567	−
2	37227.98	1.626−3	2686.15	8.390+10	3.124+15	1.266	1.605	−
3	35420.54	7.555−3	2823.22	3.358+11	1.189+16	1.282	1.644	−
4	33645.66	2.395−2	2972.15	9.121+11	3.069+16	1.298	1.685	−
5	31903.35	5.434−2	3134.47	1.764+12	5.629+16	1.314	1.728	−
6	30193.60	8.962−2	3311.96	2.467+12	7.448+16	1.331	1.772	−
7	28516.42	1.057−1	3506.75	2.450+12	6.987+16	1.348	1.818	−
8	26871.79	8.282−2	3721.37	1.607+12	4.319+16	1.366	1.865	−
9	25259.74	3.354−2	3958.87	5.406+11	1.365+16	1.383	1.911	−
10	23680.24	8.832−4	4222.93	1.173+10	2.777+14	1.383	1.898	−
2, 0	41784.44	5.605−5	2393.24	4.089+ 9	1.709+14	1.230	1.514	+
1	39911.88	7.944−4	2505.52	5.050+10	2.016+15	1.244	1.550	+
2	38071.87	5.096−3	2626.61	2.812+11	1.071+16	1.259	1.587	+
3	36264.43	1.940−2	2757.52	9.252+11	3.355+16	1.274	1.625	+
4	34489.56	4.803−2	2899.43	1.971+12	6.796+16	1.290	1.664	+
5	32747.25	7.899−2	3053.69	2.774+12	9.084+16	1.305	1.704	+
6	31037.50	8.255−2	3221.91	2.468+12	7.660+16	1.321	1.746	+
7	29360.31	4.538−2	3405.96	1.148+12	3.372+16	1.337	1.788	+
8	27715.69	4.371−3	3608.06	9.305+10	2.579+15	1.348	1.812	+
9	26103.63	1.156−2	3830.88	2.057+11	5.369+15	1.381	1.911	−
10	24524.14	5.812−2	4077.62	8.572+11	2.102+16	1.396	1.951	−
3, 0	42601.20	1.697−4	2347.35	1.312+10	5.589+14	1.224	1.499	−
1	40728.64	2.087−3	2455.27	1.410+11	5.744+15	1.238	1.533	−

Table 57. Franck-Condon integrals--continued

$$O_2^+ \, A^2\Pi_u - O_2 \, X^2\Pi_g \text{ Second negative system}$$

v'	v''	σ_0	$q_{v'v''}$	$\lambda_0^{(vac)}$	$q_{v'v''}\sigma_0^3$	$q_{v'v''}\sigma_0^4$	$\bar{r}$	$\overline{r^2}$	phase
	2	38888.64	1.130-2	2571.44	6.647+11	2.585+16	1.252	1.569	−
	3	37081.20	3.487-2	2696.79	1.778+12	6.593+16	1.267	1.606	−
	4	35306.32	6.558-2	2832.35	2.886+12	1.019+17	1.282	1.644	−
	5	33564.01	7.252-2	2979.38	2.742+12	9.203+16	1.297	1.682	−
	6	31854.26	3.749-2	3139.30	1.212+12	3.860+16	1.312	1.720	−
	7	30177.08	1.498-3	3313.77	4.118+10	1.243+15	1.316	1.724	−
	8	28532.45	1.804-2	3504.78	4.189+11	1.195+16	1.352	1.830	+
	9	26920.40	5.723-2	3714.66	1.117+12	3.006+16	1.367	1.869	+
	10	25340.90	4.664-2	3946.19	7.590+11	1.923+16	1.383	1.912	+
4,	0	43390.83	4.096-4	2304.63	3.346+10	1.452+15	1.218	1.484	+
	1	41518.26	4.373-3	2408.58	3.129+11	1.299+16	1.231	1.518	+
	2	39678.26	1.990-2	2520.27	1.243+12	4.931+16	1.246	1.552	+
	3	37870.82	4.904-2	2640.56	2.664+12	1.009+17	1.260	1.588	+
	4	36095.95	6.717-2	2770.39	3.159+12	1.140+17	1.274	1.624	+
	5	34353.63	4.320-2	2910.90	1.751+12	6.017+16	1.289	1.660	+
	6	32643.89	4.057-3	3063.36	1.411+11	4.607+15	1.298	1.681	+
	7	30966.70	1.264-2	3229.27	3.753+11	1.162+16	1.327	1.763	−
	8	29322.08	4.858-2	3410.40	1.225+12	3.591+16	1.340	1.797	−
	9	27710.02	3.518-2	3608.80	7.486+11	2.074+16	1.355	1.835	−
	10	26130.53	8.205-4	3826.94	1.464+10	3.825+14	1.351	1.808	−
5,	0	44153.32	8.386-4	2264.83	7.218+10	3.187+15	1.212	1.470	−
	1	42280.75	7.768-3	2365.14	5.871+11	2.482+16	1.226	1.503	−
	2	40440.75	2.954-2	2472.75	1.954+12	7.903+16	1.239	1.537	−
	3	38633.31	5.708-2	2588.44	3.291+12	1.272+17	1.253	1.571	−
	4	36858.44	5.325-2	2713.08	2.666+12	9.828+16	1.267	1.606	−
	5	35116.12	1.386-2	2847.69	6.001+11	2.107+16	1.280	1.636	−
	6	33406.38	3.437-3	2993.44	1.281+11	4.281+15	1.307	1.714	+
	7	31729.19	3.739-2	3151.67	1.194+12	3.790+16	1.316	1.733	+
	8	30084.57	3.586-2	3323.96	9.765+11	2.938+16	1.330	1.768	+
	9	28472.51	1.778-3	3512.16	4.105+10	1.169+15	1.334	1.768	+
	10	26893.02	1.957-2	3718.44	3.807+11	1.024+16	1.370	1.880	−
6,	0	44888.67	1.513-3	2227.73	1.369+11	6.144+15	1.207	1.457	+
	1	43016.11	1.216-2	2324.71	9.677+11	4.163+16	1.220	1.489	+
	2	41176.11	3.841-2	2428.59	2.681+12	1.104+17	1.233	1.522	+
	3	39368.67	5.667-2	2540.09	3.458+12	1.361+17	1.247	1.555	+
	4	37593.79	3.199-2	2660.01	1.700+12	6.389+16	1.260	1.588	+
	5	35851.48	4.596-4	2789.29	2.118+10	7.593+14	1.257	1.565	+
	6	34141.73	2.093-2	2928.97	8.328+11	2.843+16	1.294	1.677	−
	7	32464.55	3.900-2	3080.28	1.334+12	4.332+16	1.307	1.709	−
	8	30819.92	7.807-3	3244.65	2.286+11	7.044+15	1.318	1.733	−
	9	29207.87	9.420-3	3423.74	2.347+11	6.856+15	1.347	1.817	+
	10	27628.37	3.910-2	3619.47	8.246+11	2.278+16	1.358	1.845	+
7,	0	45596.89	2.469-3	2193.13	2.341+11	1.067+16	1.201	1.445	−
	1	43724.33	1.720-2	2287.06	1.438+12	6.286+16	1.215	1.476	−
	2	41884.32	4.477-2	2387.53	3.290+12	1.378+17	1.228	1.508	−
	3	40076.88	4.863-2	2495.20	3.130+12	1.255+17	1.241	1.540	−
	4	38302.01	1.295-2	2610.83	7.275+11	2.787+16	1.253	1.568	−
	5	36559.70	3.967-3	2735.25	1.938+11	7.087+15	1.277	1.634	+
	6	34849.95	3.372-2	2869.44	1.427+12	4.975+16	1.286	1.655	+
	7	33172.76	2.079-2	3014.52	7.589+11	2.518+16	1.299	1.685	+
	8	31528.14	7.124-4	3171.77	2.233+10	7.039+14	1.339	1.806	−
	9	29916.08	2.958-2	3342.68	7.920+11	2.369+16	1.335	1.783	−
	10	28336.59	2.199-2	3529.01	5.003+11	1.418+16	1.347	1.814	−
8,	0	46277.97	3.709-3	2160.86	3.676+11	1.701+16	1.197	1.433	+
	1	44405.41	2.239-2	2251.98	1.961+12	8.706+16	1.209	1.463	+

Table 57. Franck-Condon integrals--continued

$O_2^+ A^2\Pi_u - O_2 X^2\Pi_g$ Second negative system

v'	v''	τ_o	$q_{v'v''}$	$\lambda_o^{(vac)}$	$q_{v'v''}\sigma_o^3$	$q_{v'v''}\sigma_o^4$	$\bar{r}$	$\bar{r^2}$	phase
	2	42565.41	4.758-2	2349.33	3.669+12	1.562+17	1.222	1.495	+
	3	40757.97	3.604-2	2453.51	2.440+12	9.947+16	1.235	1.525	+
	4	38983.09	2.082-3	2565.21	1.233+11	4.808+15	1.243	1.539	+
	5	37240.78	1.552-2	2685.23	8.016+11	2.985+16	1.267	1.607	−
	6	35531.03	3.202-2	2814.44	1.436+12	5.103+16	1.279	1.636	−
	7	33853.85	3.900-3	2953.87	1.513+11	5.122+15	1.287	1.651	−
	8	32209.22	1.328-2	3104.70	4.436+11	1.429+16	1.314	1.729	+
	9	30597.17	2.956-2	3268.28	8.468+11	2.591+16	1.326	1.756	+
	10	29017.67	1.891-3	3446.18	4.621+10	1.341+15	1.328	1.753	+

THE CALCULATED ARRAY EXTENDED THROUGH (8,10). Q LESS THAN 1.0-6 HAVE BEEN OMITTED.

$O_2^+ b^4\Sigma_g^- - a^4\Pi_u$ First negative system

v'	v''	τ_o	$q_{v'v''}$	$\lambda_o^{(vac)}$	$q_{v'v''}\sigma_o^3$	$q_{v'v''}\sigma_o^4$	$\bar{r}$	$\bar{r^2}$	phase
0,	0	16666.74	2.642-1	5999.97	1.223+12	2.038+16	1.338	1.792	+
	1	15651.85	2.918-1	6389.02	1.119+12	1.751+16	1.302	1.694	−
	2	14657.60	2.063-1	6822.40	6.495+11	9.521+15	1.272	1.617	+
	3	13684.00	1.195-1	7307.80	3.061+11	4.189+15	1.246	1.552	−
	4	12731.04	6.207-2	7854.82	1.281+11	1.631+15	1.224	1.496	+
	5	11798.73	3.024-2	8475.49	4.968+10	5.861+14	1.204	1.446	−
	6	10887.06	1.418-2	9185.22	1.830+10	1.992+14	1.185	1.402	+
1,	0	17829.38	4.274-1	5608.72	2.423+12	4.319+16	1.379	1.903	+
	1	16814.49	2.369-2	5947.25	1.126+11	1.894+15	1.309	1.701	−
	2	15820.25	3.924-2	6321.01	1.554+11	2.458+15	1.322	1.755	−
	3	14846.65	1.199-1	6735.53	3.925+11	5.827+15	1.282	1.646	+
	4	13893.69	1.330-1	7197.51	3.568+11	4.957+15	1.254	1.573	−
	5	12961.37	1.037-1	7715.23	2.259+11	2.927+15	1.231	1.514	+
	6	12049.70	6.765-2	8298.96	1.183+11	1.426+15	1.210	1.462	−
2,	0	18957.76	2.446-1	5274.88	1.666+12	3.159+16	1.430	2.042	+
	1	17942.87	1.755-1	5573.25	1.014+12	1.819+16	1.398	1.960	+
	2	16948.62	1.409-1	5900.18	6.861+11	1.163+16	1.337	1.783	−
	3	15975.02	7.518-3	6259.77	3.065+10	4.896+14	1.264	1.576	+
	4	15022.06	2.216-2	6656.88	7.511+10	1.128+15	1.302	1.705	+
	5	14089.75	7.382-2	7097.36	2.065+11	2.909+15	1.264	1.600	−
	6	13178.08	9.346-2	7588.36	2.139+11	2.818+15	1.238	1.534	+
3,	0	20051.86	5.862-2	4987.07	4.726+11	9.476+15	1.496	2.233	+
	1	19036.97	3.473-1	5252.94	2.396+12	4.562+16	1.442	2.081	+
	2	18042.73	2.316-2	5542.40	1.360+11	2.455+15	1.453	2.129	+
	3	17069.13	1.416-1	5858.53	7.042+11	1.202+16	1.350	1.822	−
	4	16116.17	6.065-2	6204.95	2.539+11	4.091+15	1.302	1.690	+
	5	15183.85	9.424-4	6585.94	3.299+ 9	5.009+13	1.174	1.313	−
	6	14272.18	1.942-2	7006.64	5.645+10	8.057+14	1.281	1.649	−

THE CALCULATED ARRAY EXTENDED THROUGH (3, 6). Q LESS THAN 1.0-6 HAVE BEEN OMITTED.

TABLE 57. *Franck-Condon integrals*—Continued

$O_2\ A\ ^3\Sigma_u^+ - X\ ^3\Sigma_g^-$ Herzberg I system

Franck-Condon factors

v'' v'	0	1	2	3	4	5	6	7	8	9	10	11	12
0	1.809-6	3.339-5	2.916-4	1.605-3	6.248-3	1.840-2	4.260-2	7.935-2	1.214-1	1.546-1	1.654-1	1.495-1	1.140-1
1	1.488-5	2.383-4	1.765-3	8.012-3	2.479-2	5.519-2	8.985-2	1.052-1	8.298-2	3.500-2	1.510-3	1.512-2	6.765-2
2	6.300-5	8.761-4	5.494-3	2.041-2	4.924-2	7.924-2	8.158-2	4.457-2	4.492-3	1.049-2	5.486-2	7.589-2	4.343-2
3	1.836-4	2.222-3	1.179-2	3.553-2	6.516-2	7.053-2	3.593-2	1.434-3	1.700-2	5.478-2	4.681-2	6.822-3	9.761-3
4	4.201-4	4.439-3	1.989-2	4.816-2	6.469-2	4.103-2	3.900-3	1.162-2	4.595-2	3.559-2	1.700-3	1.847-2	5.157-2
5	7.975-4	7.382-3	2.794-2	5.368-2	4.998-2	1.343-2	2.713-3	3.372-2	3.537-2	3.171-3	1.414-2	4.233-2	1.828-2
6	1.307-3	1.066-2	3.412-2	5.134-2	3.040-2	8.570-4	1.669-2	3.605-2	1.034-2	4.851-3	3.357-2	1.962-2	6.872-4
7	1.874-3	1.354-2	3.679-2	4.277-2	1.386-2	1.724-3	2.668-2	2.223-2	3.734-5	2.013-2	2.515-2	6.205-4	1.826-2
8	2.375-3	1.536-2	3.570-2	3.168-2	4.153-3	7.860-3	2.642-2	8.092-3	4.344-3	2.454-2	8.205-3	4.749-3	2.553-2
9	2.624-3	1.539-2	3.097-2	2.090-2	4.588-4	1.232-2	1.946-2	1.184-3	1.068-2	1.771-2	4.555-4	1.313-2	1.612-2
10	2.462-3	1.332-2	2.370-2	1.231-2	4.947-5	1.249-2	1.152-2	2.020-5	1.203-2	9.046-3	6.301-4	1.390-2	5.925-3
11	1.715-3	8.762-3	1.426-2	6.011-3	3.515-4	8.568-3	5.372-3	4.550-4	8.314-3	3.434-3	1.676-3	8.748-3	1.340-3

r centroids

v'' v'	0	1	2	3	4	5	6	7	8	9	10	11	12	13	14	15
0	1.346	1.362	1.378	1.395	1.412	1.430	1.448	1.467	1.485	1.507	1.528	1.550	1.573	1.597	1.621	1.647
1	1.339	1.354	1.370	1.386	1.403	1.420	1.438	1.456	1.474	1.493	1.513	1.535	1.562	1.584	1.607	1.632
2	1.331	1.346	1.362	1.377	1.394	1.410	1.427	1.444	1.463	1.483	1.506	1.525	1.545	1.570	1.592	1.619
3	1.324	1.339	1.354	1.369	1.385	1.401	1.417	1.437	1.455	1.473	1.492	1.512	1.533	1.558	1.579	1.602
4	1.318	1.332	1.347	1.362	1.377	1.392	1.409	1.428	1.447	1.463	1.482	1.503	1.524	1.542	1.568	1.590
5	1.312	1.326	1.340	1.355	1.370	1.383	1.401	1.422	1.437	1.455	1.473	1.494	1.510	1.532	1.558	1.576
6	1.307	1.320	1.334	1.348	1.363	1.378	1.395	1.413	1.430	1.448	1.467	1.482	1.505	1.523	1.544	1.569
7	1.302	1.315	1.329	1.343	1.360	1.373	1.391	1.405	1.422	1.443	1.457	1.475	1.495	1.515	1.534	1.558
8	1.298	1.311	1.324	1.337	1.354	1.369	1.384	1.397	1.416	1.435	1.451	1.469	1.489	1.508	1.526	1.549
9	1.294	1.307	1.320	1.333	1.350	1.366	1.379	1.394	1.412	1.428	1.447	1.464	1.481	1.501	1.519	1.539
10	1.291	1.304	1.316	1.329	1.347	1.362	1.374	1.390	1.410	1.423	1.443	1.461	1.477	1.496	1.516	1.534
11	1.289	1.302	1.314	1.326	1.344	1.359	1.371	1.387	1.406	1.421	1.440	1.457	1.473	1.492	1.511	1.530

Data from unpublished results of Jarmain, communicated to Degen et al. [104]. Many r centroids have been adjusted by Jarmain to give a smoother curve of r centroid vs. λ.

TABLE 58. *Absolute band strengths* $S_{v'v''}$ [a] *for the A* $^3\Sigma_u^+ - X\ ^3\Sigma_g^-$ *bands*

v'' v'	0	1	2	3	4	5	6	7	8	9	10	11	12
0	2·39^{-12}[b]	4·08^{-11}	3·28^{-10}	1·66^{-9}	5·94^{-9}	1·60^{-8}	3·37^{-8}	5·71^{-8}	7·90^{-8}	9·06^{-8}	8·69^{-8}	7·00^{-8}	4·73^{-8}
1	2·04^{-11}	3·03^{-10}	2·07^{-9}	8·67^{-9}	2·47^{-8}	5·03^{-8}	7·49^{-8}	7·99^{-8}	5·72^{-8}	2·18^{-8}	8·46^{-10}	7·58^{-9}	3·02^{-8}
2	8·95^{-11}	1·15^{-9}	6·70^{-9}	2·30^{-8}	5·11^{-8}	7·56^{-8}	7·13^{-8}	3·56^{-8}	3·26^{-9}	6·90^{-9}	3·26^{-8}	4·05^{-8}	2·07^{-8}
3	2·70^{-10}	3·03^{-9}	1·49^{-8}	4·16^{-8}	7·04^{-8}	7·01^{-8}	3·30^{-8}	1·20^{-9}	1·30^{-9}	3·80^{-9}	2·94^{-9}	3·86^{-9}	4·96^{-9}
4	6·36^{-10}	6·25^{-9}	2·60^{-8}	5·84^{-8}	7·25^{-8}	4·24^{-8}	3·71^{-9}	1·01^{-9}	3·66^{-8}	2·59^{-8}	1·10^{-9}	1·10^{-8}	2·77^{-8}
5	1·24^{-9}	1·07^{-8}	3·77^{-8}	6·72^{-8}	5·80^{-8}	1·44^{-8}	2·68^{-9}	3·06^{-8}	2·94^{-8}	2·41^{-9}	9·77^{-9}	2·65^{-8}	1·03^{-8}
6	2·09^{-9}	1·59^{-8}	4·74^{-8}	6·62^{-8}	3·64^{-8}	9·48^{-10}	1·70^{-8}	3·39^{-8}	8·92^{-9}	3·83^{-9}	2·42^{-8}	1·29^{-8}	4·08^{-10}
7	3·07^{-9}	2·07^{-8}	5·24^{-8}	5·67^{-8}	1·70^{-8}	1·96^{-9}	2·81^{-8}	2·16^{-8}	3·33^{-11}	1·65^{-8}	1·88^{-8}	4·23^{-10}	1·13^{-9}
8	3·97^{-9}	2·40^{-8}	5·20^{-8}	4·30^{-8}	5·23^{-9}	9·19^{-9}	2·86^{-8}	8·08^{-9}	4·00^{-9}	2·07^{-8}	6·34^{-9}	3·35^{-9}	1·64^{-8}
9	4·47^{-9}	2·45^{-8}	4·60^{-8}	2·89^{-8}	5·91^{-10}	1·47^{-8}	2·15^{-8}	1·21^{-9}	1·01^{-8}	1·54^{-8}	3·62^{-10}	9·54^{-9}	1·07^{-8}
10	4·25^{-9}	2·15^{-8}	3·58^{-8}	1·73^{-8}	6·48^{-11}	1·52^{-8}	1·30^{-8}	2·11^{-11}	1·16^{-8}	8·01^{-9}	5·12^{-10}	1·03^{-8}	4·02^{-9}
11	2·99^{-9}	1·43^{-8}	2·17^{-8}	8·55^{-9}	4·66^{-10}	1·05^{-8}	6·13^{-9}	4·81^{-10}	8·11^{-9}	3·08^{-9}	1·38^{-9}	6·61^{-9}	9·24^{-10}

[a] $S_{v'v''}$ is in atomic units $(a_0e)^2$.

[b] The superscript indicates the power of ten by which the entry is to be multiplied.

Data from Hasson et al. [174].
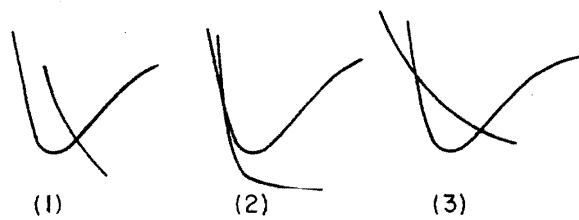
FIGURE 1.   Three types of crossing between a bound and a repulsive state
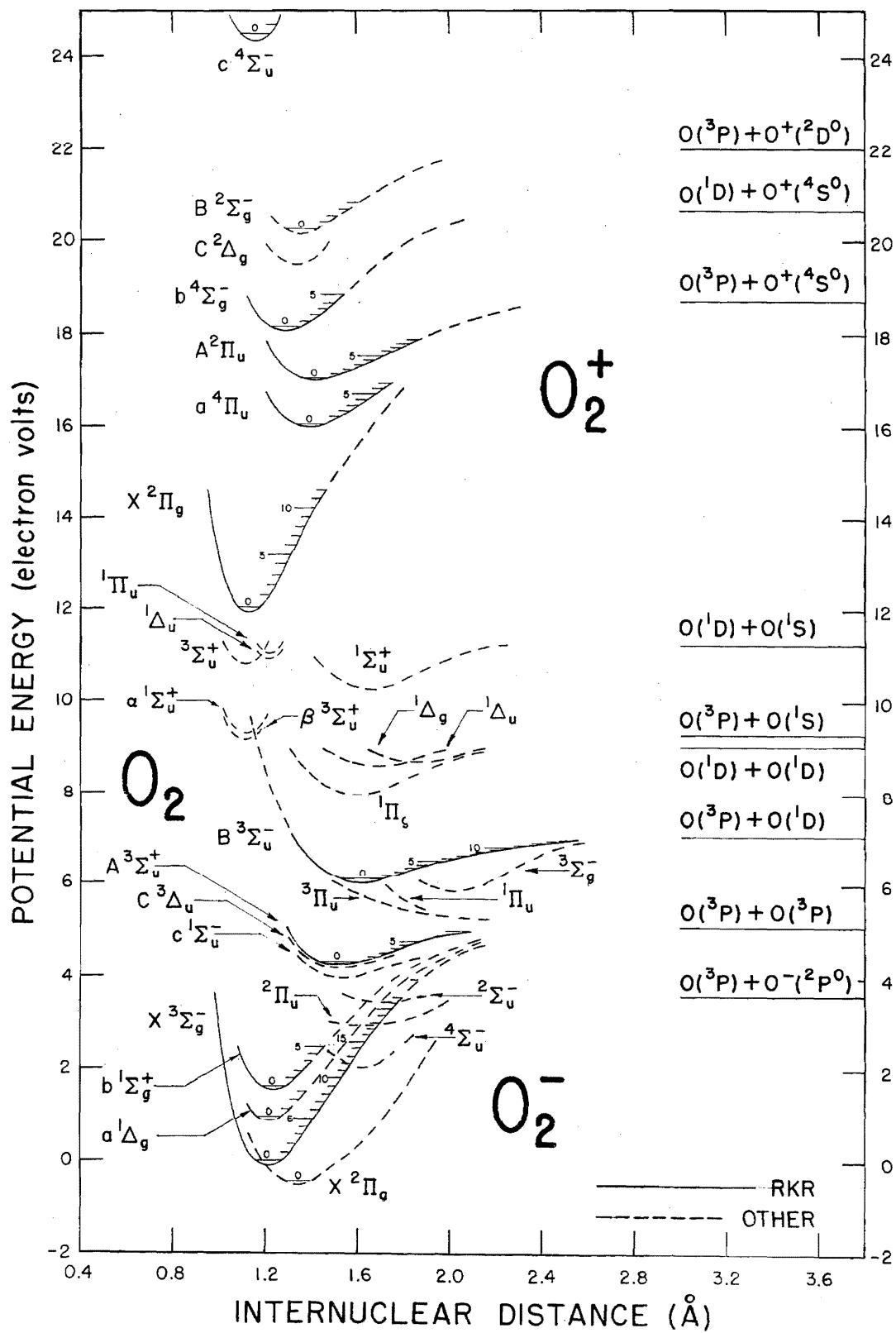
FIGURE 2.   Potential energy curves for O_2^-, O_2, and O_2^{+*}

*Enlarged copies of figure 2 may be obtained from the author upon request.

14. Acknowledgments

15. References

The references cited below have been traced from a number of standard sources [186, 316, 337, 154]. Recent references have been traced through the use of:

(a) Herzberg, G., and Howe, L. L., "Bibliography of Spectra of Diatomic Molecules, 1950–1960", Natl. Res. Council of Canada, Ottawa.

(b) Mulliken, R. S., "Bibliography of Diatomic Molecules, 1950–1960", Dept. of Physics, University of Chicago, Chicago.

(c) Phillips, J. G., and Davis, S. P., Newsletter, "Analysis of Molecular Spectra", Dept. of Physics, University of California, Berkeley.

These sources have been supplemented by the use of Current Contents and Chemical Abstracts.

Abbreviations and citations are based mainly on the listing in Access, Key to the Source Literature of the Chemical Sciences (American Chemical Society, Columbus, Ohio, 1969).

[1] Aboud, A. A., Curtis, J. P., Mercure, R., and Rense, W. A., Oxygen gas continuous absorption in the extreme ultraviolet, J. Opt. Soc. Amer. 45, 767–8 (1955).

[2] Abrahams, S. C., and Kalnajs, J., The crystal structure of α-potassium superoxide, Acta Cryst. 8, 503–6 (1955).

[3] Ackerman, M., and Biaume, F., Structure of the Schumann-Runge bands from the 0–0 to the 13–0 bands, J. Mol. Spectrosc. 35, 73–82 (1970).

[4] Ackerman, M., Biaume, F., and Kockarts, G., Absorption cross sections of the Schumann-Runge bands of molecular oxygen, Planet. Space Sci. 18 (11), 1639–51 (1970).

[5] Adiks, T. G., and Dianov-Klokov, V. I., Molecular parameters of the O_2 absorption band at 0.7620 μ and their use in calculating the transmission function, Academy of Sciences, USSR, Izvestia, Atmospheric and Oceanic Physics 4(10), 605–9 (1968). (Translation of Izv. Akad. Nauk. SSSR, Fiz Atmos. Okeana 4(10), 1052–9 (1968).) Chem. Abstr. 70: 72506 (1969).

[6] Akimoto, H., and Pitts, J. N., Jr., Emission spectra of O_2 ($^1\Delta_g$) trapped in solid oxygen at 4.2 °K, J. Chem. Phys. 53, 1312–15 (1970).

[7] Alberti, F., Ashby, R. A., and Douglas, A. E., Absorption spectra of O_2 in the a $^1\Delta_g$, b $^1\Sigma_g^+$, and X $^3\Sigma_g^-$ states, Can. J. Phys. 46, 337–42 (1968).

[8] Albritton, D. L., Schmeltekopf, A. L., and Zare, R. N., Evidence in support of the vibrational renumbering of the O_2^+ $^2\Pi_g$ ground state, J. Chem. Phys., 51(4), 1667 (1969).

9] Albritton, D. L., Schmeltekopf, A. L., and Zare, R. N., Diatomic Intensity Factors (Harper and Row, in preparation).

[10] Alder, F., and Yu, F. C., On the spin and magnetic momen of O^{17}, Phys. Rev. 81, 1067–8 (1951).

[11] Al-Joboury, M. I., May, D. P., and Turner, D. W., Molecula photoelectron spectroscopy. Part III. The ionization poten tials of oxygen, carbon monoxide, nitric oxide, and acetylene J. Chem. Soc. (London), 616–22 (1965).

[12] Al-Joboury, M. I., and Turner, D. W., Molecular photoelectroi spectroscopy. Part II. A summary of ionization potentials J. Chem. Soc. (London), 4434–41 (1964).

[13] Ammé, R. C., and Utterback, N. G., Effects of ion beam ex citation on charge transfer cross section measurements in Atomic Collision Processes, Proc. Third Intern. Conferenci on the Physics of Electronic and Atomic Collisions, held a University College, London 22–26 July, 1963, pp. 847–853 M. R. C. McDowell ed. (North-Holland Publ. Co., Amster dam, 1964).

[14] Anderson, R. S., Johnson, C. M., and Gordy, W., Resonan absorption of oxygen at 2.5 millimeter wavelength. Phys Rev. 83, 1061–2 (1951).

[15] Anderson, R. S., Smith, W. V., and Gordy, W., Line-breadth of the fine structure of the microwave spectrum of oxygen Phys. Rev. 82, 264 (1951).

[16] Anderson, R. S., Smith, W. V., and Gordy, W., Line-breadths of the microwave spectrum of oxygen, Phys. Rev. 87, 561–8 (1952).

[17] Arnold, J. S., Browne, R. J., and Ogryzlo, E. A., The red emission bands of molecular oxygen, Photochem. and Photobiol. 4, 963–9 (1965).

[18] Arnold, S. J., Kubo, M., and Ogryzlo, E. A., Relaxation and reactivity of singlet oxygen, p. 133–42 in Adv. in Chem. Ser. No. 77, 1968 (Amer. Chem. Soc.), Oxidation of Organic Compounds. Vol. III, Ozone Chemistry, Photo and Singlet Oxygen and Biochemical Oxidations, Proc. Intern. Oxida tion Symposium, arranged by Stanford Research Inst. ii San Francisco, Calif., 28 Aug.–1 Sept., 1967

[19] Artman, J. O., and Gordon, J. P., Absorption of microwaves by oxygen in the millimeter wavelength region, Phys. Rev. 96, 1237–45 (1954).

[20] Asundi, R. K., The first ionization potential of oxygen molecule, Current Sci. (Bangalore) 37(6), 160 (1968).

[21] Asundi, R. K., and Ramachandrarao, C. V. S., Revised Franck-Condon factors for the ionization transition of O_2^+ and the Second Negative band system of O_2^+, Chem. Phys. Lett. 4(2), 89–92 (1969).

[22] Babcock, H. S., Some new features of the atmospheric oxygen bands, and the relative abundance of the isotopes O^{16}, O^{18}, Proc. Natl. Acad. Sci. (U.S.) 15, 471–7 (1929)

[23] Babcock, H. C., Chemical compounds in the sun., Astrophys. J. 102, 154–67 (1945).

[24] Babcock, H. D., and Herzberg, L., Fine structure of the red system of atmospheric oxygen bands, Astrophys. J. 108, 167–90 (1948).

[25] Bader, R. F. W., Henneker, W. H., and Cade, P. E., Molecular charge distributions and chemical binding., J. Chem. Phys. 46, 3341–63 (1967).

[26] Badger, R. M., Wright, A. D., and Whitlock, R. F., Absolute intensities of the discrete and continuous absorption bands of oxygen gas at 1.26 and 1.065 μ and the radiative lifetime of the $^1\Delta_g$ state of oxygen, J. Chem. Phys. 43, 3341–63 (1967).

[27] Barrett, C. S., Meyer, L., and Wasserman, J., Antiferromagnetic and crystal structures of alpha oxygen., J. Chem. Phys. 47, 592–7 (1967).

[28] Barth, C. A., Emission spectra of the oxygen molecule in laboratory afterglows and the night airglow, Ph.D. Thesis, Dept. of Physics, University of Calif., Los Angeles (1958).

[29] Barth, C. A., and Kaplan, J., Herzberg oxygen bands in "air" afterglows and the night airglow, J. Chem. Phys. 26, 506–10 (1957).

[30] Barth, C. A., and Kaplan, J., The ultraviolet spectrum of the oxygen afterglow and the night airglow, J. Mol. Spectrosc. **3**, 583–7 (1959).

[31] Bass, A. M., and Garvin, D., On the concentrations of vibrationally excited O_2 formed in the flash photolysis of NO_2, J. Chem. Phys. **40**, 1772–3 (1964).

[32] Bassani, F., Montaldi, E., and Fumi, F. G., Electronic states of diatomic molecules: the O_2^+ molecular ion, Nuovo Cimento Ser. 10 **3**, 893–901 (1956).

[33] Bates, D. R., The intensity distribution in the nitrogen band systems emitted from the earth's upper atmosphere., Proc. Roy. Soc. (London) **A196**, 217–50 (1949).

[34] Bates, D. R., and Massey, H. S. W., The negative ions of atomic and molecular oxygen, Phil. Trans. Roy. Soc. (London) **A239**, 269–304 (1943).

[35] Battaglia, A., and Cattani, M., Line broadening of oxygen in the microwave region at low pressures, Nuovo Cimento Ser. 10 **54B**, 293–303 (1968).

[36] Ben-Aryeh, Y., Spectral emissivity of the Schumann-Runge bands of oxygen, J. Opt. Soc. Amer. **58**, 679–84 (1968).

[37] Berkowitz, J., Ehrhardt, H., and Tekaat, T., Spectra and angular distribution of photoelectrons from atoms and molecules., Z. Physik. **200**, 69–83 (1967).

[38] Berry, R. S., Electronic spectroscopy by electron spectroscopy, Annu. Rev. Phys. Chem. **20**, 357–406 (1969).

[39] Berry, R. S., Mackie, J. C., Taylor, R. L., and Lynch, R., Spin-orbit coupling and electron-affinity determinations from radiative capture of electrons by oxygen atoms, J. Chem. Phys. **43**, 3067–74 (1965).

[40] Bethke, G. W., Oscillator strengths in the far ultraviolet. II. Oxygen Schumann-Runge bands. J. Chem. Phys. **31**, 669–73 (1959).

[41] (a) Bhagavantam, S., Raman effect in gases: I. Some experimental results, Indian J. Phys. **6**, 319–30 (1931).
    (b) Bhagavantam, S., Raman effect in gases: II. Some theoretical considerations, Indian J. Phys. **6**, 331–44 (1931).
    (c) Bhagavantam, S., Raman effect in gases: III. Comparison of theory and experiment, Indian J. Phys. **6**, 557–62 (1931).

[42] Bhale, G. L., and Rao, P. R., Isotope shifts in the second negative bands of O_2. Proc. Indian Acad. Sci. Sect. A **67**(6), 350–7 (1968).

[43] Biberman, L. M., Erkovich, S. P., and Soshnikov, V. N., The transition probability in the Schumann-Runge band system of the O_2 molecule., Opt. Spectrosc. (USSR) **7**, 346–7 (1959).

[44] Birnbaum, G., Microwave pressure broadening and its application to intermolecular forces, chapt. 9, p. 487–548, in Hirschfelder, J. O., (ed), Intermolecular Forces, (Advances in Chemical Physics, vol. **12**, Interscience Publ., New York, 1967).

[45] Bixon, M., Raz, B., and Jortner, J., Resonances in the photodissociation continuum of diatomic molecules, Mol. Phys. **17**, 593–601 (1969).

[46] Blake, A. J., Carver, J. H., and Haddad, G. N., Photo-absorption cross section of molecular oxygen between 1250 Å and 2350 Å, J. Quant. Spectrosc. Radiat. Transfer **6**, 451–9 (1966).

[47] Blickensderfer, R. P., and Ewing, G. E., Spectroscopic evidence for binary O_2 clusters in the gas phase, J. Chem. Phys. **47**, 331–2 (1967).

[48] (a) Blickensderfer, R. P., and Ewing, G. E., Collision-induced absorption spectrum of gaseous oxygen at low temperatures and pressures. I. The $^1\Delta_g \leftarrow {}^3\Sigma_g$ system, J. Chem. Phys. **51**, 873–83 (1969).
    (b) Blickensderfer, R. P., and Ewing, G. E., Collision-induced absorption spectrum of gaseous oxygen at low temperatures and pressures. II. The simultaneous transitions $^1\Delta_g + {}^1\Delta_g \leftarrow {}^3\Sigma_g^- + {}^3\Sigma_g^-$ and $^1\Delta_g + {}^1\Sigma_g^+ \leftarrow {}^3\Sigma_g^- + {}^3\Sigma_g^-$, J. Chem. Phys. **51**, 5284–9 (1969).

[49] Boness, M. J. W., and Schulz, G. J., Structure of O_2 [-] Phys. Rev. **A2**, 2182–6 (1970).

[50] Boursey, E., Roncin, J., and Damany, N., Schumann-Runge bands of O_2 trapped in solid matrices, Chem. Phys. Lett. **5**, 584–6 (1970).

[51] Bowers, K. D., Kamper, R. A., and Lustig, C. D., Paramagnetic resonance absorption in molecular oxygen, Proc. Roy. Soc. (London) **A251**, 565–74 (1959).

[52] Bozóky, L., New study of the band spectrum of the ionized oxygen molecule, Magyar Tudomanyos Akademia, Matematikai és Természettudományi Értesitö (Budapest) [Math. Naturw. Anz. ungar, Akad. Wiss] **54**, 557–87 (1936).

[53] Bozóky, L., Rotational analysis of O_2^+, $^2\Pi \rightarrow {}^2\Pi$ bands, Z. Physik. **104**, 275–90 (1937).

[54] Bozóky, L., and Schmid, R., Additional first negative oxygen bands, Phys. Rev. **48**, 465 (1935).

[55] Bozóky, L., and Schmid, R., Zeeman effect in the first negative oxygen bands, Phys. Rev. **48**, 466 (1935).

[56] Brandt, W. H., Quartet states in diatomic molecules intermediate between cases a and b, Phys. Rev. **50**, 778–80 (1936).

[57] Branscomb, L. M., Emission of the atmospheric oxygen bands in discharges and afterglows, Phys. Rev. **86**, 258 (1952).

[58] Branscomb, L. M., Burch, D. S., Smith, S. J., and Geltman, S., Photo-detachment cross section and the electron affinity of atomic oxygen, Phys. Rev. **111**, 504–13 (1958).

[59] Branton, G. R., Frost, D. D., Makita, R., McDowell, C. A., and Stenhouse, I. A., Photoelectron spectra of some polyatomic molecules, Phil. Trans. Roy. Soc. London **A268**, 77–85 (1970).

[60] (a) Bridge, N. J., and Buckingham, A. D., Polarization of laser light scattered by gases, J. Chem. Phys. **40**, 2733–4 (1964).
    (b) Bridge, N. J., and Buckingham, A. D., The polarization of laser light scattered by gases, Proc. Roy. Soc. (London) **A295**, 334–49 (1966).

[61] Brion, C. E., Ionization of oxygen by "monoenergetic" electrons, J. Chem. Phys. **40**, 2995–8 (1964).

[62] Brix, P., and Herzberg, G., Fine structure of the Schumann-Runge bands near the convergence limit and the dissociation energy of the oxygen molecule, Can. J. Phys. **32**, 110–35 (1954).

[63] Broida, H. P., and Gaydon, A. G., The Herzberg bands of O_2 in an oxygen afterglow and in the night-sky spectrum, Proc. Roy. Soc. (London) **A222**, 181–95 (1954).

[64] Budó, A., Rotational structure of $^4\Sigma \rightarrow {}^4\Pi$ bands, Z. Physik **105**, 73–80 (1937).

[65] Budó, A., and Kovács, I., A-doubling of $^4\Pi$ terms, Physik. Z. **45**, 122–6 (1944).

[66] (a) Budó, A., and Kovács, I., On the $^4\Pi$ state of the O_2^+ molecule, Acta Phys. (Budapest) **4**, 273–90 (1955).
    (b) Budó, A., and Kovács, I., On the $^4\Pi$ state of the O_2^+ molecule, J. Chem. Phys. **23**, 751–2 (1955).

[67] (a) Burch, D. E., Gryvnak, D. A., and Patty, R. R., Absorption by the 7620 Angstrom oxygen band, Philco Research Labs., Newport Beach, Calif. Publication No. U-2908, 48 p. (1964). [Chem. Abstr. **63**, 5125a (1965)].
    (b) Burch, D. E., and Gryvnak, D. A., Strengths, widths, and shapes of the oxygen lines near 13,100 cm⁻¹ (7620 Å), Appl. Opt. **8**, 1493–9 (1969).

[68] Burch, D. S., Smith, S. J., and Branscomb, L. M., Photodetachment of O_2^-, Phys. Rev. **112**, 171 5 (1958).

[69] Burkhalter, J. H., Anderson, R. S., Smith, W. V., and Gordy, W., The fine structure of the microwave absorption spectrum of oxygen, Phys. Rev. **79**, 651–5 (1950).

[70] Buttrey, D. E., McChesney, H. R., and Hooker, L. A., Broadening of spectral lines of air molecules, 96 p. (Air Force Weapons Laboratory, Research and Technology Division, Kirtland Air Force Base, New Mexico, 1967). Tech. Rept. No. AFWL-TR-66-144, Contract AF 29(601)-7072.

[71] Byrne, J., New Bands in the second negative system of oxygen, Proc. Phys. Soc. (London) 78, 1074–5 (1961).

[72] (a) Cabannes, J., and Rousset, A., Depolarization factor of Raman lines in nitrogen, oxygen and carbon dioxide, Compt. Rendus Acad. Sci. (Paris), 202, 1825–8 (1936).

(b) Cabannes, J., and Rousset, A., Raman effect in gases under normal pressure, Compt. Rendus Acad. Sci. (Paris), 206, 85–8 (1938).

[73] Cairns, B. R., Infrared spectroscopic studies of solid oxygen, Ph. D. Thesis, University of California, Berkeley, (1965).

[74] Cairns, B. R., and Pimentel, G. C., Infrared spectra of solid α- and β-oxygen, J. Chem. Phys. 43, 3432–8 (1965).

[75] Cantone, B., Emma, V., and Grasso, F., Fine structure near the ionization threshold of Kr, O_2, NO by electron impact, Adv. in Mass Spectrom. 4, 599–605, Proc. Conf. held in Berlin, Sept. 1967, E. Kendrick, (ed) (The Institute of Petroleum, London, 1968).

[76] Carroll, P. K., Predissociation in the Schumann-Runge bands of oxygen, Astrophys. J. 129, 794–800 (1959).

[77] Carroll, P. K., and Hurley, A. C., Identification of an electronic transition of N_2^{2+}, J. Chem. Phys. 35, 2247–8 (1961).

[78] Cashion, J. K., Simple formulas for the vibrational and rotational eigenvalues of the Lennard-Jones 12–6 potential, J. Chem. Phys. 48, 94–103 (1968).

[79] hamberlain, J. W., On the presence of oxygen bands in the ultraviolet airglow spectrum, Astron. J. 59, 183–4 (1954).

[80] hamberlain, J. W., The ultraviolet airglow spectrum, Astrophys. J. 121, 277–86 (1955).

[81] hamberlain, J. W., The blue airglow spectrum, Astrophys. J. 128, 713–17 (1958).

[82] hamberlain, J. W., Fan, C. Y., and Meinel, A. B., A new O_2 band in the infrared auroral spectrum, Astrophys. J. 120, 560–2 (1954).

[83] Child, M. S., Repulsive potential curves from predissociation data, J. Mol. Spectrosc. 33(3), 487–93 (1970).

[84] (a) Childs, W. H. J., Absorption measurements and transition probabilities for the A(0,0) and B(0,1) bands of oxygen, Phil. Mag. Ser. 7 14, 1049–60 (1932).

(b) Childs, W. H. J., Equivalent widths in the A and B bands of oxygen, Astrophys. J. 77, 212–20 (1933).

[85] Childs, W. H. J., and Mecke, R., Intensity measurements in the atmospheric oxygen band λ7600, Z. Physik 68, 344–61 (1931).

[86] Cho, C. W., Allin, E. J., and Welsh, H. L., Structure of the infrared "atmospheric" bands in liquid oxygen, J. Chem. Phys. 25, 371–2 (1956).

[87] Cho, C. W., Allin, E. J., and Welsh, H. L., Effect of high pressures on the infrared and red atmospheric absorption band systems of oxygen, Can. J. Phys. 41, 1991–2002 (1963).

[88] Churchill, D. R., Armstrong, B. H., Johnston, R. R., and Muller, K. G., Absorption coefficients of heated air: A tabulation to 24,000 °K, J. Quant. Spectrosc. Radiat. Transfer 6, 371–42 (1966).

[89] (a) Codling, K., and Madden, R. P., New Rydberg series in molecular oxygen near 500Å, J. Chem. Phys. 42, 3935–8 (1965).

(b) Codling, K., Private communication.

[90] Collin, J. E., and Natalis, P., Ionic states and photon impact-enhanced vibrational excitation in diatomic molecules by photoelectron spectroscopy. Photoelectron spectra of N_2, CO and O_2, Intern. J. Mass Spectrom. and Ion Phys. 2, 231–45 (1969).

[91] Connes, J., and Gush, H. P., Infrared spectroscopy of the night sky by Fourier transforms, J. Phys. Radium 20, 915–17 (1959).

[92] Conway, D. C., Attachment of low-energy electrons to oxygen, J. Chem. Phys. 36, 2549–57 (1962).

[93] Cook, G. R., and Ching, B. K., Absorption, photoionization, and fluorescence of some gases of importance in the study of the upper atmosphere, 225 p. (Aerospace Corp., El. Segundo,

Calif., 1965). Report No. TDR–469 (9260–01)–4, Contract No. AF04(695)–469, AD 458631.

[94] Cook, G. R., and Ching, B. K., Penetration of solar ultraviolet in oxygen windows, Trans. Amer. Geophys. Union 48, 187 (1967). Abstract P. 187.

[95] Cook, G. R., and Metzger, P. H., Photoionization and absorption cross sections of O_2 and N_2 in the 600- to 1000-Å region, J. Chem. Phys. 41, 321–36 (1964).

[96] Crawford, M. F., Welsh, H. L., and Locke, J. L., Infrared absorption of oxygen and nitrogen induced by inter-molecular forces, Phys. Rev. 75, 1607 (1949).

[97] Creighton, J. A., and Lippincott, E. R., Vibrational frequency and dissociation energy of the superoxide ion. I. Chem. Phys. 40, 1779–80 (1964).

[98] Curcio, J. A., Drummeter, L. F., and Knestrick, G. L., An atlas of the absorption spectrum of the lower atmosphere from 5400 Å to 8520 Å, Appl. Opt. 3, 1401–9 (1964).

[99] Curry, J., and Herzberg, G., On the ultraviolet absorption bands of oxygen (Schumann-Runge bands), Ann. Physik (Leipzig) 19, 800–8 (1934).

[100] Dalgarno, A., and McElroy, M. B., The fluorescence of solar ionizing radiation, Planet. Space Sci. 13, 947–57 (1965).

[101] Daly, N. R., and Powell, R. E., Electron collisions in oxygen, Proc. Phys. Soc. (London) 90, 629 35 (1967).

[102] Degen, V., Intensity measurements on the Herzberg I band system of oxygen, Ph. D. Thesis, Dept. of Physics, U. of Western Ontario, London, Canada, 1966.

[103] Degen, V., The Herzberg II ($c~^1\Sigma_u^- - X~^3\Sigma_g^-$) system of O_2 in emission in the oxygen-argon afterglow, Can. J. Phys. 46, 783–7 (1968), erratum ibid, 46, 2850 (1968).

[104] Degen, V., Innanen, S. H., Hébert, G. R., and Nicholls, R. W. Identification Atlas of Molecular Spectra. 6. The $O_2~A~^3\Sigma_u^-$ $X~^3\Sigma_g^-$ Herzberg I system, York University, Centre for R search in Experimental Space Science and Dept. of Physic Toronto, Canada, Nov. 1968.

[105] Degen, V., and Nicholls, R. W., Intensity measurements in t laboratory on the O_2 Herzberg I ($A~^3\Sigma_u^- - X~^3\Sigma_g^-$) band syst in an oxygen-argon afterglow, J. Geophys. Res. 71, 3781 (1966).

[106] Degen, V., and Nicholls, R. W., Intensity measurements on tl $A~^3\Sigma_u^+ - X~^3\Sigma_g^-$ Herzberg I band system of O_2, J. Phys. B (A Mol. Phys.) 2, 1240–50 (1969). [Proc. Phys. Soc. (London)

[107] Dianov-Klokov, V. I., On the question of the origin of the spe trum of liquid and compressed oxygen, Opt. Spectrosc. (USSR) 6, 290–3 (1959).

[108] Dianov-Klokov, V. I., Absorption spectrum of oxygen at pressures from 2 to 35 atm. in the region from 12,600 to 3600 Å, Opt. Spectrosc. (USSR) 16, 224–7 (1964).

[109] Dianov-Klokov, V. I., On the bands of the $(O_2)_2$ complex in the near infrared absorption spectrum of the atmosphere, Opt. Spectrosc. (USSR), 17, 76–7 (1964).

[110] Dianov-Klokov, V. I., Absorption by gaseous oxygen and its mixtures with nitrogen in the 2800–2350 Å range, Opt. Spectrosc. (USSR), 21, 233–6 (1966).

[111] Dibeler, W. H., and Walker, J. A., Mass-spectrometric study of photoionization. VI. O_2, CO_2, COS, and CS_2, J. Opt. Soc. Amer. 57, 1007–12 (1967).

[112] Dieke, G. H., and Babcock, H. D., The structure of the atmospheric absorbtion bands of oxygen, Proc. Natl. Acad. Sci. (U.S.), 13, 670–8 (1927).

[113] Ditchburn, R. W., and Heddle, D. W. O., Absorption cross-sections in the vacuum ultra-violet II. The Schumann-Runge bands of oxygen (2000 to 1750 Å), Proc. Roy. Soc. London Ser. A226, 509–21 (1954).

[114] Ditchburn, R. W., and Young, P. A., The absorption of molecular oxygen between 1850 and 2500 Å, J. Atmos. Terr. Phys. 24, 127–39 (1962).

[115] Dixon, R. N., and Hull, S. E., The photo-ionization of π-electrons from O_2, Chem. Phys. Lett. 3(6), 367–70 (1969).

[116] Donovan, R. J., Kirsch, L. J., and Husain, D., O_2 ($a\ ^1\Delta_g$) in the photolysis of ozone, monitored by kinetic absorption spectroscopy in the vacuum ultra-violet, Chem. Phys. Lett. 7(4), 453–4 (1970).

[117] Doolittle, P. H., Schoen, R. I., and Schubert, K. E., Dissociative photoionization of O_2, J. Chem. Phys. 49, 5108–15 (1968).

[118] Dorman, F. H., and Morrison, J. D., Ionization potentials of doubly charged oxygen and nitrogen, J. Chem. Phys. 39, 1906–7 (1963).

[119] Dufay, J., Possible interpretation of certain intense radiation of the night sky in the ultraviolet region, Compt. Rend. Acad. Sci. (Paris), 213, 284–6 (1941).

[120] Dufay, J., Notes on selective absorption in the earth's atmosphere. 1.—Description of the spectrum of the setting sun from 4600 Å to 6900 Å, Ann. Astrophys. (Paris) 5, 93–113 (1942).

[121] Dufay, J., Spectra of the night sky in the near infrared, C. R. Acad. Sci. (Paris) 231, 1531–3 (1950).

[122] Dufay, M., Desesquelles, J., Druetta, M., and Eidelsberg, M., Study of excitation of nitrogen and oxygen by proton impact, Ann. Geophys. (Paris) 22, 614–27 (1966).

[123] Durie, R. A., The spectra of flames supported by flourine, Proc. Roy. Soc. (London) A211, 110–21 (1952).

[124] Eddy, J. A., Léna, P. J., and MacQueen, R. M., The far infrared transmission of the upper atmosphere, J. Atmos. Sci. 26, 1318–28 (1969).

[125] Edqvist, O., Lindholm, E., Selin, L. E., and Asbrink, L., On the photoelectron spectrum of O_2, Phys. Scripta 1, 25–30 (1970).

[126] Ellis, J. W., and Kneser, H. O., Combination relations in the absorption spectrum of liquid oxygen, Z. Physik 86, 583–91 (1933).

[127] Ellsworth, V. M., and Hopfield, J. J., Oxygen bands in the ultraviolet, Phys. Rev. 29, 79–84 (1927).

[128] Evenson, K. M., Broida, H. P., Wells, J. S., Mahler, R. J., and Mizushima, M., Electron paramamagnetic resonance absorption in oxygen with the HCN laser, Phys. Rev. Lett. 21, 1038–40 (1968).

[129] Falick, A. M., Mahan, B. H., and Myers, R. J., Paramagnetic resonance spectrum of the $^1\Delta_g$ oxygen molecule, J. Chem. Phys. 42, 1837–8 (1965).

[130] Fan, C. Y., Emission spectra excited by electronic and ionic impact, Phys. Rev. 103, 1740–5 (1956).

[131] Farmer, A. J. D., Fabian, W., Lewis, B. R., Lokan, K. H., and Haddad, G. N., Experimental oscillator strengths for the Schumann Runge band system in oxygen, J. Quant. Spectrosc. Radiat. Transfer 8, 1739–46 (1968).

[132] Feast M. W., Emission Schumann-Runge O_2 bands, Nature (London) 162, 214–5 (1948).

[133] Feast, M. W., On the Schumann-Runge O_2 bands emitted at atmospheric pressure, Proc. Phys. Soc. (London) A62, 114–21 (1949).

[134] Feast, M. W., The Schumann-Runge O_2 emission bands in the region 3100–2500 Å, Proc. Phys. Soc. (London) A63, 549–56 (1950).

[135] Feast, M. W., New O_2^+ second negative bands: a note on O_3 and O II emission spectra, Proc. Phys. Soc. (London) A63, 557–63 (1950).

[136] Feast, M. W., and Garton, W. R. S., The Schumann-Runge bands of O_2 in emission and absorption in the quartz ultra-violet region, Unpublished draft (1950). Supplied in private communication by W. R. S. Garton.

[137] Fesefeldt, H., Measurement of oxygen bands in the violet and ultra-violet spectral regions, Z. Wiss. Photogr., Photophys., Photobiol. 25, 33–60 (1927).

[138] Findlay, F. D., Relative band intensities in the atmospheric and infrared atmospheric systems of molecular oxygen, Can. J. Phys. 47, 687–91 (1969).

[139] Fink, E. H., and Welge, K. H., Lifetime and extinction cross sections of electronically excited states of N_2O^+. NO, O_2^+, CO^+, and CO, Z. Naturforsch. 23a, 358–76 (1968).

[140] Finkelnburg, W., On the interpretation of the O_4 spectrum and the existence of polyatomic polarization molecules, Z. Physik 90, 1–10 (1934).

[141] Finkelnburg, W., and Steiner, W., On the absorption spectrum of highly compressed oxygen and the existence of O_4 molecules. I. The ultraviolet bands between 2900 and 2300 Å, Z. Physik. 79, 69–88 (1932).

[142] (a) Fitzsimmons, R. V., Study of vibrationally excited oxygen by high-resolution absorption spectroscopy, Ph. D. Thesis, Physical Chemistry, Indiana Univ. (1963), [Univ. Microfilms, 64–5451, Ann Arbor, Michigan].

(b) Fitzsimmons, R. V., and Bair, E. J.; Distribution and relaxation of vibrationally excited oxygen in flash photolysis of ozone, J. Chem. Phys. 40, 451–8 (1964).

[143] Flory, P. J., Predissociation of the oxygen molecule, J. Chem. Phys. 4, 23–7 (1936).

[144] Fraga, S., and Ransil, B. J., Studies in molecular structure. V. Computed spectroscopic constants for selected diatomic molecules of the first row, J. Chem. Phys. 35, 669–78 (1961).

[145] Freund, R. S., Dissociation by electron impact of oxygen into metastable quintet and long-lived high-Rydberg atoms (preprint, 1970).

[146] Frosch, R. A., and Foley, H. M., Magnetic hyperfine structure in diatomic molecules, Phys. Rev. 88, 1337–49 (1952).

[147] Frost, D. C., and McDowell, C. A., The ionization and dissociation of oxygen by electron impact, J. Amer. Chem. Soc. 80, 6183–7 (1958).

[148] Frost, D. C., McDowell, C. A., and Vroom, D. A., Photoelectron kinetic energy analysis in gases by means of a spherical analyser, Proc. Roy. Soc. (London) A296, 566–79 (1967).

[149] Füchtbauer, C., and Holm, E., The ultra-violet absorption bands of oxygen as dependent on temperature; and a short-wave-length spectrum of iodine, Physik. Z. 26, 345–9 (1925).

[150] Fumi, F. G., and Parr, R. G., Electronic states of diatomic molecules: The oxygen molecule, J. Chem. Phys. 21, 1864–8 (1953).

[151] Gaily, T. D., Optical absorption of molecular oxygen near 1215 Angstroms, J. Opt. Soc. Amer. 59, 536–8 (1969).

[152] Garton, W. R. S., and Feast, M. W., Schumann-Runge absorption bands in heated oxygen, Nature (London) 165, 281–2 (1950).

[153] Gaydon, A. G., A laboratory source of the Herzberg bands of O_2, p. 262–3 in the Airglow and the Aurorae (papers presented at symposium held at Belfast, Sept. 1955) E. B. Armstrong and A. Dalgarno (eds.) (Pergamon Press, London, New York, 1956).

[154] Gaydon, A. G., Dissociation Energies and Spectra of Diatomic Molecules, 3rd. edition; (Chapman and Hall Ltd., London, 1968).

[155] Gebbie, H. A., Burroughs, W. J., and Bird, G. R., Magnetic dipole rotation spectrum of oxygen, Proc. Roy. Soc. (London) A310, 579–90 (1969).

[156] Gebbie, H. A., Burroughs, W. J., Harries, J. E., and Cameron, R. M., Submillimeter wave spectroscopy of the earth's atmosphere above 39,000 feet, Astrophys. J. 154, 405–8 (1968).

[157] Gebbie, H. A., Burroughs, W. J., Robb, J. A., and Bird, G. R., Observation of the magnetic dipole rotation spectrum of oxygen, Nature (London) 212, 66–7 (1966).

[158] Geiger, J., and Schröder, B., High-resolution energy-loss spectrum of molecular oxygen, J. Chem. Phys. 49, 740–4 (1968).

[159] Geschwind, S., and Gunther-Mohr, G. R., The spin and quadrupole moment of O^{17}, Phys. Rev. 85, 474–7 (1952).

[160] (a) Giauque, W. F., and Johnston, H. L., An isotope of oxygen, mass 18. Interpretation of the atmospheric absorption bands, J. Amer. Chem. Soc. 51, 1436–41 (1929).

(b) Giauque, W. F., and Johnston, H. L., An isotope of oxygen, mass 17, in the earth's atmosphere, J. Amer. Chem. Soc. 51, 3528–34 (1929).

51] Gilmore, F. R., Potential energy curves for N_2, NO, O_2, and corresponding ions, J. Quant. Spectrosc. Radiat. Transfer 5, 369–89 (1965).

52] Ginter, M. L., and Battino, R., On the calculation of potential curves by the Rydberg-Klein-Rees method, I. Experimental limitations, extrapolation procedures, and applications to the third-group hydrides, J. Chem. Phys. 42, 3222–9 (1965).

53] Glockler, G., and Lind, S.C., The Electrochemistry of Gases and other Dielectrics (J. Wiley and Sons, Inc., New York, 1939).

54] Goldstein, R., and Mastrup, F. N., Absorption coefficients of the O_2 Schumann-Runge continuum from 1270 Å $\leftrightarrow$ 1745 Å using a new continuum source, J. Opt. Soc. Amer. 56, 765–9 (1966).

55] Gush, H. P., and Buijs, H. L., The near infrared spectrum of the night airglow observed from high altitude, Can. J. Phys. 42, 1037–45 (1964).

66] Hagstrum, H. D., and Tate, J. T., Ionization and dissociation of diatomic molecules by electron impact, Phys. Rev. 59, 354–70 (1941).

67] Halmann, M., The far-ultraviolet absorption spectrum of $^{18}O_2$, $^{17}O^{18}O$, and $^{16}O^{18}O$, J. Chem. Soc. (London), 3729–33 (1964).

68] (a) Halmann, M., and Laulicht, I., Isotope effects on vibrational transition probabilities. The Schumann-Runge absorption bands of $^{16}O_2$ and $^{18}O_2$, J. Chem. Phys. 42, 137–9 (1965).

(b) Halmann, M., and Laulicht, I., Isotope effects on vibrational transition probabilities. II. Electronic transitions of isotopic nitrogen, nitric oxide, and oxygen molecules, J. Chem. Phys. 43, 438–48 (1965).

(c) Halmann, M., and Laulicht, I., Isotope effects on vibrational transition probabilities. III. Ionization of isotopic H_2, N_2, O_2, NO, CO, and HCl molecules, J. Chem. Phys. 43, 1503–9 (1965).

(d) Halmann, M., and Laulicht, I., Isotope effects on vibrational transition probabilities. V. Electronic transitions of isotopic O_2, N_2, C_2, and H_2 molecules, J. Chem. Phys. 44, 2398–2405 (1966).

(e) Halmann, M., Isotope effects on Franck-Condon factors. VI. Pressure-broadened absorption intensities of the Schumann-Runge bands of $^{16}O_2$ and $^{18}O_2$, J. Chem. Phys. 44, 2406–8 (1966).

[169] Halmann, M., and Laulicht, I., Isotope effects on Franck-Condon factors. VII. Vibrational intensity distribution in the H_2 Lyman, H_2 Werner, O_2 Schumann-Runge, N_2 First Positive, N_2 Vegard-Kaplan, and LiH $(A-X)$ systems based on RKR potentials. J. Chem. Phys. 46, 2684–9 (1967).

[170] Halmann, M., and Laulicht, I., Isotope effects on Franck-Condon factors: Intensity distribution in the rotational structure of the O_2 Schumann-Runge and the H_2 and D_2 Lyman band systems, J. Quant. Spectrosc. Radiat. Transfer 8, 935–44 (1968).

[171] Halverson, F., Comments on potassium superoxide structure, J. Phys. Chem. Solids 23, 207–14 (1962).

[172] Harris, R., Blackledge, M., and Generosa, J., Rydberg-Klein-Rees (RKR) Franck-Condon factors for the O_2 Schumann-Runge system including high vibrational quantum numbers, J. Mol. Spectrosc. 30, 506–12 (1969).

[173] Hasson, V., Hébert, G. R., and Nicholls, R. W., Measured transition probabilities for bands of the Schumann-Runge (B $^3\Sigma_u^- - X\ ^3\Sigma_g^-$) band system of molecular oxygen, J. Phys. B (At. Mol. Phys.) 3(8), 1188–91 (1970), [Proc. Phys. Soc. (London)].

[174] Hasson, V., Nicholls, R. W., and Degen, V., Absolute intensity measurements on the $A\ ^3\Sigma_u^+ - X\ ^3\Sigma_g^-$ Herzberg I band system of molecular oxygen, J. Phys. B (At Mol. Phys.) 3 (8), 1192–4 (1970), [Proc. Phys. Soc. (London)].

[175] Hébert, G. R., Innanen, S. H., and Nicholls, R. W., Identification atlas of molecular spectra. 4. The O_2 $B\ ^3\Sigma_u^- - X\ ^3\Sigma_g^-$ Schumann-Runge system, York University, Centre for Research in Experimental Space Science and Dept. of Physics, Jan., 1967, Toronto, Ontario, Canada.

[176] Hébert, G. R., and Nicholls, R. W., The λ2763 Å (0, 9) band of the O_2 Schumann-Runge system, J. Atmos. Terr. Phys. 21, 213–15 (1968).

[177] Hébert, G. R., and Nicholls, R. W., Intensity measurements in emission on 29 bands of the O_2 Schumann-Runge system, Proc. Phys. Soc. (London) A78, 1024–37 (1961).

[178] Heddle, D. W. O., Photodissociation in the Schumann-Runge system of oxygen, J. Chem. Phys. 32, 1889–90 (1960).

[179] Heller, R., Theory of some van der Waals molecules, J. Chem. Phys. 9, 154–63 (1941).

[180] Hendrie, J. M., and Kusch, P., Radio-frequency Zeeman effect in O_2, Phys. Rev. 107, 716–23 (1957).

[181] Herczog, A., and Wieland, K., Absorption bands of the Schumann-Runge system of O_2 at high pressure and temperature, Helv. Phys. Acta 23, 432–6 (1950).

[182] Herman, L., Absorption spectrum of oxygen, Ann. Phys. (Paris) 11, 548–611 (1939).

[183] Herman, L., Herman, R., and Rakotoarijimy, D., Study of a radio-frequency discharge in oxygen, J. Phys. Radium 22, 1–8 (1961).

[184] Herman, R. C., Hopfield, H. S., and Hornbeck, G. A., Photographic infrared emission bands of O_2 from the $CO-O_2$ flame, J. Chem. Phys. 17, 220–1 (1949).

[185] Herzberg, G., A new "forbidden" absorption band system of the O_2 molecule, Naturwiss. 20, 577 (1932).

[186] Herzberg, G., Spectra of Diatomic Molecules, Second Edition (D. Van Nostrand Co., Inc., New York, 1950).

[187] Herzberg, G., Forbidden transitions in diatomic molecules II. The $^3\Sigma_u^+ \leftarrow\ ^3\Sigma_g^-$ absorption bands of the oxygen molecule, Can. J. Phys. 30, 185–210 (1952).

[188] Herzberg, G., Forbidden transitions in the spectra of diatomic molecules, Trans. Roy. Soc. Can. Ser. 3 46 (Sect. 3), 1–21 (1952).

[189] Herzberg, G., Forbidden transitions in diatomic molecules III. New $^1\Sigma_u^- \leftarrow\ ^3\Sigma_g^-$ and $^3\Delta_u \leftarrow\ ^3\Sigma_g^-$ absorption bands of the oxygen molecule, Can. J. Phys. 31, 657–69 (1953).

[190] Herzberg, G., Forbidden transitions in diatomic molecules, Mem. Soc. Roy. Sci. Liege, Collect. in 8°, Ser. 5 17, 121–55 (1969).

[191] Herzberg, L., and Herzberg, G., Fine structure of the infrared atmospheric oxygen bands, Astrophys. J. 105, 353–9 (1947).

[192] Hijikata, K., On the fluorine molecule II. Energy levels of F_2 and F_2^+, J. Chem. Phys. 34, 231–9 (1961).

[193] Hill, R. M., and Gordy, W., Zeeman effect and line breadth studies of the microwave lines of oxygen, Phys. Rev. 93, 1019–22 (1954).

[194] Holzer, W., Murphy, W. F., Bernstein, H. J., and Rolfe, J., Raman spectrum of O_2 ion in alkali halide crystals, J. Mol. Spectrosc. 26, 543–5 (1968).

[195] Hopfield, J. J., New oxygen spectra in the ultraviolet, Phys. Rev. 36, 789 (Abstract 22) (1930).

[196] Hornbeck, G. A., and Hopfield, H. S., Spectroscopic investigation of the carbon monoxide-oxygen reaction, J. Chem. Phys. 17, 982–7 (1949).

[197] Huber, K. P., Rydberg series in the absorption spectrum of the NO molecule, Helv. Phys. Acta 34, 929–58 (1961).

[198] Hudson, R. D., Critical review of ultraviolet photoabsorption cross sections for molecules of astrophysical and aeronomic interest, Rev. Geophys. Space Phys. 9, 305–406 (1971).

[199] (a) Hudson, R. D., and Carter, V. L., Absorption of oxygen at elevated temperatures (300 to 900 K) in the Schumann-Runge system, J. Opt. Soc. Amer. 58, 1621–9 (1968).

(b) Hudson, R. D., and Carter, V. L., Absorption of oxygen at elevated temperatures (300 to 900 K) in the Schumann-Runge system, 88 p., (Space and Missile Systems Organization, Air Force Systems Command, Los Angeles Air Force Station, Los Angeles, California, 1968). Report No. SAMSO TR 68-452, Aerospace No. TR-0200(9260-01)-2.

[200] Hudson, R. D., and Carter, V. L., Predissociation in N_2 and O_2, Can. J. Phys. 47, 1840–5 (1969).

- [201] Hudson, R. D., Carter, V. L., and Breig, E. L., Predissociation in the Schumann-Runge band system of O_2: Laboratory measurements and atmospheric effects, J. Geophys. Res., Space Phys. 74, 4079–86 (1969).

[202] Hudson, R. D., Carter, V. L., and Stein, J. A., An investigation of the effect of temperature on the Schumann-Runge absorption continuum of oxygen 1580–1950 Å., J. Geophys. Res. 71, 2295–8 (1966).

[203] Huffman, R. E., Absorption cross-sections of atmospheric gases for use in aeronomy, Can. J. Chem. 47, 1823–40 (1969).

[204] Huffman, R. E., Larrabee, J. C., and Tanaka, Y., Absorption coefficients of oxygen in the 1060–580 Å wavelength region, J. Chem. Phys. 40, 356–65 (1964).

[205] Huffman, R. E., Larrabee, J. C., and Tanaka, Y., New absorption spectra of atomic and molecular oxygen in the vacuum ultraviolet, I. Rydberg series from OI ground state and new excited O_2 bands, J. Chem. Phys. 46, 2213–33 (1967).

[206] Huffman, R. E., Tanaka, Y., and Larrabee, J. C., Nitrogen and oxygen absorption cross-sections in the vacuum ultra-violet, Disc. Faraday Soc. No. 37, 159–66 (1964).

[207] Hulst, H. C., van de, The atmospheric oxygen bands, Ann. Astrophys. (Paris) 8, No. 1/2, 12–25 (1945).

[208] Hurley, A. C., Potential energy curves for doubly positive diatomic ions Part II. Predicted states and transitions of N_2^{2+}, O_2^{2+}, and NO_2^+ [i.e. NO^{2+}] J. Mol. Spectrosc. 9, 18–29 (1962).

[209] Hurley, A. C., and Maslen, V. W., Potential curves for doubly positive diatomic ions, J. Chem. Phys. 34, 1919–25 (1961).

[210] Hurst, G. S., and Bortner, T. E., Negative ions of oxygen, Radiation Research, Suppl. 1, 547–57 (1959).

[211] Inouc, Y., On the ionization mechanism in the ionosphere, Jap. J. Geophys. 1, 21–120 (1957).

[212] Itoh, T., and Ohno, K., Modified atomic orbital method, II. The electronic structure of the oxygen molecule, J. Chem. Phys. 25, 1098–1101 (1956).

[213] Jain, D. C., and Sahni, R. C., Transition probabilities for the ionization of N_2, O_2, NO and CO molecules, Intern. J. Quantum Mech. 2, 325–32 (1968).

[214] James, T. C., The analysis of intensity data in diatomic molecules. A criticism of the r-centroid approach, J. Mol. Spectrosc. 20, 77–87 (1966).

[215] Jarmain, W. R., Franck-Condon factors from Klein-Dunham potentials for bands of the Schumann-Runge system of O_2, Can. J. Phys. 41, 414–16 (1963).

[216] Jarmain, W. R., Franck-Condon factors from Klein-Dunham potentials for the $v''=0$ progression of the Schumann-Runge system of O_2, Can. J. Phys. 41, 1926–9 (1963).

[217] Jarmain, W. R., O_2 Schumann-Runge Franck-Condon factors, densities (≳1969), unpublished results.

[218] Jarmain, W. R., and Nicholls, R. W., A theoretical study of the O_2 $X\,^3\Sigma_g^- - B\,^3\Sigma_u^-$ photodissociation continuum, Proc. Phys. Soc. (London) A84, 417–24 (1964).

[219] Jarmain, W. R., and Nicholls, R. W., A theoretical study of the $v''=0, 1, 2$ progressions of bands and adjoining photodissociation continua of the O_2 Herzberg I system. Proc. Phys. Soc. (London) A90, 545–53 (1967).

[220] (a) Jeunehomme, M., Oscillator strengths of the negative systems of oxygen, J. Chem. Phys. 44, 4253–8 (1966).

(b) Jeunehomme. M., Private communication to D. E. Shemansky and A. Vallance Jones (See ref. [353]).

[221] Johnson, R. C., Ultra-violet emission bands associated with oxygen, Proc. Roy. Soc. (London) A105, 683–97 (1924).

[222] Jonathan, N., Smith, D. J., and Ross, K. J., High-resolution vacuum ultraviolet photoelectron spectroscopy of transient species: $O_2(^1\Delta_g)$, J. Chem. Phys. 53, 3758–9 (1970).

[223] Jordan, T. H., Streib, W. E., Smith, H. W., and Lipscomb, W. N., Single-crystal studies of β–F_2 and of γ–O_2, Acta Cryst. 17, 777–8 (1964).

[224] Judge, D. L., Fluorescence spectra of the molecular ions of O_2^+, N_2^+, and CO^+ excited by vacuum ultraviolet radiation, Ph. D. Thesis, Dept. of Physics, Univ. of Southern Calif., Los Angeles, 1965.

[225] Kahan, W., Detection of the microwave ν_{27}- line of molecular oxygen produced in the high atmosphere, Nature (London) 195, 30–2 (1962).

[226] Kaplan, J., The atmospheric bands of oxygen, Phys. Rev. 71, 274 [abstract] (1947).

[227] Kayama, K., and Baird, J. C., Spin-orbit effects and the fine structure in the $^3\Sigma_g^-$ ground state of O_2, J. Chem. Phys. 46, 2604–18 (1967).

[228] Keck, J. C., Allen, R. A., and Taylor, R. L., Electronic transition moments for air molecules, J. Quant. Spectrosc. Radiat. Transfer 3, 335–53 (1963).

[229] Keck, J., Camm, J., and Kivel, B., Absolute emission intensity of Schumann-Runge radiation from shock heated oxygen, J. Chem. Phys. 28, 723–4 (1958).

[230] Keck, J. C., Camm, J. C., Kivel, B., and Wentink, T., Jr., Radiation from hot air. Part II. Shock tube study of absolute intensities, Ann. Phys. (N.Y.) 7, 1–38 (1959).

[231] Keys, L. K., Magnetic susceptibility and resonance studies on adsorbed oxygen: Formation of O_4 species, Ph. D. Thesis, Physical Chemistry, The Pennsylvania State University, 1965.

[232] Kivel, B., Excited states of negative ions of atomic oxygen, 16 p., (AVCO–Everett Research Lab., Everett, Mass., 1966) Research Report 246, Contract No. AF 04 (684)–690.

[233] Knauss, H. P., and Ballard, S. S., Rotational structure of the Schumann-Runge bands of oxygen in the vacuum region, Phys. Rev. 48, 796–9 (1935).

[234] Knobler, C. M., On the existence of a molecular oxygen dimer, Doctoral thesis, Leiden University, Leiden (1961). Drukkerij Pasmans, 'S-Gravenhage, 1961.

[235] Konishi, A., Wakiya, K., Yamamoto, M., and Suzuki, H., Cross sections of the excitation of the $a\,^1\Delta_g$, $b\,^1\Sigma_g^+$, and $A\,^3\Sigma_u^+$ and $C\,^3\Delta_u$ states in O_2 by electron impact, J. Phys. Soc. Japan 29, 526 (1970).

[236] Kotani, M., Mizuno, Y., Kayama, K., and Ishiguro, E., Electronic structure of simple homonuclear diatomic molecules I. Oxygen molecule, J. Phys. Soc. Japan 12, 707–36 (1957).

[237] Kovács, I., The role of the spin–spin interaction in the multiplet splitting of the $^4\Pi$ state of the O_2^+ molecule, Acta Phys. (Budapest) 10, 255 8 (1959).

[238] Kovács, I., and Weniger, S., Interpretation of the anomalous separation of the multiplet components of the $^4\Pi$ state of the ionized oxygen molecule, J. Phys. Radium 23, 377–80 (1962).

[239] Koval, A. G., Koppc, V. T., and Fogcl, Ya. M., Emission spectra of rarefied molecular gases excited by fast electrons, Kosmich. Issled., Akad. Nauk SSSR 4(1), 74–88 (1966). [Chem. Abstr. 65: 11549a (1966)].

[240] Krassovsky, V. I., On the detection of the infra-red night-airglow, p. 86–90 in Armstrong, E. B.; Dalgarno, A. (eds.), The Airglow and the Aurora (Pergamon Press, London, 1956).

[241] Krassovsky, V. I., Shefov, N. N., and Yarin, V. I., Atlas of the airglow spectrum 3,000–12,400 Å, Planet. Space Sci. 9, 883–915 (1962).

[242] (a) Krindach, N. I., Kudryavtsev, R. M., Sobolev, N. N., Tunitskii, L. N., and Faizullov, F. S., Determination of the electronic transition moments of the Schumann-Runge band system in oxygen. I., Opt. Spectrosc. (USSR) 14, 188–93 (1963).

(b) Krindach, N. I., Sobolev, N. N., and Tunitskii, L. N., Determination of the electronic transition moments of the Schumann-Runge bands of the oxygen molecule. II., Opt. Spectrosc. (USSR) 15, 161–4 (1963).

(c) Krindach, N. I., Sobolev, N. N., and Tunitskii, L. N., Determination of the electronic transition moments of the Schumann-Runge bands of the oxygen molecule. III., Opt. Spectrosc. (USSR) 15, 326–30 (1963).

[243] (a) Krishna, V. G., Simultaneous and induced electronic transitions in oxygen. I., J. Chem. Phys. 50, 792–9 (1969).

(b) Krishna, V. G., and Cassen, T., Simultaneous and induced electronic transitions in oxygen. II., J. Chem. Phys. 51, 2140–5 (1969).

[244] Krupenie, P. H., and Benesch, W., Electronic transition moment integrals for first ionization of CO and the A–X transition in CO+. Some limitations on the use of the r-centroid approximation, J. Res. Natl. Bur. Stand. (U.S.) 72A, (Phys. and Chem.) No. 5, 495–503 (1968).

[245] Ladenburg, R., Van Voorhis, C. C., and Boyce, J. C., Absorption of oxygen in the region of short wave-lengths, Phys. Rev. 40, 1018–20 (1932).

[246] Lal, L., New bands in the Schumann-Runge system of the oxygen molecule, Nature (London) 161, 477–8 (1948).

[247] Lal, L., New bands in the second negative or ultraviolet band system of O_2^+ molecule $(^2\Pi_u \to {}^2\Pi_g)$, Phys. Rev. 73, 255 1948).

[248] Lal, L., Prediction of a new electronic level of the O_2^+ molecule, Sci. Culture (Calcutta) 13, 343–4 (1948).

[249] Landau, A., Allin, E. J., and Welsh, H. L., The absorption spectrum of solid oxygen in the wavelength region from 12,000 Å to 3,300 Å, Spectrochim. Acta 18, 1–19 (1962).

[250] (a) LeBlanc, F. J., A rotational analysis of the Hopfield oxygen bands, M. S. Thesis, Dept. of Physics, Boston College. 1959.

(b) LeBlanc, F. J., Electronic states of Hopfield's oxygen emission bands, J. Chem. Phys. 38, 487–8 (1963).

[251] Leclercq, J., Theoretical calculation of Rydberg levels of molecular oxygen, Ann. Astrophys. (Paris) 30(1), 93–9 (1967).

[252] Lichten, W., Some new metastable states of molecules, J. Chem. Phys. 37, 2152–4 (1962).

[253] Lindholm, E., Rydberg series in small molecules IV. Rydberg series in O_2, Ark. Fysik (Stockholm) 40, 117–24 (1969).

[254] Linnett, J. W., Binding in some diatomic molecules, J. Chem. Soc. (London), 275–87 (1956).

[255] (a) Linton, C., New identifications in the oxygen second negative system, Nature (London) 212, 1358 (1966).

(b) Linton, C., Ph. D. Thesis, Spectroscopy Dept., Imperial College, London, England, 1966.

[256] Lochte-Holtgreven, W., and Dieke, G. H., On the ultraviolet bands of the neutral oxygen molecule, Ann. Physik. (Leipzig) 3, 937 77 (1929).

[257] MacQueen, R. M., Eddy, J. A., and Léna, P. J., New far infrared observations of atmospheric molecular lines, Nature (London) 220, 1112–13 (1968).

[258] Marr, G. V., The electronic transition moment for the Schumann-Runge band system of O_2, Can. J. Phys. 42, 382–6 (1964).

[259] (a) Matsunaga, F. M., and Watanabe, K., Absorption coefficients of O_2 in the vacuum ultraviolet, 20 p. (Hawaii Inst. of Geophysics, Honolulu, Dec. 1961). Contribution No. 33, Sci. Report No. 5, Contract No. AF19(604)–4576. AD 272,606.

(b) Watanabe, K., private communication.

[260] Matsunaga, F. M., and Watanabe, K., Total and photoionization coefficients and dissociation continua of O_2 in the 580–1070 Å region, Sci. of Light (Tokyo) 16, 31–42 (1967).

[261] McCormac, B. M., and Omholt, A., (eds.), Atmospheric Emissions, Proc. of the NATO Advanced Study Institute held at the Agricultural College of Norway, Ås, Norway, July 29–Aug. 9, 1968 (Van Nostrand Reinhold Co., New York, 1969).

[262] McGowan, W., and Kerwin, L., Collisions of long-lived excited ions of oxygen and nitrogen, Can. J. Phys. 42, 2086–101 (1964).

[263] McGrath, W. D., and Norrish, R. G. W., Production of vibrationally excited oxygen molecules in the flash photolysis of ozone, Nature (London) 180, 1272–3 (1957).

[264] McGrath, W. D., and Norrish, R. G. W., Studies of the reactions of excited oxygen atoms and molecules produced in

the flash photolysis of ozone, Proc. Roy. Soc. (London) A254, 317–26 (1960).

[265] McKnight, J. S., and Gordy, W., Measurement of the submillimeter-wave rotational transition of oxygen at 424 kMc/sec, Phys. Rev. Lett. 21, 1787–9 (1968).

[266] (a) McLennan, J. C., and McLeod, J. H., On the Raman effect with liquid oxygen and with liquid nitrogen, Trans. Roy. Soc. Can., Third Ser: 22, (Sect. 3) 413–16 (1928).

(b) McLennan, J. C., and McLeod, J. H., The Raman effect with liquid oxygen, nitrogen, and hydrogen. Nature (London) 123, 160 (1929).

[267] Mecke, R., and Baumann, W., On a new atmospheric oxyge band at λ7710, Z. Physik 73, 139–46 (1931).

[268] Meckler, A., Electronic energy levels of molecular oxygen, . Chem. Phys. 21, 1750–62 (1953).

[269] Meeks, M. L., and Lilley, A. E., The microwave spectrum (oxygen in the earth's atmosphere, J. Geophys. Res. 68 1683–1703 (1963).

[270] Meinel, A. B., O_2 emission bands in the infrared spectrum o the night sky, Astrophys. J. 112, 464–8 (1950).

[271] Metzger, P. H., and Cook, G. R., A reinvestigation of the ab sorption cross-sections of molecular oxygen in the 1050–1800 Å region, J. Quant. Spectrosc. Radiat. Transfer 4, 107–16 (1964).

[271a] Michels, H. H., and Harris, F. E., Adiabatic potential curves for the system O + O−, p. 1170–1 in Branscomb, L. M. et al. (eds.), Electronic and Atomic Collisions, Abstracts of papers of the 7th International Conference on the Physics of Electronic and Atomic Collisions, held at Amsterdam, The Netherlands, 26–30 July 1971 (North-Holland, Amsterdam, 1971).

[272] Miller, J. H., Boese. R. W., and Giver, L. P., Intensity measurements and rotational intensity distribution for the oxygen A-band, J. Quant. Spectrosc. Radiat. Transfer, 9, 1507–17 (1969).

[273] Miller, S. L., The microwave absorption spectrum of oxygen, Ph. D. Thesis, Dept. of Physics, Columbia Univ. (New York), 1952.

[274] Miller, S. L., Javan, A., and Townes, C. H., The spin of O^{18} Phys. Rev. 82, 454–5 (1951).

[275] Miller, S. L., and Townes, C. H., The microwave absorption spectrum of $(O^{16})_2$ and $O^{16}O^{17}$, Phys. Rev. 90, 537– (1953).

[276] Miller, S. L., Townes, C. H., and Kotani, M., The electro structure of O_2, Phys. Rev. 90, 542–3 (1953).

[277] Miller, T. A., Rotational moment, rotational g factor, electror orbital g factor, and anisotropy of the magnetic susceptibili of $^1\Delta$ O_2, J. Chem. Phys. 54, 330–7 (1971).

[278] Millon, J., and Herman, L., The emission spectrum of pur oxygen, Compt. Rend. Acad. Sci. (Paris), 218, 152–3 (194

[279] Mizushima, M., and Hill, R. M., Microwave spectrum of O_2 Phys. Rev. 93, 745–8 (1954).

[280] Moffitt, W., The electronic structure of the oxygen molecule, Proc. Roy. Soc. (London) A210, 224–45 (1951).

[281] Moore, C. E., Atomic Energy Levels, Natl. Bur. Stand. (U.S.) Circ. 467, Vol. 1 (1949).

[282] Mulay, L. N., and Keys, L. K., Evidence for O_4. Magnetic studies on adsorption of oxygen, J. Amer. Chem. Soc. 86, 4489–91 (1964).

[283] Mulliken, R. S., Interpretation of the atmospheric bands of oxygen, Phys. Rev. 32, 880–7 (1928).

[284] Mulliken, R. S., The interpretation of band spectra: Part III. Electron quantum numbers and states of molecules and their atoms, Rev. Mod. Phys. 4, 1–86 (1932).

[285] Mulliken, R. S., Intensities of electronic transitions in molecular spectra. II., charge transfer spectra, J. Chem. Phys. 7, 20–34 (1939).

[286] Mulliken, R. S., Electron affinity of O_2, Phys. Rev. 115, 1225–6 (1959).

[287] Mulliken, R. S., and Stevens, D. S., New O_2^+ bands. Dissociation energy of O_2^+ and ionization potential of O_2, Phys. Rev. **44**, 720–3 (1933).

[288] Murrell. J. N., and Taylor, J. M., Predissociation in diatomic spectra with special reference to the Schumann-Runge bands of O_2, Mol. Phys. **16**, 609–21 (1969).

[289] Myers, B. F., and Bartle, E. R., Shock-tube study of the radiative combination of oxygen atoms by inverse predissociation, J. Chem. Phys. **48**, 3935–44 (1968).

[290] Namioka, T., Ogawa, M., and Tanaka, Y., The b $^4\Sigma_g^- \leftarrow X$ $^3\Sigma_g^-$ Rydberg series of the oxygen molecule, Paper B–20 (Science Council of Japan, Tokyo, Dec. 1962), Proc. Intern. Symp. on Molecular Structure and Spectroscopy, 1st, Tokyo (1962).

[291] (a) Nevin, T. E., Rotational analysis of the first negative band spectrum of oxygen, Phil. Trans. Roy. Soc. (London) **A237**, 471–507 (1938).
   (b) Nevin, T. E., Rotational analysis of the first negative band spectrum of oxygen. II., Proc. Roy. Soc. (London) **A174**, 371–8 (1940).
   (c) Nevin, T. E., and Murphy, T., Analysis of the (0, 3) band of the first negative system of the O_2^+ molecule, Proc. Roy. Irish Acad. **A46**, 169–81 (1941).

[292] Nicholls, R. W. The Franck-Condon factor ($q_{v'v''}$) array to high vibrational quantum numbers for the O_2 (B $^3\Sigma_u^- - X$ $^3\Sigma_g^+$ [i.e. $^3\Sigma_g^-$]) Schumann-Runge band system, Can. J. Phys. **38**, 1705–11 (1960).

[293] Nicholls, R. W., Laboratory astrophysics, J. Quant. Spectrosc. Radiat. Transfer **2**, 433–49 (1962).

[294] Nicholls, R. W., Transition probabilities of aeronomically important spectra, Ann. Geophys. (Paris) **20**, 144–81 (1964).

[295] Nicholls, R. W., Franck-Condon factors for the O_2^+ first and second negative band systems, Can. J. Phys. **43**, 1390–4 (1965).

[296] Nicholls, R. W., Franck-Condon factors to high vibrational quantum numbers V. O_2 band systems, J. Res. Natl. Bur. Stand. (U.S.) **69A** (Phys. and Chem.), 369–73 (1965).

[297] Nicholls, R. W., Franck-Condon factors for ionization transitions of O_2, CO, NO and H_2 and for the NO$^+$ ($A^1 - \Sigma X^1\Sigma$ [i.e. A $^1\Sigma - X$ $^1\Sigma$]) band system, J. Phys. B (At. Mol. Phys.) **1**, 1192–1211 (1968) [Proc. Phys. Soc. (London)].

[298] Nicholls, R. W., Aeronomically important transition probability data, Can. J. Chem. **47**, 1847–56 (1969).

[299] Nicholson, A. J. C., Photo-ionization efficiency curves. Measurement of ionization potentials and interpretation of fine structure, J. Chem. Phys. **39**, 954–61 (1963).

[300] Nordheim-Pöschl, G., Orbital valence and direction properties in the theory of chemical binding. I., Ann. Phys. (Leipzig) **26**, 258–80 (1936).

[301] Noxon, J. F., Observation of the (b $^1\Sigma_g^+ - a$ $^1\Delta_g$) transition in O_2, Can. J. Phys. **39**, 1110–19 (1961).

[302] Ogawa, M., Absorption spectrum of electrically excited oxygen molecules in the ultraviolet region, Sci. of Light (Tokyo) **15**, 97–114 (1966).

[303] Ogawa, M., Tanaka-Takamine Rydberg series of O_2, Can. J. Phys. **46**, 312–13 (1968).

[304] Ogawa, M., Absorption coefficients of O_2 at the Lyman-alpha line and its vicinity, J. Geophys. Res. Space Phys. **73**, 6759–63 (1968); errata ibid **74**, 1320 (1969).

[305] Ogawa, M., Absorption coefficients of oxygen in the metastable state, a $^1\Delta_g$, J. Chem. Phys. **53**, 3754–5 (1970).

[306] Ogawa, M., and Chang, H., Absorption spectrum of electrically excited oxygen molecules. Part II., Sci. of Light (Tokyo) **17**, 45–56 (1968).

[307] Ogawa, M., and Yamawaki, K. R., Absorption coefficients of O_2 at the Lyman-α line and of other O_2 transmission windows, Appl. Opt. **9**, 1709–11 (1970).

[308] Ogawa, M., and Yamawaki, K. R., Forbidden absorption bands of O_2 in the argon continuum region, Can. J. Phys. **47**, 1805–11 (1969).

[309] Orville-Thomas, W. J., A bond-order/bond-length relation f oxygen-oxygen bonds, J. Mol. Spectrosc. **3**, 588–91 (1959).

[310] Ory, H. A., and Gittleman, A. P., Unusual variation of Franck Condon factors for the O_2 Schumann-Runge band system Astrophys. J. **139**, 357–64 (1964).

[311] Ossenbrüggen, W., Term representation of the band spectra of the neutral oxygen molecule, Z. Physik **49**, 167–216 (1928).

[312] Pack, J. L., and Phelps, A. V., Electron attachment and detachment. I. Pure O_2 at low energy, J. Chem. Phys. **44**, 1870–83 (1966).

[313] Panofsky, H. A., Profiles in the alpha band of atmospheric oxygen, Astrophys. J. **97**, 180–5 (1943).

[314] (a) Parthasarathy, S., Light-scattering in relation to molecular structure: new data for depolarization in 39 gases, Indian J. Phys **7**, 139–57 (1932).
   (b) Parthasarathy, S., Light scattering in gases, Indian J. Phys. **25**, 21–4 (1951).

[315] Pattabhiramayya, P., The dispersion and optical anisotropy of molecular oxygen in relation to its absorption spectrum, Proc. Indian Acad. Sci. **A7**, 235–44 (1938).

[316] Pearse, R. W. B., and Gaydon, A. G., The Identification of Molecular Spectra, 3rd. ed. (J. Wiley and Sons, New York, 1963).

[317] Prasad, A. N., and Craggs, J. D., Electron detachment in oxygen, Electronic Lett. **1**, 118–19 (1965).

[318] Present, R. D., The theory of $^3\Sigma^+ - ^3\Sigma^-$ transitions in band spectra, Phys. Rev. **48**, 140–8 (1935).

[319] Price, W. C., Developments in photo-electron spectroscopy, p. 221–36 in Hepple, P. W., (ed.), Molecular Spectroscopy, (Institute of Petroleum and Elsevier, Inc., London, 1968).

[320] Price, W. C., and Collins, G., The far ultraviolet absorption spectrum of oxygen, Phys. Rev. **48**, 714–9 (1935).

[321] Prikhotko, A., Kuhemann, M., and Federitenko, A., The absorption spectrum of solid oxygen. I., Phys. Z. Sowjet. **7**, 410–31 (1935).

[322] Pritchard, R. H., Bender, C. F., and Kern, C. W., Fine structure interactions in the ground state of O_2, Chem. Phys. Lett. **5**, 529–32 (1970).

[323] Pulskamp, C. A., Oxygen absorption bands, Ph. D. thesis, Dept. of Physics, U. of Calif., 1929.

[324] Rakotoarijimy, D., Weniger, S., and Grenat, H., Extension of the Schumann-Runge band system of molecular oxygen in the near ultraviolet in absorption and emission, Compt. Rend. Acad. Sci. (Paris) **246**, 2883–6 (1958).

[325] Rao, P. S. R., Vibrational intensities of the O_2^+ (first negative) bands, Proc. Phys. Soc. (London) **A81**, 240–3 (1963).

[326] (a) Rasetti, F., On the Raman effect in diatomic gases. II., Proc. Natl. Acad. Sci. (U.S.) **15**, 515–19 (1929).
   (b) Rasetti, F., Incoherent scattered radiation in diatomic molecules, Phys. Rev. **34**, 367–71 (1929).
   (c) Rasetti, F., On the rotational Raman spectrum of nitrogen and oxygen, Z. Physik. **61**, 598–601 (1930).

[327] Rasetti, F., On a fluorescence spectrum of oxygen, Proc. Natl. Acad. Sci. (U.S.) **15**, 411–14 (1929).

[328] Renschler, D. L., Hunt, J. L., McCubbin, T. K., Jr., and Polo, S. R., Triplet structure of the rotational Raman spectrum of oxygen, J. Mol. Spectrosc. **31**, 173–6 (1969).

[329] Rettschnick, R. P. H., and Hoytink, G. J., Collision induced electronic transitions of oxygen, Chem. Phys. Lett. **1**, 145–8 (1967).

[330] Richards, W. G., and Barrow, R. F., The calculation of potential curves for diatomic molecules from experimental data, Proc. Phys. Soc. (London) **83**, 1045–9 (1964).

[331] Riess, I. and Ben-Aryeh, Y., Application of the quantum Franck-Condon principle to predissociation in oxygen, J. Quant. Spectrosc. Radiat. Transfer **9**, 1463–8 (1969).

[332] Roach, F. E., Forbidden transitions in the upper atmosphere, Mem. Soc. Roy. Sci. Liege, Collect in 8°, Ser. 5 **17**, 175–85 (1969).

[333] Robin, J., Experimental study of the perturbation of visible and ultraviolet absorption spectra of oxygen, nitric oxide, and the resonance lines of certain metals at high pressures, J. Recherches centre natl. recherche sci., Labs. Bellevue (Paris) 10, No. 47, 89–140 (1959).

[334] Robinson, D., and Nicholls, R. W., Intensity measurements on on the O_2^+ second negative, CO Ångstrom and third positive, and NO α and β molecular band systems, Proc. Phys. Soc. (London) A71, 957–64 (1958).

[335] Robinson, G. W., Intensity enhancement of forbidden electronic transitions by weak intermolecular interactions J. Chem. Phys. 46, 572–85 (1967).

[336] (a) Rolfe, J., Low-temperature emission spectrum of O_2^- in alkali halides, J. Chem. Phys. 40, 1664–70 (1964).
(b) Rolfe, J., private communication.
(c) Rolfe, J., Holzer, W., Murphy, W. F., and Bernstein, H. J., Some spectroscopic constants for O_2^- ions in alkali halide crystals, J. Chem. Phys. 49, 963 (1968).

[337] Rosen, B. (ed.), Constantes selectionees; donnees spectroscopiques concernant les molecules diatomiques, etabli par R. F. Barrow et al. (Tables de constantes et donnees numeriques, 4) (Hermann, Paris, 1951).

[338] Runge, C., On a new band spectrum of oxygen, Physica 1, 254–61 (1921).

[339] Saha, B., Rotational Raman scattering in liquid oxygen, Indian J. Phys. 14, 123–8 (1940).

[340] Samson, J. A. R., Angular distributions of photoelectrons and partial photoionization cross sections, Phil. Trans. Roy. Soc. London A268, 141–6 (1970).

[341] (a) Samson, J. A. R., and Cairns, R. B., Absorption and photoionization cross sections of O_2 and N_2 at intense solar emission lines, J. Geophys. Res. 69, 4583–90 (1964).
(b) Samson, J. A. R., and Cairns, R. B., Total absorption cross sections of H_2, N_2, and O_2 in the region 550–200 Å, J. Opt. Soc. Amer. 55, 1035 (1965).

[342] Samson, J. A. R., and Cairns, R. B., Ionization potential of O_2, J. Opt. Soc. Amer. 56, 769–75 (1966).

[343] Schadee, A., The relation between the electronic oscillator strength and the wavelength for diatomic molecules, J. Quant. Spectrosc. Radiat. Transfer 7, 169–83 (1967).

[344] Schaefer, H. F., III, and Harris, F. E., Ab initio calculations on 62 low-lying states of the O_2 molecule, J. Chem. Phys. 48, 4946–55 (1968).

[344a] Schaefer, H. F., III, and Miller, W. H., Curve crossing of the $B\ ^3\Sigma_u^-$ and $^3\Pi_u$ states of O_2 and its relation to predissociation in the Schumann-Runge bands, J. Chem. Phys. 55, 4107–15 (1971).

[345] Schlapp, R., Intensities in singlet-triplet bands of diatomic molecules, Phys. Rev. 39, 806–15 (1932).

[346] Schlapp, R., Fine structure in the $^3\Sigma$ ground state of the oxygen molecule, and the rotational intensity distribution in the atmospheric oxygen bands, Phys. Rev. 51, 342–5 (1937).

[347] (a) Schmid, R., Zeeman effect in the atmospheric oxygen bands; production of a strong magnetic field over a length of 80 cm, Phys. Rev. 49, 271 (1936).
(b) Schmid, R., Budó, A., and Zemplen, J., On the Zeeman effect of the atmospheric oxygen band lines, Z. Physik 103, 250–62 (1936).
(c) Zemplen, J. M., The Zeeman effect of atmospheric oxygen bands, Magyar Tudomanyos Akademia, Matematikai es Termesyettudomanyi Ertesito (Budapest) [Math. naturw. Anz. ungar. Akad. Wiss.] 55, 373–99 (1937).

[348] Schnepp, O., and Dressler, K., Schumann-Runge bands of O_2 in solid phases: spectroscopic measurements of intermolecular potentials, J. Chem. Phys. 42, 2482–9 (1965).

[349] Schoen, R. I., Retarding potential measurements of electrons photoemitted by N_2, CO, and O_2, J. Chem. Phys. 40, 1830–6 (1964).

[350] Schoen, R. I., Laboratory measurements of photoionization, photoexcitation, and photodetachment, Can. J. Chem. 47, 1879–99 (1969).

[351] Schulz, G. J., and Dowell, J. T., Excitation of vibrational and electronic levels in O_2 by electron impact, Phys. Rev. 128, 174–7 (1962).

[352] Shapiro, M. M., and Gush, H. P., The collision-induced fundamental and first overtone bands of oxygen and nitrogen, Can. J. Phys. 44, 949–63 (1966).

[353] Shemansky, D. E., and Vallance Jones, A., Type-B red aurora; the O_2^+ first negative system and the N_2 first positive system, Planet. Space Sci. 16, 115–30 (1968).

[354] Singh, N. L., and Lal, L., New bands in the first negative (or visible) O_2^+ band-system, Sci. Culture (Calcutta) 9, 89 (1943).

[355] Singh, R. B., and Rai, D. K., Potential energy curves for O_2^+, N_2^+, and CO^+, J. Mol. Spectrosc. 19, 424–34 (1966).

[356] Sitnik, G. F., and Khlystov, A. I., Determination of the electronic transition probability of the red "atmospheric" system of the O_2 molecule bands, Akad. Nauk (USSR), Izv. Atmospheric and Oceanic Phys. 4, (10), 1120–2 (1968).

[357] Sjogren, H., and Lindholm, E., Ionization and dissociative ionization of O_2 after electron and ion impact, Ark. Fysik (Stockholm) 32, 275–84 (1966).

[358] Smith, A. L., The role of autoionization in molecular photoelectron spectra, Phil. Trans. Roy. Soc. London A268, 77–85 (1970).

[359] Smith, A. L., and Johnston, H. L., The molecular spectra of condensed oxygen and the O_4 molecule, J. Chem. Phys. 20, 1972–3 (1952).

[360] Sobolev, N. N., The experimental determination of electron-transition strengths in diatomic molecules, p. 9–25 in (Proceedings) XII International Conference on Spectroscopy (XII Colloquium Spectroscopicum Internationale), Exeter, 11–17 July 1965, (Hilger and Watts Ltd, London, 1965).

[361] Spence, D., and Schulz, G. J., Vibrational excitation by electron impact in O_2, Phys. Rev. A 2, 1802–11 (1970).

[362] Spohr, R., and von Puttkamer, E., Photoelectron energy measurement and Franck-Condon factors for vibrational transitions of several molecular ions, Z. Naturforsch. 22a, 705–10 (1967).

[363] Stafford, L. F., and Tolbert, C. W., Shapes of oxygen absorption lines in the microwave frequency region, J. Geophys. Res. 68, 3431–5 (1963).

[364] Stansbury, E. J., Crawford, M. F., and Welsh, H. L., Determination of rates of change of polarizability from Raman and Rayleigh intensities, Can. J. Phys. 31, 954–61 (1953).

[365] Stevens, D. S., The rotational analysis of the first negative group of oxygen (O_2^+) bands, Phys. Rev. 38, 1292–1311 (1931).

[366] Stoicheff, B. P., High resolution Raman spectroscopy, p. 91–174 in Thompson, H. W. (ed.), Advances in Spectroscopy, vol. 1 (Interscience Publ., Inc., New York, 1959).

[367] Sullivan, J. O., and Holland, A. C., A congeries of absorption cross sections for wavelengths less than 3000 Å, 170 p., U.S. Natl. Aeron. Space Admin. NASA–CR–371 (1966). (For sale by Clearinghouse for Federal Scientific and Technical Information. Springfield. Va. 22151.)

[368] Tabisz, G. C., Allin, E. J., and Welsh, H. L., Interpretation of the visible and near-infrared absorption spectra of compressed oxygen as collision-induced electronic transitions, Can. J. Phys. 47, 2859–71 (1969).

[369] Tanaka, Y., On the new absorption bands of the oxygen molecule in the far ultraviolet region, J. Chem. Phys. 20, 1728–33 (1952).

[370] Tanaka, Y., Jursa, A. S., and LeBlanc, F. J., Hopfield's emission bands of O_2 in the region 1900–2350 Å, J. Chem. Phys. 24, 915–6 (1956).

[371] Tanaka, Y., and Takamine, T., Vibrational structure of the $^4\Sigma_g^-$ (O_2^+) $\leftarrow$ $^3\Sigma_g^-$ Rydberg series of O_2, Sci. Pap. Inst. Phys.-Chem. Res. (Tokyo) 39, 437–46 (1942).

[372] Tatum, J. B., The Interpretation of intensities in diatomic molecular spectra, Astrophys. J. Suppl. No. 124, vol. 16. 21–56 (1967).

[373] Thompson, B. A., Harteck, P., and Reeves, R. R. Jr., Ultra-violet absorption coefficients of CO_2, CO, O_2, H_2O, N_2O, NH_3, NO, SO_2, and CH_4 between 1850 and 4000 Å, J. Geophys. Res. **68**, 6431–6 (1963).

[374] Tinkham, M., Theory of the fine structure of the molecular oxygen ground state with an experimental study of its micro-wave paramagnetic spectrum, Ph. D. thesis, Dept. of Physics, Massachusetts Inst. of Technology, 1954.

[375] Tinkham, M., and Strandberg, M. W. P., Theory of the fine structure of the molecular oxygen ground state, Phys. Rev. **97**, 937–51 (1955).

[376] Tinkham, M., and Strandberg, M. W. P., Interaction of molec-ular oxygen with a magnetic field, Phys. Rev. **97**, 951–66 (1955).

[377] Tinkham, M., and Strandberg, M. W. P., Line breadths in the microwave magnetic resonance spectrum of oxygen, Phys. Rev. **99**, 537–9 (1955).

[378] Tischer, R., On the *EPR* spectrum of molecular oxygen, Z. Naturforsch. **22a**, 1711–24 (1967).

[379] Townes, C. H., Holden, A. N., and Merrit, F. R., Microwave spectra of some linear *XYZ* molecules, Phys. Rev. **74**, 1113–33 (1948).

[380] Treanor, C. E., and Wurster, W. H., Measured transition probabilities for the Schumann-Runge system of oxygen, J. Chem. Phys. **32**, 758–66 (1960).

[381] Trumpy, B., Rotational Raman spectrum of O_2 at high pressure, Z. Physik **84**, 282–8 (1933).

[382] Tsai, S. C., and Robinson, G. W., Why is condensed oxygen blue?, J. Chem. Phys. **51**, 3559–68 (1969).

[383] Turner, D. W., High resolution molecular photoelectron spec-troscopy. I. Fine structure in the spectra of hydrogen and oxygen, Proc. Roy. Soc. (London) **A307**, 15–26 [1968].

[384] Turner, D. W., and May, D. P., Franck-Condon factors in ionization: Experimental measurements using molecular photoelectron spectroscopy, J. Chem. Phys. **45**, 471–6 (1966).

[385] Vallance Jones, A., and Harrison, A. W., $^1\Delta_g - ^3\Sigma_g^-$ O_2 infrared emission band in the twilight airglow spectrum, J. Atmos. Terr. Phys. **13**, 45–60 (1958).

[386] Vance, D. W., Auger electron emission from clean Mo bom-barded by positive ions. III. Effect of electronically excited ions, Phys. Rev. **169**, 263–72 (1968).

[387] (a) Vanderslice, J. T., Mason, E. A., and Maisch, W. G., Inter-actions between ground state oxygen atoms and molecules: O–O and O_2–O_2, J. Chem. Phys. **32**, 515–24 (1960).

    (b) Vanderslice, J. T., Mason, E. A., Maisch, W. G., and Lip-pincott, E. R., Potential curves for N_2, NO, and O_2, J. Chem. Phys. **33**, 614–15 (1960).

[388] van Vleck, J. H., Magnetic dipole radiation and the atmospheric absorption bands of oxygen, Astrophys. J. **80**, 161–70 (1934).

[389] Vassy, A., and Vassy, M. E., Research on atmospheric absorp-tion. II., J. Phys. Radium **10**, 403–12 (1939).

[390] (a) Vegard, L., and Kvifte, G., An auroral spectrogram and the results derived from it, Geofysiske publikasjoner, Norske. Videnskaps-Akad., Oslo **18**, No. 3, 1–23 (1951). [Chem. Abstr. 48:1142e (1954)].

    (b) Vegard, L., Composition, variations and excitation of the auroral luminescence spectra, Geofysiske publikasjoner, Norske. Videnskaps-Akad., Oslo **19**, No. 9, 1–59 (1956).

[391] (a) Volman, D. H., Photochemical evidence relative to the ex-cited states of oxygen, J. Chem. Phys. **24**, 122–4 (1956).

    (b) Volman, D. H., Photochemical oxygen-hydrogen reaction at 1849 Å, J. Chem. Phys. **25**, 288–92 (1956).

[392] Wacker, P., Mizushima, M., Peterson, J. D., and Ballard, J. R., Microwave spectral tables: Diatomic molecules, Natl. Bur. Stand. (U.S.) Monogr. 70, vol. 1 (1964).

[393] Wacks, M. E., Franck-Condon factors for the ionization of CO, NO and O_2, J. Chem. Phys. **41**, 930–6 (1964).

[394] Wacks, M. E., and Krauss, M., Franck-Condon factors and the shape of ionization efficiency curves, J. Chem. Phys. **35**, 1902–3 (1961).

[395] Waelbroeck, F., and Bauer, S. H., Intense Schumann-Runge source, J. Opt. Soc. Amer. **49**, 102–3 (1959).

[396] Wallace, L., Band-head wavelengths of C_2, CH, CN, CO, NH NO, O_2, OH, and their ions, Astrophys. J. Suppl. No. 68, vol. 7, 165–290 (1962).

[397] Wallace, L., and Hunten, D. M., The dayglow of the oxygen A band, J. Geophys. Res. **73**, 4813–34 (1968).

[398] (a) Wark, D. Q., and Mercer, D. M., Absorption in the atmosphere by the oxygen "A" band, Appl. Opt. **4**, 839–45 (1965).

    (b) Wark, D. Q., and Mercer, D. M., errata, ibid, **5**, 1469 (1966).

    (c) Wark, D. Q., and Mercer, D. M., Lines of 0–0 band for three isotopes (unpublished). See footnote of [398(a)], p. 840.

[399] Watanabe, K., Ultraviolet absorption processes in the upper atmosphere, Adv. in Geophys. **5**, 153–221 (1958).

[400] Watanabe, K., Inn, E. C. Y., and Zelikoff, M., Absorption co-efficients of oxygen in the vacuum ultraviolet, J. Chem. Phys. **21**, 1026–30 (1953).

[401] Watanabe, K., and Marmo, F. F., Photoionization and total ab-sorption cross section of gases. II. O_2 and N_2 in the region 850–1500 Å, J. Chem. Phys. **25**, 965–71 (1956).

[402] Watari, W., Electronic states of F_2 and O_2 molecules, Progr. Theor. Phys. (Kyoto) **8**, 524–30 (1952).

[403] Watson, J. K. G., Rotational line intensities in $^3\Sigma - ^1\Sigma$ electronic transitions, Can. J. Phys. **46**, 1637–43 (1968).

[404] Wayne, R. P., Singlet molecular oxygen, Advances in Photo-chemistry **7**, 311–71 (1969). (Eds.) Pitts, J. N. Jr., Hamond, G. N., and Noyes, W. A., Jr. (Interscience Publishers, New York, 1969).

[405] Weber, A., and McGinnis, E. A., The Raman spectrum of gaseous oxygen, J. Mol. Spectrosc. **4**, 195–200 (1960).

[406] Weber, A., Porto, S. P. S., Cheesman, L. E., and Barrett, J. J., High-resolution Raman spectroscopy of gases with *cw*-laser excitation, J. Opt. Soc. Amer. **57**, 19–28 (1967).

[407] Weissler, G. L., and Lee, P., Absorption coefficients of oxygen in the vacuum ultraviolet, J. Opt. Soc. Amer. **42**, 200–3 (1952).

[408] Weniger, S., Spectrum of the ionized oxygen molecule in the near infrared, J. Phys. Radium **23**, 225–37 (1962).

[409] Wentink, T., Jr., Isaacson, L., and Spindler, R. J., Research on the opacity of low temperature air: oscillator strengths and transition moments of band systems of N_2, O_2, and NO, 164 p., (Air Force Weapons Laboratory, Research and Technology Div., Kirtland Air Force Base, New Mexico, 1965). Report No. AFWL–TR–65139, Contract AF29(601)–6438.

[410] Wentink, T., Jr., Marram, E. P., Isaacson, L., and Spindler, R. J., Ablative Material Spectroscopy, vol. I, Experimental Determi-nation, of Molecular Oscillator Strengths, 138 p. (Air Force Weapons Lab., Research and Technology Div., Kirtland Air Force Base, New Mexico, 1967). Tech. Rept. No. AFWL–TR–67–30, vol. I, Contract No. AF29(601)–7117.

[411] West, B. G., and Mizushima, M., Absorption spectrum of the oxygen molecule in the 55–65 Gc region, Phys. Rev. **143**, 31–2 (1966).

[412] Whitlow, S. H., and Findlay, F. D., Single and double electronic transitions in molecular oxygen, Can. J. Chem. **45**, 2087–91 (1967).

[413] Wilheit, T. T., Jr., and Barrett, A. H., Microwave spectrum of molecular oxygen, Phys. Rev. **A1**, 213–15 (1970).

[414] Wilkinson, P. G., and Mulliken, R. S., Dissociation processes in oxygen above 1750 Å, Astrophys. J. **125**, 594–600 (1957).

[415] Wulf, O. R., A progression relation in the molecular spectrum of oxygen occurring in the liquid and in the gas at high pres-sure, Proc. Natl. Acad. Sci. (U.S.) **14**, 609–13 (1928).

[416] Wurster, W. H., and Treanor, C. E., Transition probabilities for O_2 radiation in the near ultraviolet, 24 p. (Cornell Aeronautical Laboratory, Inc., Buffalo, N.Y., 1958. — Available from U.S. Clearinghouse for Federal Scientific and Technical Informa-tion). Report No. QM–1209–A–1, PB Rept. 140, 457, AD–162 145.

[417] Yoshino, K., and Tanaka, Y., Rydberg absorption series and ionization energies of the oxygen molecule. I., J. Chem. Phys. 48, 4859–67 (1968).

[418] Yoshino, T., and Bernstein, H. J., Intensity in the Raman effect VI. The photoelectrically recorded Raman spectra of some gases, J. Mol. Spectrosc. 2, 213–20 (1958).

[419] Young, R. A., and Black, G., Excited-state formation and destruction in mixtures of atomic oxygen and nitrogen, J. Chem. Phys. 44, 3741–51 (1966).

[420] Young, R. A., and Sharpless, R. L., Chemiluminescent reactions involving atomic oxygen and nitrogen, J. Chem. Phys. 39, 1071–102 (1963).

[421] Zare, R. N., Rotational line strengths: the O_2^+ b $^4\Sigma_g^-$ $-$ a $^4\Pi_u$ band system, in (Rao, K. N., and Mathews, C. W., eds.) Molecular Spectroscopy: Modern Research (Academic Press, N.Y., planned for publication in 1972).

[422] Zimmerer, R. W., and Mizushima, M., Precise measurement of the microwave absorption frequencies of the oxygen molecule and the velocity of light, Phys. Rev. 121, 152–5 (1961).

Appendix A. Notation and Terminology

The spectroscopic notation used in this report is that adopted in Herzberg's book [186] as modified by recommendations of the Triple Commission on Spectroscopy [J. Opt. Soc. Amer. 43, 425–30 (1953); 52, 476–7 (1962); 53, 883–5 (1963)]. A number of specific conventions used are itemized below.

(1) Wavenumber in cm^{-1} is denoted by σ; ν is reserved for frequency in Hz.

(2) N is total angular momentum of electrons and nuclei exclusive of spin (case b, b', d), formerly denoted by K.

(3) Rotational angular momentum of the nuclei, formerly denoted N, is now denoted by R.

(4) Dissociation energy is written as D^0 or D^e; rotational constants (for the zero level or equilibrium value, respectively) are denoted as usual by D_0 and D_e.

(5) A transition is always represented with a dash, as $^2\Pi - {}^2\Sigma$ transition. The upper state is always written first. $\leftarrow$ means absorption; $\rightarrow$ means emission, for an electronic, vibration-rotation, or rotational (here, microwave) transition. In reporting the magnetic dipole rotation spectrum of O_2, whether in the microwave or far IR region, authors have not used a consistent notation. The notation assumed here is that used for electronic transitions.

(6) A perturbation by one state of another is indicated as e.g., ($^1\Delta^1\Pi$) perturbation, following an early notation of Kovács. (Conventions used in some early papers include $^1\Delta \times {}^1\Pi$ or $^1\Delta$, $^1\Pi$.)

(7) A progression of bands is indicated as follows:
   (a) $v'' = 0$ progression
   (b) $(v' - 0)$ progression

(8) Reciprocal dispersion is given in Å/mm. However, following the colloquial use of many spectroscopists this quantity is referred to as dispersion.

(9) In the tables, wavelengths above 2000 Å are air wavelengths unless otherwise specified; below 2000 Å vacuum wavelengths are listed.

(10) The known band degradation is indicated by R (red-degraded) or V (violet-degraded) in the headings of section 3 as well as in tables 1 and 3 to 30.

(11) Rotational constants in tables 36 to 52 are given in units of cm^{-1}.

(12) Zero-point energy is abbreviated by ZPE.

(13) First negative system (or group) is abbreviated as (1–), etc. An alternate abbreviation used in the literature is 1NG, etc.

The following items apply to table 1:

(1) Vibrational constants and term values T are assumed to be derived from data on band origins. (Herzberg [186] denotes these by the letter Z.) In conformity with Herzberg, H denotes constants derived from head measurements.

(2) $[r_e]$ means r_0; $[B_e]$ means B_0; $[\omega_e]$ means $\Delta G(\tfrac{1}{2})$, as in Herzberg's book.

(3) ( ) means uncertain.

(4) T_0 is the mean height (in case of multiplets) above X, $v = 0$, $J = 0$.

(5) States which are predissociated have Pr written in the column for dissociation products.

(6) All numerical data are in units of cm^{-1} unless otherwise indicated.

(7) References cited include only those from which the numerical data have been extracted. Other pertinent references are cited in the appropriate sections of this report.

(8) The tabulated molecular constants are largely those from which the RKR potentials have been derived, and represent the best fit to the vibrational term values or rotational constants where these have been compiled from various sources.

(9) To avoid confusion of sign conventions several formulas are listed below:
   Vibrational terms:

$$G(v) = \omega_e(v + \tfrac{1}{2}) - \omega_e x_e(v + \tfrac{1}{2})^2$$
$$+ \omega_e y_e(v + \tfrac{1}{2})^3 + \omega_e z_e(v + \tfrac{1}{2})^4$$

i.e., a negative value of $\omega_e x_e$ from the table would mean a positive anharmonic term.
Rotational terms:

$$F_v(J) = B_v J(J + 1) - D_v J^2(J + 1)^2 + H_v J^3(J + 1)^3$$

where $(-D_v)$ is always < 0, and

$$B_v = B_e - \alpha_e(v + \tfrac{1}{2}) + \gamma_e(v + \tfrac{1}{2})^2 + \delta_e(v + \tfrac{1}{2})^3$$

$$D_v = D_e + \beta_e(v + \tfrac{1}{2})$$

$$H_v \sim H_e$$

The Dunham coefficients are given by

$$G(v) = \sum_{i=1} Y_{i0}(v+\tfrac{1}{2})^i$$

and

$$B_v = \sum_{i=0} Y_{i1}(v+\tfrac{1}{2})^i$$

The tabulated coefficients are really $Y_{10} \sim \omega_e$, $-Y_{20} \sim \omega_e x_e$, etc.

(10) Footnotes which give supplementary information pertaining to the individual electronic states are indicated at the end of table 1 and are identified by the electronic state. Table 1 has been left free of superscripts.

(11) The tabulated ZPE include the Dunham correction which adds an amount given by

$$Y_{00} - \frac{B_e}{4} + \frac{\alpha_e \omega_e}{12 B_e} + \frac{\alpha_e^2 \omega_e^2}{144 B_e^3} - \frac{\omega_e x_e}{4}$$

Appendix B. Physical Constants[1,2,3] and Conversion Factors

$$c = 2.9979250(10) \times 10^{10} \text{ cm-s}^{-1}$$
$$h = 6.626196(50) \times 10^{-27} \text{ erg-s}$$
$$N_0 = 6.022169(40) \times 10^{23} \text{ mole}^{-1}$$
$$1 \text{ eV} = 8065.465(27) \text{ cm}^{-1}$$
$$\mu_A(^{16}O_2) = 7.9974575 \text{ a.m.u.}$$
$$\mu_A(^{16}O_2^+) = 7.9973203 \text{ a.m.u.}$$
$$\mu = \mu_A/N_0 \text{ in g.}$$

Atomic masses·
$$^{16}O = 15.9949150 \text{ a.m.u.}$$
$$^{17}O = 16.999133 \text{ a.m.u.}$$
$$^{18}O = 17.9991600 \text{ a.m.u.}$$
$$k_e(^{16}O_2) = 47.1194 \times 10^{-2} \omega_e^2 \ (\omega_e \text{ in cm}^{-1}; k_e \text{ in dyne-cm}^{-1})$$

$$k_e(^{16}O_2^+) = 47.1186 \times 10^{-2} \omega_e^2$$

$$r_e(^{16}O_2) = 1.451868858 \sqrt{\frac{1}{B_e}} \ (B_e \text{ in cm}^{-1}; r_e \text{ in Å})$$

$$r_e(^{16}O_2^+) = 1.451881312 \sqrt{\frac{1}{B_e}}$$

The "Tabelle der Schwingungszahlen" of Kayser has been superseded by Natl. Bur. Stand. (U.S.) Monograph 3, "Table of Wavenumbers," by Coleman, Bozman, and Meggers (1960) which is based on the 1953 formula for dispersion in standard air of Edlen. For low resolution work the older tables are adequate.

¹ The molecular reduced masses are calculated from the data of Mattauch. Thiele, and Wapstra, 1964 Atomic Mass Table. Nuclear Physics 67, 1–31 (1965) which are based on the unified atomic mass scale with ¹²C = 12.

² The reduced mass $\mu_A(O_2^+)$ was calculated by assuming 5.48593 (10⁻⁴) a.m.u. for the mass of the electron and assuming that ionization removes an electron from one O atom (1 a.m.u. = 1/12 mass of ¹²C).

³ The fundamental physical constants and conversion factors are those from the critical compilation of Taylor, Parker, and Langenberg, Rev. Mod. Phys. 41, 375–496 (1969). The uncertainties in these values (enclosed in parentheses) represent one standard deviation. The value for N₀ is likely subject to change in the near future and its uncertainty should be assumed as 3 times the quoted value.

Appendix C. Rotational Constants and Multiplet Splitting for the O_2 Ground State

For the level $X \, ^3\Sigma_g^-$, $v=0$, there has for many years existed an apparent discrepancy between the values for B_0 and D_0 determined from electronic spectra and microwave spectra [69]. Fine-structure analyses of O_2 electronic transitions have been based on the use of values for B_0 and D_0 which were determined graphically by Babcock and Herzberg [24] in 1948. Even the most recently published papers [302, 33] have used the graphical method for determining rotational constants, though now a least squares fit by computer is preferable.

Babcock and Herzberg derived their constants from

$$\frac{\Delta_2 F_2''(N)}{N+\tfrac{1}{2}} = (4B'' - 6D'') - 8D''(N+\tfrac{1}{2})^2$$

and obtained

$$B_0 = 1.437770 \pm 0.000015 \text{ cm}^{-1}$$
$$D_0 = (4.913 \pm 0.020)10^{-6} \text{ cm}^{-1}.$$

Lofthus, using a computer and the method of least squares on the same data (at the request of the author) has obtained

$$B_0 = 1.437836 \ (\text{standard deviation } 0.000055)$$

$$D_0 = 4.986(10^{-6}) \ (\text{standard deviation } 0.050(10^{-6}).$$

If the error is assumed as three standard deviations we obtain

$$B_0 = 1.4378 \pm 0.0002 \text{ cm}^{-1}$$

$$D_0 = (4.99 \pm 0.15)10^{-6} \text{ cm}^{-1}.$$

(The error assumed by Babcock and Herzberg seems too small.)

If the coefficients are derived from a formula which does not unduly weight the effect of small N, i.e.,

$\Delta_2 F_2''(N) = (4B'' - 6D'')(N + \frac{1}{2}) - 8D''(N + \frac{1}{2})^3$, the results are

$$B_0 = 1.437891 \text{ (standard deviation, 0.000055)}$$

$$D_0 - 5.022(10^{-6}) \text{ (standard deviation, 0.050(10}^{-6}).$$

With error limits assumed as three standard deviations we get

$$B_0 = 1.4379 \pm 0.0002 \text{ cm}^{-1}$$

$$D_0 = (5.02 \pm 0.15)10^{-6} \text{ cm}^{-1}.$$

The numerical values obtained from the two refittings are the same within the assumed uncertainty.

Because of the result obtained by Lofthus, Albritton et al. [9] reanalyzed all of Babcock and Herzberg's data using a more extensive theory of the fine structure for the ground state and obtained the same values for B_0 [1.43784] and D_0 as those obtained by Lofthus.

In fitting the fine structure of the b $^1\Sigma_g^+ - X$ $^3\Sigma_g^-$ bands and obtaining the rotational constants (B_0, D_0) and spin coupling constants (λ, γ) for the ground state, Babcock and Herzberg [24] used the formulas of Schlapp [346] for the multiplet structure of the $^3\Sigma_g^-$ state. In Schlapp's theoretical formulation λ is (1) an approximate measure of spin-spin interaction of the unpaired electrons, and (2) a measure of deviation from strict Hund's coupling case b [in which the electron spin is completely decoupled from the molecular axis]. γ (or μ as is used in subsequent papers) is a measure of the interaction of the unpaired electron spins with the magnetic field due to rotation of the molecule. Second order contributions to B, λ, and γ arise from both spin-orbit and rotational effects.

More recent extensions of the fine structure theory of the ρ-type triplet have been used for fitting the microwave spectrum of O_2. In recent papers by West and Mizushima [411], Wilheit and Barrett [413], and Tischer [378] the same effective Hamiltonian is used for the ρ-type triplet:

$$H = BN^2 + 2/3\lambda(3S_z^2 - S^2) + \mu N \cdot S$$

with $B = B_0 + B_1 N(N+1)$ $\qquad [B_1 = -D_0]$
$\qquad \lambda = \lambda_0 + \lambda_1 N(N+1)$
$\qquad \gamma = \gamma_0 + \gamma_1 N(N+1)$.

The N-dependent contributions to the parameters arise from centrifugal distortion of the molecule. From the solution of the secular equation are obtained expressions for the multiplet term values and the absorption frequencies. Tischer formally introduced two parameters which are orders of magnitude smaller than the others, and when neglected in his fitting, give expressions identical to those obtained by Wilheit and Barrett [413]. Kayama and Baird [227], by contrast with these authors, used the rigorous microscopic Hamiltonian for the spin-

orbit coupling and deduced mixing of the ground state predominantly with $^1\Sigma_g^+$ (but also with $^1\Pi_g$ and $^3\Pi_g$), rather than with only $^3\Pi_g$, as had the others—but the expressions for the term values have the same form as those of Wilheit and Barrett and of Tischer, and the formulation differs only in the interpretation of the several contributions to λ and γ.

Many values for B_0 determined from microwave measurements have been based on a particular theory (formula) fitted to the observed fine structure. Microwave values of D_0 have not been reliable. McKnight and Gordy [265] have seemingly obtained for the first time a value for B_0 that is independent of fine structure theory. They related their measurements of rotational and fine structure frequencies to a formula involving only coefficients B_0, D_0, H_0. The formula is

$$\frac{E(3,3) - E(1,1)}{h} = \nu(1,2 \to 3,2) - \nu_{1+} + \nu_{3-}$$

$$= 10B_0 - 140D_0 + 1720H_0.$$

Quoting their numbers, we have

$$424,763.80 \pm 0.20 - 56264.778 \pm 0.01 + 62486.255 \pm 0.01$$

$$= 430,985.28 \pm 0.20 \text{ MHz}.$$

Now $1720 H_0 < 0.01$ MHz is not considered further. Thus

$$B_0 = \frac{430,985.28 \pm 0.20 + 140 D_0}{10}$$

McKnight and Gordy used Babcock and Herzberg's value for D_0. By using the refitted value (5.022 ± 0.050) 10^{-6} cm$^{-1} = (0.1506 \pm 0.0015)$ MHz [with $140 D_0 = (21.08 \pm 0.21)$ MHz] we obtain

$$B_0 = 43100.636 \pm 0.029 \text{ MHz} = 1.437682$$
$$\pm 0.0000015 \text{ cm}^{-1}.[1]$$

As has been pointed out by Tischer [378], the simplified theory of Schlapp [346] provided Babcock and Herzberg [24] with a value of B, not B_0, where $B = B_0 - \mu_1 + 2/3\lambda_1$. McKnight and Gordy [265] then also obtained B, not B_0 for

$$F_2(N) = N(N+1)(B_0 - \mu_1 + 2/3\lambda_1) - D_0 N^2(N+1)^2.$$

[1] More recent (tentative) unpublished results communicated by M. Mizushima give

$$B_0 = 43100.6355 \text{ MHz} = 1.437682 \text{ cm}^{-1}$$

$$D_0 = 0.15259 \text{ MHz} = 5.0899(10^{-6}) \text{ cm}^{-1}$$

$$H_0 = -0.0000650 \text{ MHz} = 2.17(10^{-9}) \text{ cm}^{-1}.$$

These coefficients were determined from a simultaneous fit to fine-structure microwave measurements (unpublished) as well as to the data of McKnight and Gordy [265]. More extensive microwave measurements still in progress (K. Evenson, M. Mizushima) are likely to lead to improved values for all fine structure parameters.

By using the values of μ_1 and λ_1 from the various authors [411, 413, 378] a correction of -0.039 MHz is obtained to the value of B deduced from the results of McKnight and Gordy [265]. This gives $B_0 = 43100.597$ MHz $= 1.437681$ cm^{-1} as the best value which is not independent of the fine structure theory. In addition, the centrifugal distortion correction in the expression for λ may be slightly incorrect (T. A. Miller, private communication). Whether the new formalism will have a significant effect on the numerical value for B_0 is not yet known.

Appendix D. Molecular Constants Derived from the O_2^+ $A\,^2\Pi_u - X\,^2\Pi_g$ Transition.

A computer least squares fit has been made by Lofthus to the fine structure measurements on bands of the O_2^+, $A-X$ system of Stevens and of Bozóky. The band origins, weighted by the reciprocal of the square of the computed standard deviations, have been used by the author to obtain a revised set of molecular constants for the $A-X$ transition. A similar set of constants, fitted to all observed band heads, has also been computed by the author. Below, a comparison is made between the results for the extensive set of R_2 band heads and the relatively few, but more reliable, band origins. Standard deviations are quoted only for coefficients fitted to band origins.

Error has been assumed as three standard deviations; the head and origin results overlap one another and are consistent with one another. Unexpectedly, the array of more than one hundred band heads is best fitted in a least squares sense by quadratic functions of both v' and v''. The rather small uncertainty in $\omega_e x_e$ for both states, however, fails to reflect the significantly different values obtained when $\omega_e y_e$'s are used, singly, or together. The $\omega_e y_e$'s are not statistically significant, but do produce relatively large change in $\omega_e x_e$'s from those quoted above.

	Heads	S.D.	Origins	S.D.
σ_e	R_2 40483 R_2 40683	5 5	40572.3	3.7
$\sigma(0-0)$ calc.	39978 40178		40070	
$A\,^2\Pi_u$ ω_e	896.7	0.6	898.17	0.37
$\omega_e x_e$	13.45	0.03	13.57	0.02
ZPE	445.0		445.7	
$X\,^2\Pi_g$ ω_e	1907.2	1.07	1905.1	0.75
$\omega_e x_e$	16.44	0.06	16.28	0.04
ZPE	949.5		948.5	